Destabilization of Alzheimer's Amyloid-β Fibrils by Natural Compounds: An All-Atom Molecular Dynamics Simulation Study

A thesis submitted

in partial fulfilment of the requirements

for the degree of

Doctor of Philosophy

by

SHIVANI GUPTA

(Roll No.: 166107106)

Department of Chemical Engineering

Indian Institute of Technology Guwahati

Guwahati–781039

Assam, India

August 2022

DEDICATED

TO

MY PARENTS

AND

BROTHER

STATEMENT

I do hereby declare that the content embodied in this thesis entitled "**Destabilization of Alzheimer's Amyloid-β Fibrils by Natural Compounds: An All-Atom Molecular Dynamics Simulation Study"** is the result of investigations carried out by me at Department of Chemical Engineering, Indian Institute of Technology Guwahati, Guwahati, India, under the guidance of Prof. Ashok Kumar Dasmahapatra.

In keeping with the general practice of reporting scientific observations, the thesis has been prepared without resorting to plagiarism and due acknowledgement and citation has been made wherever the work described is based on the findings of other investigations.

Date:

Place: IIT Guwahati, India

August 2022

Shivani Gupta

(Roll No. 166107107)

CERTIFICATE

This is to certify that the thesis entitled **"Destabilization of Alzheimer's Amyloid-β Fibrils by Natural Compounds: An All-Atom Molecular Dynamics Simulation Study (Roll No.: 166107106)**, a research scholar in the Department of Chemical Engineering, Indian Institute of Technology Guwahati, for the award of the degree of Doctor of Philosophy, is a record of the original research work carried out by him under my supervision and guidance.

The thesis has fulfilled all requirements as per the regulations of the institute and in my opinion has reached the standard needed for submission. The work documented in this thesis have not been submitted to any other University or Institute for the award of any degree.

Date: 15th March,'23

Prof. Ashok Kumar Dasmahapatra
Professor
Department of Chemical Engineering
Indian Institute of Technology Guwahati
Guwahati–781039, Assam, India.

ACKNOWLEDGEMENTS

The entire duration of this doctoral program has been full of memorable and enriching experiences for me. Not only have I been fortunate enough to understand my limitations and improve upon them on a professional front, but I have also learned valuable lessons that have made me a better person. As I near the tenure of my PhD study, I would like to express my earnest and heartfelt gratitude to the people who have supported me throughout the journey. First and foremost, I would like to thank my thesis supervisor Prof. Ashok Kumar Dasmahapatra for his patience, wisdom and guidance which aided me to endure and resolve challenges that I encountered during my PhD tenure. I sincerely thank him for allowing me the latitude to explore scientific pursuits and provide a guiding light throughout this study. I am grateful to the members of my doctoral committee, Prof. Tamal Banerjee, Dr. Amit Kumar and Dr. Priyadarshi Satpati, for accepting to evaluate my thesis and provide insightful comments.

During my PhD study, I had the wonderful experience of learning from my lab seniors Dr. Chitrita Kundu, Dr. Pavan Krishna Kanchi, Dr. Shatrudhan Palsaniya and Dr. Siddharth Thakur who not only assisted me in developing technical knowledge but also provided constant encouragement.

I am thankful to the members of our research group Sophia Leimapokpam, Suvendu Mandal, Imran Hussain, Banalata Kaibarta, Prateek Singh, Sadika and Gourab Nandy for providing a collaborative and healthy research environment. I earnestly appreciate the help, support and guidance from each of them. I would be grateful to all the faculty members and staff of the Department of Chemical Engineering, and High Performance Computational Facility at departmental (FIST CLUSTER) and institute level (PARAM-ISHAN), IIT Guwahati.

Most importantly, I would like to thank my support system, which includes Dr. Jenasree Hazarika, Dr. Nihal Gujre, Dr. Kushagra Agarwal, Bhaskar Kalita, Dr. Sutapa Das, Dr. Surabhi Patel, Dr. Anusuya Talukdar, Dr. Trishnamoni Gautom, Dr. Jinesh Machale, Kajal Ingtipi, Saptarshi Da, Rahul Yadav, Nilesh Khalse, Neelkamal Kalita, Sayani Adhikari, Nikhil Dhongde and Gaurav Sharma for their constant faith, patience and all the love and care and good times that we had during my PhD tenure.

Last but not the least, this thesis would not have been complete without the endless trust and support of my parents Lt. Ramesh Gupta and Mrs. Snehlata Gupta and my brother Akhil Gupta. Without my family I would not have been here and anywhere. Their love, blessings and trust in me is my biggest strength.

Last but not least, I want to express my gratitude to everyone who has been directly or indirectly involved in my work over the years.

ABSTRACT

Alzheimer's Disease (AD) which is a progressive, neurodegenerative and geriatric disease is multi-faceted in nature with genetic, environmental and some unknown mechanism associated with it. The main culprit behind the etiology of the disease is believed to be the extraneuronal senile plaques made up of Amyloid-Beta (Aβ) proteins and intraneuronal neurofibrillary tangles (NFTs) of hyperphosphorylated tau protein. Amongst these two, Aβ fibrils have been reported to be the principal clinical hallmark due to its direct involvement in the neurotoxicity and degeneration leading to AD.

The therapeutic approaches have been broadly classified into two viz. inhibition of the aggregation of the Aβ monomers and disaggregation of the preformed Aβ fibrils. The use of β-sheet breakers, nanoparticles, small molecules and natural compounds have been studied for the same purpose. The failure of the clearance of the drugs from inhibition strategy has motivated the in depth investigations for the disaggregation approach. In this view the role of natural compounds have been preferred owing to their natural non-toxicity and biocompatibility with the human system.

In the present work, various natural compounds from different category have been studied by means of Molecular Dynamics (MD) simulation, wherein they were made to interact with disease relevant Aβ fibril (PDB ID: 2BEG). Herein the caffeine from alkaloids, caffeic acid, gallic acid, epigallocatechin and ellagic acid from polyphenols, omega-3 polyunsaturated fatty acids (PUFAs) and lycopene from terpene have been investigated. The mechanistic details on the interaction of caffeine (CFF) with preformed Aβ fibril has been obtained wherein the destabilization of the fibril is observed. Four major phenolics from plants have been screened

by docking and studied by MD simulation for their destabilization potential. The outcome of the study observed ellagic acid (REF) as the best binder and destabilizer of Aβ fibril wherein it binds to chain A of the fibril by accessing fibrillar cavity. The significant role of Omega -3 fatty acids, Eicosapentaenoic acid (EPA) and Docosahexaenoic acid (HXA) specifically in destabilization of the Aβ fibril has been assessed. The crucial role of EPA and HXA in maintaining brain integrity and destabilization potential on Aβ fibril, makes them a suitable drug candidate for treating AD. The amphiphilic nature of these PUFAs was found to be the supportive for the better binding with the fibril, wherein polar head binds to K28 (positively charged residue) and long carbon tail to the hydrophobic residues of the fibril. This brings effective destabilization by compromising the inherent hydrophobic interactions coupled with loss of β sheet content. The detailed analysis of lycopene as a potential destabilizer of different polymorphic form of Aβ fibril has been done. The lycopene was found to interact with the surface and cavity of the fibril depending on the architecture. Conclusively, from all the studies, the major governing principles behind destabilization of the fibril was observed by loss of H-bonds, breakage of salt-bridges and loss of hydrophobic interactions in the fibril upon ligand introduction. The loss of β-sheet content indicates the collapse of highly organized structure indicating disorganization in the presence of the ligand curbing neurotoxicity of the fibril. The need to investigate the fate of the destabilized fibril upon removal of the ligand has also been conducted. This study highlights the enhancement of the destabilized structure upon removal of the ligand, REF in this case, thereby inhibiting the refibrillation, indicates towards the non-neurotoxicity of the fibril obtained. This establishes the efficacy and prophecy of destabilization of preformed Aβ fibril by natural compounds as a promising therapeutic approach for treating AD.

Table of Contents

Introduction

Motivation and Objectives

Modelling and Simulation Method

Destabilization of Aβ Protofilament by Caffeine: Insights from all atom MD Simulations

Destabilization potential of phenolics on Aβ Fibril: Mechanistic insights from Molecular Dynamics Simulation

Destabilization of Aβ fibrils by Omega-3 Polyunsaturated Fatty Acids: A Molecular Dynamics study

Lycopene Destabilizes Preformed Aβ Fibrils: Mechanistic Insights from All-Atom Molecular Dynamics Simulation

Enhanced Stability of a Disaggregated Aβ Fibril on Removal of Ligand Inhibits Refibrillation: An All Atom Molecular Dynamics Simulation Study

Conclusion and Future Scope

List of Tables

List of Figures

List of Abbreviations

AD	**Alzheimer's Disease**
MD	**Molecular Dynamics**
SPC	**Simple Point charge**
SPC/E	**Extended Simple Point charge**
MM-PBSA	**Molecular Mechanics Poisson-Boltzmann Surface Area Method**
CFF	**Caffeine**
DHC	**Caffeic Acid**
REF	**Ellagic Acid**
EGT	**Epigallocatechin**
GDE	**Gallic Acid**
PUFA	**Poly Unsaturated Fatty Acid**
EPA	**Eicosapentaenoic acid**
HXA	**Docosahexaenoic acid**
LNL	**Alpha-linolenic acid**
LYC	**Lycopene**

Chapter 1

Introduction

1.1 Proteins

Proteins (Greek *proteios*, which means "first" or "foremost") are the macromolecules that form the building blocks of any living system.[1] They are the expression of all the information hidden in cellular DNA. They are the workhorses of the cell and have crucial role in functioning of any living system. They play significant role as enzymes, hormones, neurotransmitters, cytokines, growth factors, cellular products, transcription factors and basically all functions.

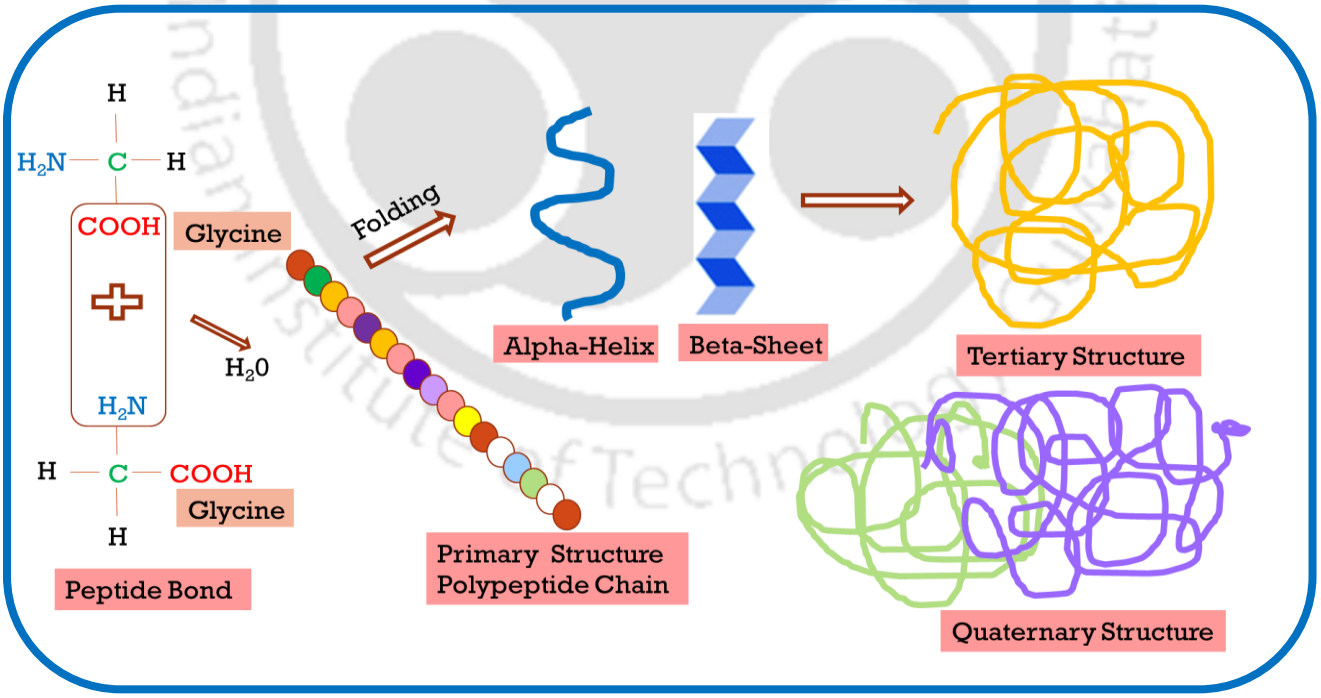

Fig. 1.1. Levels of Organization in a protein

A polypeptide chain, the primary structure of a protein composed of 20 amino acids, which arrange themselves in a unique pattern explaining the functional repository of an organism. The information for folding are inclusive to primary structure that defines structure and functionality of any protein.[2] The overall stability of proteins relies upon peptide bonds at primary level and hydrogen bonding, di-sulfide linkages, salt bridges and hydrophobic interactions at secondary, tertiary and higher levels of organization (Fig. 1.1). The answer to the existing enormous functional repository of the proteins lies in the possible arrangements of amino acids in an exclusive pattern and conformations by virtue of amino acid sequences.

1.2 Protein Folding

The multidimensional structure of a protein translates into a specified function, which is fundamental to the biology of all living systems. Protein folding is the key feature which helps in attaining a certain structure by the protein thereby imparting stability to carry out desired functions.[3] The primary structure holds all the cues for folding, which is a prerequisite for its specified biological activity.[4] In 1968, Levinthal proposed that a protein folds rapidly because its constituent amino acids interact locally thus limiting the conformational space that the protein has to explore and forcing the protein to follow a funnel-like energy landscape (energy funnel).[5] The Levinthal paradox explains the capability of proteins to traverse through the enormous conformational space of possible states within a microsecond.

The protein thus formed, has specific fate (described in Fig. 1.2) to either (1) fold, (2) remain unfolded or (3) misfold. All these states can interchange between each other at any point

of time with unclear reasons. This entire regulation is maintained by the protein homeostatic machinery in humans that checks upon any erroneous productions.

A protein sequence must satisfy two requirements: one is thermodynamic and other one is kinetic. The thermodynamic requirement is that the protein should adopt a unique folded conformation (native state), which is stable under physiological conditions. The kinetic requirement is that the denatured polypeptide chain can fold into the native conformation within a reasonable time.[6] Ellis, in 1987, explained that the folding is a spontaneous process mediated by another class of proteins called chaperones. Sometimes the proteins are not able to fold properly leading to loss of function as observed in cystic fibrosis, Tay-Sachs disease and various forms of cancers.

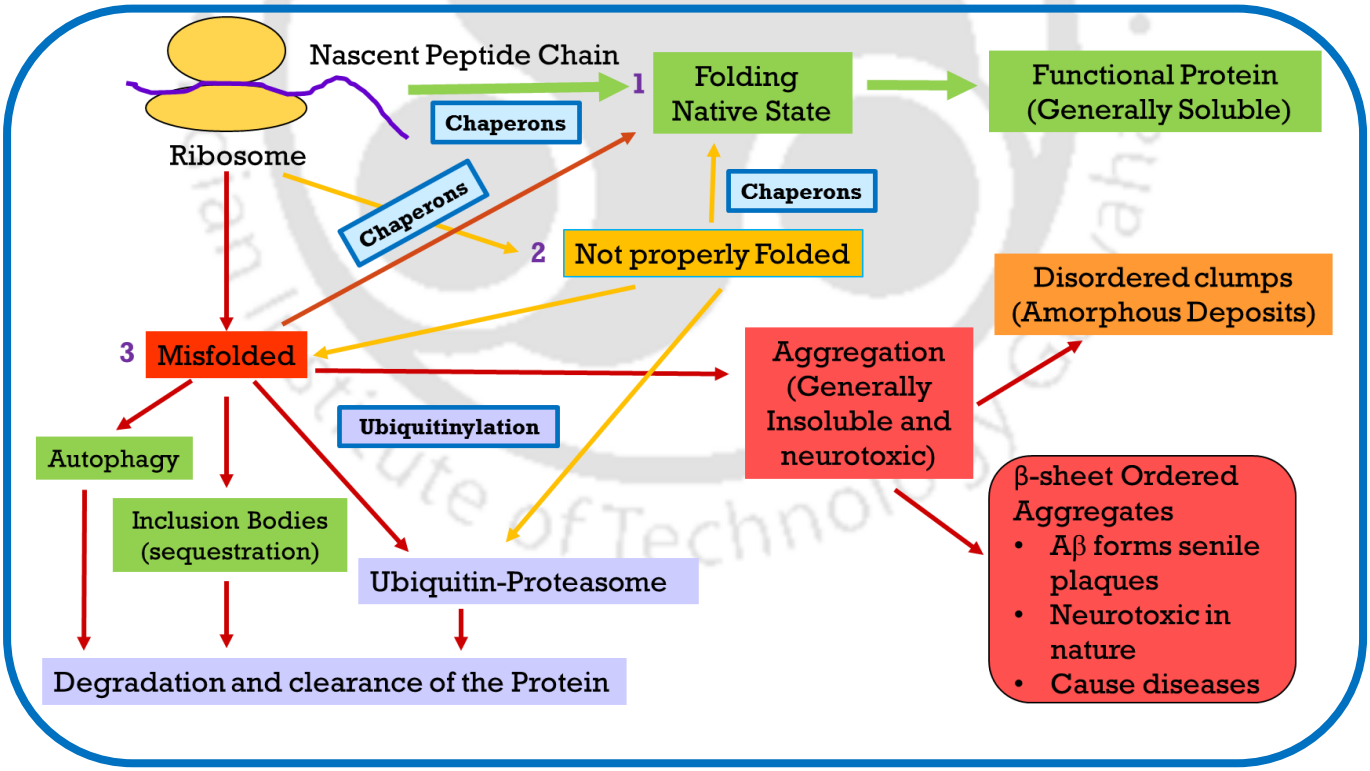

Fig. 1.2. Fate of Protein: Conformational Stability (Adapted from Chiti and Dobson, 2017)[7]

Collectively, the ubiquitin proteasome system and chaperons constitute the protein homeostatic machinery. Despite of involvement of several check points, proteins tend to misfold in the cellular space, which lead to so many disease conditions.

1.3 Protein Misfolding: Proteinopathies

Cellular proteostatic collapse, mutation, oxidative stress, erroneous post-translational modifications and ageing[8,9] encourages protein to attain a misfolded state.[10] Misfolded proteins are generally sequestered and degraded by proteasome and autophagy in the cellular space but sometimes evade this regulation facility. Henceforth, the misfolded protein gets aggregated due to protein overload and triggers the agglomeration amongst themselves. The protein aggregation eventually gives rise to various disorders, collectively called as proteinopathies.[11-12] These misfolded conformers obtain alternative energy minima, even more stable than the native state. The coexistence of unfolded, misfolded, folded and intermediate folded state creates a pool of different conformations in a cellular space at any instance.[13] Remarkably, they often able to interact with other native copies of the same protein and catalyze their transition into the misfolded toxic state.[14] Because of this ability, they are known as infective conformers. The newly made toxic proteins repeat the cycle in a self-sustaining loop, amplifying the toxicity and thus leading to a catastrophic effect that eventually kills the cell or impairs its function.

Misfolding of proteins triggers conversion of soluble form (random coil) of protein into highly ordered fibrillar aggregates (β-sheet) which are mostly insoluble, known as amyloid fibrils or plaques. The phenomena of formation of amyloid fibrils is called as amyloidosis.[15] The major

factors contributing towards agglomeration of misfolded proteins are hydrophobicity, propensity of amino acid sequence to form β-sheets and low net charge of peptide.[16-17]

The proteinopathies caused from misfolding of different proteins can be localized to a certain organ or can spread to different parts of the body i.e. systemic in nature. Type-2 diabetes, caused by toxic aggregates of the islet amyloid polypeptide (IAPP) cause cytotoxicity of β cells of pancreas and spread over other organs as well that manifests in sugar imbalance and thus hyperglycemia in the body.[18]

1.4 Functional Amyloids

Despite of the well-known detrimental effects of amyloids, they still play some crucial structural and physiological roles in living systems from microbes to humans.[19] The tight regulation of functional amyloids preventing toxicity to humans adds to their significant existence and functions in humans.[20] The notoriety is overshadowed by their following roles.

- Melanin biosynthesis is guided by fibrous structures of Pmel17 (premelanosome protein) protein during melanosome formation which are very important for skin pigmentation and prevention from skin cancer.[21]
- Tissue-type plasminogen activator act as a regulatory structure in formation and clot clearance mechanisms by activating Blood clotting factor XII protein and the entire cascade mechanism thereafter.[22]
- Aβ fibrils also play essential role in protecting brain from pathogens by creating a trap, thereby possessing antimicrobial, antibacterial and antifungal properties.[23]

- Aβ intercepts oncogenic virus and suppresses tumor growth, act as sealant for Blood brain barrier (BBB) and maintains synaptic communication in hippocampus region of the brain thereby contributing to memory consolidation in humans.[24]

1.5 Neurodegenerative Disorders

The neurodegenerative proteinopathies are of bigger concern owing to their higher prevalence in the society and the socio-economic burden adhere to it. Neurodegenerative disorders (NDs) like Alzheimer's Disease (AD), Parkinson's Disease (PD) and Huntington's disease (HD), Amyotrophic Lateral Sclerosis (ALS) are characterized by an array of misfolded proteins as described in Table 1.1 that agglomerates abnormally[25] to form insoluble aggregates, hindering the normal functioning of the brain.[26]

Table 1.1. Common NDs and their Causative Proteins[25]

S. No.	Disease	Aggregating Protein	Characteristic Pathology
1	Alzheimer's Disease (AD)	Aβ peptide	Amyloid Plaques
		Tau	Neurofibrillary Tangles
		α-synuclein	Lewy Bodies
2	Parkinson's Disease (PD)	α-synuclein	Lewy Bodies and Neurites

3	Huntington's Disease (HD)	Huntington with tandem glutamine repeats	Intracellular inclusions and cytoplasmic aggregates
4	Amyotrophic Lateral Sclerosis (ALS)	Superoxide Dismutase	Inclusions of disarrayed neurofilaments in lower motor neurons

1.6 Alzheimer's Disease

AD is a multi-faceted chronic, neurodegenerative, progressive, and geriatric disease with unclear roots and mechanisms.[27] Firstly reported in 1907 by Alois Alzheimer, AD is multidimensional in nature owing to its association with genetics (familial),[28] lifestyle and environmental factors (sporadic) that interplay for the disease incidences. AD is the most prevalent amongst NDs and is increasing at an uncontrolled rate.[29] According to the World Alzheimer's report,2021 by WHO, 55 million people across the globe are living with dementia, which is forecasted to reach to 78 million by 2030.[30] The number of people getting affected by this debilitating disease is increasing at an uncontrollable rate expected to reach to 152 million people by 2050 globally as quoted by Alzheimer's disease International (ADI).[31] Dementia is explained as a cognitive impairment comprising of memory loss leading to poor judgment, inability to process daily information, and

social withdrawal affecting the normal sustenance of a person. The devitalizing effects of dementia connotes personal, societal and global healthcare burden adhered to AD.

The typical histopathological hallmarks of AD are reported to be senile Aβ plaques of Aβ proteins, extraneuronal in location[29] and neurofibrillary tangles made up of hyper phosphorylated tau proteins present intraneuronally.[32]

1.7 Hypothesis related to AD

Many hypothesis have been proposed explaining the causes for AD, with Amyloid cascade hypothesis being the most supported, studied and accepted one.

1.7.1 *Cholinergic Hypothesis:* This theory postulates the decline in amount of acetylcholine, a neurotransmitter, to be the reason for memory deficit in AD patients.[32] This age old hypothesis indicates enhanced activity of acetylcholinesterase enzyme that breakdowns acetylcholine thereby hindering synaptic communication, affecting cognitive abilities severely.[33]

1.7.2 *Tau Hypothesis:* The tau hypothesis states about involvement of neurofibrillary tangles (NFTs) made up of hyperphosphorylated tau protein in pathology of AD and other tauopathies.[32] Mis-stabilization of tau protein leads to synaptic impairment and mitochondrial integrity.[34] Tau has been reported to have inter-relation with Aβ peptides in causing neurotoxicity.[35]

1.7.3 *Amyloid Cascade Hypothesis (ACH):* According to the amyloid cascade hypothesis, insoluble mature Aβ fibrils formed by aggregation of Aβ peptides during amyloidogenic pathway, reported to be the main culprit behind AD and its etiology.[36] Aβ plaques trigger a cascade from neuritic injury for the formation of NFTs via tau protein that eventually leads to neuronal dysfunction in AD (Fig. 1.3).

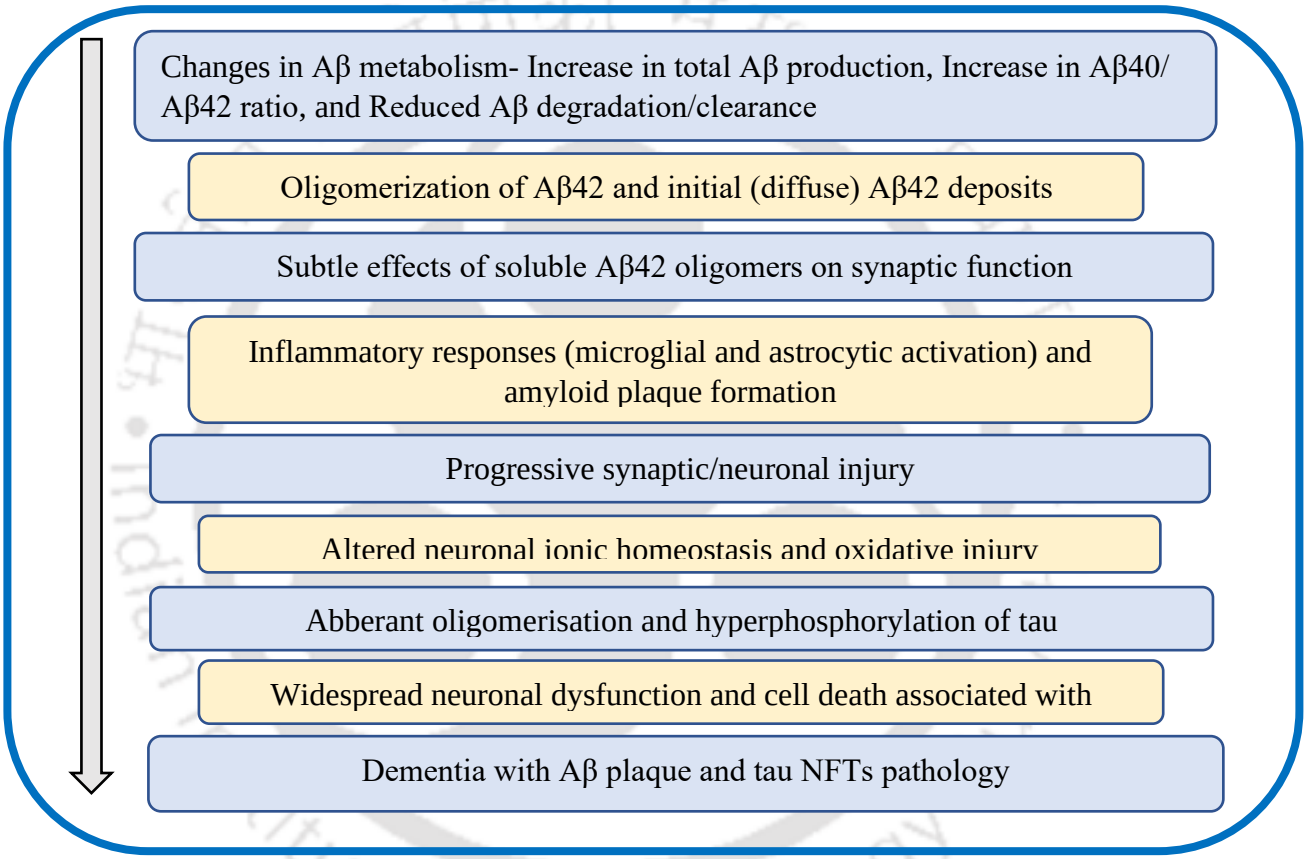

Fig. 1.3. Amyloid cascade hypothesis (Adapted from Hardy and Selkoe,'2002)[37]

1.7.4 *Aβ Oligomer Hypothesis (AβO):* The soluble intermediate products formed during fibrillation are called as AβO claimed to be more toxic than Aβ mature fibrils.[38] The presence of AβO

in AD patients and mouse models entrenches the toxic and pathogenic role of AβO in progression of AD.[39]

The greater acceptance of ACH hypothesis is pertinent to significant and direct involvement of senile Aβ plaques in AD. There have been various drugs proposed time to time to treat AD that consider different drug targets such as, acetylcholinesterase, tau proteins and Aβ for therapeutic purposes. The failure of drugs in clinical trials has encouraged the interest and investigation towards anti amyloid therapy.[40] The long age debate between the pathological potential of Aβ fibrils and AβO is still undergoing that needs a lot of investigations. Although in the eye of the currently available evidences, Aβ fibrils are found to be neurotoxic causing etiology of AD.

1.8 Aβ Production

The proteolytic processing of APP (Amyloid Precursor Protein), which is a 639-770 residue long protein, present in chromosome 21 forms Aβ peptide by two different pathways viz. normal non-amyloidogenic and toxic amyloidogenic pathway (as illustrates in Fig. 1.4). The non-amyloidogenic cleavage of APP by α-secretase enzyme results in production of α-APP fragments and C-terminal fragments, α(C83) having neuroprotective effects.[41] The product from this pathway has proposed to have vital functional roles as discussed in section 1.4.

However, the alternating amyloidogenic enzymatic cleavage of APP also leads to Aβ biogenesis but neurotoxic this time. This happens due to sequential cleavage of β and γ secretase to form Aβ peptide having 37-42 residue long. In both of the pathways a common fragment called

AICD (APP intracellular domain) is produced, which upon phosphorylation, facilitates the interaction of APP with various cytosolic factors that regulates its intracellular trafficking.[42] The major isoforms produced are 40 and 42 residue long, with 42 reported to be the more aggregation prone, rigid and toxic one.[43] Aβ peptide formed from this pathway then undergoes aggregation to form neurotoxic Aβ fibrils, interfering with the normal synaptic functioning. The Aβ fibril is the pathological hallmark and of greater clinical importance, as explained by amyloid cascade hypothesis below.[44–46] The mechanism of fibrillation and structure has been explained in the subsequent sections.

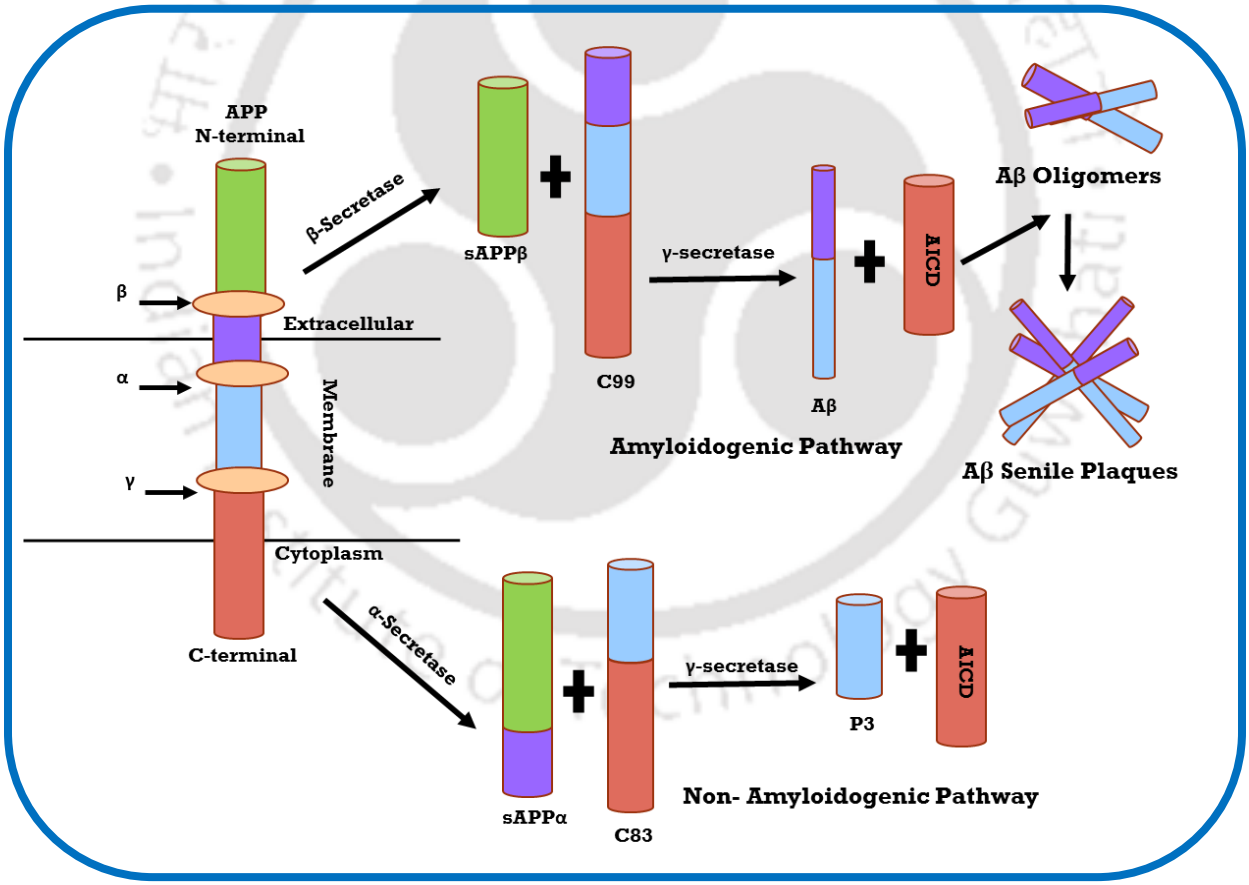

Fig. 1.4. Overview of APP Processing (Adapted from Chow et al.,2011)[42]

1.9 Mechanism of Fibrillation

Amyloid fibrillation is a self-assembly phenomenon of misfolded Aβ peptides into a more stable and organized structure. The most widely accepted model is "Nucleation dependent polymerization mechanism".[47] The fibrillation process commences with the misfolded state of Aβ protein that gets clumped with formation of intermediate soluble oligomers followed by the formation of mature insoluble neurotoxic fibrillar aggregates. Furthermore, secondary nucleation can form higher order aggregates via fibrils interacting with upcoming monomers, soluble oligomers or even fibrils. The kinetic studies by ThT assay (Thioflavin-T) provides insight on the sigmoidal nature of fibrillation process wherein four different phases viz. (i) Lag phase (ii) Elongation phase (iii) Polymerization phase and (iv) Secondary nucleation phase exists.[48] The ThT is the most acceptable dye that gives the clear picture on fibrillation, which is directly proportional to the amount of fibrils present.

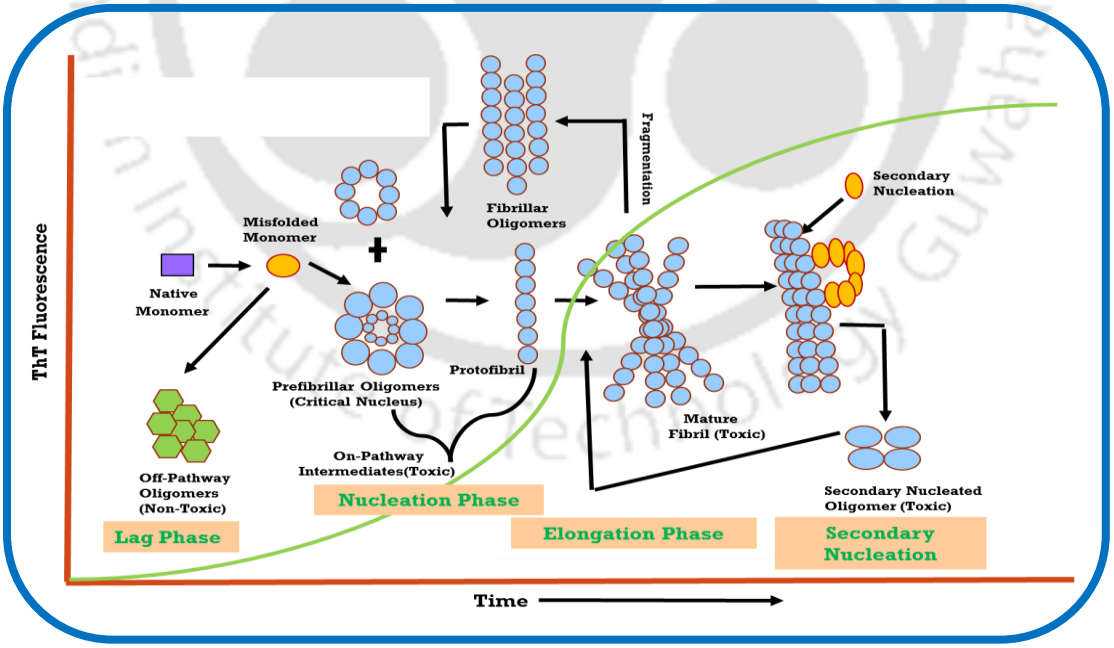

Fig. 1.5. Fibrillation Mechanism (Adapted from Taneja et al., 2015)[49]

As illustrated in Fig. 1.5 above, the lag phase comprises of formation of a critical nucleus having sufficient number of monomers to enter elongation phase. A nucleus is defined as the state wherein the rate of formation exceeds the rate of dissociation of monomers. After that, monomers attach to each other and form protofibril (during elongation phase), which can dissociate by fragmentation or can form mature fibrils. After a critical concentration of the mature fibril is reached, the secondary nucleation takes over the elongation phase and result in higher order aggregates. All the structures formed during the entire fibrillation process are toxic with variable degree and the formation is concentration dependent.[49]

1.10 Structure of Amyloid Fibril

As explained in above section 1.3, hydrophobicity and β-sheet propensity of amino acids in Aβ peptide (Fig. 1.6) drives its aggregation and organization in a β-sheet structure. This entails further pathway of aggregation and senile plaque formation.

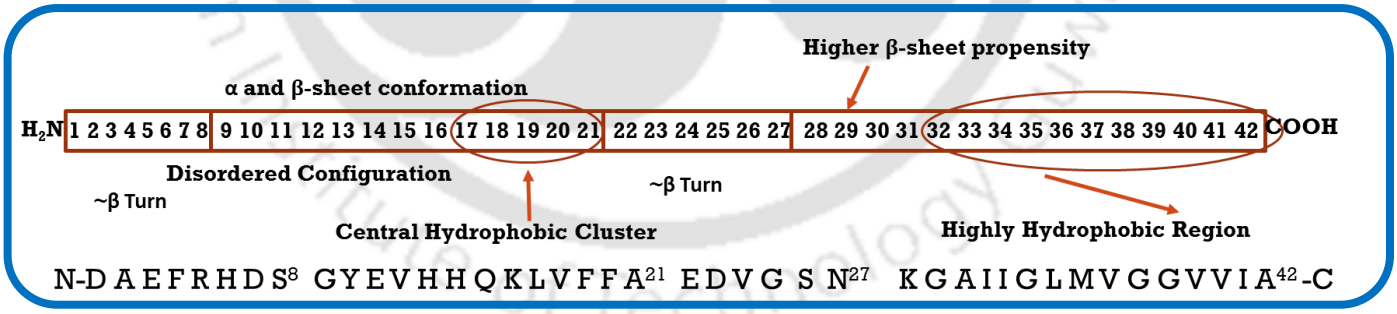

Fig. 1.6. Amyloid Beta Peptide (1-42) Sequence[50]

Aβ fibrils are recognized by fibrillar morphology and cross β-sheet arrangement as mark of identification and, are insoluble and protease resistant in nature. The conventional methods such as single crystal X-ray crystallography and solution nuclear magnetic resonance (NMR)

spectroscopy cannot be used owing to insolubility of the fibrils. Therefore, X-ray fiber diffraction, electron microscopy (EM), solid state (ss) NMR, Fourier transform infra- red spectroscopy (FTIR) and circular dichroism (CD) can be used to study amyloid structures. The information about the structure of Aβ fibrils is crucial in order to gain knowledge about fibrillation mechanism which in turn facilitates understanding of Aβ as an important biomarker, drug target and structure-based drug designing in lieu to cure AD.

All the amyloid fibrils in general possess following characteristics, which form basis of their structural studies as well as identification.[51,52]

- Conformational switching from α-helix or random coil to a β-strand configuration.
- The fibril appears to be composed of several protofilaments twisted around each other as revealed from a cross-sectional view
- Some polypeptides having Poly-Q repeats have inherent property to form amyloids.
- Structural monitoring done by binding dyes like Thioflavin-T (ThT), congo red that gives green birefringence when examined under cross polarized light.
- Aβ have shown that β-sheet may be arranged parallel or anti-parallel with inter-strand distance of 4.8 Aº and inter sheet distance as 6-12 Aº (Fig. 1.7).
- Fibrils possess cross β structure in which stacked β-strands are oriented perpendicularly (Fig. 1.7) to fibrillar axis as studied by X-ray crystallography and ss-NMR (solid state-Nuclear Magnetic Resonance).
- The mechanical strength and stability as reported by AFM studies is attributed to highly organized structure due to cross β sheet structures.[53]

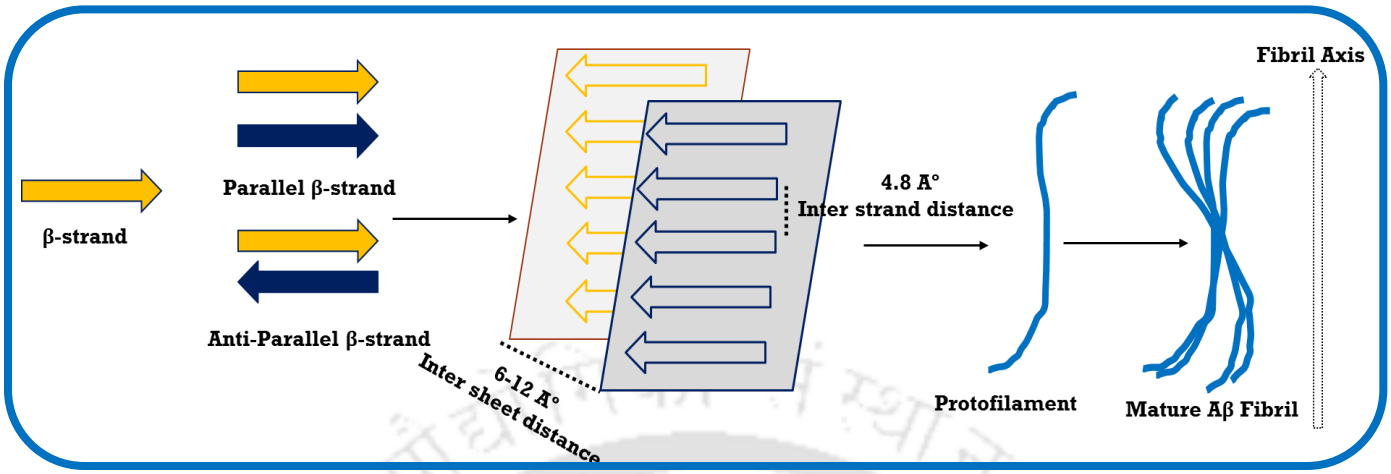

Fig. 1.7. Aβ Fibrils: Different Patterns of β-strands (Adapted from Loquet et al,'2018).[54]

1.11 Therapeutic Strategies for treatment of AD

The role of Aβ as critical initiator and propagator of AD has well been discussed in the earlier section of the thesis. On the molecular level, the anti-amyloid therapy has different points for intervention, starting from decreasing Aβ production, modulating its transport, inhibition of aggregation of Aβ monomers and Aβ immunotherapy to disaggregation of Aβ fibrils.[55] A brief introduction of all these therapeutic approaches is discussed as follows:

- **Decreasing Aβ production**: Increasing activity of α-secretase and reducing γ-secretase may enhance non-amyloidogenic pathway of APP metabolism. Epigallocatechin-gallate from green tea has been reported to enhance α-secretase activity.[56] Eight FDA approved NSAIDs have also been reported to lower $A\beta_{42}$ *in-vivo* by targeting γ-secretase activity.[57]

- **Modulating Aβ transport**: The role of Apolipoprotein (apoE4) as major transporter of cholesterol and Aβ from blood to brain has been indespensable.[58] The crucial role in transportation of Aβ from blood to brain qualifies apoE as suitable target for modulating the Aβ transport, despite being a genetic risk factor that can modify deposition of Aβ in the cerebrovasculature. Various compounds targeting apoE such as, bexarotene, pyrazolines and probucol etc. have been reported to target apoE to alter its production, its lipidation, and lower blood cholesterol level leading to Aβ clearance.[59]

- **Inhibition of Aggregation of Aβ:** The failure associated with restraining production of Aβ monomers, directs the prevention of inhibition of Aβ fibrillation as a promising strategy. There have been various natural compounds reported as potential anti-aggregators of Aβ monomers, such as, melatonin, curcumin, wgx-50, brazilin, morin, resveratrol, tashinone.[60] They prevent aggregation of Aβ monomers and hence evade neurotoxicity and thereby restoring normal cognitive functioning.

- **Aβ immunotherapy:** Anti-amyloid immunization is the basis of this line of treatment to inhibit Aβ proliferation and fibrillation. Monoclonal antibodies[61] when tested in transgenic mice, found promising in targeting Aβ protein and plaques thereby curing AD. However, failure in clinical trials dwindles their effective role in treating AD. The FDA approval of biogen's Aducanumab under Aβ immunotherapy has triggered a scientific division globally.[62]

- **Destabilization of preformed Aβ fibrils:** Another line of treatment for AD is believed to be the destabilization of the preformed Aβ fibrils. Nanoparticles,[63,64] β-sheet breakers,[65] and natural compounds[66–69] are reported as potential destabilizers of Aβ fibrils.

All these interventions either manages the progression of the disease or ease the symptomatic discomfort. Meanwhile, the skepticism about the disease mechanism streamlines investigation of potential drugs involving inhibition of aggregation of Aβ monomers or destabilization of Aβ fibrils.[70] Failure of numerous drug leads in clinical trials accessed for inhibition strategy ignited the consideration of destabilization of preformed Aβ fibrils as a fruitful alternative line of treatment of AD.

1.12 Destabilization of Aβ Fibril by Natural Compounds

Disaggregation of Aβ fibrils is relatively newer strategy that needs detailed investigation to gain insights on the molecular details and potential of this therapeutic approach. The perturbations introduced in the Aβ fibrillar structure curbs toxicity caused by the fibril and restrains the formation of higher order aggregates as well, explaining dual advantage of this therapy.

The antioxidant, anti-cancerous, neuroprotection and various other health benefits of natural compounds add to their suitability to be used as drugs for a wide array of human diseases, including AD.[71–75] Natural products can be obtained from numerous living systems including marine, plant, and animal resources. Amongst all the origins of natural compounds, the plant-based phytochemicals are the safest choice due to fair availability, extractability and broad spectrum of applicability.[76–78] Some of them are: resveratrol, a polyphenol present in red wine and trans-

εvinferin[79], curcumin,[80] ferulic acid,[81] tannic acid,[82] serotonin, melatonin and other indole compounds.[83] Dihydrochalcone, a bioactive from daemonorops draco tree[84] have been reported for its anti-amyloidogenic property, inferred from its role in destabilizing Aβ fibril. The destabilization effect of morin[85] was well studied mechanistically by means of MD simulation.

The computational studies not only traverse atomic-scale mechanisms by means of MD simulations but also validates *in-vitro* findings.[86] Brazilin[87] and hematoxylin[88] from Sappan wood were reported to redirect Aβ monomers and mature fibrils into unstructured Aβ aggregates when studied by *in-vitro* methods and MD simulation, restricting their primary and secondary nucleation. A recent finding on inhibition and destabilization of Aβ monomer and Aβ protofibril, studied computationally, by a hybrid of resveratrol and clioquinol reinforces the importance of phenolic compounds in prospecting new drug candidates for AD.[89] Finding new drug candidates from plants to treat AD by means of computational studies is exemplary and a continuously evolving process.

The destabilization of Aβ fibrils by natural compounds as studied by MD simulation is the focus of the present study. Herein, various compounds and classes of natural compounds have been accessed in the subsequent chapters via MD simulation for their destabilization potential.

1.13 Computational Tools for the Atomistic details in different aspects of AD

The importance of computational tools for studying any processes in science has been exemplary due to desire for mimicking the system, saving resources to a greater extent, and helps in preplanning and validating the experimental studies more comprehensively. The role of computational tools particularly MD simulation, has been quite significant in case of AD,

specifically studying Aβ protein that lies in skepticism associated with AD. The unknown roots of disease occurrence, progression and possible therapeutic treatment has encouraged the use of computational tools for studying various aspects of these diseases to understand the mechanism better and plan the experimental studies and vice versa. The computational studies complements well in understanding the polymorphic nature of the disease in context to Aβ monomers, protofibril and fibrils that translates into different phenotype.[90] The polymorphism has been suggested to be related to the different environmental conditions that dictates different self-assembly and conformations of the Aβ monomer.[91] Mutational studies as studied by computational tools explained the significance of even one amino acid substitution, crucial for increment or decrement for the toxicity of the Aβ thus formed.[92] Computational studies ease the same set of calculations at different pH level, so as to gain more insights in the pH related structural and functional toxicity of the fibril.[93]

Hence, the computational tools find greater utility in better assessment of the protein-ligand interactions, the prerequisite for entire drug designing process.[94,95] The molecular level understanding on crucial interactions between protein and the ligand forms the basis of drug screening, drug discovery, drug designing and drug testing along with the efficacy of the drug.[96] The protein-ligand interaction studies are therefore important to avoid failure of the proposed drugs in the clinical trials. This study in turn saves the substantial amount of effort, time and cost invested in proposing one drug lead compound. The use of computational tools along with the experimental studies saves energy, time and cost and enhances the possibility of the development of promising therapeutic approach for treatment of AD.

1.14 Summary

Unfortunately, there have been 115 years since the discovery of AD but the unclear roots, elusive mechanism of progression, lack of biomarkers and question on suitable drug targets makes it troublesome for people working in this field. The constantly growing incidences and plight of people worldwide ads to the misery of this debilitating disease. The socio-economic burden cannot be neglected but cannot be answered also due to lack of any promising treatment for AD. Although, recently only one monoclonal antibody got FDA approval but has created a division in the scientific community over acceptance. Inspite of availability of vast pool of reports, findings, observations and manuscripts for AD in all the domains of mechanism, diagnosis and treatment, any promising treatment still appears a distant dream.

In the present thesis, after going through the literature available, we have concentrated on determining the destabilization of Aβ fibrils by natural compounds, studied by MD simulation, thereby proposing drug leads to cure AD. There have been various compounds from varied classes of bioactives that are scrutinized and reported for the treatment of AD in the present work. The destabilization strategy as therapeutic intervention needs special attention due to its dual advantage. This strategy helps in desisting the progression of the disease and prevent further aggregation as well thereby ensuring a holistic cure and not just the palliative one.

Conclusively, the use of computational tools may help in initial screening and understanding of the drug leads in terms of their efficacy, mechanism of action and dosage. The information thus obtained can be tested by *in-vitro* and *in-vivo* methods ensuring a larger possibility of clearance in clinical trials. The amalgamation of computational and experimental approach can help find drug leads from natural compounds cure to AD.

1.15 Organization of the Thesis

A brief introduction to the Alzheimer's disease and the culprit protein associated with it, is provided in **Chapter 1**. In **Chapter 2**, the motivation and objectives of the thesis have been discussed. In **Chapter 3**, we discuss the methodology of the molecular docking, molecular dynamics simulation protocols and MM-PBSA tools. **Chapter 4** we present a study where we determine the destabilization potential of Caffeine molecule on Aβ protofibril. The **Chapter 5** presents studies with screening of different phenolics for the destabilization potential. In **Chapter 6**, another class of natural compounds, i.e. Omega-3, healthy acid fatty acids have been studied for disruption profile of Aβ fibril. **Chapter 7** contains the investigation of lycopene (from terpene family) for its destabilization potential on Aβ fibril. The **Chapter 8** checks upon the refibrillation possibility after the ligand is removed from the destabilized structure. Finally, in **Chapter 9**, we present a summary of the thesis with a discussion on the scope for future studies.

REFERENCES

1 M. Vendruscolo, J. Zurdo, C. E. MacPhee and C. M. Dobson, Protein folding and misfolding: a paradigm of self–assembly and regulation in complex biological systems, *Philosophical Transactions of the Royal Society of London. Series A: Mathematical, Physical and Engineering Sciences*, 2003, **361**, 1205–1222.

2 W. Widłak, *Molecular Biology*, Springer Berlin Heidelberg, Berlin, Heidelberg, 2013, vol. 8248.

3 L. M. Luheshi and C. M. Dobson, Bridging the gap: From protein misfolding to protein misfolding diseases, *FEBS Letters*, 2009, **583**, 2581–2586.

4 Anfinsen, Folding of Protein Chains, *Science*, 1973, **181**, 223–230.

5 C. Levinthal, Are there pathways for protein folding?, *J. Chim. Phys.*, 1968, **65**, 44–45.

6 C. M. Dobson, A. Šali and M. Karplus, Protein Folding: A Perspective from Theory and Experiment, *Angewandte Chemie International Edition*, 1998, **37**, 868–893.

7 F. Chiti and C. M. Dobson, Protein Misfolding, Amyloid Formation, and Human Disease: A Summary of Progress Over the Last Decade, *Annual Review of Biochemistry*, 2017, **86**, 27–68.

8 J. W. Kelly, Alternative conformations of amyloidogenic proteins govern their behavior, *Curr Opin Struc Biol*, 1996, **6**, 11–17.

9 C. Soto, Protein misfolding and disease; protein refolding and therapy, *FEBS Letters*, 2001, **498**, 204–207.

10 W. E. Balch, R. I. Morimoto, A. Dillin and J. W. Kelly, Adapting Proteostasis for Disease Intervention, *Science*, 2008, **319**, 916–919.

11 L. M. Blancas-Mejía and M. Ramirez-Alvarado, Systemic Amyloidoses, *Annual Review of Biochemistry*, 2013, **82**, 745–774.

12 C. M. Dobson, Principles of protein folding, misfolding and aggregation, *Seminars in Cell & Developmental Biology*, 2004, **15**, 3–16.

13 F. U. Hartl and M. Hayer-Hartl, Converging concepts of protein folding in vitro and in vivo, *Nature Structural & Molecular Biology*, 2009, **16**, 574–581.

14 P. Brundin, R. Melki and R. Kopito, Prion-like transmission of protein aggregates in neurodegenerative diseases, *Nature Reviews Molecular Cell Biology*, 2010, **11**, 301–307.

15 I. Moreno-Gonzalez and C. Soto, Misfolded protein aggregates: Mechanisms, structures and potential for disease transmission, *Seminars in Cell & Developmental Biology*, 2011, **22**, 482–487.

16 T. Konno, Amyloid-induced aggregation and precipitation of soluble proteins: An electrostatic contribution of the Alzheimer's ??(25-35) amyloid fibril, *Biochemistry*, 2001, **40**, 2148–2154.

17 F. Chiti, M. Stefani, N. Taddei, G. Ramponi and C. M. Dobson, Rationalization of the effects of mutations on peptide andprotein aggregation rates, *Nature*, 2003, **424**, 805.

18 A. Mukherjee, D. Morales-Scheihing, P. C. Butler and C. Soto, Type 2 diabetes as a protein misfolding disease, *Trends in Molecular Medicine*, 2015, **21**, 439–449.

19 S. A. Levkovich, E. Gazit and D. Laor Bar-Yosef, Two Decades of Studying Functional Amyloids in Microorganisms, *Trends in Microbiology*, 2021, **29**, 251–265.

20 M. P. Jackson and E. W. Hewitt, Why are functional amyloids non-toxic in humans?, *Biomolecules*, 2017, **7**, 1–13.

21 D. M. Fowler, A. V. Koulov, W. E. Balch and J. W. Kelly, Functional amyloid – from bacteria to humans, *Trends in Biochemical Sciences*, 2007, **32**, 217–224.

22 O. Kranenburg, B. Bouma, L. M. J. Kroon-Batenburg, A. Reijerkerk, Y.-P. Wu, E. E. Voest and M. F. B. G. Gebbink, Tissue-Type Plasminogen Activator Is a Multiligand Cross-β Structure Receptor, *Current Biology*, 2002, **12**, 1833–1839.

23 D. K. V. Kumar, S. H. Choi, K. J. Washicosky, W. A. Eimer, S. Tucker, J. Ghofrani, A. Lefkowitz, G. McColl, L. E. Goldstein, R. E. Tanzi and R. D. Moir, Amyloid-β peptide protects against microbial infection in mouse and worm models of Alzheimer's disease, *Science Translational Medicine*, 2016, **8**, 340ra72-340ra72.

24 H. M. Brothers, M. L. Gosztyla and S. R. Robinson, The Physiological Roles of Amyloid-β Peptide Hint at New Ways to Treat Alzheimer's Disease, *Frontiers in Aging Neuroscience*, 2018, **10**, 411–424.

25 P. Sweeney, H. Park, M. Baumann, J. Dunlop, J. Frydman, R. Kopito, A. McCampbell, G. Leblanc, A. Venkateswaran, A. Nurmi and R. Hodgson, Protein misfolding in neurodegenerative diseases: implications and strategies, *Translational Neurodegeneration*, 2017, **6**, 6.

26 D. Eisenberg and M. Jucker, The Amyloid State of Proteins in Human Diseases, *Cell*, 2012, **148**, 1188–1203.

27 R. Mayeux and Y. Stern, Epidemiology of Alzheimer Disease, *Cold Spring Harbor Perspectives in Medicine*, 2012, **2**, a006239–a006239.

28 K. Bettens, K. Sleegers and C. Van Broeckhoven, Genetic insights in Alzheimer's disease, *The Lancet Neurology*, 2013, **12**, 92–104.

29 G. R. Grøntvedt, T. N. Schröder, S. B. Sando, L. White, G. Bråthen and C. F. Doeller, Alzheimer's disease, *Current Biology*, 2018, **28**, R645–R649.

30 A. D. International and M. University, World Alzheimer Report 2021, *Alzheimer's Disease International*, 2021, 2–314.

31 2022 Alzheimer's disease facts and figures, *Alzheimer's & Dementia*, 2022, **18**, 700–789.

32 C. Ballatore, V. M. Y. Lee and J. Q. Trojanowski, Tau-mediated neurodegeneration in Alzheimer's disease and related disorders, *Nature Reviews Neuroscience*, 2007, **8**, 663–672.

33 R. M. Lane, M. Kivipelto and N. H. Greig, Acetylcholinesterase and Its Inhibition in Alzheimer Disease, *Clinical Neuropharmacology*, 2004, **27**, 141–149.

34 S. S. Shafiei, M. J. Guerrero-Muñoz and D. L. Castillo-Carranza, Tau Oligomers: Cytotoxicity, Propagation, and Mitochondrial Damage, *Frontiers in Aging Neuroscience*, 2017, **9**, 1–9.

35 Ilie-Cosmin Stancu, Bruno Vasconcelos, Dick Terwel and Ilse Dewachter, Models of beta-amyloid induced Tau-pathology: the long and folded road to understand the mechanism

Molecular Neurodegeneration, *Molecular Neurodegeneration*, 2014, **9**, 1750–1326.

36 G. S. Bloom, Amyloid-β and Tau, *JAMA Neurology*, 2014, **71**, 505.

37 J. Hardy and D. J. Selkoe, The Amyloid Hypothesis of Alzheimer's Disease: Progress and Problems on the Road to Therapeutics, *Science*, 2002, **297**, 353 LP – 356.

38 I. Benilova, E. Karran and B. De Strooper, The toxic Aβ oligomer and Alzheimer's disease: an emperor in need of clothes, *Nature Neuroscience*, 2012, **15**, 349–357.

39 Y. Zhang, L. Lu, J. Jia, L. Jia, C. Geula, J. Pei, Z. Xu, W. Qin, R. Liu, D. Li and N. Pan, A Lifespan Observation of a Novel Mouse Model: In Vivo Evidence Supports Aβ Oligomer Hypothesis, *PLoS ONE*, 2014, **9**, e85885.

40 L.-K. Huang, S.-P. Chao and C.-J. Hu, Clinical trials of new drugs for Alzheimer disease, *Journal of Biomedical Science*, 2020, **27**, 18.

41 F. Corrigan, C. L. L. Pham, R. Vink, P. C. Blumbergs, C. L. Masters, C. van den Heuvel and R. Cappai, The neuroprotective domains of the amyloid precursor protein, in traumatic brain injury, are located in the two growth factor domains, *Brain Research*, 2011, **1378**, 137–143.

42 V. W. Chow, M. P. Mattson, P. C. Wong and M. Gleichmann, An Overview of APP Processing Enzymes and Products, *NeuroMolecular Medicine*, 2010, **12**, 1–12.

43 Y. Yan and C. Wang, Aβ42 is More Rigid than Aβ40 at the C Terminus: Implications for Aβ Aggregation and Toxicity, *Journal of Molecular Biology*, 2006, **364**, 853–862.

44 G. Evin and A. Weidemann, Biogenesis and metabolism of Alzheimer's disease Aβ amyloid peptides, *Peptides*, 2002, **23**, 1285–1297.

45 R. Kayed, E. Head, J. L. Thompson, T. M. McIntire, S. C. Milton, C. W. Cotman and C. G. Glabe, Common Structure of Soluble Amyloid Oligomers Implies Common Mechanism of Pathogenesis, *Science*, 2003, **300**, 486–489.

46 M. A. Findeis, The role of amyloid β peptide 42 in Alzheimer's disease, *Pharmacology & Therapeutics*, 2007, **116**, 266–286.

47 T. P. J. Knowles, C. A. Waudby, G. L. Devlin, S. I. A. Cohen, A. Aguzzi, M. Vendruscolo,

E. M. Terentjev, M. E. Welland and C. M. Dobson, An Analytical Solution to the Kinetics of Breakable Filament Assembly, *Science*, 2009, **326**, 1533–1537.

48 K. Gade Malmos, L. M. Blancas-Mejia, B. Weber, J. Buchner, M. Ramirez-Alvarado, H. Naiki and D. Otzen, ThT 101: a primer on the use of thioflavin T to investigate amyloid formation, *Amyloid*, 2017, **24**, 1–16.

49 V. Taneja, M. Verma and A. Vats, Toxic species in amyloid disorders: Oligomers or mature fibrils, *Annals of Indian Academy of Neurology*, 2015, **18**, 138.

50 K. Y. Wu, D. Doan, M. Medrano and C. A. Chang, Modeling structural interconversion in Alzheimers' amyloid beta peptide with classical and intrinsically disordered protein force fields, *Journal of Biomolecular Structure and Dynamics*, 2021, 1–18.

51 L. C. Serpell, Alzheimer's amyloid fibrils: structure and assembly, *Biochimica et Biophysica Acta (BBA) - Molecular Basis of Disease*, 2000, **1502**, 16–30.

52 R. N. Rambaran and L. C. Serpell, Amyloid fibrils, *Prion*, 2008, **2**, 112–117.

53 T. Fukuma, A. S. Mostaert and S. P. Jarvis, Explanation for the mechanical strength of amyloid fibrils, *Tribology Letters*, 2006, **22**, 233–237.

54 A. Loquet, N. El Mammeri, J. Stanek, M. Berbon, B. Bardiaux, G. Pintacuda and B. Habenstein, 3D structure determination of amyloid fibrils using solid-state NMR spectroscopy, *Methods*, 2018, **138**–**139**, 26–38.

55 J. Cao, J. Hou, J. Ping and D. Cai, Advances in developing novel therapeutic strategies for Alzheimer's disease, *Molecular Neurodegeneration*, 2018, **13**, 64.

56 A. Smith, B. Giunta, P. C. Bickford, M. Fountain, J. Tan and R. D. Shytle, Nanolipidic particles improve the bioavailability and α-secretase inducing ability of epigallocatechin-3-gallate (EGCG) for the treatment of Alzheimer's disease, *International Journal of Pharmaceutics*, 2010, **389**, 207–212.

57 J. L. Eriksen, S. A. Sagi, T. E. Smith, S. Weggen, P. Das, D. C. McLendon, V. V. Ozols, K. W. Jessing, K. H. Zavitz, E. H. Koo and T. E. Golde, NSAIDs and enantiomers of flurbiprofen target γ-secretase and lower Aβ42 in vivo, *Journal of Clinical Investigation*,

2003, **112**, 440–449.

58 J. Fan, J. Donkin and C. Wellington, Greasing the wheels of Aβ clearance in Alzheimer's Disease: The role of lipids and apolipoprotein E, *BioFactors*, 2009, **35**, 239–248.

59 T. Williams, D. R. Borchelt and P. Chakrabarty, Therapeutic approaches targeting Apolipoprotein E function in Alzheimer's disease, *Molecular Neurodegeneration*, 2020, **15**, 8.

60 K. Pagano, S. Tomaselli, H. Molinari and L. Ragona, Natural Compounds as Inhibitors of Aβ Peptide Aggregation: Chemical Requirements and Molecular Mechanisms, *Frontiers in Neuroscience*, 2020, **14**, 1–18.

61 B. Bohrmann, K. Baumann, J. Benz, F. Gerber, W. Huber, F. Knoflach, J. Messer, K. Oroszlan, R. Rauchenberger, W. F. Richter, C. Rothe, M. Urban, M. Bardroff, M. Winter, C. Nordstedt and H. Loetscher, Gantenerumab: A Novel Human Anti-Aβ Antibody Demonstrates Sustained Cerebral Amyloid-β Binding and Elicits Cell-Mediated Removal of Human Amyloid-β, *Journal of Alzheimer's Disease*, 2012, **28**, 49–69.

62 J. S. Perlmutter, Aducanumab: look before leaping, *Nature Medicine*, 2021, **27**, 1499–1499.

63 N. Guzior, A. Wieckowska, D. Panek and B. Malawska, Recent development of multifunctional agents as potential drug candidates for the treatment of Alzheimer's disease., *Current medicinal chemistry*, 2015, **22**, 373–404.

64 S. Sudhakar and E. Mani, Rapid Dissolution of Amyloid β Fibrils by Silver Nanoplates, *Langmuir*, 2019, **35**, 6962–6970.

65 B. S. and S. C., β-Sheet Breakers for Alzheimers Disease Therapy, *Current Drug Targets*, 2004, **5**, 553–558.

66 X. Han and G. He, Toward a Rational Design to Regulate β-Amyloid Fibrillation for Alzheimer's Disease Treatment, *ACS Chemical Neuroscience*, 2018, **9**, 198–210.

67 C. Wu, J. Scott and J. E. Shea, Binding of congo red to amyloid protofibrils of the alzheimer Aβ 9-40 peptide probed by molecular dynamics simulations, *Biophysical Journal*, 2012, **103**, 550–557.

68 P. Alam, S. K. Chaturvedi, M. K. Siddiqi, R. K. Rajpoot, M. R. Ajmal, M. Zaman and R. H. Khan, Vitamin k3 inhibits protein aggregation: Implication in the treatment of amyloid diseases, *Scientific Reports*, 2016, **6**, 1–11.

69 J. C. Saunders, L. M. Young, R. A. Mahood, M. P. Jackson, C. H. Revill, R. J. Foster, D. A. Smith, A. E. Ashcroft, D. J. Brockwell and S. E. Radford, An in vivo platform for identifying inhibitors of protein aggregation, *Nature Chemical Biology*, 2016, **12**, 94–101.

70 L. Estrada and C. Soto, Disrupting β-Amyloid Aggregation for Alzheimer Disease Treatment, *Current Topics in Medicinal Chemistry*, 2006, **7**, 115–126.

71 P. Deshpande, N. Gogia and A. Singh, Exploring the efficacy of natural products in alleviating Alzheimer's disease, *Neural Regeneration Research*, 2019, **14**, 1321.

72 J. Xiao and R. Shao, EDITORIAL (Natural Products for Treatment of Alzheimer's Disease and Related Diseases: Understanding their Mechanism of Action), *Current Neuropharmacology*, 2013, **11**, 337–337.

73 T. T. Bui and T. H. Nguyen, Natural product for the treatment of Alzheimer's disease, *Journal of Basic and Clinical Physiology and Pharmacology*, 2017, **28**, 413–423.

74 D. J. Newman and G. M. Cragg, Natural products as sources of new drugs over the 30 years from 1981 to 2010, *Journal of Natural Products*, 2012, **75**, 311–335.

75 A. Dey, R. Bhattacharya, A. Mukherjee and D. K. Pandey, Natural products against Alzheimer's disease: Pharmaco-therapeutics and biotechnological interventions, *Biotechnology Advances*, 2017, **35**, 178–216.

76 P. Williams, A. Sorribas and M.-J. R. Howes, Natural products as a source of Alzheimer's drug leads, *Nat. Prod. Rep.*, 2011, **28**, 48–77.

77 G. D'Onofrio, D. Sancarlo, Q. Ruan, Z. Yu, F. Panza, A. Daniele, A. Greco and D. Seripa, Phytochemicals in the Treatment of Alzheimer's Disease: A Systematic Review, *Current Drug Targets*, 2017, **18**, 1487–1498.

78 Habtemariam, Natural Products in Alzheimer's Disease Therapy: Would Old Therapeutic Approaches Fix the Broken Promise of Modern Medicines?, *Molecules*, 2019, **24**, 1519.

79 E. Vion, G. Page, E. Bourdeaud, M. Paccalin and J. Guillard, Molecular and Cellular Neuroscience Trans ε -viniferin is an amyloid- β disaggregating and anti-in fl ammatory drug in a mouse primary cellular model of Alzheimer ' s disease, *Molecular and Cellular Neuroscience*, 2018, **88**, 1–6.

80 G. Orteca, F. Tavanti, Z. Bednarikova, Z. Gazova, G. Rigillo, C. Imbriano, V. Basile, M. Asti, L. Rigamonti, M. Saladini, E. Ferrari and M. C. Menziani, Curcumin derivatives and Aβ-fibrillar aggregates: An interactions' study for diagnostic/therapeutic purposes in neurodegenerative diseases, *Bioorganic & Medicinal Chemistry*, 2018, **26**, 4288–4300.

81 K. Ono, M. Hirohata and M. Yamada, Ferulic acid destabilizes preformed β-amyloid fibrils in vitro, *Biochemical and Biophysical Research Communications*, 2005, **336**, 444–449.

82 K. Ono, K. Hasegawa, H. Naiki and M. Yamada, Anti-amyloidogenic activity of tannic acid and its activity to destabilize Alzheimer's β-amyloid fibrils in vitro, *Biochimica et Biophysica Acta (BBA) - Molecular Basis of Disease*, 2004, **1690**, 193–202.

83 R. Hornedo-Ortega, G. Da Costa, A. B. Cerezo, A. M. Troncoso, T. Richard and M. C. Garcia-Parrilla, In Vitro Effects of Serotonin, Melatonin, and Other Related Indole Compounds on Amyloid-β Kinetics and Neuroprotection, *Molecular Nutrition and Food Research*, 2018, **62**, 1–12.

84 Y. Jin, Y. Sun, J. Lei and G. Wei, Dihydrochalcone molecules destabilize Alzheimer's amyloid-β protofibrils through binding to the protofibril cavity, *Physical Chemistry Chemical Physics*, 2018, **20**, 17208–17217.

85 J. A. Lemkul and D. R. Bevan, Destabilizing Alzheimer's Aβ 42 Protofibrils with Morin: Mechanistic Insights from Molecular Dynamics Simulations, *Biochemistry*, 2010, **49**, 3935–3946.

86 J. Nasica-Labouze, P. H. Nguyen, F. Sterpone, O. Berthoumieu, N.-V. Buchete, S. Coté, A. De Simone, A. J. Doig, P. Faller, A. Garcia, A. Laio, M. S. Li, S. Melchionna, N. Mousseau, Y. Mu, A. Paravastu, S. Pasquali, D. J. Rosenman, B. Strodel, B. Tarus, J. H. Viles, T. Zhang, C. Wang and P. Derreumaux, Amyloid β Protein and Alzheimer's Disease: When Computer Simulations Complement Experimental Studies, *Chemical Reviews*, 2015, **115**,

3518–3563.

87 W. J. Du, J. J. Guo, M. T. Gao, S. Q. Hu, X. Y. Dong, Y. F. Han, F. F. Liu, S. Jiang and Y. Sun, Brazilin inhibits amyloid β-protein fibrillogenesis, remodels amyloid fibrils and reduces amyloid cytotoxicity, *Scientific Reports*, 2015, **5**, 1–10.

88 Y. Tu, S. Ma, F. Liu, Y. Sun and X. Dong, Hematoxylin inhibits amyloid β-protein fibrillation and alleviates amyloid-induced cytotoxicity, *Journal of Physical Chemistry B*, 2016, **120**, 11360–11368.

89 R. K. Saini, S. Shuaib, D. Goyal and B. Goyal, Insights into the inhibitory mechanism of a resveratrol and clioquinol hybrid against Aβ 42 aggregation and protofibril destabilization: A molecular dynamics simulation study, *Journal of Biomolecular Structure and Dynamics*, 2019, **37**, 3183–3197.

90 J. Nasica-Labouze, P. H. Nguyen, F. Sterpone, O. Berthoumieu, N.-V. Buchete, S. Coté, A. De Simone, A. J. Doig, P. Faller, A. Garcia, A. Laio, M. S. Li, S. Melchionna, N. Mousseau, Y. Mu, A. Paravastu, S. Pasquali, D. J. Rosenman, B. Strodel, B. Tarus, J. H. Viles, T. Zhang, C. Wang and P. Derreumaux, Amyloid β Protein and Alzheimer's Disease: When Computer Simulations Complement Experimental Studies, *Chemical Reviews*, 2015, **115**, 3518–3563.

91 G. Bitan, M. D. Kirkitadze, A. Lomakin, S. S. Vollers, G. B. Benedek and D. B. Teplow, Amyloid β-protein (Aβ) assembly: Aβ40 and Aβ42 oligomerize through distinct pathways, *Proceedings of the National Academy of Sciences*, 2003, **100**, 330–335.

92 C. Liang, R. Ni, J. E. Smith, W. S. Childers, A. K. Mehta and D. G. Lynn, Kinetic Intermediates in Amyloid Assembly, *Journal of the American Chemical Society*, 2014, **136**, 15146–15149.

93 W. Xu, C. Zhang, P. Derreumaux, A. Gräslund, L. Morozova-Roche and Y. Mu, Intrinsic Determinants of Aβ12–24 pH-Dependent Self-Assembly Revealed by Combined Computational and Experimental Studies, *PLoS ONE*, 2011, **6**, e24329.

94 G. Sliwoski, S. Kothiwale, J. Meiler and E. W. Lowe, Computational Methods in Drug Discovery, *Pharmacological Reviews*, 2014, **66**, 334–395.

95 C. Sotriffer and G. Klebe, Identification and mapping of small-molecule binding sites in proteins: computational tools for structure-based drug design, *Il Farmaco*, 2002, **57**, 243–251.

96 T. P. Lybrand, in *Computational Approaches to Biochemical Reactivity*, eds. G. Náray-Szabó and A. Warshel, Kluwer Academic Publishers, Boston, 2002, pp. 363–374.

Chapter 2

Motivation and Objectives

2.1 Motivation

Inhibition of aggregation of amyloid-beta (Aβ) peptides by natural compounds have been explored extensively for their implication as a potential therapeutic strategy to treat AD.[1–4] However, failure of any proposed drugs in clinical trials, based on this anti-aggregation approach raised global concerns. Tramiprosate, a naturally occurring compound from seaweed have been discontinued in 2007 after phase 3 clinical trial due to lack of consistent cognitive performance data.[5] Colostrinin, a proline rich polypeptide have also been discontinued in 2009 after phase 2 clinical trial due to lack of efficacy reported in cognitive assessment over period of 15 days to a month.[6] These are the few examples that explains inhibition of aggregation as an insignificant therapeutic strategy, and hence triggers the investigation of an alternate therapeutic approach to treat AD.

The failure of the drugs proposed for inhibition of aggregation, motivates exploration of disaggregation of the neurotoxic Aβ senile plaques (made up of aggregation of Aβ monomers), as an alternative promising therapeutic intervention for AD. The FDA (Food and Drug Administration) approval of aducanumab (a monoclonal antibody targeting Aβ deposits in the brain)[7] affirms the probable success of other drugs as well for disaggregation of senile plaques. However, the mere approval does not stop the quest and need to find new drugs for AD, pertinent to the controversy associated with the approved drug.[8] The literature available on the disaggregation of preformed aggregates by natural compounds and the underlying mechanism is

limited and needs immediate attention. Therefore, a detailed investigation of natural compounds as potential disruptors of the Aβ fibrils have been taken into consideration for the present work. There are some advantages associated with the disaggregation of preformed fibrils, reported in the literature, that are outlined as follows:

1. Disaggregation mechanism has lot of potential in clearing preformed Aβ fibrils.
2. The natural compounds could be a preferred choice as drug owing to their inherent biocompatibility and no toxicity.
3. Disaggregation of Aβ deposits as a therapeutic strategy posits additional advantage of prevention of further aggregation of deformed aggregates, ensuring non neurotoxicity.
4. The detailed investigation in the mechanism of disaggregation can be done thoroughly by computational studies involving molecular dynamics (MD) simulation.

2.2 Objectives

The major objective of the thesis is to investigate various natural compounds for their destabilization potential on preformed Aβ fibrils. The present work focus upon searching different compounds from major classes of the natural compounds from both plant and animal sources.

For this purpose, four major classes have been considered - Alkaloids, Polyphenols, Fatty acids and Terpenoids. Single or many molecules from each class have been considered to check for their destabilization potential on Aβ fibrils. From alkaloids, caffeine (CFF), a popular psychostimulant, has been considered. Different polyphenol compounds having antioxidant properties such as, caffeic acid (DHC), gallic acid (GDE) and ellagic acid (REF) from phenolic acid category and epigallocatechin (EGT) from flavonoids have been investigated. Three major Omega-3 polyunsaturated fatty acids (PUFAs) viz. Eicosapentaenoic acid (EPA),

Docosahexaenoic acid (HXA) and Alpha-linolenic acid (LNL) have been considered. The essential role of these PUFAs in maintaining brain integrity have prompted their selection for the present work. Lycopene (LYC), a carotenoid, reported for its highest antioxidant potential from terpenoids (largest class amongst phytochemicals) have also been studied in the thesis.

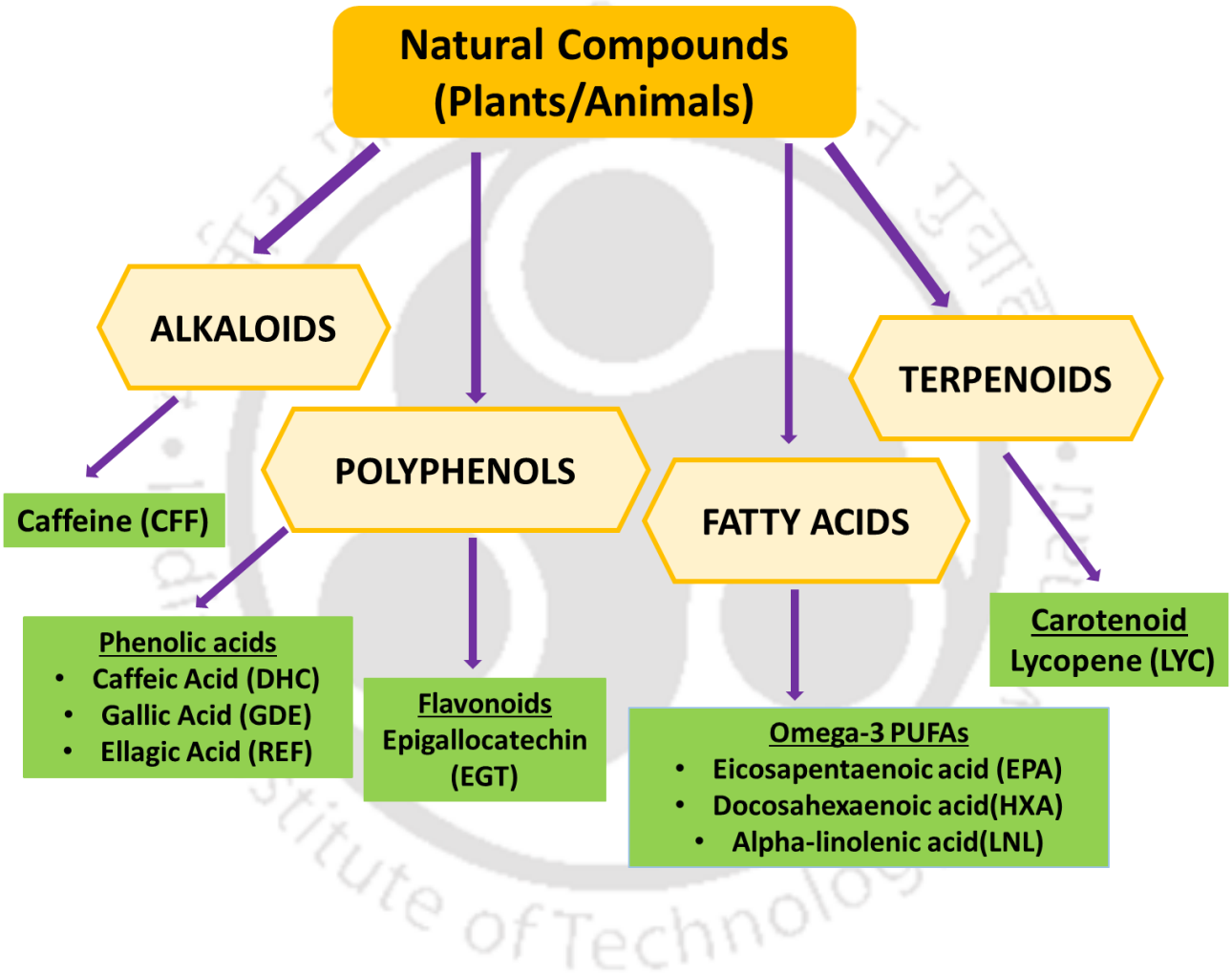

Fig. 2.1. Natural compound from different classes

The point of similarity in all these natural compounds are as follows:

- Their antioxidant and overall health benefits and other pharmacological effects.

- Role in neuroprotection coupled with penetration in blood brain barrier makes them suitable for formulating any neurodegenerative disease in general.
- Reports available on interaction with Aβ plaques encourages their selection for current study.
- Limited scientific reports on the direct destabilization of the Aβ fibril for these compounds instigates their selection for current work.
- All these natural compounds have been investigated for their destabilization potential of Aβ fibrils by means of MD simulation. The objectives that are organized as different chapters in the thesis are summarized below.

2.2.1 Destabilization of Aβ Protofilament by Caffeine: Insights from all-atom MD Simulations

We have implemented MD simulation by randomly inserting one Caffeine molecule in Aβ fibril. The all-atom simulation has provided an in-depth understanding on the mechanism of caffeine molecule in destabilizing Aβ fibril. There have been various parameters that were evaluated to determine the extent of disruption of the fibril by caffeine, such as, RMSD, R_g, RMSF, secondary structure content, H-bonds, salt bridges and hydrophobic interactions.

2.2.2 Destabilization potential of Phenolics on Aβ Fibril: Mechanistic insights from Molecular Dynamics Simulation

We have considered four different phenolic compounds for this objective. Herein, Caffeic acid, Epigallocatechin, Gallic acid and Ellagic acid from various fruits and nuts have been considered and tested for their destabilization potential on Aβ fibril. For screening the best binder towards

fibril, docking has been conducted, followed by MD simulation. The determinants for disruption of Aβ fibril were RMSD, RMSF, R_g, H-bonds and hydrophobic interactions. The detailed binding energy profiling has been evaluated by MM-PBSA tool to evaluate binding affinity and residues involves in binding of the ligand with the fibril.

2.2.3 Destabilization of Aβ Fibril by Omega-3 Polyunsaturated Fatty Acids: A Molecular Dynamics study

For this objective, another class of nootropic substances has been considered i.e. omega-3 fatty acids owing to their crucial role in promoting brain health. Herein, we present the destabilization potential of three ω-3 PUFAs viz., Eicosapentaenoic acid (EPA), Docosahexaenoic acid (HXA) and α-linolenic acid (LNL) by Molecular Dynamics simulation. The destabilization potential was gauged by various parameters, such as, RMSD, β-sheet content by DSSP tool, H-bonds and hydrophobic interactions. The MM-PBSA tool was employed to determine the binding energy between various chains of Aβ fibril in the presence of ω-3 PUFAs.

2.2.4 Lycopene Destabilizes Preformed Aβ Fibrils: Mechanistic Insights from All-Atom Molecular Dynamics Simulation

For this objective, lycopene, another natural compound from biggest class of secondary metabolites called terpenes, has been considered to check for destabilization of different polymorphs (viz., 2NAO and 2BEG) of Aβ fibrils. One molecule of lycopene has been introduced in a hexameric Aβ fibril and MD simulation was conducted. All the systems were analyzed via RMSD, R_g, SASA, RMSF and H-bonds, β-sheet content and other key residue interactions. The

higher concentration of the lycopene (sixty molecules i.e. Aβ-LYC_{60}) has also been assessed for higher destabilization of the fibril.

2.2.5 Enhanced Stability of a Disaggregated Aβ Fibril on Removal of Ligand Inhibits Refibrillation: An All-atom Molecular Dynamics Simulation Study

For this objective, the effect of removal of ligand has been measured for its probability for refibrillation or enhanced stability of the destabilized complex. For this, the ellagic acid (Aβ-REF") and caffeine (Aβ-CFF") has been removed from their respective destabilized complexes and simulated for 1 μs. Following this, RMSD, R_g, and SASA values have been calculated for Aβ-Water, Aβ-REF" and Aβ-CFF" systems to evaluate the extent of destabilization.

All these objectives have been explained and discussed in a detailed manner with the obtained results in the subsequent chapters in the thesis.

REFERENCES

1 Q. Nie, X. Du and M. Geng, Small molecule inhibitors of amyloid β peptide aggregation as a potential therapeutic strategy for Alzheimer's disease, *Acta Pharmacologica Sinica*, 2011, **32**, 545–551.

2 Q. Wang, X. Yu, L. Li and J. Zheng, Inhibition of Amyloid-β ; Aggregation in Alzheimer's Disease, *Current Pharmaceutical Design*, 2014, **20**, 1223–1243.

3 X.-L. Bu, P. P. N. Rao and Y.-J. Wang, Anti-amyloid Aggregation Activity of Natural Compounds: Implications for Alzheimer's Drug Discovery, *Molecular Neurobiology*, 2016, **53**, 3565–3575.

4 P. Velander, L. Wu, F. Henderson, S. Zhang, D. R. Bevan and B. Xu, Natural product-based amyloid inhibitors, *Biochemical Pharmacology*, 2017, **139**, 40–55.

5 P. S. Aisen, S. Gauthier, S. H. Ferris, D. Saumier, D. Haine, D. Garceau, A. Duong, J. Suhy, J. Oh, W. C. Lau and J. Sampalis, Tramiprosate in mild-to-moderate Alzheimer's disease – a randomized, double-blind, placebo-controlled, multi-centre study (the Alphase Study), *Archives of Medical Science*, 2011, **1**, 102–111.

6 A. Bilikiewicz and W. Gaus, Colostrinin (a naturally occurring, proline-rich, polypeptide mixture) in the treatment of Alzheimer's disease, *Journal of Alzheimer's Disease*, 2004, **6**, 17–26.

7 M. Shi, F. Chu, F. Zhu and J. Zhu, Impact of Anti-amyloid-β Monoclonal Antibodies on the Pathology and Clinical Profile of Alzheimer's Disease: A Focus on Aducanumab and Lecanemab, *Frontiers in Aging Neuroscience*, 2022, **14**, 1–11.

8 F. Tagliavini, P. Tiraboschi and A. Federico, Alzheimer's disease: the controversial approval of Aducanumab, *Neurological Sciences*, 2021, **42**, 3069–3070.

Chapter 3

Modelling and Simulation Method

The entire work revolves around the interaction of various natural compounds, primarily secondary plant metabolites with Aβ fibril to determine their destabilization potential via MD simulations. The thesis has been segregated into different chapters, wherein Aβ oligomer is made to interact with different natural compounds. The overall general scheme employs molecular docking, MD simulation and MMPBSA tool evaluation for detailed binding energy assessment. Three major methods that needs to be explained here are Docking, MD simulation and MMPBSA calculation. There are few in-built tools in GROMACS and some external software and tools that are explained in subsequent sections.

3.1 Defining Protein and Ligand System

3.1.1 Aβ fibril as protein receptor

(a) 2BEG.pdb (pentamer)

To study the interaction between any protein and ligand, firstly these two systems need to be retrieved from the RSCB database as pdb structures in GROMACS readable format. In the current work, the protein taken into consideration are the Aβ fibrils of various lengths, which forms

neurotoxic senile plaques that are believed to be neurotoxic in nature. The three-dimensional structure of $A\beta_{17-42}$ oligomer (PDB ID: 2BEG)[1] was taken from the protein data bank (PDB) designated as receptor. The pentamer is a U-shaped structure having chain length of 26 residues, starting from 17 and ending till 42. The initial 16 residues are disordered and has very less contribution to the overall stability of this fibril that is why neglected in the disease relevant structure. This Aβ oligomer is a pentamer structure spanning from residues 17-42, which forms the characteristic β-sheet, a prerequisite for fibrillization and stable organization. The characteristic β-sheet structure is further divided into three regions; β1 region (18-26 residues), turn region (27-30 residues), and β2 region (31-42 residues), as depicted in Fig. 3.1. There are five chains in 2BEG protofibril, designated as A, B, C, D, and E, having the same primary sequence with A and E being the terminal hains.

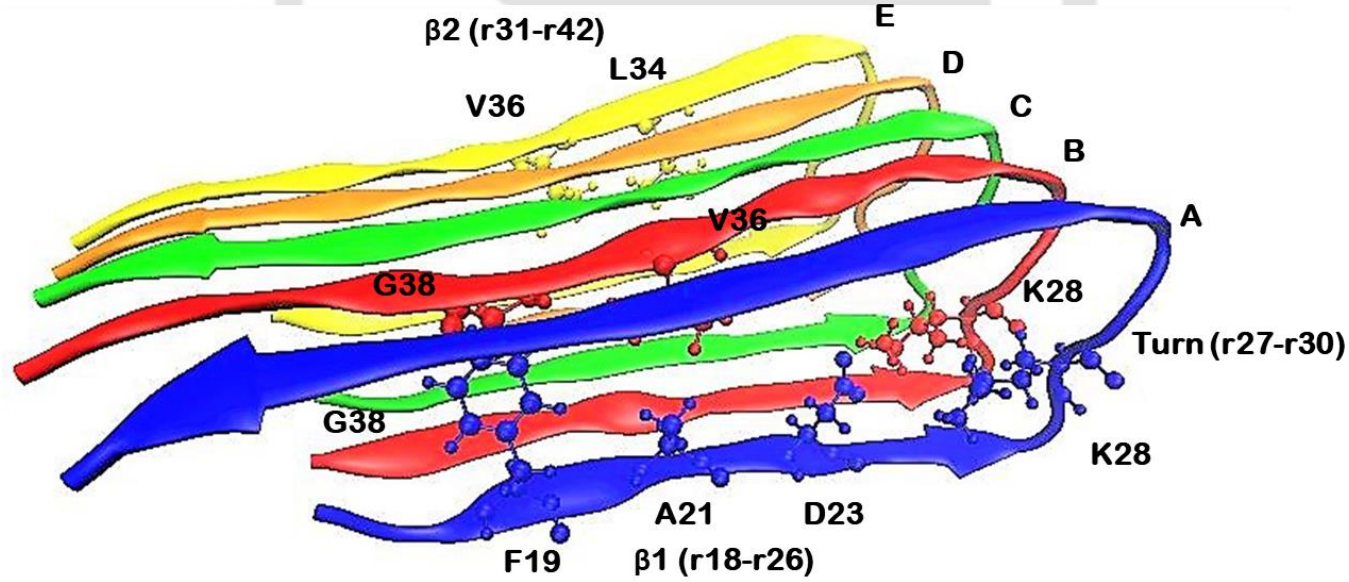

Fig. 3.1. Initial model of $A\beta_{17-42}$ (2BEG.pdb) constructed from solid state NMR.

There have been various interactions reported in pentamer that are within a single chain (intra-chain) and between two chains (inter-chain), which provides stability and strength to the structure.[1] The salt bridge interaction between D23 (Asp, Aspartic acid) and K28 (Lys, Lysine) residue is one of the crucial interactions that provide stability to the entire fibril. A similar electrostatic interaction between Cα of K28 residues for inter-chain pairs provides strength to the backbone of the fibril. The other key hydrophobic interactions include contact between different residues pairs viz. A21-V36, L34-V36 and F19-G38 for both intra and inter-chain pairs. The uses of 2BEG as the representative model for Aβ fibril have been a preferred choice by numerous studies owing to its well-established and a very stable structure, employed in numerous studies.[2–5]

(b) 2NAO.pdb (hexamer)

The Aβ fibril considered for the current study is the disease relevant, dimeric, LS shaped fibril that appears as a double horseshoe structure.[6] Each monomeric unit consists of three chains making it a hexameric fibril, wherein chains are arranged in two subunits as A, B, C, and D, E and F, as depicted by VMD representation in Fig.3.2. All the six chains are full residues length from 1 to 42, wherein residues 1-14 are reported to be partially ordered and in β-strand conformation. The 15-42 residues are relatively densely packed and forms the double horseshoe shape structure consisting of maximally buried residues with hydrophobic side chains. The fibrillar sequence is further divided into five β-sheet regions observed for all chains, wherein residues 2-6 represents β1 region, 15-18 (β2 region), 26-28 (β3 region), 30-32 (β4 region) and 39-42 marks β5 region. Each chain has characteristic cross β-sheet, the prerequisite for fibrillation and stable organization of amyloids.

In Fig. 3.2, all the six chains of the hexamer have been depicted from A, B and C in one unit and D, E and F in another unit. The N and C terminus has been mentioned. All five beta regions viz., β1to β5 has been illustrated in CPK representation in colour red, green, pink, cyan and purple colour for β1, β2, β3, β4 and β5, respectively. The same arrangement has been observed in all other five chains as well.

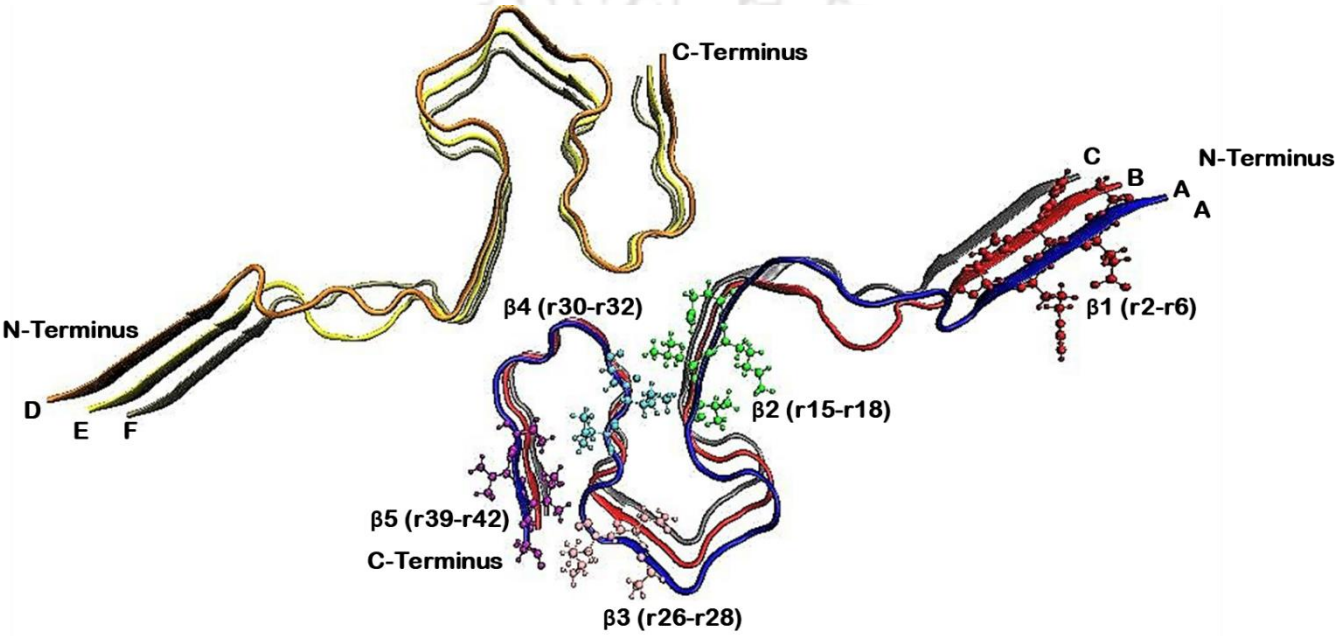

Fig. 3.2. Initial model of Aβ$_{42}$ (2NAO.pdb) constructed from solid state NMR.

3.1.2. Natural Compounds as Ligands

There have been an array of natural compounds that are considered as ligands for interaction with the Aβ fibril to check their destabilization potential. We have considered Caffeine (CFF) in Chapter 4 and four polyphenolic compounds viz., Caffeic acid (DHC), Epigallocatechin (EGT),

Gallic acid (GDE) and Ellagic acid (REF) in Chapter 5 as potential ligands. Similarly, in Chapter 6 we have screened destabilization potential of three major ω-3 PUFAs, which are Eicosapentaenoic acid (EPA), Docosahexaenoic acid (HXA) and alpha-linolenic acid (LNL). In Chapter 7, a terpene molecule called lycopene has been considered for its destabilization potential on Aβ fibril. After covering major classes of natural compounds, the after effect of ligand removal has been tested. For this purpose, the ligand Ellagic acid and caffeine has been removed from the destabilized structure and simulated for 1μs.

The retrieval and topology generation for individual ligand has been explained in the respective chapters.

3.2 Molecular Docking of Protein and the ligand

Molecular Docking studies were performed using AutoDock Suite 4.2.1 with the help of MGL tools 1.5.6.[7] This tool has been used in Chapter 5, wherein all the phenolic compounds have been docked in Aβ fibril and then MD simulation was conducted. The detailed approach for docking and related parameters have been well defined in section 5.2.1 of Chapter 5.

3.3 Molecular Dynamics Simulations

Simulations imitate the real system in the closest form and model them in mathematical equation for understanding and predictive purpose. The general idea behind MD is the capturing of all the possible configuration that a particle can pass through, if allowed to move in time infinitely. Hence, the selection of the time scale in MD is dependent on the size and complexity of the system under

consideration. The successive configurations of any system, in MD, is generated by integrating the Newton's second law of motion over a defined time step. The equation below gives the motion of the particle of mass m_i with coordinate x_i with F_{x_i}being the force exerted on the particle in that direction as described in Equation 3.1.

$$\frac{d^2x_i}{dt^2} = \frac{F_{x_i}}{m_i} \qquad \textbf{(3.1)}$$

The building blocks towards defining the equation for the calculations of energy and force is called the force field that defines the accuracy of the simulation further. It is a combination of bonded and non-bonded interactions terms. The bonded interaction terms (first four terms in Equation 3.2) such as bond distance r_0, bond angles θ_0, dihedral angles δ and improper angles Ψ_0 (to maintain the planarity of the ring) which describe a part of the total potential U_{total} due to interactions between bonded atoms. The non-bonded interaction includes van der Waals interactions, modeled by the Lennard–Jones potential, and electrostatic interactions, modeled by Coulomb's potential.

$$U_{total} = \sum_{bonds} k_{r\,(r-r_0)^2} + \sum_{angles} k_{\theta\,(\theta-\theta_0)^2} + \sum_{dihedrals} k_{\varphi\,(1+\cos[n\varphi-\gamma])} + \sum_{impropers} k_{\omega\,(\omega-\omega_0)^2} + \sum_{i<j}^{atoms} \in_{ij} \left[\left(\frac{r_m}{r_{ij}}\right)^{12} - 2\left(\frac{r_m}{r_{ij}}\right)^{6}\right] + \sum_{i<j}^{atoms} \frac{q_i q_j}{4\pi\epsilon_0 r_{ij}} \qquad \textbf{(3.2)}$$

In equation 3.2, potential energy terms in a force field are on right and energy function used to derive atomic forces for molecular movement is in left. Herein, r is the bond length; θ is the bond

angle; ϕ is the dihedral angle; ω is the improper dihedral angle; r_{ij} is the distance in between atom i and j; k_r, k_θ, k_φ, and k_ω are force constants; r_0, θ_0 and ω_0 are equilibrium positions; ϵ_{ij} is related to the Lennard–Jones well depth; r_m is the distance at which the potential reaches its minimum; q_i and q_j are the charges on the respective atoms; and ϵ_0 is the dielectric constant.

All these potential terms are calculated at every time step and updated as the simulation runs keeping periodic boundary conditions and minimum image convention maintained. The individual MD approach for different ligands has been explained in the respective chapters defining force field, parameterization of both protein and the ligand and other parameters necessary for simulation. In Chapter 4, section 4.2.2 highlights the simulation strategy for caffeine and Aβ fibril. Similarly, section 5.2.2 of Chapter 5 explains the MD simulation approach for phenolic compounds and Aβ fibril. The section 6.2.2 of Chapter 6 and section 7.2.2 of Chapter 7 gives simulation strategy for PUFAs and lycopene with Aβ fibril respectively. A general workflow of the MD simulation has been illustrated in Fig. 3.3.

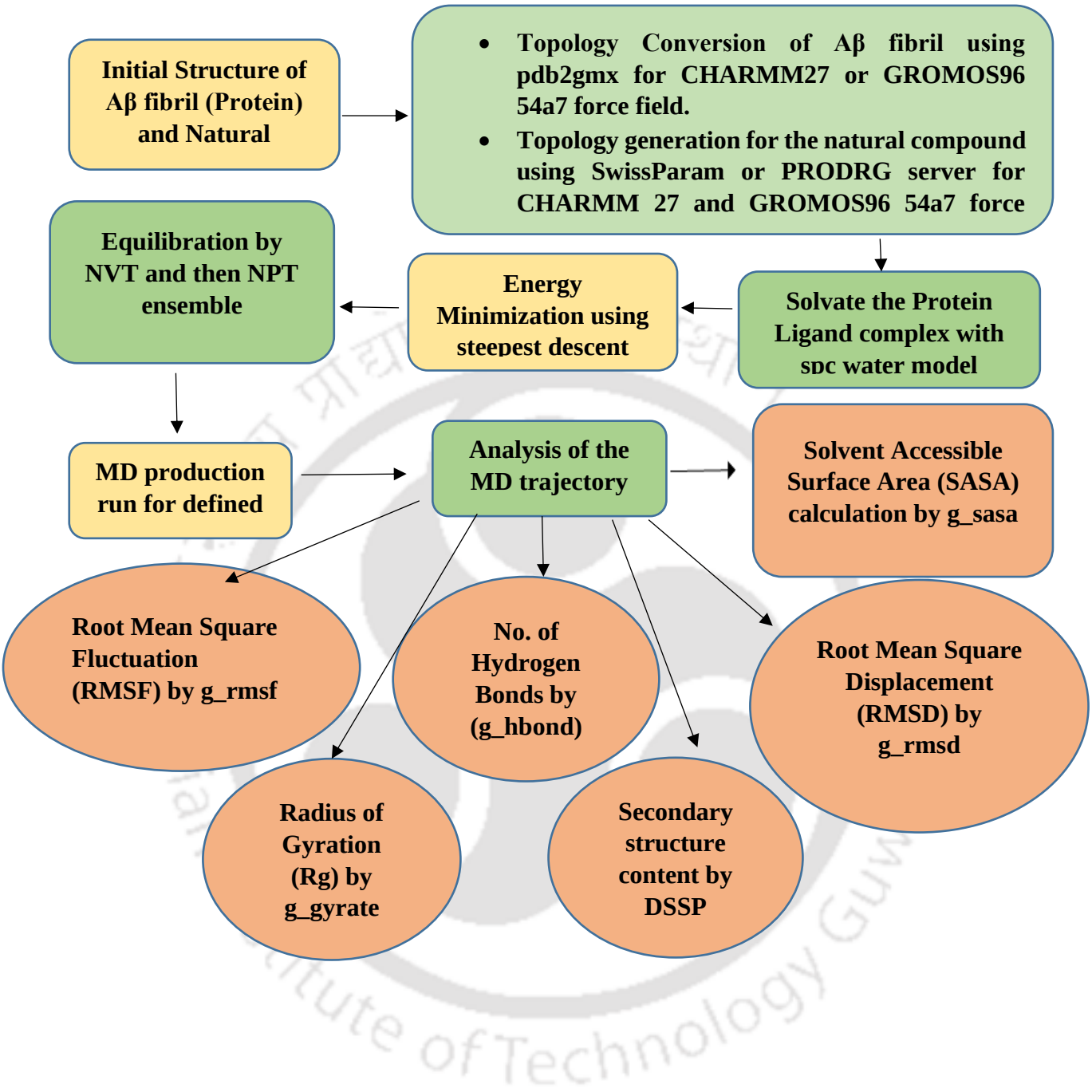

Fig. 3.3. General scheme for workflow of MD simulation

3.4 Analysis of the MD Trajectory

We have calculated various parameters using different tools defined within the GROMACS v5.1.1 package. All the parameters used in the entire thesis, has been mentioned in the analysis sections of the respective chapters. This includes 4.2.3, 5.2.3, 6.2.3, 7.2.3 and 8.2.3 in Chapter 4, 5, 6, 7 and 8, respectively. A special external tool called MM-PBSA has been set up with GROMACS to estimate the binding affinity between protein and the ligand. The basic definition and usage has been explained in section 5.2.4, section 6.2.4 and section 8.2.4 in Chapter 5, 6 and 8, respectively. The commands has been given in Appendix A for all the tools.

REFERENCES

1 T. Lührs, C. Ritter, M. Adrian, D. Riek-Loher, B. Bohrmann, H. Döbeli, D. Schubert and R. Riek, 3D structure of Alzheimer's amyloid-β(1–42) fibrils, *Proceedings of the National Academy of Sciences*, 2005, **102**, 17342–17347.

2 J. A. Lemkul and D. R. Bevan, Destabilizing Alzheimer's Aβ 42 Protofibrils with Morin: Mechanistic Insights from Molecular Dynamics Simulations, *Biochemistry*, 2010, **49**, 3935–3946.

3 S. Gupta and A. K. Dasmahapatra, Caffeine destabilizes preformed Aβ protofilaments: insights from all atom molecular dynamics simulations, *Physical Chemistry Chemical Physics*, 2019, **21**, 22067–22080.

4 A. Kumar, S. Srivastava, S. Tripathi, S. K. Singh, S. Srikrishna and A. Sharma, Molecular insight into amyloid oligomer destabilizing mechanism of flavonoid derivative 2-(4′ benzyloxyphenyl)-3-hydroxy-chromen-4-one through docking and molecular dynamics simulations, *Journal of Biomolecular Structure and Dynamics*, 2016, **34**, 1252–1263.

5 G. Kuang, N. A. Murugan, Y. Tu, A. Nordberg and H. Ågren, Investigation of the Binding Profiles of AZD2184 and Thioflavin T with Amyloid-β(1–42) Fibril by Molecular Docking and Molecular Dynamics Methods, *The Journal of Physical Chemistry B*, 2015, **119**, 11560–11567.

6 M. A. Wälti, F. Ravotti, H. Arai, C. G. Glabe, J. S. Wall, A. Böckmann, P. Güntert, B. H. Meier and R. Riek, Atomic-resolution structure of a disease-relevant Aβ(1–42) amyloid fibril, *Proceedings of the National Academy of Sciences*, 2016, **113**, E4976–E4984.

7 G. M. Morris, R. Huey, W. Lindstrom, M. F. Sanner, R. K. Belew, D. S. Goodsell and A. J. Olson, AutoDock4 and AutoDockTools4: Automated docking with selective receptor flexibility, *Journal of Computational Chemistry*, 2009, **30**, 2785–2791.

Chapter 4

Destabilization of Aβ Protofilament by Caffeine: Insights from all atom MD Simulations

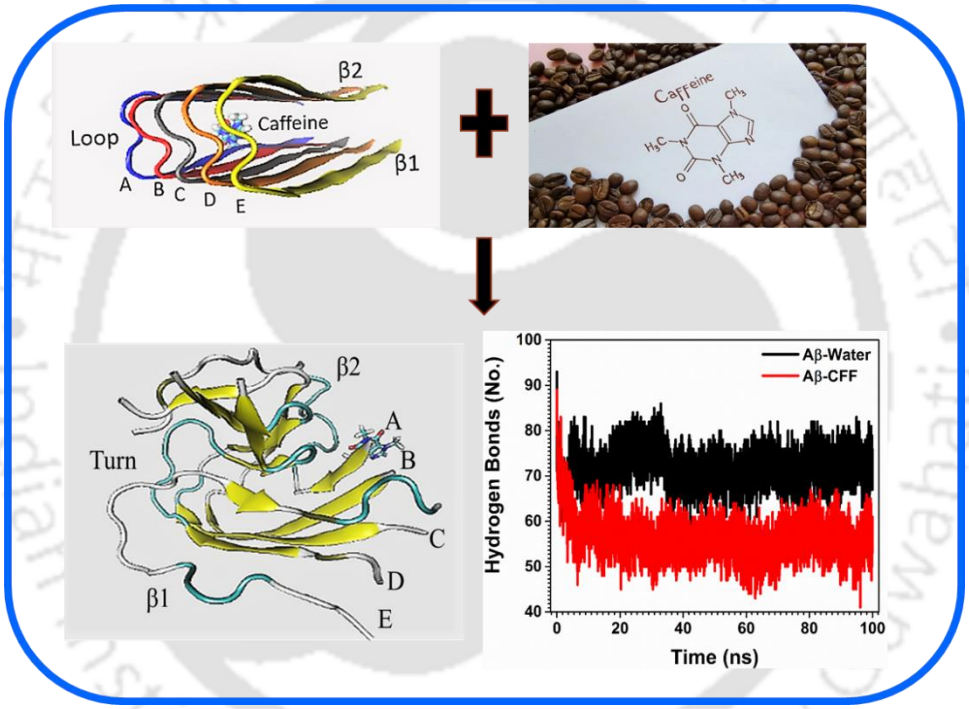

In this chapter, we presented the interaction between caffeine (CFF) molecule and Aβ fibril$_{17\text{-}42}$. The molecular dynamics simulations studies give insights about the destabilization potential of the caffeine on the fibril. The disrupted configuration of fibril thus obtained, not only reduce instances of neurotoxicity but also prevents further aggregation. We observed that reduction in β sheet content and breakage of H-bonds are the main drivers behind distorted structure of the fibril. These observations enable us to establish CFF as a potential dug lead to treat AD by destabilizing the Aβ fibril.

4.1 INTRODUCTION

Neurodegenerative disorders like Alzheimer's Disease (AD), Parkinson's Disease (PD) and Huntington's disease (HD) associate themselves with an array of misfolded proteins that aggregates abnormally[1–9] to form insoluble assemblages hindering normal functioning of brain.[10,11] AD is described as a chronic, progressive, geriatric and incurable neurodegenerative disorder having largest share of dementia across the global population.[12] Amyloid beta fibril is of greater clinical importance as it directs formation of NFTs as well, which worsens the case further as explained by amyloid cascade hypothesis.[13–16]

Therapeutic strategies for treating AD are broadly classified into two categories: inhibition of fibrillation of amyloid-beta monomers and destabilization of preformed amyloid beta fibrils. There has been a wide array of compounds prospected for their efficiency to inhibit fibrillation and destabilization of fibrils targeting Aβ monomer and Aβ fibrils respectively traversing atomic-scale mechanisms by means of Molecular Dynamics simulations.

The potential associated with the *in-silico* studies establishes ground for the interplay and essential linkage between *in-vitro* and *in-vivo* with *in-silico* studies.[17] A recent report involving inhibition and destabilization of Aβ monomer and Aβ protofibril by a hybrid of resveratrol and clioquinol explains the importance of computational studies in prospecting new drug candidates.[18] The inhibitory mechanism of Erythrosine B on Aβ peptides was studied employing molecular modeling.[19] Recently, EGCG (Epigallocatechin-3-gallate), Ibuprofen, fluorescent dyes (ThT and PIB, as identifiers) and modified β-sheet breakers are reported to have significant effect upon the Amyloid beta toxicity by inhibiting aggregation or by converting toxic aggregates into unstructured non-toxic aggregates as indicated from *in-silico* studies.[20] The destabilization of Aβ

protofibril by arginine-based short peptides found to be very much promising.[21] Fluorinated compounds have been shown to inhibit fibrillation of Aβ monomeric form as well as to destabilize preformed Aβ fibrils.[22]

The destabilization of Aβ fibrils upon interaction with FDA approved drugs[23,24] nanoparticles[25,26] and natural compounds[27–30] is considered to be a fruitful alternative line of treatment for AD. Importance of natural compounds in treating diseases has been studied and applied since ancient times owing to their inherent biocompatibility and general intoxicity to the biological system. Many compounds of biological origin have been tested *in-vitro* and *in-silico* for their neuroprotective ability. Active compounds in green tea (EGCG)[31,32] and bioactives such as melanoidins and 5-0-caffeoylquinic acid[33] present in raw green coffee as well as in roasted coffee, target pre-formed Aβ fibrils and disrupt them to form disordered monomers as evidenced by *in-vitro* and *in-silico* studies.[34–36]

The mediterranean diet consisting of fruits, vegetables, citrus, nuts and fish is rich in antioxidants, healthy fatty acids and a range of several minerals and vitamins, that are reported to delay the onset of AD and declines cognitive impairment.[37–40] Coffee consumption dates back to centuries ago and is the second most leading beverage consumed across the globe.[41] The health benefits of coffee entails anti-oxidant, anti-inflammatory, anti-carcinogenic, prevention of cardio vascular diseases and reduced risk of NDs.[42–44] Caffeine (1,3,7-trimethylxanthine), present majorly in coffee, is an alkaloid in chemical identity and a natural psychostimulant[45] having neuroprotective ability thereby a potential role in preventing AD as supported by numerous *in-vitro* and animal studies.[46,47] Caffeine was found to have reducing effect on plasma and brain Aβ levels when tested in Alzheimer's transgenic mice,[48] and the Aβ neurotoxicity is found to be reduced significantly in SHSY5Y cell lines in the presence of caffeine with a wide range of

concentration.[49] Caffeine relieves the overall oxidative stress by adopting different mechanisms that includes inhibiting formation of ROSs, improving mitochondrial function in neurotoxic situations, reducing inflammation in brain and by moderating apoptosis that prevents AD as is evidenced by studies on rat brain.[50–52] The crucial role of caffeine in inhibiting aggregation of Aβ peptides into neurotoxic fibrils by means of self-aggregation of caffeine molecules around hydrophobic residues of Aβ have been studied by MD studies.[53] The role of caffeine in destabilizing preformed Aβ fibrils needs a detailed investigation that triggers conduction of MD simulation studies to check the efficacy of caffeine as a potential and promising anti-amyloidogenic agent to prevent the onset of AD.

The underpinning mechanism of destabilizing Aβ fibrils, which is poorly understood till date, is a prerequisite to design drugs with higher efficacy in lieu to fetch approval in clinical trials. The atomistic details obtained by Molecular Dynamics (MD) simulation help in finding the mechanism involved by providing insights on key interactions involved in disruption of Aβ fibrils. In the current work, the caffeine molecule is allowed to interact with the Aβ protofibril, 2BEG, in explicit solvent (water) system with CHARMM22* force field. The MD simulation was conducted on GROMACS MD simulation package[54] and analyzed by an array of different tools. The substantial increase in RMSD and radius of gyration along with the loss of β-sheet content demarcate a loss in organized fibril structure. The disruption of H-bonds (hydrogen bonds) and breaking of hydrophobic contacts further weakens the fibril structure, ultimately leading to its destabilization. The results thus obtained, establishes caffeine as a potent disruptor of Aβ fibril thereby improved cognitive function and delayed onset of the disease and thus a promising cure for AD.

4.2 METHODS

4.2.1 System setup

The model system for human amyloid beta protofilament ($A\beta_{17-42}$) as obtained from solid State NMR has been retrieved from RSCB PDB (protein data bank) with the PDB ID-2BEG, a pentameric oligomer.[55] The protofibril structure consists of five chains, named as A, B, C, D and E, having strand-loop-strand motif as depicted in VMD representation of 2BEG in Fig. 4.1a. The entire length of the amyloid beta protofibril has been divided into two major regions - disordered N-terminal region spanning from residue 1 to 17 (truncated), and mature and stable β sheet region from 18 to 42.[55] The β sheet region has been further classified into three different regions: β1 (18 to 26 residues), turn (27 to 30 residues) and β2 (31 to 42 residues). The coordinate file for caffeine molecule was taken from CFF ligand summary page from RSCB PDB and is depicted in Fig. 4.1b as viewed by VMD package. Caffeine is being studied as a potential molecule to destabilize preformed amyloid beta fibrils; hence setting up of two simulation systems, one with caffeine (Aβ-CFF) and other without caffeine (Aβ-Water), has been done for a comparative analysis. The molecular dynamics (MD) simulation and calculation has been done over ($A\beta_{17-42}$) protofibril structure ranging from 17-42 residues.

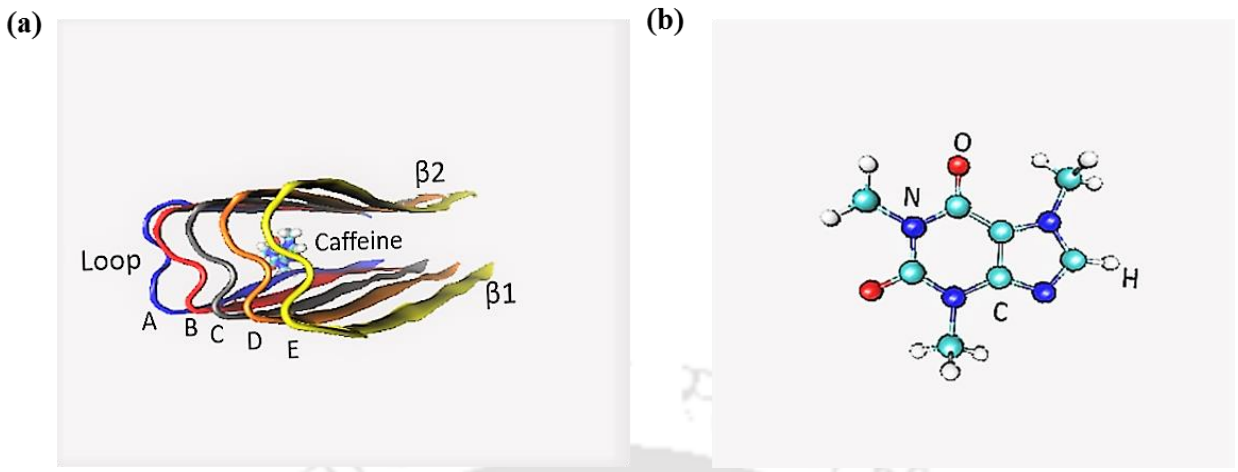

Fig. 4.1. (a) - Initial structure of 2BEG protofibril with Caffeine molecule and (b) - Structure of Caffeine molecule both viewed in VMD Package.

4.2.2 Simulation Method

All the atomistic MD simulations have been performed in isothermal isobaric ensemble (NPT) using GROMACS v5.1.1 with CHARMM22*[56,57] with CMAP corrections for proteins (Chemistry at HARvard Macromolecular Mechanics) force field.[58–60] Various simulations have already been performed to study the inherent stability of $A\beta_{17-42}$ protofibril[61] with different force fields, such as, OPLS-AA,[62] Amber 99SB-ILDN,[63] GROMOS 96 53a6,[64] Amber ff03[65] and CHARMM22* for proteins[56,66–69] with TIP3P water model to explicitly solvate the $A\beta_{17-42}$ protofibril. However, to the best of our knowledge, a combination of employing CHARMM22* force field with SPC water model for $A\beta_{42}$ was not executed, though well reported for other proteins[70,71], which in turn motivated us to select CHARMM force field along with SPC water model for simulating our system. The initial structure of caffeine taken from ZINC[72] database as mol2 script, was submitted to Swiss-Param[73] to generate topology file, CFF.itp, which is a prerequisite to make it readable by GROMACS package. There are numerous MD studies conducted wherein biological entities viz.

DNA, RNA, proteins including Aβ are made to interact with different small molecules. In all these studies the small molecules including natural compounds and nanoparticles are parameterized using SWISS-PARAM.[74–78] Hence, the parameterization of caffeine by SWISS-PARAM is validated and trusted. The details on the CFF.itp file has been given in Appendix 1at the end of the thesis. The 2BEG protofibril is simultaneously converted to .gro file from pdb structure by pdb2gmx tool, which act as initial feed for simulation. The topology for caffeine and protein have been combined into a single topology file, complex.gro, depicting the protein-ligand interaction. The caffeine molecule is allowed to place itself randomly around Aβ fibril in a manner similar to the one reported in various studies involving morin,[64] wgx-50,[65] norepinephrine[79] and dihyrochalcone[63] as ligands. Both the systems (viz., Aβ-Water and Aβ-CFF) were solvated in a $6.8 \times 6.8 \times 6.8$ nm^3 cubic box with water, represented by SPC water model.[80] Five sodium ions were added to the system to make it neutral. Following this, system was energy minimized using the steepest descent method. The energy minimized structure is then subjected to equilibration employing NVT and NPT ensemble. The equilibrated structure then finally simulated for 100 ns at temperature of 300 K and a pressure of 1 atm. The temperature and pressure coupling was done by velocity-rescaling method[81] and parinello-rahman method, respectively.[82] The LINCS algorithm[83] was applied to constrain the lengths of all bonds. The electrostatic interactions were calculated by PME (particle mesh Ewald method)[84] with a cutoff distance of 1.0 nm and the van der Waals interactions were treated using a cutoff of 1.0 nm as well. The periodic boundary conditions were applied in all the directions in all the systems. All the simulations were repeated thrice to check the reproducibility, and results have been averaged over three simulations. The commands for setting up the simulation has been given in Appendix A.

4.2.3 Analysis

Different tools executable by GROMACS 5.1.1 were employed to calculate various parameters to obtain simulation details. To make an assessment on structural stability of the pentamer, we have calculated RMSD (Root Mean Square Deviation), RMSF (Root Mean Square Fluctuation), radius of gyration (R_g), along with SASA (Solvent Accessible Surface Area), number of h, salt bridge and hydrophobic interactions. The Cα RMSD for Aβ-water and Aβ-CFF, for individual chains and for different regions has been calculated by g_rms tool. The tool, g_gyrate was used to calculate R_g of protein for both the systems i.e. in absence and presence of caffeine. Aβ-CFF system was further analyzed by calculating residue wise RMSF, and average SASA for all chains by g_rmsf and g_sas, respectively. The stability of the protofibril on addition of caffeine molecule was determined by enumerating number of H-bonds in protofibril with the help of g_hbond tool. The total number of H-bonds has been quantified by counting acceptor and donor group with a cut off distance of 0.35 nm. The numbers of interpeptide H-bonds have also been calculated between chain A and B, and chain D and E, for both the systems (viz., Aβ-CFF and Aβ-water) to assess the stability of terminal chains with respect to their neighboring ones. The modification in secondary structure has been determined by DSSP (Dictionary of secondary structure) content by using DSSP tool followed by generation of a color plot by g_xpm2ps tool.

Further, to scrutinize more about the destabilization of protofibril when caffeine is interacted, the distance between Cα-Cα K28 (Lysine at 28th position) has been measured by g_mindist for chain A and B, and D and E, for both the systems. The salt bridge disruption upon interaction with caffeine has been established by determining the distance between D23 (Aspartic acid at 23rd position) and K28 (Lysine at 28th position) for chain A and B for both the systems. The hydrophobic contacts are known to provide strength and stability contributed by A21 (Alanine on

21st position), F19 (Phenylalanine at 19th position) V36 (Valine on 36th Position) and G38 (Glycine at 38th position), where A21 interacts with V36, and F19 interacts with G38. The hydrophobic interactions have been gauged in terms of minimum distance between above mentioned residues of chain A and B, and chain B and C. The intrachain hydrophobic interaction for chain E was calculated by the distance between L34 (Leucine at 34th position) and V36 present in chain E. All the structures were visualized and represented with the help of VMD (Visual Molecular Dynamics) package.[85] The commands for all the tools have been given in Appendix A.

4.3 RESULTS AND DISCUSSIONS

The effect of caffeine on Aβ protofibril begins with VMD representation of simulated structure followed by RMSD, R_g and RMSF calculation. The higher beta sheet content, important for Aβ protofibril formation, is measured by DSSP. The destabilization effect of the caffeine molecule on Aβ fibril has been evaluated by calculating number of H-bonds, backbone stability, salt bridges and hydrophobic contacts for different chains in the following sections.

4.3.1 Validation of simulation data with experimental results

Before proceeding towards destabilization effect of caffeine on $A\beta_{17-42}$ protofibril, MD ensembles obtained after 100 ns simulation were monitored for convergence. We have calculated chemical shifts in backbone Cα and Cβ by using ShiftX2[86] package, which gives details about matching of MD ensembles produced by MD simulations with experimental data. For this, the NMR chemical shifts have been calculated using ShiftX2 program for 2BEG and Ensembles obtained after 100 ns

simulation of Aβ-CFF system. The correlation between two values is 0.99, establishing the validation of simulation data with the experimental one (see Fig. 4.2a and b) for Cα and Cβ, respectively sharing similarity with result observed in several studies reported in the literature.[18,87]

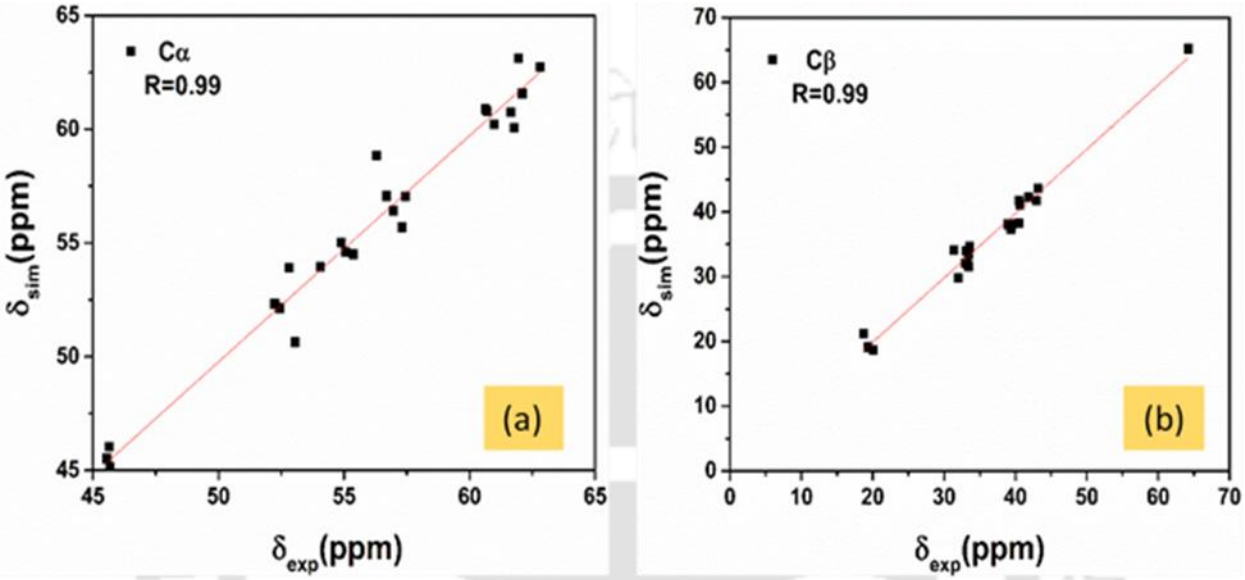

Fig. 4.2. Correlation between the theoretical and experimental NMR chemical shifts for Cα and Cβ atoms of Aβ42 protofibril structure is shown in panel a, and b, respectively. The unit of NMR chemical shift is ppm.

Three-bond J-coupling constants in Fig. 4.3 have also been calculated by Karplus equation using Vuister and bax equation[88,89] shows close agreement between experimental and simulated values for J coupling constant for Aβ42 protofibril.[90]

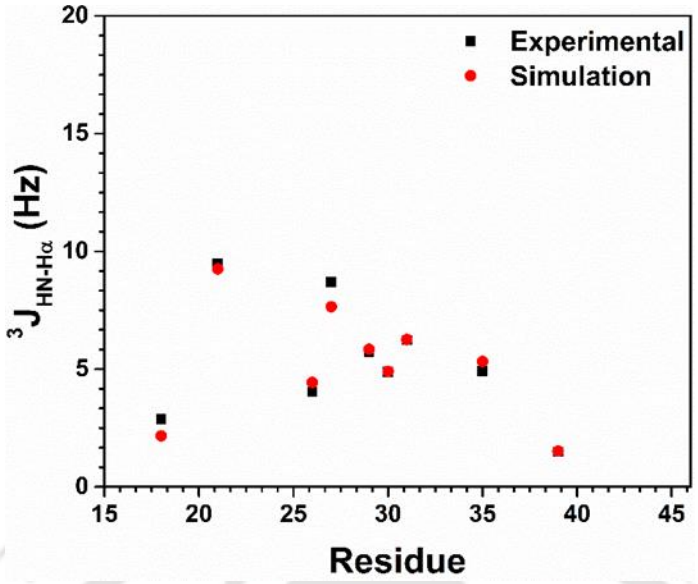

Fig. 4.3. Comparison of simulated 3JHN-Hα coupling constants of the Aβ42 residues (red) with experimental measurements.

4.3.2 Simulation of Aβ protofibril in water and caffeine

The visual inspection of the trajectory obtained by Aβ alone (with water i.e. Aβ-water system) simulated for 100 ns suggested that in the presence of water, the Aβ protofibril remains stable with little twisting at the edges of the peptide chains as shown in Fig. 4.4a. The β1 and β2 regions showed twisting such that β-strands were not entirely coplanar resulting in an increased level of side chain packing, which helps in stabilizing the amyloid fibril structure as mentioned in earlier reports.[91,92] The rationale behind dissolving the $A\beta_{17-42}$ system in water is to elucidate the significant role of water in the stabilization of $A\beta_{17-42}$ protofibril structure.[64]

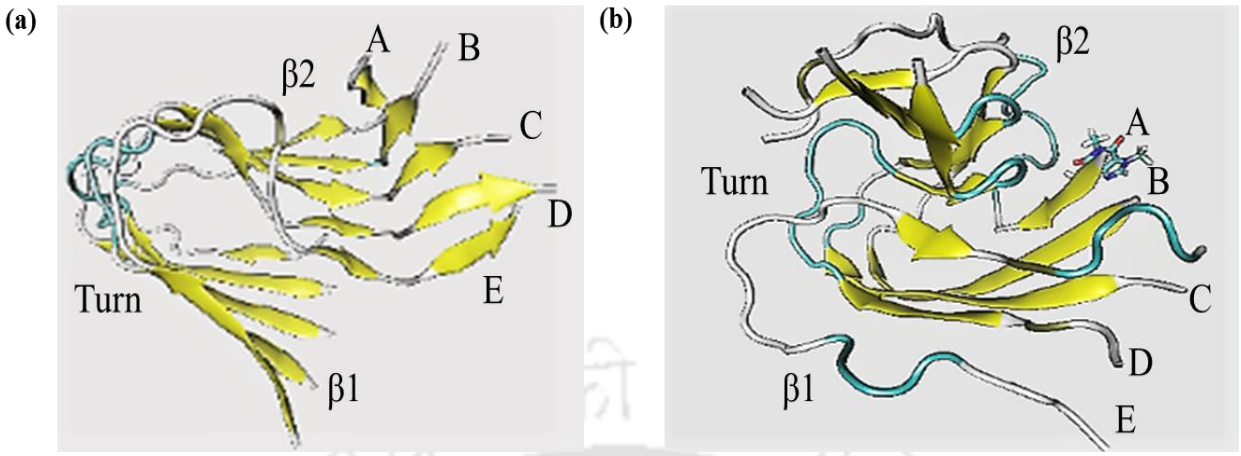

Fig. 4.4. (a) - Final Configuration of 2BEG in water, (b) - Final Configuration of 2BEG when 1 molecule of CFF is added for 100 ns.

The other reason is to have a control system (viz., without caffeine) for better investigation of the effect of caffeine on $A\beta_{17-42}$ protofibril. Hence, it was extremely important to run a simulation of 100 ns of $A\beta_{17-42}$ protofibril with CHARMM22* force field and SPC water model. Fig. 4.4b clearly depicts disordered arrangement of the fibril structure with the edge chains losing their β-sheet content, highlighted by yellow in other chains, parting from the intact structure pointing towards destabilization of the $A\beta_{17-42}$ protofibril structure in the presence of caffeine. The disruptive effect of caffeine has been further assessed by studying different parameters, which is explained in sections below.

4.3.3 Destabilization in the turn and β2 regions

The global structural stability of $A\beta_{17-42}$ protofibril has been assessed by calculating Cα-RMSD over trajectory of 100 ns. The Cα-RMSD for both the systems (viz., Aβ-Water and Aβ-CFF) has been computed, and marked by black and red color, respectively in Fig. 4.5a. The Cα-RMSD of protein for Aβ-water averages to 0.7 nm, which increased to 0.96 nm in case of Aβ-CFF system, indicating a destabilization effect of caffeine on $A\beta_{17-42}$ protofibril. A comparison on Cα-RMSD between protein (Pro) only and protein ligand (Pro-Lig) as combination in Aβ-CFF system (Fig. 4.5b) reveals that the Pro-Lig system shows a higher value (1.48 nm) compared to the Pro system (0.96 nm). The enhanced value of Cα-RMSD of Pro-Lig system construes the contribution of caffeine interaction in decreasing structural stability of the preformed protofibril.

To elucidate further about the most affected region of protofibril, Cα-RMSD of β1, turn and β2 region, as defined in section 2, has been calculated and shown in Fig. 4.5c. The trend in Fig. 4.5c clearly shows that the effect of caffeine is more pronounced in β2 and turn region as compared to β1 region. It has been reported earlier that the instability of β2 region inhibits fibril elongation, which obstructs the aggregation process,[93] highlighting the crucial role of β2 region in fibrillogenesis. The edge chains (viz., chain A and E) in the pentamer structure, displayed relatively higher level of disruption compared to the rest of the chains, as concluded by higher value of Cα-RMSD of 1.33 nm and 0.99 nm for chain A and E, respectively (see Fig. 4.5d).

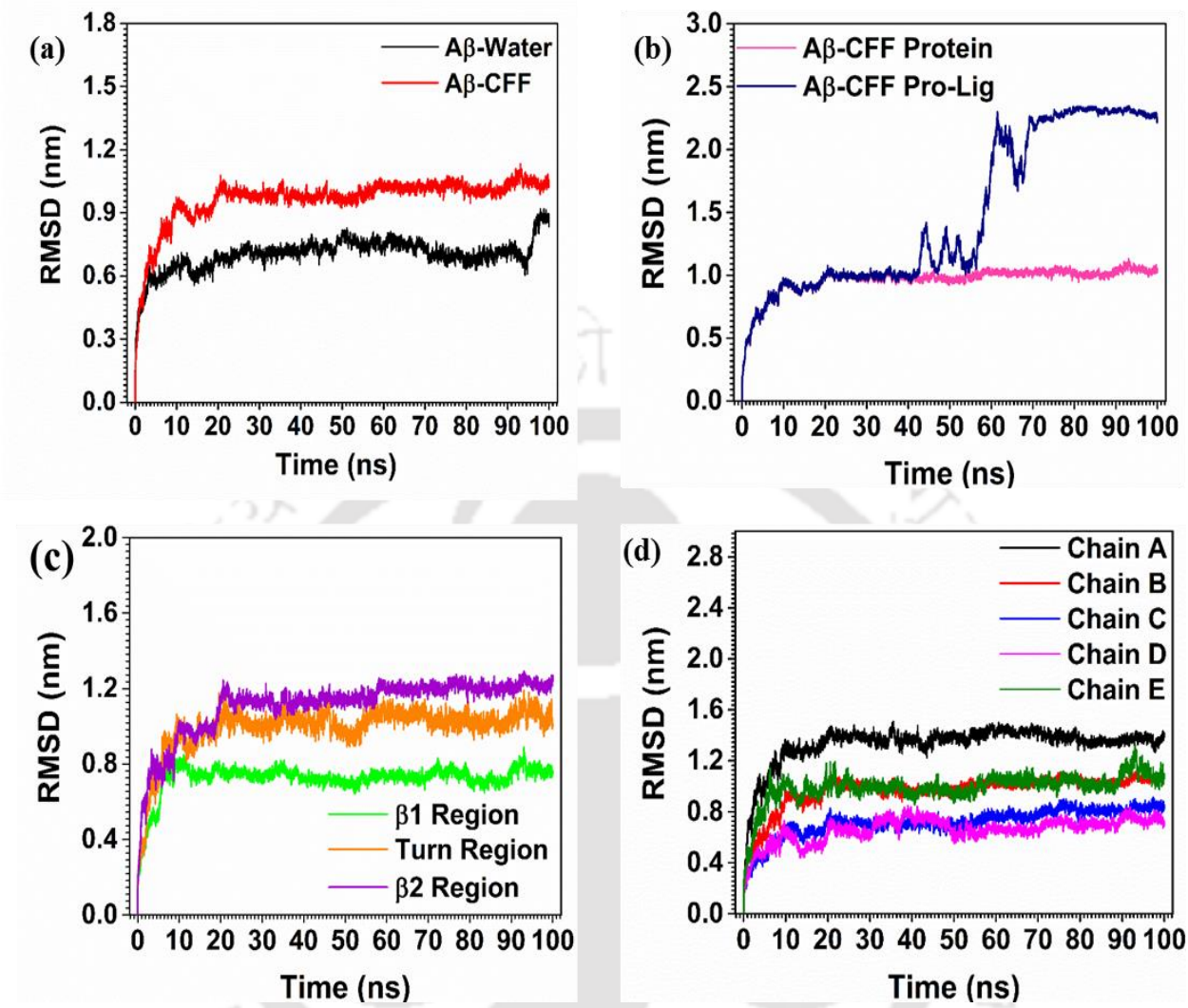

Fig. 4.5. Cα RMSD as function of time (a) - Aβ –Water and Aβ-CFF, (b) - Aβ-CFF Protein and Pro-Lig System, (c) - Aβ-CFF β1 Region, Turn and β2 Region, (d) - Aβ-CFF for all chains.

Conclusively, the disruptive effect of caffeine on $A\beta_{17-42}$ protofibril can clearly be interpreted by the higher Cα-RMSD values for different selections like entire protein, individual chains of the pentamer and different regions like β1 region, turn and β2 region over a trajectory of 100 ns.

4.3.4 Structural Stability of $A\beta_{17-42}$ protofibril

Radius of gyration (R_g) is a measure of compactness of any protein structure. Fig. 4.6 presents the R_g values average over three sets of simulation (100 ns each) with a good reproducibility along with statistical significance.

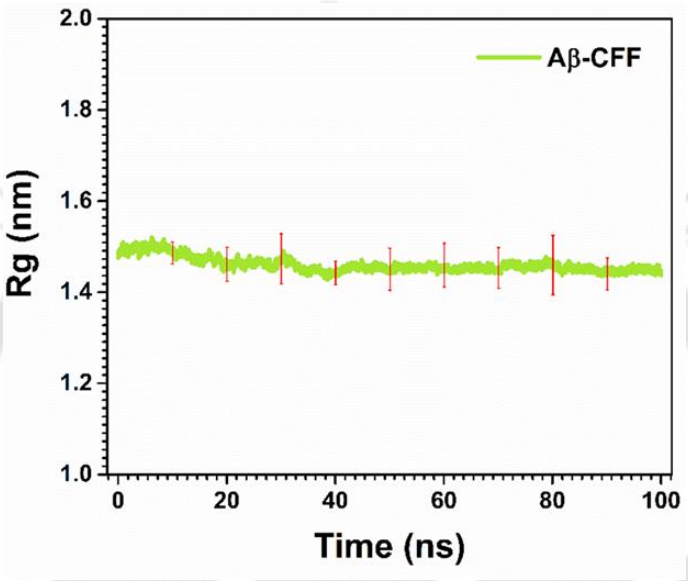

Fig. 4.6. Statistical significance of all three simulation runs by mean and standard deviation across R_g for all three sets in Aβ-CFF for 100 ns.

In Fig. 4.7a, R_g of protein for Aβ-Water and Aβ-CFF systems after 100 ns simulation was found to be 14.3 Å and 14.96 Å, respectively, suggesting the role of caffeine in disarranging pentameric structure. A larger fluctuation in R_g implies a higher perturbation, which increases mobility of five chains of $A\beta_{17-42}$ protein. The conformity by simulation outcome of study employing $A\beta_{17-42}$ protofibril and D744, fluorinated compound, showed similar increase in R_g in Aβ protofibril-D744 complex than protofibril alone.[87] The increase in R_g clearly indicate the potency of caffeine in destabilizing Aβ fibril contributing towards curing AD.

The SASA is an important property to determine protein conformation in water, and gives a fair idea on the area that is exposed to solvent, accounting interactions with hydrophobic and hydrophilic residues.[94] The SASA for side chain atoms for $A\beta_{17-42}$ protofibril in Fig. 4.7b illustrated higher value of turn region for chain A, while β1 and β2 region for chain E in the presence of caffeine molecule. The average value of SASA for Chain A, B, C, D and E is 0.82, 0.41, 0.36, 0.50 and 0.87 nm^2, respectively. The greater SASA values for terminal chains reflect upon loss of hydrophobicity and an increase in hydrophilicity, which leads to an elevated loosening of these chains from the pentamer structure. The findings are in corroboration with the belief that helix conformation of a protein correlates with its hydrophilicity.[95] The results thus obtained, are in correspondence with the simulation study conducted on Aβ monomer and a β- sheet breaker (LPFFD), wherein they found decrement of hydrophobicity of the C-terminal residues of monomer on binding of LPFFD inhibiting further aggregation.[96] Similar trends were observed from simulation study wherein caffeine molecules were checked for their potential to inhibit aggregation of switch peptides.[53] The fluctuations in SASA also indicate towards binding induced conformational changes in the protein that facilitate better protein ligand interaction as reported by computational studies on different monomers.[97] The role of caffeine in increasing solvent accessible area and introducing conformational changes adds to its capability for better interaction with Aβ protofibril hence introduce more flexibility in edge chains, necessary for destabilization.

The RMSF value per residue for each chain of Aβ-CFF system for 100 ns has been shown in Fig. 4.7c, which depicted larger fluctuations in the β2 region of the pentamer. Interestingly, this trend is found to be in close agreement with Cα-RMSD trend of these regions (see Fig. 4.5c). The consonance of this finding have been provided by destabilization studies by means of MD simulation conducted on Aβ protofibril with morin, wherein maximum fluctuations were recorded

for turn and β_2 regions.[64] The relatable spiked RMSF values have been reported in simulation study wherein, wgx-50 was found to destabilize Aβ protofibril by introducing higher flexibilities in terminal chains assisting interaction of wgx-50 with β2 region of the terminal chains of the pentamer.[65] Caffeine being able to interact with Aβ protofibril, destabilizes it by introducing higher flexibility in the terminal chains which establishes it as a potential fibril breaker to barricading progression of AD.

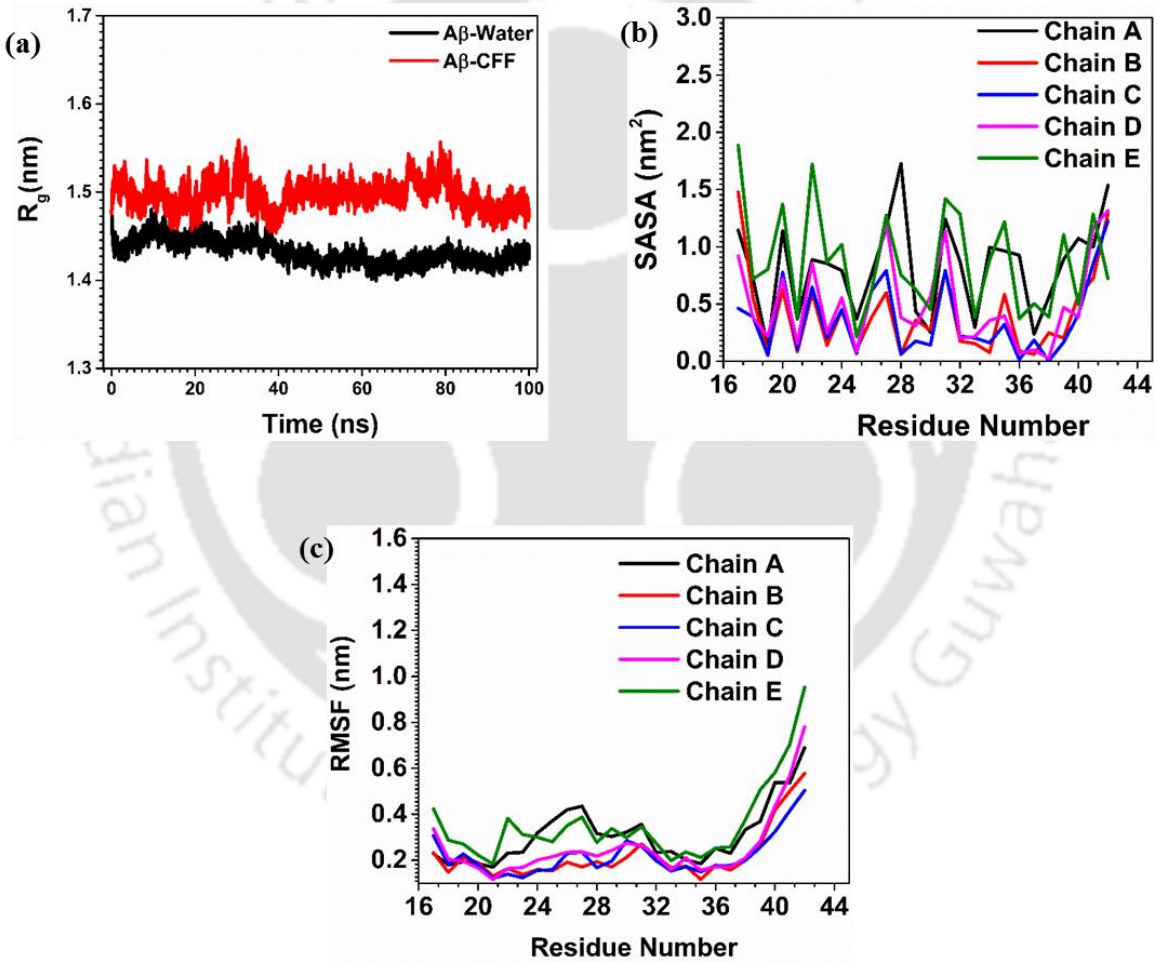

Fig. 4.7. (a) - Rg of Protein for Aβ –Water and Aβ-CFF, (b) - SASA of all chains residue wise of Aβ-CFF (c) - RMSF of all chains of Aβ-CFF at 100 ns.

4.3.5 Beta sheet content

The secondary structure analysis gives insights on the ability of a protein to acquire a defined secondary order conformation associated with their stability and longevity. The secondary structure has been analyzed by DSSP (Dictionary for Secondary Structure for Protein) method.[98] The evolution of secondary structure with time for Aβ-water and Aβ-CFF systems have illustrated appearance of α-helix and 3_{10}- helix in the terminal chains in Aβ-CFF system as shown in Fig. 4.8a and 8b, respectively. Decrease in the β-sheet content with concomitant increase in coil, bend and turn structure accelerated the disorganization of Aβ protofibril in the presence of caffeine. The graphical representation of secondary structures as depicted in Fig. 4.8c shows a higher β-sheet content present inherently in $A\beta_{17-42}$ protein[99] in water. In contrast, Fig. 4.8d clearly pointed out an increase of coil, α-helix and 3_{10}- helix, in exchange of β-sheet content upon interaction with caffeine molecule for a trajectory of 100 ns. The results thus obtained are found in consonance with the MD simulation studies wherein a fluorinated compound, D744, is allowed to interact with $A\beta_{17-42}$ protofibril, resulting in a notable decrease in β-sheet content with increasing coil and bend conformations.[87]

The similar trends have been espied after MD simulation conducted on Aβ protofibril with norepinephrine to check for its destabilization effect on the protofibril.[79] The experimental observations based on congo red birefringence and decrease in intensity of ThT fluorescence, validates the inhibitory effect of caffeine on fibrillation of functional mimic of Aβ peptide to Aβ protofibril.[53] The β-sheet content, a prerequisite for fibrillogenesis, is investigated to check for the destabilization effect of the caffeine molecule and the resulted decrease in the same establishes caffeine as a potential anti-amyloidogenic drug lead.

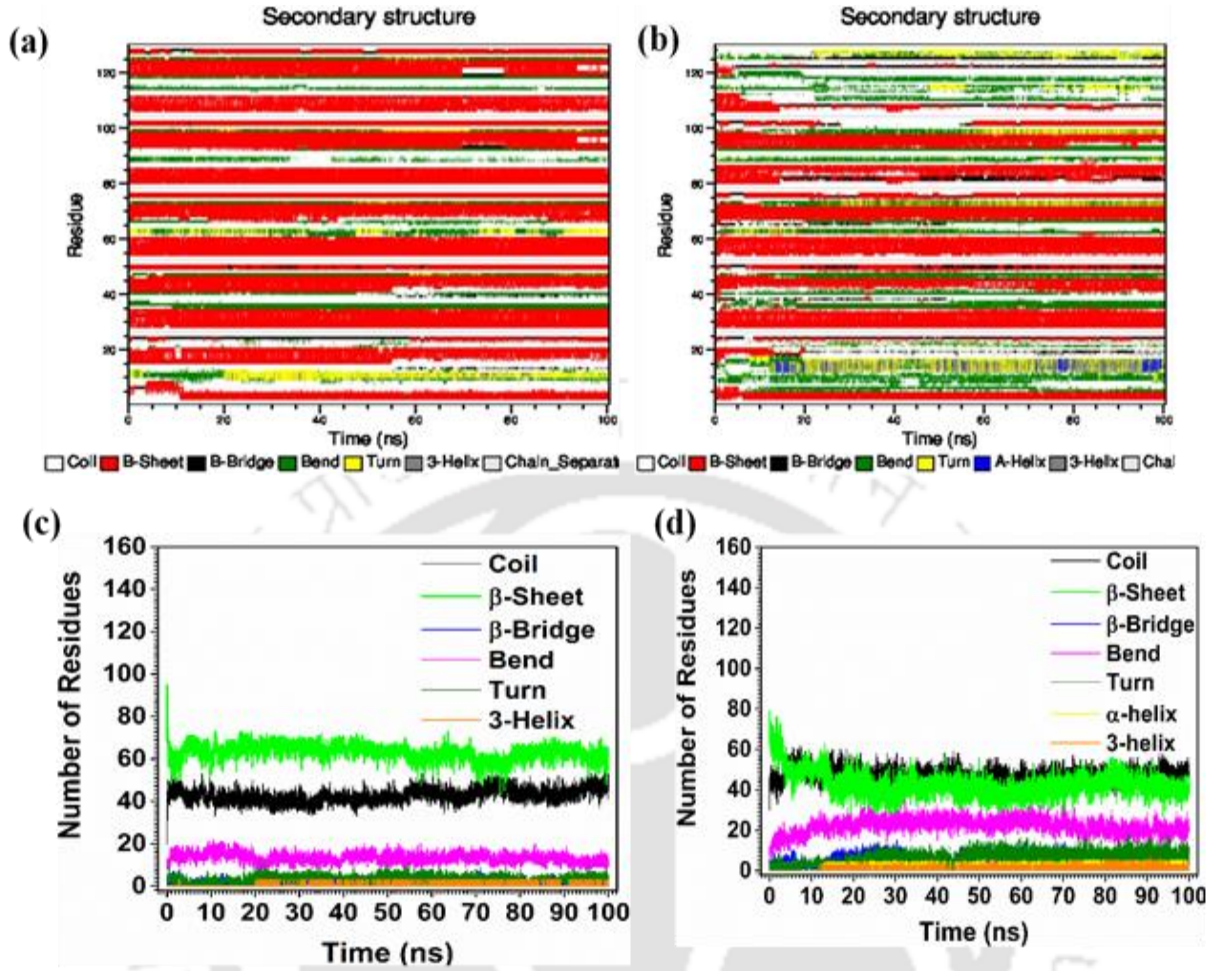

Fig. 4.8. DSSP and Secondary structure (a) - Aβ-water, (b) - Aβ-CFF system, (c) - Secondary structure for Aβ-water, (d) - Secondary structure for Aβ-CFF at 100 ns.

4.3.6 Number of H-bonds

The H-bonds are believed to play a major role in the formation of secondary structures and other higher order aggregates by contributing immensely towards structural integrity. The stability of Aβ fibrils observed by both theoretical[92] and experimental[100] investigations is described by the virtue of extensive network of H-bonding (intra and inter peptide).We calculated the average number of H-bonds including both intra- and inter-peptide H-bonds. We observed that the number

of H-bonds has been reduced from 71.960 (Aβ-water) to 56.565 (Aβ-CFF) suggesting disruption of H-bonds in the presence of caffeine (see Fig. 4.9a). Additionally, the number of H-bonds between chain A and B have been calculated over 100 ns trajectory, where a reduction from 14.793 in Aβ-water to 8.362 in Aβ-CFF (see Fig. 4.9b) was recorded. The number of backbone H-bonds between chain D and E has also been reduced significantly from 18.750 for Aβ-water to 7.282 for Aβ-CFF (see Fig. 4.9c). This significant decrement in H-bonds clearly indicate destabilization of Aβ protofibril structure attributed to loss of H-bonds in the presence of caffeine.

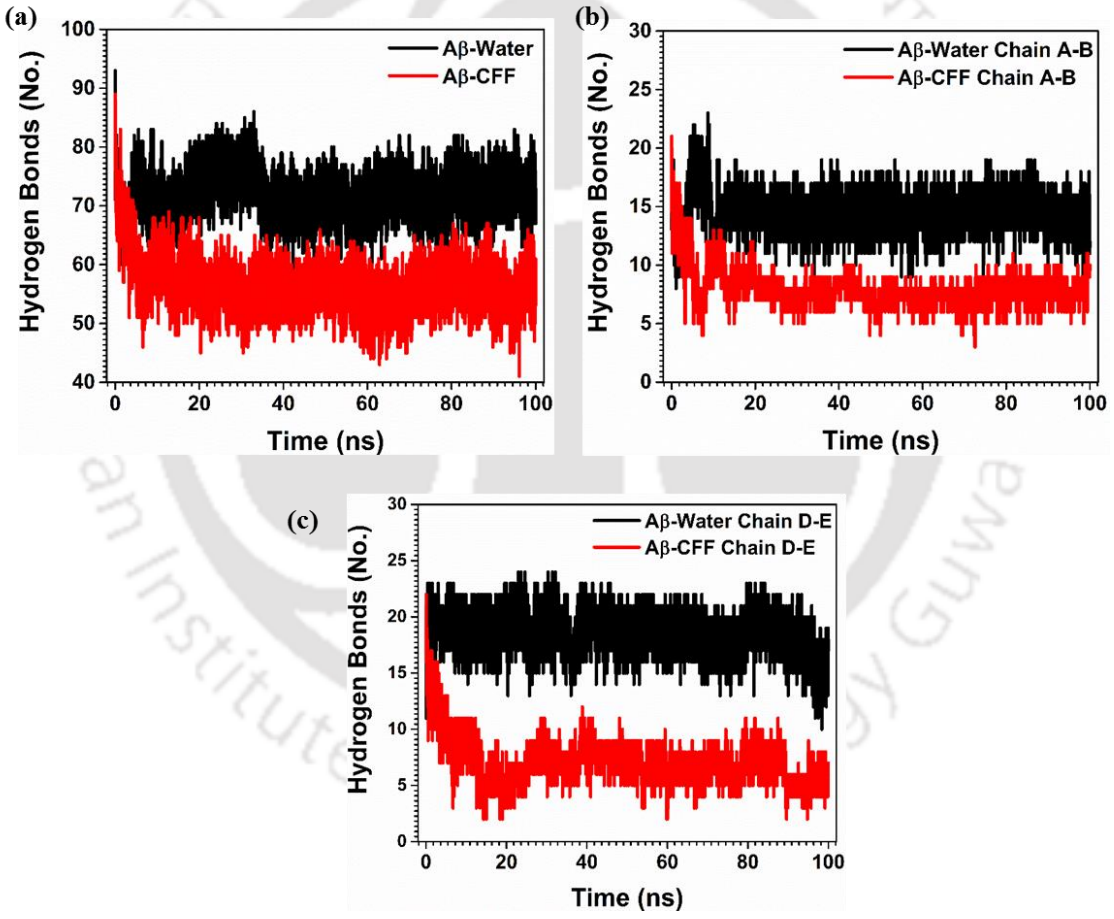

Fig. 4.9. (a) – No. of overall H-Bonds of Aβ-Water and Aβ-CFF system, (b) - Intra H-bonding between Chain A and Chain B for Aβ-water and Aβ-CFF system, (c) - Intra H-bonding between Chain D and Chain E for Aβ-water and Aβ-CFF system.

The findings are in parity with other MD simulation study on Aβ protofibril wherein, the protofibril was made to interact with morin, a natural compound found in fruits and berries resulted in loss of interchain H-bonds in edge chains.[64] The observation was well supported by similar decrease in interchain H-bonds when wgx-50, compound from Sichuan pepper, was allowed to insert into Aβ protofibril.[65]

To elucidate further, the number of H-bonds have been calculated for individual regions of Aβ protofibril structure for both the systems (see Table 4.1). It is observed from Table 4.1 that the number of H-bonds has been reduced significantly in β1, turn and β2 region, affecting β2 region in the most severe way. These results clearly highlighted the destabilization effect of caffeine on β2 region, which is known to play a crucial role in fibril growth and elongation.[101]

Table 4.1. H-Bonds of Aβ-water and Aβ-CFF systems for β1, turn and β2 region

Region	Aβ-Water	Aβ-CFF
β1	21.174 ± 0.46	16.954 ± 0.40
Turn	6.674 ±0.29	3.104 ± 0.25
β2	31.967 ± 0.16	21.075 ± 0.09

Disrupting H-bonds across β1 region led to relatively slow growth of fibrils, where the stability is at a stake.[61] Evidently, caffeine disrupts H-bonds causing destabilization of Aβ protofibril,

attributed to the intrinsic property of caffeine to form H-bonds with the protein system, due to presence of three hydrogen-accepting sites.[102]

4.3.7 Backbone and Salt Bridge stability

The inter-chain K28 Cα-Cα distance was estimated for neighboring chains and found to be 1.584 nm for chain A and B, and 1.161 nm for chain D and E, respectively (see Fig. 4.10a). These observed values were much higher in contrast to 0.57 nm in A and B, and 0.56 nm in D and E without caffeine molecule, which marked their disruption, thereby declining stability of the peptide chains. These results are in congruity with the simulation study conducted on Aβ protofibril with dihydrochalcone as the ligand.[63]

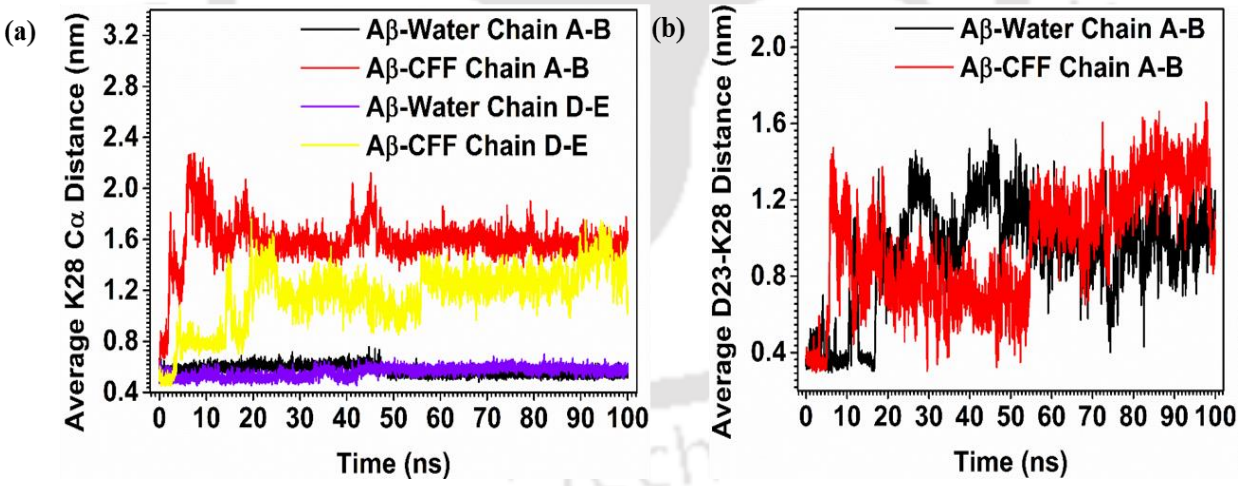

Fig. 4.10. (a) – Inter-chain K28 Cα- Cα distance between Chain A-B for Aβ-water and Aβ-CFF system, (b) - Average D23-K28 distance between Chain A-B for Aβ-water and Aβ-CFF system.

Salt bridge, an electrostatic interaction (intra-peptide and inter-peptide), involving D23 and K28 residues, reported to be a major contributor towards stability of fibril structure and governs fibrillation rate of full length $A\beta_{17-42}$.[55,103–106] The substantial increase in the interchain distance between D23 of chain A and K28 of chain B is marked, (see Fig. 4.10b), resulted in interruption with salt bridge formation. However, a slight increase can also be observed in control (Aβ-Water) system, but the value for the Aβ-CFF system goes beyond 0.52 nm that impedes with salt bridge formation.

This increase in the D23-K28 distance highlights the disruption of chain A from the pentamer. The relatable results on disruptive effect of molybdenum sulphide nanoparticles on terminal chains by breaking salt-bridges of Aβ protofibril are in conformance with our finding.[107] Overall, caffeine by interfering with K28 Cα-Cα bonding and salt bridges, expresses itself as potential natural compound to destabilize preformed Aβ protofibril thereby keeping a check on progression of AD.

4.3.8 Hydrophobic Contacts

The hydrophobic contacts for various residues viz. A21 and V36, L34 and V36 and F19 and G38 for all individual chains and neighboring chains have been calculated. The increased interchain distance between A21 and V36 for chain A and B, and chain B and C in Aβ-CFF system, as shown in Fig. 4.11a and 4.11b respectively. This increased distance implies loss of hydrophobic contacts between these chains. Moreover, the intrachain distance between L34 and V36 residues for chain E as shown in Fig. 4.11c, found to be increased in Aβ-CFF system, indicating the loosening of terminal chain E. Other hydrophobic interactions involving F19 and G38, was also analyzed for

interchain distance between chain A and B (see Fig. 4.11d), which was recorded higher in the presence of caffeine.

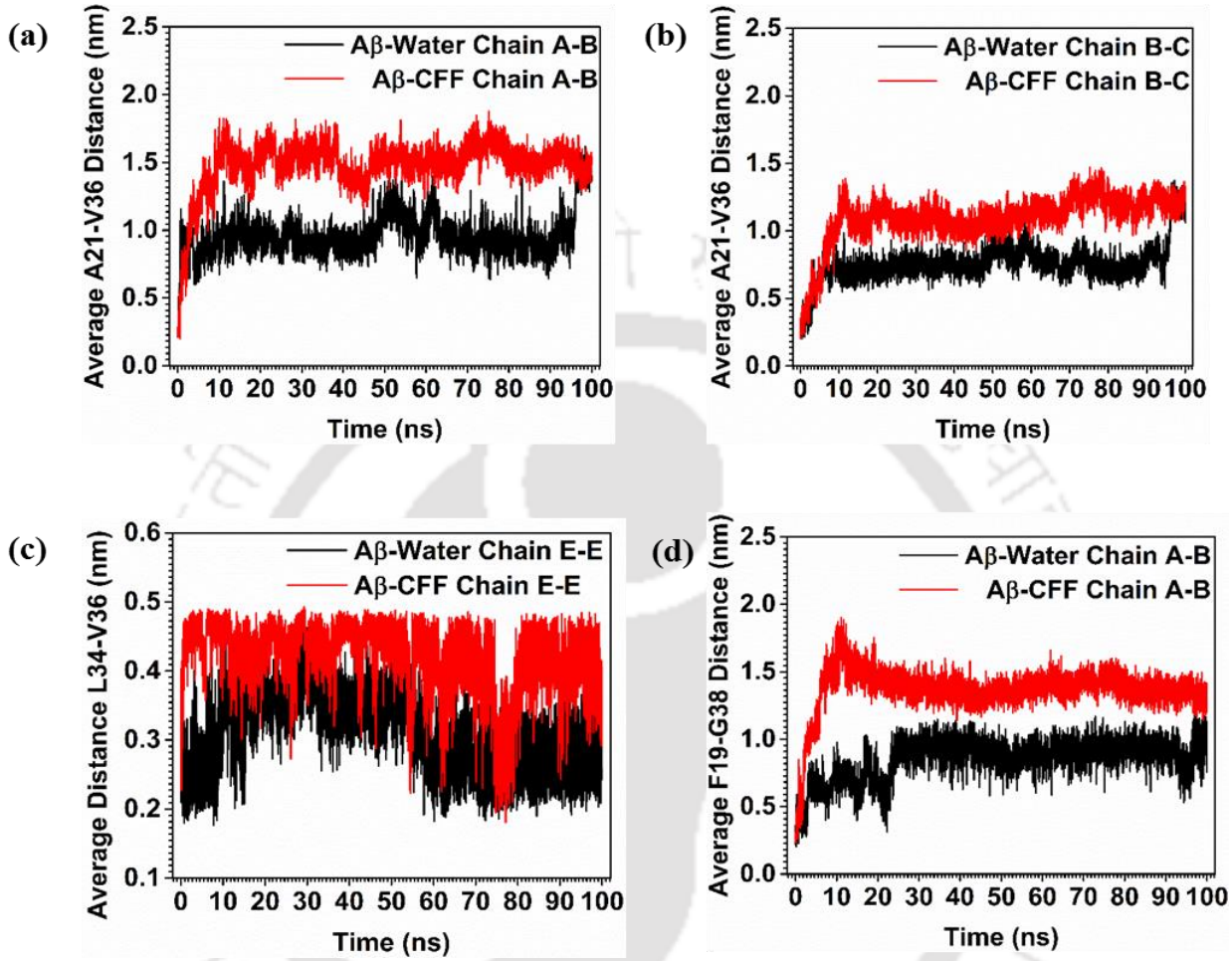

Fig. 4.11. (a) - Interchain A21-V36 distance between Chain A-B for Aβ-water and Aβ-CFF system (b)- Interchain A21-V36 distance between Chain B-C for Aβ-water and Aβ-CFF system (c)- Intrachain L34-V36 distance between Chain E for Aβ-water and Aβ-CFF system (d)- Interchain F19-G38 distance between Chain A-B for Aβ-water and Aβ-CFF system.

The noteworthy increase in the distance between residues A21-V36, and F19-G38 in Aβ-CFF system for chain A-B, B-C, and L34-V36 intra-chain distance for chain E gave insights on

weakening of these bonds in the presence of caffeine. The hydrophobic stability of $A\beta_{17-42}$ pentameric structure gets highly compromised reinforcing binding of caffeine molecule to hydrophobic β2 region of the protofibril. These results have been found in parity with simulation studies conducted on Aβ protofibril involving morin[64] and β- sheet breakers.[22] Similar findings were also recorded in case of chemically synthesized drugs having anti-cholinesterase activity tested *in-vitro* as well as by simulation, leading to disruption of preformed Aβ fibrils.[108]

According to PASA (Principle of Amyloid Self-Assembly),[104] the structures that have maximum intra- and inter-peptide hydrophobic interactions and salt bridges have higher tendency towards fibrillation. Hydrophobic core comprising the β2 portion of the aggregate has been proclaimed to be the crucial stabilizing element in Aβ aggregation process.[61] The results obtained clearly indicate that an increase in inter-residual distance leading to breakage of hydrophobic contacts destabilizes Aβ protofibril in the presence of caffeine.

4.4 CONCLUSIONS

In this **chapter,** the MD simulation details of interaction of caffeine with Aβ protofibril have been presented in order to expound molecular details about destabilization effect of caffeine molecule on Aβ protofibril. The VMD representation of simulated structure showed perturbations and deflection of terminal chains from the rest of the protofibril. The structural instability caused due to insertion of caffeine was verified by RMSD analysis where higher deviation was observed for β2 region of edge chains without much effect observed for other chains in the pentamer. The magnitude of radius of gyration and RMSF also recorded higher fluctuations in the presence of caffeine. The secondary structure conformation showed transition from β-sheet to turn

configuration along with formation of both α-helix and 3_{10} helix in the terminal chain when simulated for 100 ns. The destabilization of Aβ protofibril is attributed to the disruption of H-bonds over entire pentamer, largely between chain A and B, and chain D and E causing chain A and E to loosen up from Aβ pentamer. The interchain K28 Cα-Cα distance between chain A and B, and chain D and E enlarged, resulted in disruption of these crucial interactions. The D23-K28 salt bridge, known to provide stability, was disrupted with a substantial increase in average interchain distance between them. The interchain hydrophobic contacts between A21-V36 for chain A and B, and chain B and C was disturbed as distance increased between neighboring chains, in presence of caffeine. The results obtained from MD simulation provides mechanistic details about role of caffeine in destabilizing Aβ fibril that establishes caffeine as a potent anti-amyloidogenic drug. This finding also opens up new arenas for further investigation of natural compounds for their potential applicability to control neurotoxicity, and thus proposes a preventive therapeutic strategy towards preventing Alzheimer's disease.

REFERENCES

1 C. Swart, W. Haylett, C. Kinnear, G. Johnson, S. Bardien and B. Loos, Neurodegenerative disorders: Dysregulation of a carefully maintained balance?, *Experimental Gerontology*, 2014, **58**, 279–291.

2 M. S. Forman, J. Q. Trojanowski and V. M.-Y. Lee, Neurodegenerative diseases: a decade of discoveries paves the way for therapeutic breakthroughs, *Nature Medicine*, 2004, **10**, 1055–1063.

3 E. Laskowska, D. Kuczyńska-Wiśnik and B. Lipińska, Proteomic analysis of protein homeostasis and aggregation, *Journal of Proteomics*, 2019, **198**, 98–112.

4 P. Salahuddin, M. K. Siddiqi, S. Khan, A. S. Abdelhameed and R. H. Khan, Mechanisms of protein misfolding: Novel therapeutic approaches to protein-misfolding diseases, *Journal of Molecular Structure*, 2016, **1123**, 311–326.

5 T. N. Shamsi, T. Athar, R. Parveen and S. Fatima, A review on protein misfolding, aggregation and strategies to prevent related ailments, *International Journal of Biological Macromolecules*, 2017, **105**, 993–1000.

6 D. M. Skovronsky, V. M.-Y. Lee and J. Q. Trojanowski, NEURODEGENERATIVE DISEASES: New Concepts of Pathogenesis and Their Therapeutic Implications, *Annual Review of Pathology: Mechanisms of Disease*, 2006, **1**, 151–170.

7 F. E. Cohen and J. W. Kelly, Therapeutic approaches to protein misfolding diseases, *Nature*, 2003, **426**, 905–909.

8 C. M. Dobson, Protein folding and misfolding., *Nature*, 2003, **426**, 884–90.

9 P. A. Temussi, L. Masino and A. Pastore, From Alzheimer to Huntington: why is a structural understanding so difficult?, *EMBO Journal*, 2003, **22**, 355–361.

10 F. Chiti and C. M. Dobson, Protein Misfolding, Functional Amyloid, and Human Disease, *Annual Review of Biochemistry*, 2006, **75**, 333–366.

11 D. Eisenberg and M. Jucker, The Amyloid State of Proteins in Human Diseases, *Cell*, 2012,

148, 1188–1203.

12 G. R. Grøntvedt, T. N. Schröder, S. B. Sando, L. White, G. Bråthen and C. F. Doeller, Alzheimer's disease, *Current Biology*, 2018, **28**, R645–R649.

13 G. Evin and A. Weidemann, Biogenesis and metabolism of Alzheimer's disease Aβ amyloid peptides, *Peptides*, 2002, **23**, 1285–1297.

14 R. Kayed, Common Structure of Soluble Amyloid Oligomers Implies Common Mechanism of Pathogenesis, *Science*, 2003, **300**, 486–489.

15 J. Hardy and D. J. Selkoe, The Amyloid Hypothesis of Alzheimer's Disease: Progress and Problems on the Road to Therapeutics, *Science*, 2002, **297**, 353 LP – 356.

16 M. A. Findeis, The role of amyloid β peptide 42 in Alzheimer's disease, *Pharmacology & Therapeutics*, 2007, **116**, 266–286.

17 J. Nasica-Labouze, P. H. Nguyen, F. Sterpone, O. Berthoumieu, N. V. Buchete, S. Coté, A. De Simone, A. J. Doig, P. Faller, A. Garcia, A. Laio, M. S. Li, S. Melchionna, N. Mousseau, Y. Mu, A. Paravastu, S. Pasquali, D. J. Rosenman, B. Strodel, B. Tarus, J. H. Viles, T. Zhang, C. Wang and P. Derreumaux, Amyloid β Protein and Alzheimer's Disease: When Computer Simulations Complement Experimental Studies, *Chemical Reviews*, 2015, **115**, 3518–3563.

18 R. K. Saini, S. Shuaib, D. Goyal and B. Goyal, Insights into the inhibitory mechanism of a resveratrol and clioquinol hybrid against Aβ42 aggregation and protofibril destabilization: A molecular dynamics simulation study, *Journal of Biomolecular Structure and Dynamics*, 2019, **37**, 3183–3197.

19 J. Lee, I. Kwon, S. S. Jang and A. E. Cho, Investigation of the effect of erythrosine B on amyloid beta peptide using molecular modeling, *Journal of Molecular Modeling*, 2016, **22**, 92.

20 H.-M. Fan, Q. Xu and D.-Q. Wei, in *Translational Bioinformatics and Its Application*, eds. D.-Q. Wei, Y. Ma, W. C. S. Cho, Q. Xu and F. Zhou, Springer Netherlands, Dordrecht, 2017, pp. 135–151.

21 S. S. Barale, R. S. Parulekar, P. M. Fandilolu, M. J. Dhanavade and K. D. Sonawane, Molecular Insights into Destabilization of Alzheimer's Aβ Protofibril by Arginine Containing Short Peptides: A Molecular Modeling Approach, *ACS Omega*, 2019, **4**, 892–903.

22 S. Shuaib, R. K. Saini, D. Goyal and B. Goyal, Insights into the Inhibitory Mechanism of Dicyanovinyl-Substituted J147 Derivative against Aβ 42 Aggregation and Protofibril Destabilization: A Molecular Dynamics Simulation Study, *ChemistrySelect*, 2017, **2**, 1645–1657.

23 D. Goyal, A. Kaur and B. Goyal, Benzofuran and Indole: Promising Scaffolds for Drug Development in Alzheimer's Disease, *ChemMedChem*, 2018, **13**, 1275–1299.

24 E. Mezeiova, K. Chalupova, E. Nepovimova, L. Gorecki, L. Prchal, D. Malinak, K. Kuca, O. Soukup and J. Korabecny, Donepezil Derivatives Targeting Amyloid-β cascade in Alzheimer`s Disease, *Current Alzheimer Research*, 2019, **16**, 1–27.

25 N. Guzior, A. Wieckowska, D. Panek and B. Malawska, Recent development of multifunctional agents as potential drug candidates for the treatment of Alzheimer's disease., *Current medicinal chemistry*, 2015, **22**, 373–404.

26 S. Sudhakar and E. Mani, Rapid Dissolution of Amyloid β Fibrils by Silver Nanoplates, *Langmuir*, 2019, **35**, 6962–6970.

27 X. Han and G. He, Toward a Rational Design to Regulate β-Amyloid Fibrillation for Alzheimer's Disease Treatment, *ACS Chemical Neuroscience*, 2018, **9**, 198–210.

28 C. Wu, J. Scott and J. E. Shea, Binding of congo red to amyloid protofibrils of the alzheimer Aβ 9-40 peptide probed by molecular dynamics simulations, *Biophysical Journal*, 2012, **103**, 550–557.

29 P. Alam, S. K. Chaturvedi, M. K. Siddiqi, R. K. Rajpoot, M. R. Ajmal, M. Zaman and R. H. Khan, Vitamin k3 inhibits protein aggregation: Implication in the treatment of amyloid diseases, *Scientific Reports*, 2016, **6**, 1–11.

30 J. C. Saunders, L. M. Young, R. A. Mahood, M. P. Jackson, C. H. Revill, R. J. Foster, D. A. Smith, A. E. Ashcroft, D. J. Brockwell and S. E. Radford, An in vivo platform for

identifying inhibitors of protein aggregation, *Nature Chemical Biology*, 2016, **12**, 94–101.

31 J. Bieschke, J. Russ, R. P. Friedrich, D. E. Ehrnhoefer, H. Wobst, K. Neugebauer and E. E. Wanker, EGCG remodels mature α-synuclein and amyloid-β fibrils and reduces cellular toxicity, *Proceedings of the National Academy of Sciences*, 2010, **107**, 7710–7715.

32 D. E. Ehrnhoefer, J. Bieschke, A. Boeddrich, M. Herbst, L. Masino, R. Lurz, S. Engemann, A. Pastore and E. E. Wanker, EGCG redirects amyloidogenic polypeptides into unstructured, off-pathway oligomers, *Nature Structural &Amp; Molecular Biology*, 2008, **15**, 558.

33 C. Ciaramelli, A. Palmioli, A. De Luigi, L. Colombo, G. Sala, C. Riva, C. P. Zoia, M. Salmona and C. Airoldi, NMR-driven identification of anti-amyloidogenic compounds in green and roasted coffee extracts, *Food Chemistry*, 2018, **252**, 171–180.

34 C. Rivière, J.-C. Delaunay, F. Immel, C. Cullin and J.-P. Monti, The Polyphenol Piceid Destabilizes Preformed Amyloid Fibrils and Oligomers In Vitro: Hypothesis on Possible Molecular Mechanisms, *Neurochemical Research*, 2009, **34**, 1120–1128.

35 K. Ono, Y. Yoshiike, A. Takashima, K. Hasegawa, H. Naiki and M. Yamada, Potent anti-amyloidogenic and fibril-destabilizing effects of polyphenols in vitro: implications for the prevention and therapeutics of Alzheimer's disease, *Journal of Neurochemistry*, 2003, **87**, 172–181.

36 K. Ono, T. Hamaguchi, H. Naiki and M. Yamada, Anti-amyloidogenic effects of antioxidants: Implications for the prevention and therapeutics of Alzheimer's disease, *Biochimica et Biophysica Acta - Molecular Basis of Disease*, 2006, **1762**, 575–586.

37 K. Augustin, A. Khabbush, S. Williams, S. Eaton, M. Orford, J. H. Cross, S. J. R. Heales, M. C. Walker and R. S. B. Williams, Mechanisms of action for the medium-chain triglyceride ketogenic diet in neurological and metabolic disorders, *The Lancet Neurology*, 2018, **17**, 84–93.

38 F. Panza, M. Lozupone, V. Solfrizzi, C. Custodero, V. Valiani, A. D'Introno, E. Stella, R. Stallone, M. Piccininni, A. Bellomo, D. Seripa, A. Daniele, A. Greco and G. Logroscino, in *Role of the Mediterranean Diet in the Brain and Neurodegenerative Diseases*, eds. T.

Farooqui and A. A. B. T.-R. of the M. D. in the B. and N. D. Farooqui, Academic Press, 2018, pp. 139–155.

39 D. Vauzour, M. Camprubi-Robles, S. Miquel-Kergoat, C. Andres-Lacueva, D. Bánáti, P. Barberger-Gateau, G. L. Bowman, L. Caberlotto, R. Clarke, E. Hogervorst, A. J. Kiliaan, U. Lucca, C. Manach, A. M. Minihane, E. S. Mitchell, R. Perneczky, H. Perry, A. M. Roussel, J. Schuermans, J. Sijben, J. P. E. Spencer, S. Thuret, O. van de Rest, M. Vandewoude, K. Wesnes, R. J. Williams, R. S. B. Williams and M. Ramirez, Nutrition for the ageing brain: Towards evidence for an optimal diet, *Ageing Research Reviews*, 2017, **35**, 222–240.

40 M. C. Morris, The role of nutrition in Alzheimer's disease: epidemiological evidence, *European journal of neurology*, 2009, **16 Suppl 1**, 1–7.

41 A. A. Nuhu, Bioactive Micronutrients in Coffee: Recent Analytical Approaches for Characterization and Quantification, *ISRN Nutrition*, 2014, **2014**, 1–13.

42 M. S. Butt and M. T. Sultan, Coffee and its consumption: Benefits and risks, *Critical Reviews in Food Science and Nutrition*, 2011, **51**, 363–373.

43 A. Palmioli, C. Ciaramelli, R. Tisi, M. Spinelli, G. De Sanctis, E. Sacco and C. Airoldi, Natural Compounds in Cancer Prevention: Effects of Coffee Extracts and Their Main Polyphenolic Component, 5-O-Caffeoylquinic Acid, on Oncogenic Ras Proteins, *Chemistry - An Asian Journal*, 2017, **12**, 2457–2466.

44 A. Cano-Marquina, J. J. Tarín and A. Cano, The impact of coffee on health, *Maturitas*, 2013, **75**, 7–21.

45 M. A. Heckman, J. Weil and E. G. de Mejia, Caffeine (1, 3, 7-trimethylxanthine) in foods: A comprehensive review on consumption, functionality, safety, and regulatory matters, *Journal of Food Science*, 2010, **75**, 77–87.

46 G. W. Arendash, W. Schleif, K. Rezai-Zadeh, E. K. Jackson, L. C. Zacharia, J. R. Cracchiolo, D. Shippy and J. Tan, Caffeine protects Alzheimer's mice against cognitive impairment and reduces brain β-amyloid production, *Neuroscience*, 2006, **142**, 941–952.

47 S. Haller, M. L. Montandon, C. Rodriguez, F. R. Herrmann and P. Giannakopoulos, Impact

of coffee, wine, and chocolate consumption on cognitive outcome and MRI parameters in old age, *Nutrients*, 2018, **10**, 1–13.

48 C. Cao, J. R. Cirrito, X. Lin, L. Wang, D. K. Verges, A. Dickson, M. Mamcarz, C. Zhang, T. Mori, G. W. Arendash, D. M. Holtzman and H. Potter, Caffeine Suppresses Amyloid-β Levels in Plasma and Brain of Alzheimer's Disease Transgenic Mice, *Journal of Alzheimer's Disease*, 2009, **17**, 681–697.

49 M. Keshavarz, M. R. Farrokhi and A. Amiri, Caffeine neuroprotective mechanism against β-amyloid neurotoxicity in SHSY5Y cell line: Involvement of adenosine, ryanodine, and Nmethyl- D-aspartate receptors, *Advanced Pharmaceutical Bulletin*, 2017, **7**, 579–584.

50 C. Carelli-Alinovi, S. Ficarra, A. M. Russo, E. Giunta, D. Barreca, A. Galtieri, F. Misiti and E. Tellone, Involvement of acetylcholinesterase and protein kinase C in the protective effect of caffeine against β-amyloid-induced alterations in red blood cells, *Biochimie*, 2016, **121**, 52–59.

51 F. Ullah, T. Ali, N. Ullah and M. O. Kim, Caffeine prevents d-galactose-induced cognitive deficits, oxidative stress, neuroinflammation and neurodegeneration in the adult rat brain, *Neurochemistry International*, 2015, **90**, 114–124.

52 T. P. A. Devasagayam, J. P. Kamat, H. Mohan and P. C. Kesavan, Caffeine as an antioxidant: inhibition of lipid peroxidation induced by reactive oxygen species, *Biochimica et Biophysica Acta (BBA) - Biomembranes*, 1996, **1282**, 63–70.

53 B. Sharma, S. Kalita, A. Paul, B. Mandal and S. Paul, The role of caffeine as an inhibitor in the aggregation of amyloid forming peptides: a unified molecular dynamics simulation and experimental study, *RSC Advances*, 2016, **6**, 78548–78558.

54 D. Van Der Spoel, E. Lindahl, B. Hess, G. Groenhof, A. E. Mark and H. J. C. Berendsen, *Journal of Computational Chemistry*, 2005, 26, 1701–1718.

55 T. Lührs, C. Ritter, M. Adrian, D. Riek-Loher, B. Bohrmann, H. Döbeli, D. Schubert and R. Riek, 3D structure of Alzheimer's amyloid-β(1–42) fibrils, *Proceedings of the National Academy of Sciences*, 2005, **102**, 17342–17347.

56 S. Piana, K. Lindorff-Larsen and D. E. Shaw, How robust are protein folding simulations

with respect to force field parameterization?, *Biophysical Journal*, 2011, **100**, L47–L49.

57 M. Carballo-Pacheco and B. Strodel, Comparison of force fields for Alzheimer's A β42: A case study for intrinsically disordered proteins, *Protein Science*, 2017, **26**, 174–185.

58 A. D. MacKerell, D. Bashford, M. Bellott, R. L. Dunbrack, J. D. Evanseck, M. J. Field, S. Fischer, J. Gao, H. Guo, S. Ha, D. Joseph-McCarthy, L. Kuchnir, K. Kuczera, F. T. K. Lau, C. Mattos, S. Michnick, T. Ngo, D. T. Nguyen, B. Prodhom, W. E. Reiher, B. Roux, M. Schlenkrich, J. C. Smith, R. Stote, J. Straub, M. Watanabe, J. Wiórkiewicz-Kuczera, D. Yin and M. Karplus, All-atom empirical potential for molecular modeling and dynamics studies of proteins, *Journal of Physical Chemistry B*, 1998, **102**, 3586–3616.

59 K. Vanommeslaeghe, E. Hatcher, C. Acharya, S. Kundu, S. Zhong, J. Shim, E. Darian, O. Guvench, P. Lopes, I. Vorobyov and A. D. Mackerell, CHARMM general force field: A force field for drug-like molecules compatible with the CHARMM all-atom additive biological force fields, *Journal of Computational Chemistry*, 2009, **8**, 671–690.

60 T. Ackermann, C. L. Brooks III, M. Karplus, B. M. Pettitt. Proteins: A Theoretical Perspective of Dynamics, Structure and Thermodynamics, Volume LXXI, in: Advances in Chemical Physics, John Wiley & Sons, New York 1988. 259 Seiten, Preis: US $ 65.25, *Berichte der Bunsengesellschaft für physikalische Chemie*, 1990, **94**, 96.

61 M. F. Masman, U. L. M. Eisel, I. G. Csizmadia, B. Penke, R. D. Enriz, S. J. Marrink and P. G. M. Luiten, In Silico Study of Full-Length Amyloid β 1−42 Tri- and Penta-Oligomers in Solution, *The Journal of Physical Chemistry B*, 2009, **113**, 11710–11719.

62 G. A. Kaminski, R. A. Friesner, J. Tirado-Rives and W. L. Jorgensen, Evaluation and reparametrization of the OPLS-AA force field for proteins via comparison with accurate quantum chemical calculations on peptides, *Journal of Physical Chemistry B*, 2001, **105**, 6474–6487.

63 Y. Jin, Y. Sun, J. Lei and G. Wei, Dihydrochalcone molecules destabilize Alzheimer's amyloid-β protofibrils through binding to the protofibril cavity, *Physical Chemistry Chemical Physics*, 2018, **20**, 17208–17217.

64 J. A. Lemkul and D. R. Bevan, Destabilizing Alzheimer's Aβ 42 Protofibrils with Morin:

Mechanistic Insights from Molecular Dynamics Simulations, *Biochemistry*, 2010, **49**, 3935–3946.

65 H.-M. Fan, R.-X. Gu, Y.-J. Wang, Y.-L. Pi, Y.-H. Zhang, Q. Xu and D.-Q. Wei, Destabilization of Alzheimer's Aβ42 Protofibrils with a Novel Drug Candidate wgx-50 by Molecular Dynamics Simulations, *The Journal of Physical Chemistry B*, 2015, **119**, 11196–11202.

66 N. V. Buchete, R. Tycko and G. Hummer, Molecular dynamics simulations of Alzheimer's β-amyloid protofilaments, *Journal of Molecular Biology*, 2005, **353**, 804–821.

67 J. Wiley, The Encyclopedia of Computational Chemistry Graph Theory in Chemistry, 1998, 1169–1190.

68 E. Lindahl, P. Bjelkmar, P. Larsson, M. A. Cuendet and B. Hess, Implementation of the charmm force field in GROMACS: Analysis of protein stability effects from correction maps, virtual interaction sites, and water models, *Journal of Chemical Theory and Computation*, 2010, **6**, 459–466.

69 B. R. Brooks, C. L. Brooks, A. D. Mackerell, L. Nilsson, R. J. Petrella, B. Roux, Y. Won, G. Archontis, C. Bartels, S. Boresch, A. Caflisch, L. Caves, Q. Cui, A. R. Dinner, M. Feig, S. Fischer, J. Gao, M. Hodoscek, W. Im, K. Kuczera, T. Lazaridis, J. Ma, V. Ovchinnikov, E. Paci, R. W. Pastor, C. B. Post, J. Z. Pu, M. Schaefer, B. Tidor, R. M. Venable, H. L. Woodcock, X. Wu, W. Yang, D. M. York and M. Karplus, CHARMM: The biomolecular simulation program, *Journal of Computational Chemistry*, 2009, **30**, 1545–1614.

70 I. Caroline, S. Aguiar and R. Stefani, Investigation of Chitosan , Quercetin and Water Interactions using Free Energy Calculations and Molecular Docking.

71 J. L. Desmond, P. M. Rodger and T. R. Walsh, Testing the inter-operability of the CHARMM and SPC/Fw force fields for conformational sampling, *Molecular Simulation*, 2014, **40**, 912–921.

72 J. J. Irwin, T. Sterling, M. M. Mysinger, E. S. Bolstad and R. G. Coleman, ZINC: A Free Tool to Discover Chemistry for Biology, *Journal of Chemical Information and Modeling*, 2012, **52**, 1757–1768.

73 V. Zoete, M. A. Cuendet, A. Grosdidier and O. Michielin, SwissParam: A fast force field generation tool for small organic molecules, *Journal of Computational Chemistry*, 2011, **32**, 2359–2368.

74 M. Greiner, E. Elts, J. Schneider, K. Reuter and H. Briesen, Dissolution study of active pharmaceutical ingredients using molecular dynamics simulations with classical force fields, *Journal of Crystal Growth*, 2014, **405**, 122–130.

75 N. M. Hassan, A. A. Alhossary, Y. Mu and C. K. Kwoh, Protein-Ligand Blind Docking Using QuickVina-W with Inter-Process Spatio-Temporal Integration, *Scientific Reports*, 2017, **7**, 1–13.

76 Y. Wang, D. C. Latshaw and C. K. Hall, Aggregation of Aβ(17–36) in the Presence of Naturally Occurring Phenolic Inhibitors Using Coarse-Grained Simulations, *Journal of Molecular Biology*, 2017, **429**, 3893–3908.

77 Y. Wang, Y. He, Z. Yu, J. Gao, S. ten Brinck, C. Slebodnick, G. B. Fahs, C. J. Zanelotti, M. Hegde, R. B. Moore, B. Ensing, T. J. Dingemans, R. Qiao and L. A. Madsen, Double helical conformation and extreme rigidity in a rodlike polyelectrolyte, *Nature Communications*, 2019, **10**, 801.

78 T. Zhang, H. Yang, Z. Yang, S. Tan, J. Jin, S. Liu and J. Zhang, Sulfonated Compounds Bind with Prostatic Acid Phosphatase (PAP 248-286) to Inhibit the Formation of Amyloid Fibrils, *ChemistryOpen*, 2018, **7**, 447–456.

79 Y. Zou, Z. Qian, Y. Chen, H. Qian, G. Wei and Q. Zhang, Norepinephrine Inhibits Alzheimer's Amyloid-β Peptide Aggregation and Destabilizes Amyloid-β Protofibrils: A Molecular Dynamics Simulation Study, *ACS Chemical Neuroscience*, 2019, **10**, 1585–1594.

80 H. J. C. Berendsen, J. R. Grigera and T. P. Straatsma, The missing term in effective pair potentials, *Journal of Physical Chemistry*, 1987, **91**, 6269–6271.

81 G. Bussi, D. Donadio and M. Parrinello, Canonical sampling through velocity rescaling, *The Journal of Chemical Physics*, 2007, **126**, 014101.

82 S. Nosé and M. L. Klein, Constant pressure molecular dynamics for molecular systems,

Molecular Physics, 1983, **50**, 1055–1076.

83 B. Hess, H. Bekker, H. J. C. Berendsen and J. G. E. M. Fraaije, LINCS: A linear constraint solver for molecular simulations, *Journal of Computational Chemistry*, 1997, **18**, 1463–1472.

84 T. Darden, D. York and L. Pedersen, Particle mesh Ewald: An N ·log(N) method for Ewald sums in large systems, *The Journal of Chemical Physics*, 1993, **98**, 10089–10092.

85 W. Humphrey, A. Dalke and K. Schulten, VMD: Visual molecular dynamics, *Journal of Molecular Graphics*, 1996, **14**, 33–38.

86 B. Han, Y. Liu, S. W. Ginzinger and D. S. Wishart, SHIFTX2: Significantly improved protein chemical shift prediction, *Journal of Biomolecular NMR*, 2011, **50**, 43–57.

87 R. K. Saini, S. Shuaib and B. Goyal, Molecular insights into Aβ 42 protofibril destabilization with a fluorinated compound D744: A molecular dynamics simulation study, *Journal of Molecular Recognition*, 2017, **30**, e2656.

88 M. Karplus, Contact electron-spin coupling of nuclear magnetic moments, *The Journal of Chemical Physics*, 1959, **30**, 11–15.

89 G. W. Vuister and A. Bax, Quantitative J correlation: a new approach for measuring homonuclear three-bond J(HNH.alpha.) coupling constants in 15N-enriched proteins, *Journal of the American Chemical Society*, 1993, **115**, 7772–7777.

90 S.-H. Chong, J. Yim and S. Ham, Structural heterogeneity in familial Alzheimer's disease mutants of amyloid-beta peptides, *Molecular BioSystems*, 2013, **9**, 997.

91 N. L. Fawzi, K. L. Kohlstedt, Y. Okabe and T. Head-Gordon, Protofibril assemblies of the arctic, dutch, and flemish mutants of the alzheimer's Aβ1-40 peptide, *Biophysical Journal*, 2008, **94**, 2007–2016.

92 J. Zheng, H. Jang, B. Ma, C. J. Tsai and R. Nussinov, Modeling the Alzheimer Aβ17-42 fibril architecture: Tight intermolecular sheet-sheet association and intramolecular hydrated cavities, *Biophysical Journal*, 2007, **93**, 3046–3057.

93 N. V. Buchete and G. Hummer, Structure and dynamics of parallel β-sheets, hydrophobic

core, and loops in Alzheimer's Aβ fibrils, *Biophysical Journal*, 2007, **92**, 3032–3039.

94 W. M. Berhanu and U. H. E. Hansmann, Side-chain hydrophobicity and the stability of Aβ 16-22 aggregates, *Protein Science*, 2012, **21**, 1837–1848.

95 V. Knecht, H. Möhwald and R. Lipowsky, Conformational Diversity of the Fibrillogenic Fusion Peptide B18 in Different Environments from Molecular Dynamics Simulations, *The Journal of Physical Chemistry B*, 2007, **111**, 4161–4170.

96 C. Yang, X. Zhu, J. Li and R. Shi, Exploration of the mechanism for LPFFD inhibiting the formation of β-sheet conformation of Aβ(1-42) in water, *Journal of Molecular Modeling*, 2010, **16**, 813–821.

97 J. A. Marsh and S. A. Teichmann, Relative Solvent Accessible Surface Area Predicts Protein Conformational Changes upon Binding, *Structure*, 2011, **19**, 859–867.

98 W. Kabsch and C. Sander, Dictionary of protein secondary structure: Pattern recognition of hydrogen-bonded and geometrical features, *Biopolymers*, 1983, **22**, 2577–2637.

99 L. C. Serpell, Alzheimer's amyloid fibrils: structure and assembly, *Biochimica et Biophysica Acta (BBA) - Molecular Basis of Disease*, 2000, **1502**, 16–30.

100 M. Sunde, L. C. Serpell, M. Bartlam, P. E. Fraser, M. B. Pepys and C. C. F. Blake, Common core structure of amyloid fibrils by synchrotron X-ray diffraction, *Journal of Molecular Biology*, 1997, **273**, 729–739.

101 K. L. Sciarretta, A. Boire, D. J. Gordon and S. C. Meredith, Spatial separation of β-sheet domains of β-amyloid: Disruption of each β-sheet by N-methyl amino acids, *Biochemistry*, 2006, **45**, 9485–9495.

102 B. Sharma and S. Paul, Understanding the role of temperature change and the presence of NaCl salts on caffeine aggregation in aqueous solution: From structural and thermodynamics point of view, *Journal of Physical Chemistry B*, 2015, **119**, 6421–6432.

103 B. Ma and R. Nussinov, Stabilities and conformations of Alzheimer's -amyloid peptide oligomers (A 16-22, A 16-35, and A 10-35): Sequence effects, *Proceedings of the National Academy of Sciences*, 2002, **99**, 14126–14131.

104 B. Tarus, J. E. Straub and D. Thirumalai, Dynamics of Asp23−Lys28 Salt-Bridge Formation in Aβ 10-35 Monomers, *Journal of the American Chemical Society*, 2006, **128**, 16159–16168.

105 A. T. Petkova, W. M. Yau and R. Tycko, Experimental constraints on quaternary structure in Alzheimer's β-amyloid fibrils, *Biochemistry*, 2006, **45**, 498–512.

106 J.-X. Lu, W. Qiang, W.-M. Yau, C. D. Schwieters, S. C. Meredith and R. Tycko, Molecular Structure of β-Amyloid Fibrils in Alzheimer's Disease Brain Tissue, *Cell*, 2013, **154**, 1257–1268.

107 S. K. Mudedla, N. A. Murugan, V. Subramanian and H. Agren, Destabilization of amyloid fibrils on interaction with MoS 2 -based nanomaterials, *RSC Advances*, 2019, **9**, 1613–1624.

108 S. Brogi, S. Butini, S. Maramai, R. Colombo, L. Verga, C. Lanni, E. De Lorenzi, S. Lamponi, M. Andreassi, M. Bartolini, V. Andrisano, E. Novellino, G. Campiani, M. Brindisi and S. Gemma, Disease-modifying anti-Alzheimer's drugs: Inhibitors of human cholinesterases interfering with β-amyloid aggregation, *CNS Neuroscience and Therapeutics*, 2014, **20**, 624–632

Chapter 5

Destabilization potential of phenolics on Aβ Fibril: Mechanistic insights from Molecular Dynamics Simulation

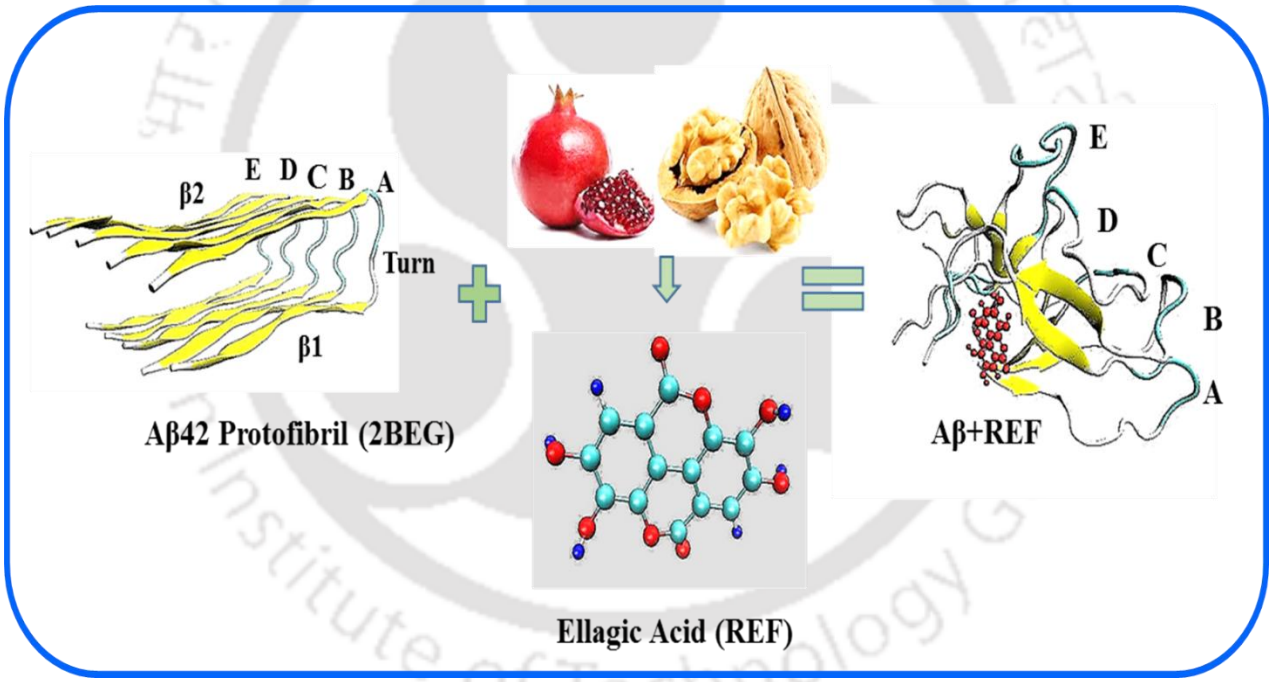

In the current study, we have investigated four phenolic compounds from food sources for their potential in destabilizing the Aβ fibril. We have employed docking to see for the best possible interaction between phenolic compound and fibril. The docking results proposed ellagic acid (REF) to be the best binder to Aβ fibril owing to the minimum binding energy. Further, to test the

destabilization effect of REF on Aβ oligomer, MD simulation was conducted. The simulation outcome obtained henceforth clearly indicates a drift of terminal chains from the Aβ oligomer, leading to the disorganization of the characteristically organized cross β structure of Aβ fibrils. The MM-PBSA results revealed the binding of REF to chain A of the Aβ oligomer. The destabilization potential of ellagic acid, as explained by the MD simulation study, establishes it as a promising drug to cure AD.

5.1 INTRODUCTION

AD is a multi-faceted chronic, progressive, and geriatric disease with unclear root causes and mechanisms.[1] The Aβ fibril is of greater clinical importance as it is the foremost step in aggregation and also directs the formation of NFTs further, as explained by amyloid cascade hypothesis.[2–5]

The clinical failure of drugs employing an anti-aggregation strategy motivated researchers to focus on destabilization as a therapeutic approach.[6] For the purpose of disrupting preformed Aβ fibrils, natural compounds have been a preferred choice owing to their biocompatibility and non-toxicity to the human system. The antioxidant, anti-cancerous, neuroprotection and various other health benefits add to the suitability of natural compounds as drugs for a wide array of human diseases, including AD.[7–11] Natural products can be obtained from numerous living systems including marine, plant, and animal resources. Amongst all the origins of natural compounds, the plant-based phytochemicals are the safest choice due to higher efficacy, fair availability, extractability and broad spectrum applicability.[12–14]

A diverse range of phytochemicals, including alkaloids, terpenoids, and polyphenols etc. have been studied for finding drug cues for AD. Curcumin from *Curcuma longa* was found to

inhibit Aβ fibril formation and destabilize preformed Aβ fibrils by *in-vitro* studies.[15] Quercetin and Rutin show their neuroprotection ability by inhibiting aggregation of Aβ monomers as well as destabilizing Aβ fibrils.[16] 7-Methyl gallic acid (methanolic extracts from *T.Chebula* and *T.arjuna* plant) was reported to inhibit and disaggregate Aβ oligomers, when tested *in-vitro*.[17] The role of melatonin, serotonin, tryptamine, and tryptophan from plant sources, studied *in-vitro,* exhibited neuroprotection ability of phytochemicals.[18] Ferulic acid has been proposed as a promising destabilizer of Aβ fibrils by *in-vitro* testing.[19] The *in-vitro* investigations proposed all these natural compounds as potential drug leads but their molecular level mechanism remains incomprehensible, so augmentation of both *in-vitro* and *in-silico* studies is desirable.[20]

The computational studies not only traverse atomic-scale mechanisms by means of MD simulations but also validate results obtained by *in-vitro* studies as well.[21] Brazilin[22] and hematoxylin[23] from the Sappan wood, when studied by in-vitro methods and coupled with MD simulation, were reported to redirect Aβ monomers and mature fibrils into unstructured Aβ aggregates, restricting their primary and secondary nucleation. A recent finding on inhibition and destabilization of Aβ monomer and Aβ protofibril, studied computationally, by a hybrid of resveratrol and clioquinol reinforces the importance of phenolic compounds in prospecting new drug candidates for AD.[24] Morin, a natural bioflavonoid from tea, coffee, red wine, and cereals were found to alter Aβ fibrils to form non-neurotoxic off-pathway aggregates.[25] Dihydrochalcone, a natural compound from pepper, has shown its ability to destabilize Aβ fibril, studied by MD simulation.[26] Recently, EGCG (Epigallocatechin-3-gallate), a tea catechin was also reported as β-sheet breaker converting neurotoxic aggregates into unstructured non-toxic clumps.[27]

The growing consensus on the use of plant-derived biophenols possessing aromatic rings[28] embarks their suitability for treating AD.[29] The antioxidant and neuroprotective abilities of

biophenols reported to delay the onset of AD.[30–33] Dry fruits (walnut, almond, and hazelnut), berries, fruits, green leafy vegetables, coffee, tea, and spices are rich sources of polyphenolic compounds. A nut-rich diet containing phenolic acids (caffeic acid, gallic acid, and ellagic acid) and a flavanol (epigallocatechin) has been considered for the present study.[34] The caffeic acid from walnut, coffee, tea, chocolate, and red wine is known to reduce Aβ-induced toxicity and improve cognitive ability when tested in mice.[35,36] Gallic acid from walnuts, pomegranate, grape seeds, and black tea were also reported to inhibit Aβ fibril formation[37] and destabilize Aβ oligomers[38], thus restraining neurotoxicity. Ellagic acid, predominantly found in pomegranates[39], chestnut, almond, walnut, strawberries, raspberries were found to diminish cognitive decline and prevents self-aggregation when tested *in-vitro* and *in-vivo*.[40,41] The epigallocatechin, present majorly in green tea and broad beans, having antioxidant and anti-aggregation properties is reported to reduce Aβ production and attenuate Aβ induced toxicity when studies were conducted in a transgenic mouse.[42] All these preliminary reports motivated us to examine the interaction and, thus, destabilization mechanism of Aβ fibrils by these phenolic compounds, thereby providing a promising cure to AD.

The atomistic details about destabilization mechanism of Aβ fibrils by MD simulation facilitate drug designing in lieu to formulate a clinically approved drug to treat AD. In the present study, four plant polyphenols, viz., caffeic acid (DHC), epigallocatechin (EGT), gallic acid (GDE), and ellagic acid (REF), have been considered for screening to select the most potent destabilizer of Aβ fibrils amongst them. The study is conducted by docking of these biophenols with Aβ oligomer that revealed ellagic acid as the best binder to Aβ oligomer. The docked complexes were then submitted to MD simulation to check for the most potential destabilizer of Aβ oligomer. The substantial increase in RMSD and radius of gyration (R_g) along with the loss of β-sheet content

and salt bridges demarcates disorganization of Aβ fibril structure in the presence of ellagic acid. The disruption of H-bonds (hydrogen bonds) and breaking of hydrophobic contacts further weakens the oligomer structure, ultimately leading to its destabilization. The results thus obtained after docking and MD simulation establishes ellagic acid as a potent disruptor of Aβ fibril and thus a promising drug for the treatment of AD.

5.2 METHODS

5.2.1 Selection of Phenolic Compounds and $A\beta_{17-42}$ Oligomer for Molecular Docking

Molecular docking Studies were performed using AutoDock Suite 4.2.1 with the help of MGL tools 1.5.6.[43] Three-dimensional structure of $A\beta_{17-42}$ oligomer (PDB ID: 2BEG)[44] was taken from the protein data bank (PDB) and was used as the receptor protein in the current study. The Aβ oligomer is a pentamer structure spanning from residues 17-42, which forms the characteristic β-sheet, the prerequisite for fibrillation and stable organization. The characteristic β-sheet structure is further divided into three regions - β1 region (18-26 residues), turn region (27-30 residues), and β2 region (31-42 residues) as depicted in Fig. 5.1a. There are five chains in 2BEG, designated as A, B, C, D, and E, having the same primary sequence with A and E being the terminal chains. The uses of 2BEG as the representative model for Aβ fibril have been a preferred choice by numerous studies owing to its well-established and a very stable structure, employed in numerous studies.[25,45–47] The ligands that are investigated in the study are phenolic compounds viz., Caffeic acid (DHC), Epigallocatechin (EGT), Gallic acid (GDE) and Ellagic acid (REF). The PDB structures for all of these ligands have been taken from the ligand summary page of protein

database as DHC.pdb, EGT.pdb, GDE.pdb, and REF.pdb, respectively, and drawn by using ChemDraw[48] as shown in Fig. 5.1b-e. After retrieval of structures for both protein and ligands, four systems have been submitted to AutoDock[49] for docking purposes. The definition for all the systems has been depicted in Table 5.1 as S0, S1, S2, S3, and S4, where S0 represents the control system i.e. without ligand. Docking preparation includes the addition of gasteiger charges to the ligand and polar hydrogen to both protein and ligand. Each ligand was docked individually with the same receptor (2BEG).

Since Aβ oligomer has no specific binding site reported, we have performed blind docking, which searches the entire protein surface for possible docking sites. The large enough search space ensures finding all the possible binding conformations between Aβ oligomer and all four phenolic compounds. The protein was set as a rigid entity, while ligands were considered as flexible moieties. The searching space was designed as a grid around Aβ oligomer of size 126 × 60 × 60 $Å^3$, with a default grid spacing of 0.375 Å. The Lamarckian genetic algorithm (GA)[43] was utilized as a searching tool for docking. The following parameters were used for docking: GA population size =150, maximum number of energy evaluations = 2.5×10^6, maximum number of generations = 27,000, mutation rate = 0.02 and crossover rate = 0.8, keeping all others as default ones. The docked conformations obtained thereafter were clustered using RMSD (Root Mean Square Deviation) tolerance of 0.20 nm. The visualization of the docked complex was carried out by VMD[50] to look for the best pose with the minimum binding energy and the residues of Aβ oligomer involved in binding with each ligand. Subsequently, we have carried out MD simulation to investigate the best candidate for the destabilization of Aβ oligomer.

5.2.2 Molecular Dynamics Simulation of docked complexes of phenolic compounds with Aβ oligomer

The docked complexes of phenolic-Aβ oligomer were subjected to MD simulation using GROMACS v5.1.1.[51] The force field employed was GROMOS 96 54a7.[52–54] The ligand topologies obtained after docking for all the four phenolic compounds (viz., DHC, EGT, GDE and REF) have been submitted to PRODRG server[55] to generate gromos defined coordinates, which are GROMACS readable. The topologies thus obtained in .gro format were combined with Aβ oligomer to form complexes as C1, C2, C3, and C4 (Table 5.1). All the complexes then were solvated in a 7 × 7 × 7 nm^3 cubic box with water, represented by the SPC water model.[56] Further the simulation procedure has been followed the same way as described in section 4.2.2 of chapter 4.

5.2.3 Analysis of MD generated trajectories

We have calculated various parameters using different tools defined within the GROMACS v5.1.1 package. There are various parameters that have been analyzed in the same way as has been explained in section 4.2.3 of chapter 4.

5.2.4 Binding Mode analysis by MM-PBSA

The binding free energy (BFE) of the Aβ oligomer with the selected phenolic compound was calculated by MM-PBSA (Molecular Mechanics Poisson-Boltzmann Surface Area method).[57–59] The package was used within the gromacs environment by g_mmpbsa tool, which calculated the overall binding energy and individual residue contribution.[60] MM-PBSA calculates the BFE from the MD trajectory based on the following equation:

$$\Delta G^{bind} = \Delta E_{MM} + \Delta G^{psolv} + \Delta G^{npsolv} - T\Delta S$$

where,$\Delta E_{MM}$is the molecular mechanics contribution in vacuum $\Delta G^{psolv}$is the polar contribution of solvation energy, calculated by the Poisson-Boltzmann equation; $\Delta G^{npsolv}$is the nonpolar contribution towards binding and is determined by solvent accessible surface area (SASA) model. The high computational demand limits the calculation of entropy contribution. In addition, the relative change in entropy contribution (ΔS) towards free energy calculation is negligible and thus can be ignored.[61] The calculation of BFE in the present study was done on the last 10 ns trajectory with Δt = 100 ps to reduce the computational time. The energetic contribution of individual residue was also quantified to identify key residues actively involved in binding with the phenolic compound. The solute and solvent dielectric constants were taken as 4 and 80, respectively.

5.3 RESULTS AND DISCUSSIONS

The system definition for this current study has been given in Table 5.1.

Table 5.1. System definition for Docking and Molecular Dynamics Simulation

System Index (Docking)	Receptor	Ligand	Complex Index (.gro) for MD simulation
S0	2BEG.pdb (Aβ oligomer)	No ligand	Control= C0.gro (Aβ+Water)
S1	2BEG.pdb (Aβ oligomer)	DHC.pdb (Caffeic Acid)	Test 1 = C1.gro (Aβ+DHC)

S2	2BEG.pdb (Aβ oligomer)	EGT.pdb (Epigallocatechin)	Test 2= C2.gro (Aβ+EGT)
S3	2BEG.pdb (Aβ oligomer)	GDE.pdb (Gallic Acid)	Test 3 = C3.gro (Aβ+GDE)
S4	2BEG.pdb (Aβ oligomer)	REF.pdb (Ellagic Acid)	Test 4 = C4.gro (Aβ+REF)

5.3.1 Molecular Docking of phenolics with Aβ oligomer

The molecular Docking of Aβ oligomer (Fig. 5.1a) with four phenolic compounds (Fig. 5.1b-e). has been explained in Table 5.2.

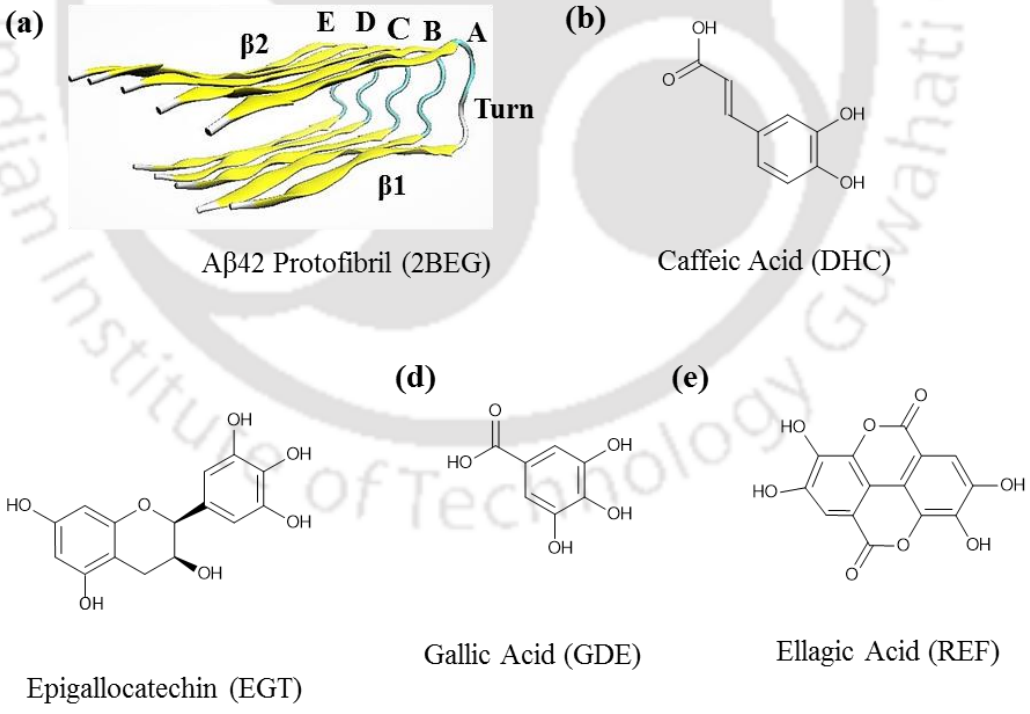

Aβ42 Protofibril (2BEG)

Caffeic Acid (DHC)

Epigallocatechin (EGT)

Gallic Acid (GDE)

Ellagic Acid (REF)

Fig. 5.1. Initial configuration of (a) 2BEG (b) DHC (c) EGT (d) GDE and (e) REF.

The present study revealed binding energy, inhibition constant, and residues involved in binding. The binding energy (ΔG , kcal/mol) was estimated as -5.17, -5.51, -3.90, and -5.68 for DHC, EGT, GDE, and REF (Table 5.2), respectively, wherein the negative sign signifies favorable binding. The lower value of ΔG for EGT (-5.51 kcal/mol) suggests that it would be a good binder to Aβ fibril as compared to earlier reports.[62] However, the lowest value for REF (-5.68 kcal/mol) marks its strong association with Aβ oligomer as compared to the other three phenolic compounds under investigation. The low value of inhibition constant signifies high binding affinity[47] and low amount of medication[63] required to inhibit the target enzyme.

The selection of REF as the best candidate is also supported by the lowest inhibition constant (Table 5.2) of REF compared to other compounds. The VMD visualization of the docked complex of $A\beta_{17-42}$ oligomer and REF, as shown in Fig. 5.2, represents various residues that are involved in binding.

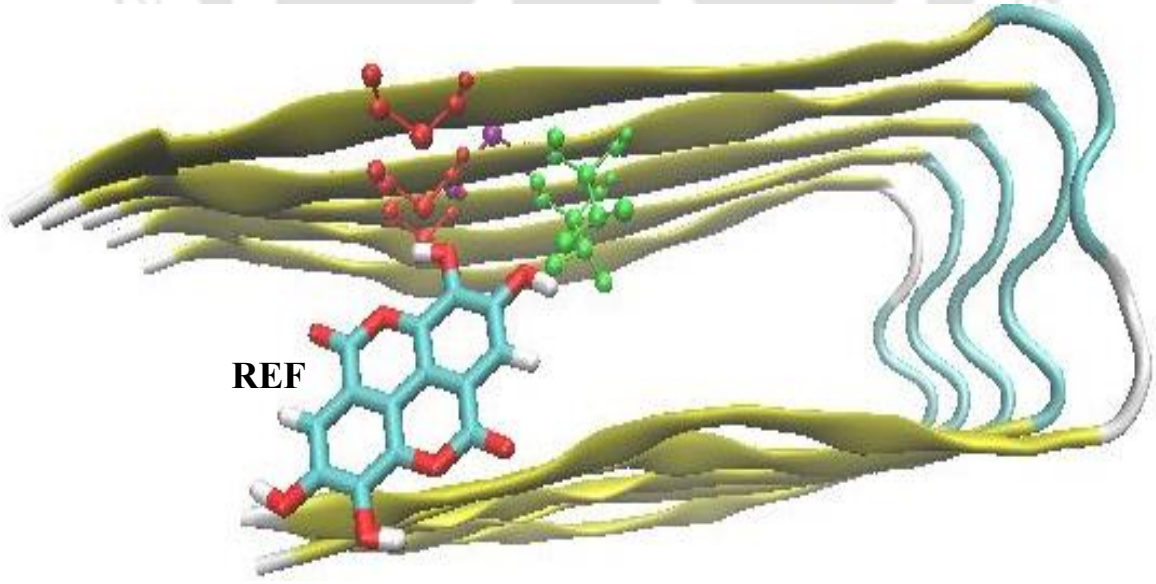

Fig. 5.2. Docking representation of Aβ oligomer with REF.

The key residues of Aβ oligomer involved in binding with REF are glycine at 37th position (G37, red) from chain A, B, and C; methionine at 35th position (M35, green) from chain B and C; and Valine at 36th position (V36, purple) from chain B (Table 5.2).

The binding of REF with hydrophobic residues of β-strands of Aβ oligomer facilitates its entry into the hydrophobic cavity. This finding is well supported by exploring various binding sites of different Aβ oligomers by numerous tracers, where the hydrophobic cavity or core is found to be the preferred binding site in Aβ fibril.[64,65] The results are also in parity with the report wherein a flavonoid derivative[46] and other flavones[66] were docked and found to destabilize Aβ oligomer. The docking investigation of different proposed drugs to Aβ oligomer[67] to test their anti-fibrillation property highlights the importance of Docking in evaluating binding affinity and best orientation possible. The selection of REF as the best binder is pertinent to its strong affinity to Aβ oligomer, which is tested further for its destabilization potential by means of MD simulation of the docked complex.

Table 5.2. Docking results with all the Phenolic Compounds

Ligand	**Binding Energy (ΔG) (kcal/mol)**	**Inhibition Constant (k_i) (μM)**	**Residues Involved**
DHC (Caffeic Acid)	-5.17	162.05	B(V18,F19); C(L17,F19); D(F19,G38,V40); E(G38)

EGT (Epigallocatechin)	-5.51	91.77	A(M35,V36); B(M35,V36,G37); C(M35,V36,G37); D(V36)
GDE (Gallic Acid	-3.90	1380	A(K28); B(N27,K28); C(N27,K28); D(G29,A30)
REF (Ellagic Acid)	-5.68	69	A(G37); B(M35,V36,G37); C(M35,G37)

5.3.2 Molecular dynamics Simulation of phenolic compounds with Aβ oligomer

The VMD visualization of the final configuration after 100 ns simulation of Aβ-water (C0) and Aβ–REF (C4) system can be viewed from Fig. 5.3a and b, respectively. The biophenols are observed to migrate to different possible binding sites along the fibrils,[68] but the average ensemble image has been depicted for all the ligands under investigation. There is a clear demarcation of the disorganization of Aβ oligomer in the presence of REF (Fig. 5.3b), which is an indication of good destabilization potential of ellagic acid. The final configurations of Aβ oligomer obtained after MD simulation in the presence of the other three phenolic compounds (viz., DHC, EGT, and GDE), are also given in Fig. 5.4b-d along with the control system (C0, Fig. 5.4a), where they did not show much deviation from the control system.

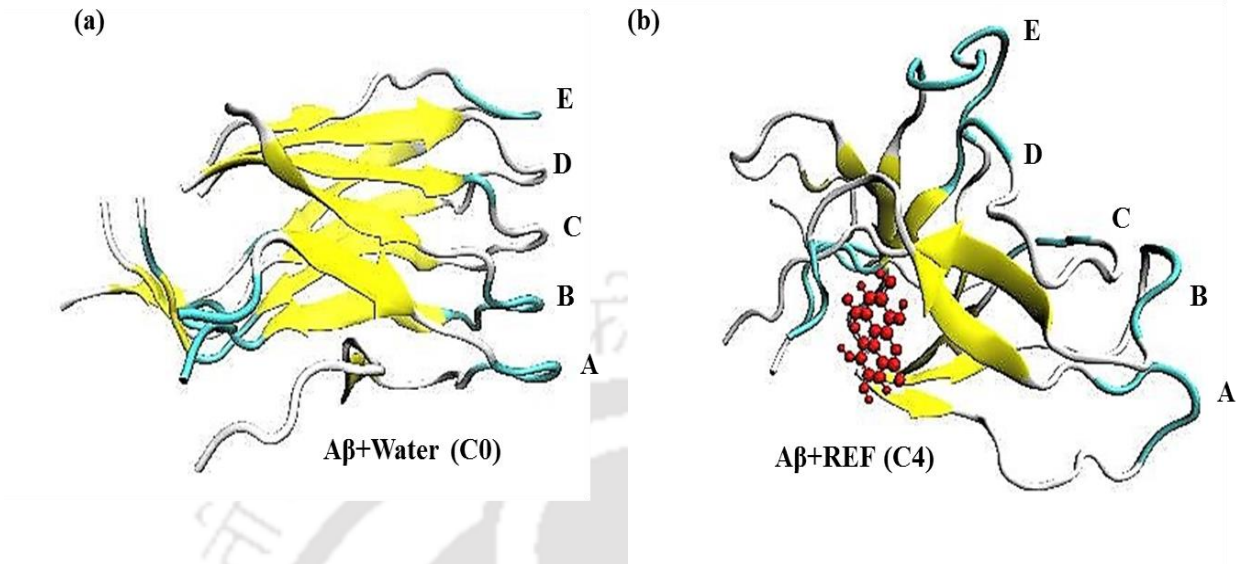

Fig. 5.3. Final Configuration of 2BEG (a) in water and (b) 1 mol of REF.

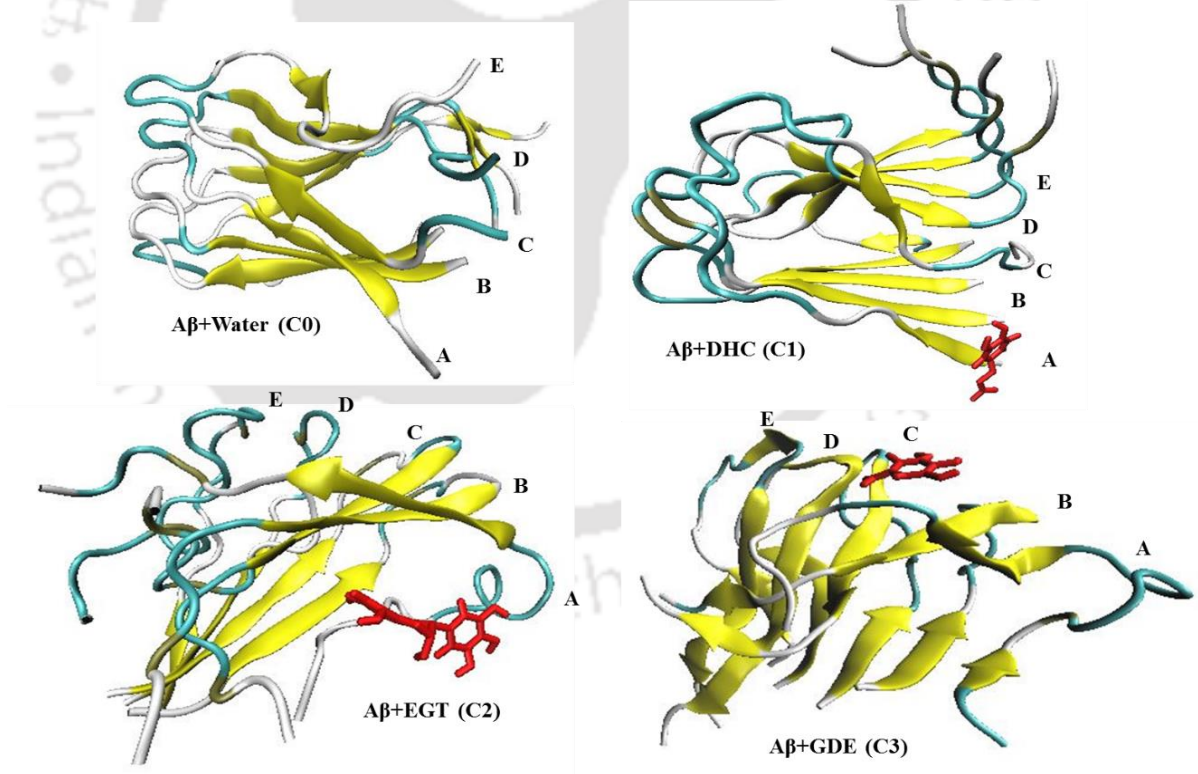

Fig. 5.4. Final configuration of Aβ with (a) water, (b) DHC, (c) EGT, and (d) GDE.

In addition to the visualization of the final structure, C_α-RMSD, R_g, Average K28-C_α distance, and D23-K28 salt bridge formation has been determined for all phenolic compounds to screen the best disruptor among all the four ligands. The highest RMSD and R_g values for Aβ oligomer in the presence of REF as compare to the other three phenolic compounds (Fig. 5.5a and b) express it as the most potential disruptor of Aβ oligomer. The increased RMSD and R_g values demonstrating structural instability of Aβ oligomer is also reported by other natural compounds which supports our findings.[24,46]

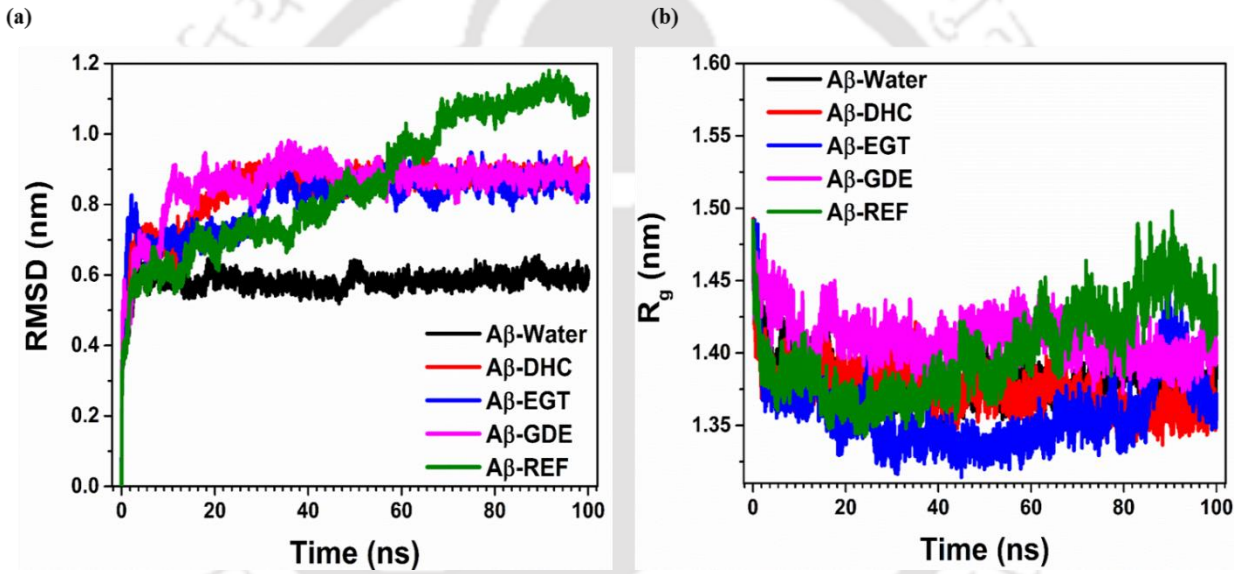

Fig. 5.5. (a) Cα-RMSD of 2BEG in water and all 4 ligands, and (b) R_g of 2BEG in water and all 4 ligands.

The K28-K28 C_α bonding between neighboring chains D and E (Fig. 5.6a) was reported to be higher in the presence of REF in comparison to the other phenolics. The distance between D23 and K28 for chains D and E, respectively, was found to be increased from 0.22 nm for Aβ-water to 0.87 nm (Fig. 5.6b) for Aβ-REF. This increased distance between K28 residues and D23 and

K28 residues from chain D and E hinders K28-K28 bonding and D23-K28 salt bridge formation, thereby resulting in the disorientation of terminal chain E from the Aβ oligomer.

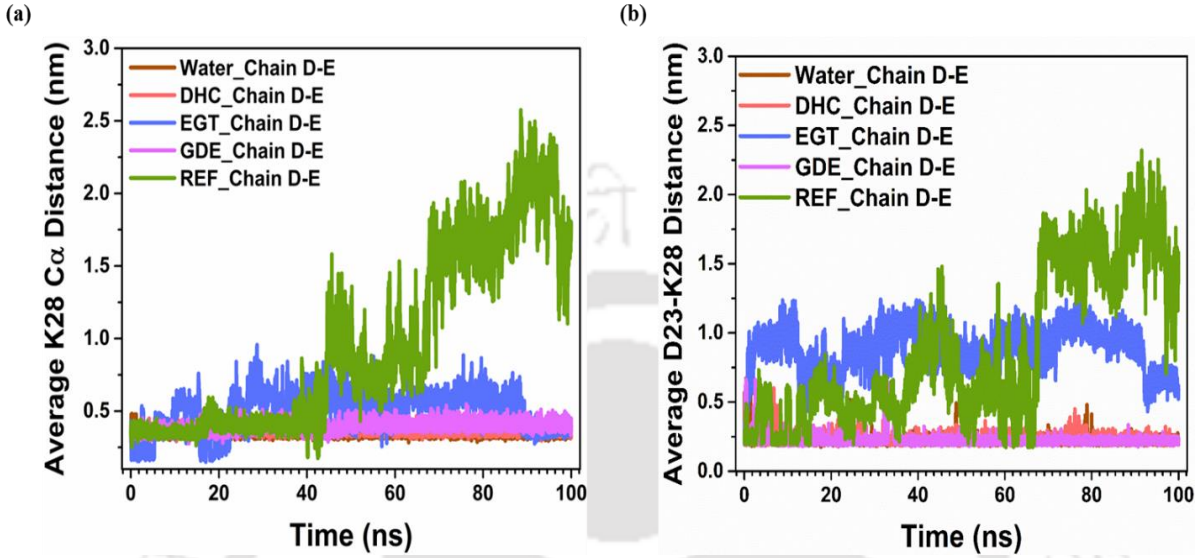

Fig. 5.6. (a) Average K28 Cα distance of chain D-E in water and all 4 ligands, and (b) Average D23-K28 distance of 2BEG in water and all 4 ligands.

Conclusively, the preliminary analysis of the MD trajectory for all the four phenolic compounds directs the selection of REF as the most efficacious destabilizer of Aβ oligomer, which needs to be analyzed further.

5.3.3 Validation of simulation data with experimental results

Before proceeding towards a more in-depth analysis of the destabilization effect of REF on Aβ oligomer, MD ensembles obtained after 100 ns simulation were validated with the NMR structure of Aβ oligomer used initially for simulation. For this purpose, the chemical shifts in backbone atoms C_α and C_β for both protein and final simulated structure have been calculated by SHIFTX2[69]

package. The input is the structural coordinates (PDB) in this software for both Aβ and Aβ-REF system. The high correlation coefficient of 0.99 between NMR chemical shifts from both the systems instated validation of simulation data with experimental study (Fig. 5.7a and b), which is also well supported by other studies.[45,70]

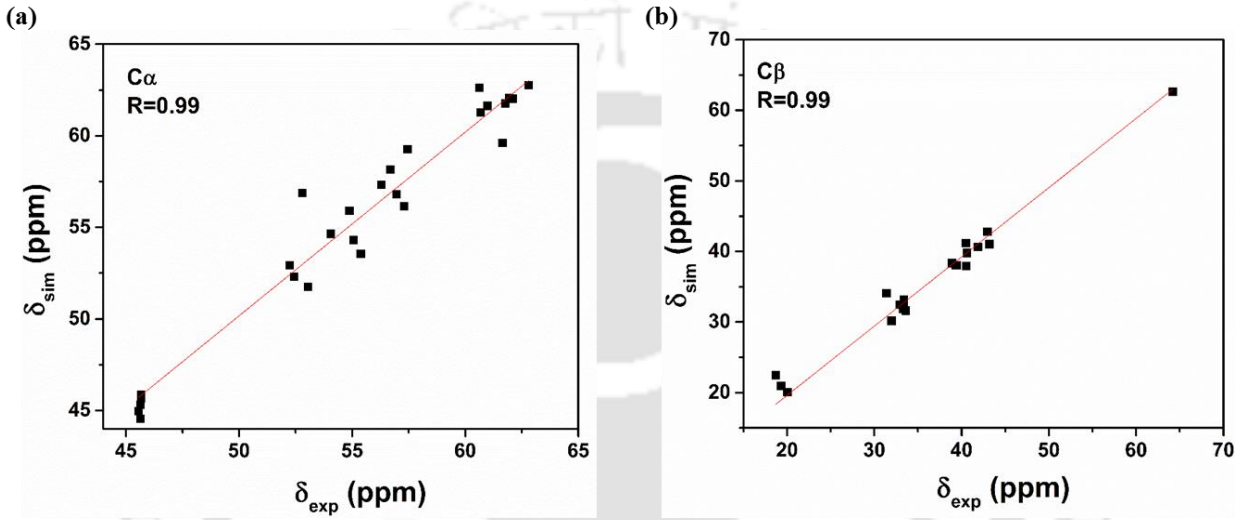

Fig. 5.7. Correlation between the theoretical and experimental NMR chemical shifts for Cα and Cβ atoms of Aβ42 protofibril structure is shown in panel (a), and (b), respectively. The unit of NMR chemical shift is in ppm.

5.3.4 Structural analysis of Aβ oligomer in the presence of Ellagic acid (REF)

The detailed structural analysis involves the determination of C_α-RMSD value around individual chains and various regions of Aβ oligomer (defined in the method section above) in the presence of REF to comprehend the most affected region. The evolution of MD trajectory with simulation time for individual chains and regions of Aβ oligomer in the presence of REF is illustrated in Fig. 5.8a and b, which exhibits chain E and turn region as the most severely affected portions. The

similar observation on destabilization of Aβ oligomer by a natural novel drug wgx-50, on account of increased Cα-RMSD value, resonates well with our findings.[71]

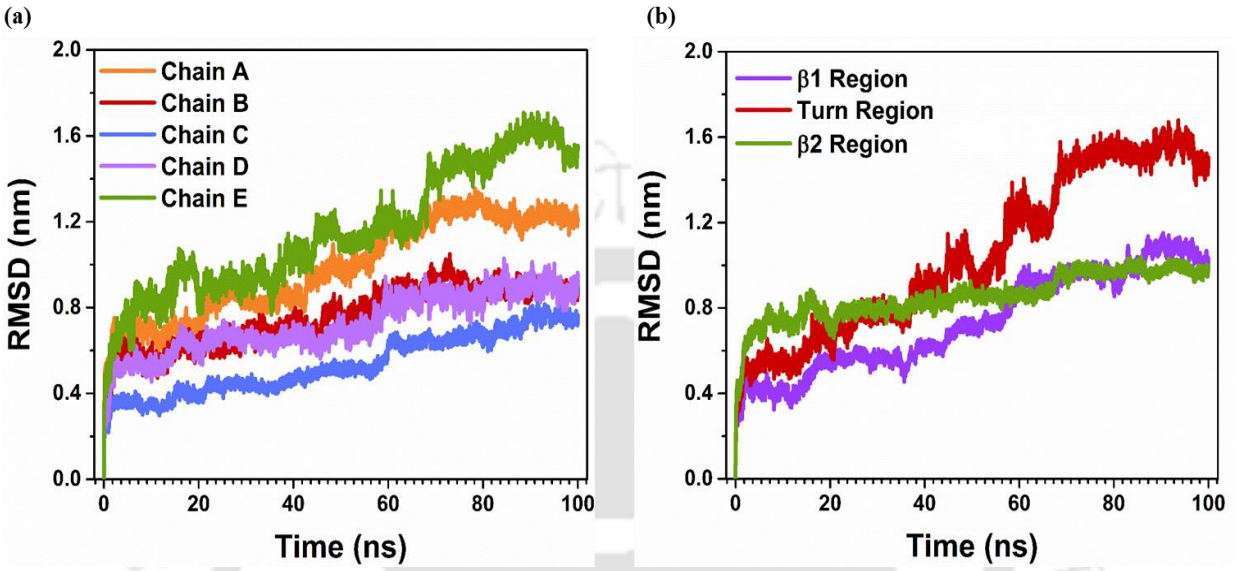

Fig. 5.8. Cα RMSD as a function of time in the presence of REF (a) for all chains, (b) β1 Region, Turn, and β2 Region.

The RMSF value for both the terminal chains (A and E), is recorded higher than the control system in the presence of REF. The clear illustration of the increased RMSF value in Fig. 5.9a and b explain the deviation of Aβ protofibril in the presence of REF, from its parent configuration. The conformity on destabilization of Aβ protofibril with Morin is shown through a similar increase in RMSF value for turn, and β_2 regions affirm the current observation.[25]

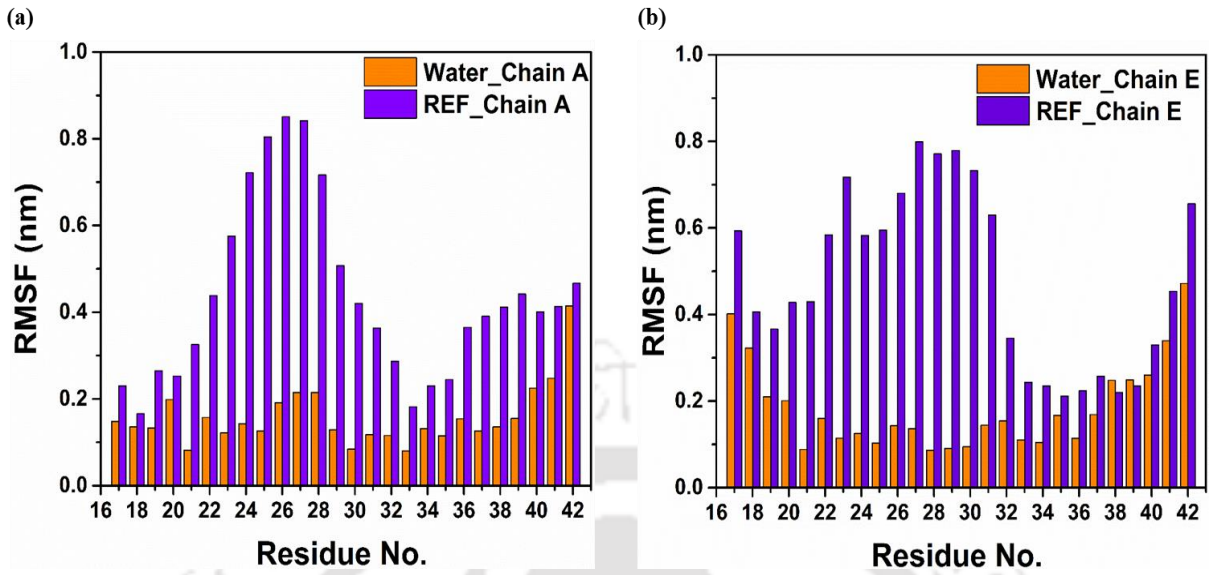

Fig. 5.9. RMSF values for Aβ fibril in the presence of REF (a) Chain A, and (b) Chain E.

The SASA value, which gives an idea about the solvent (water) accessibility of the protein accounting to its hydrophobic and hydrophilic composition, is determined.[72] This value plays a decisive role in determining the conformation of a protein when solubilized in water. Fig. 5.10 gives a pellucid portrayal of the increased SASA value from 67 nm^2 (Aβ-Water) to 72 nm^2 (Aβ-REF), which expresses enhanced solubility (viz., more exposure to solvent) of Aβ oligomer in the presence of REF. The greater SASA value for terminal chains indicates a loosening of these chains from the parent Aβ oligomer, thereby disrupting the stable conformation of Aβ. A similar increase in SASA values of Aβ protofibril by arginine containing short peptides[73] has resulted in the destabilization of Aβ protofibril corroborates well with our findings.

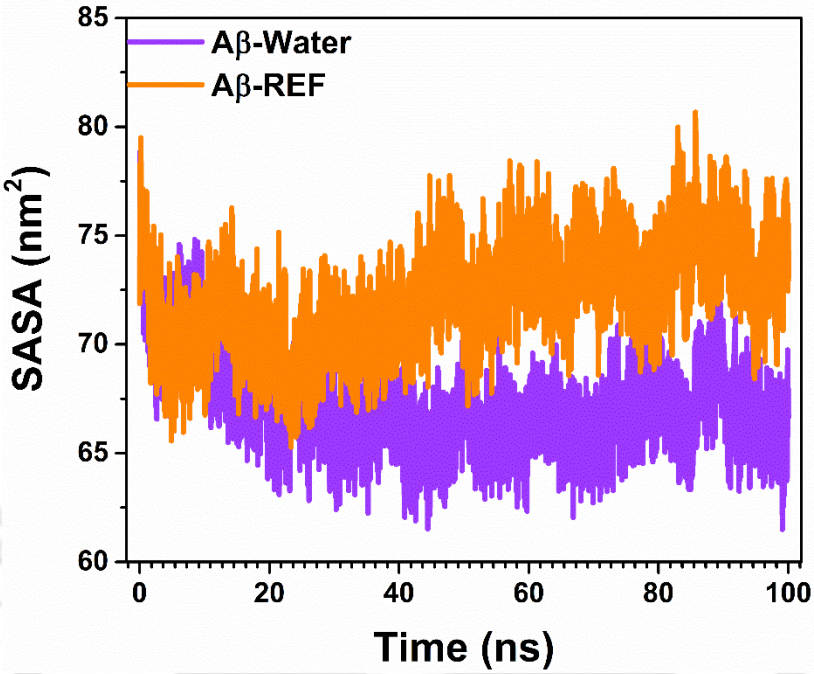

Fig. 5.10. SASA values of Aβ-Water and Aβ-REF.

Conclusively, significantly higher values observed for RMSD, RMSF, and SASA translates the potency of ellagic acid as a promising destabilizing agent of Aβ oligomers, thereby curing AD.

5.3.5 Secondary structure of Aβ oligomer and Aβ-REF complex

The secondary structure analysis by the DSSP[74] tool delivers the time evolution profile of possible secondary structure configurations achievable by Aβ oligomer. The secondary structure has a direct relation to the overall stability and longevity of the protein. The stability of Aβ fibrils has been attributed to their higher β-sheet content, which directs the formation of an organized β-fibrillar structure. The secondary structure profiling for Aβ-Water and Aβ-REF has been shown in

Fig. 5.11a and b, wherein a prominent decrease in β-sheet and bend content are recorded for the later system (viz., Aβ-REF).

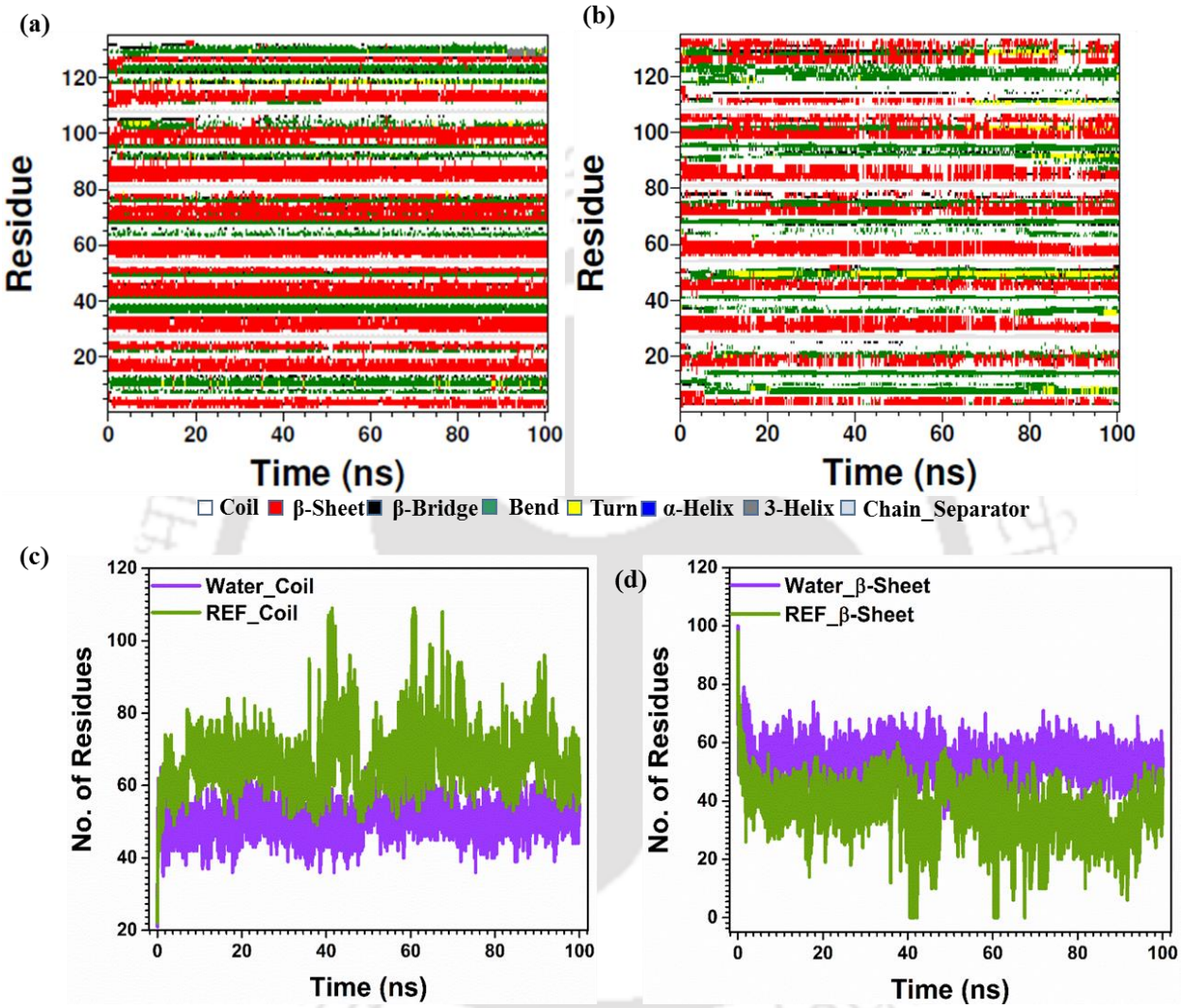

Fig. 5.11. DSSP and Secondary structure (a) Aβ-water, (b) Aβ-REF system, (c) coil content for Aβ-water and Aβ-REF, and (d) β-sheet content for Aβ-water and Aβ-REF.

The individual representation of coil and β-sheet content for both the systems has been presented in Fig. 5.11c and d, which marks an increase of 31.57% in the coil content with a simultaneous decrease of 30% in β-sheet content from Aβ-REF to the Aβ-Water. The significant

decrease in the β-sheet content ensures an obstruction to the formation of higher order aggregates barring neurotoxicity of Aβ fibrils. A similar reduction in β sheet content of Aβ oligomer leading to its destabilization in the presence of caffeine[45], a fluorinated derivative of curcumin[75] and norepinephrine[76], is found to be coherent with the current observation. The remarkable loss in β-sheet content, required for fibrillogenesis, due to ellagic acid makes it a potential anti-amyloidogenic drug lead.

5.3.6 Effect of Ellagic acid on various bonds in Aβ oligomer

There are various types of intra- and inter-molecular bonds that enable the formation and stabilization of Aβ fibrillar structure. They encompass H-bonds, salt bridges, and hydrophobic contacts. Below, we present a detailed analysis of the change in these molecular interactions in the presence of REF.

5.3.6.1 Hydrogen-Bonds

The theoretical[77] and experimental[78] studies outline the importance of an extensive H-bond network contributing towards the stability of Aβ fibrils. The formation of protein polyphenol complex is related to the presence of hydrogen binding sites both in protein and ligand.[79] We have calculated the average number of H-bonds including both intra- and inter-peptide (PP) and observed a noticeable decrease of 9.08 in number of overall H-bonds (PP) from 74.77 (Aβ-Water) to 65.89 (Aβ-REF) pointing towards the disruption of H-bonds in the presence of REF (Fig. 5.12a). A similar decrease of 2.208 in the number of inter-peptide H-bonds between chain A and B for Aβ-REF system in comparison to Aβ-Water have been depicted in Fig. 5.12b.

To elucidate further, the number of inter-peptide H-bonds between chain C and D have been recorded as 16.18 and 9.29 for Aβ-Water and 9.29 Aβ-REF, respectively (Fig. 5.12c), which gives 42.58% loss of H-bonds in Aβ-REF system.

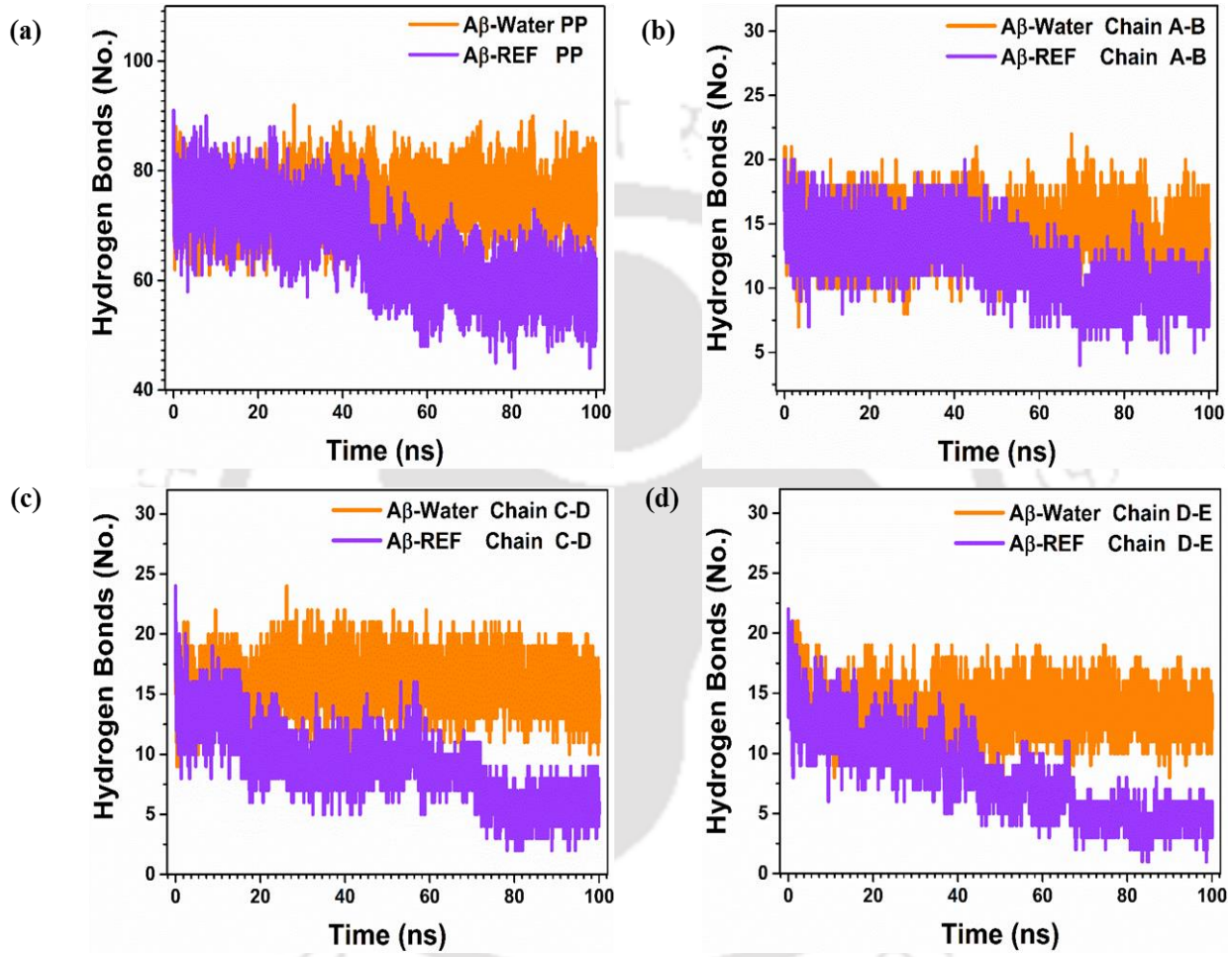

Fig. 5.12. Effect of Ellagic acid on the disruption of Hydrogen bonds (a) number of overall H-bonds of Aβ-Water and Aβ-REF system and intra H-bonding for neighboring chains for Aβ-water and Aβ-REF system, (b) between chain A and chain B, (c) between chain C and chain D, and (d) between chain D and chain E.

Similarly, the number of H-bonds calculated for chain D and E for Aβ-water is 13.863 and for Aβ-REF is 8.151 as depicted in Fig. 5.12d showed significant decrease in H-bonds in the presence of REF. The similar drop from 19 to 14 H-bonds was reported for chain A-B of the fibril in the presence of wgx-50, a novel compound from Sichuan peppers indicating destabilization thereby supporting our findings.[71] The reduction of H-bonds from 21.1 to 13.2 as reported in the presence of morin leading to destabilization of the fibril are in close agreement with the current observations.[25] The H-bond disruption of Aβ oligomer in the presence of REF prohibits fibrillar growth and elongation.

5.3.6.2 Salt-Bridges formation

Salt bridges are defined as electrostatic interactions between oppositely charged amino acid residues in any protein structure.[80,81] The formation of salt bridge is possible when the distance between anionic carboxylate of negatively charged residue such as glutamate (E) or aspartate (D), and cationic ammonium group of positively charged residue, such as arginine (R) or lysine (K) present within a cut off distance of 0.40 nm.[82] Salt bridges not only impart the stability to the protein but also influence its structural conformation, protein recognition, function, degradation pattern, and catalytic activity.[83–86]

In the present study, we have calculated the average distance between D23 and K28 residues for the entire protein in both the systems (Aβ-Water and Aβ-REF), as a function of time. The average distance for these residues was found to be increased in the presence of REF, as shown in Fig. 5.13 and 5.14. The spike in the inter-residual distance between D23 of chain A and K28 of

neighboring chain B of 0.53 nm for Aβ-REF as compare to the Aβ-Water system was observed (Fig. 5.13a). A similar increase of 0.55 nm for chain B (D23) and chain C (K28) as shown in Fig. 5.13b suggests the breaking of the bond and hence misalignment of Aβ oligomer.

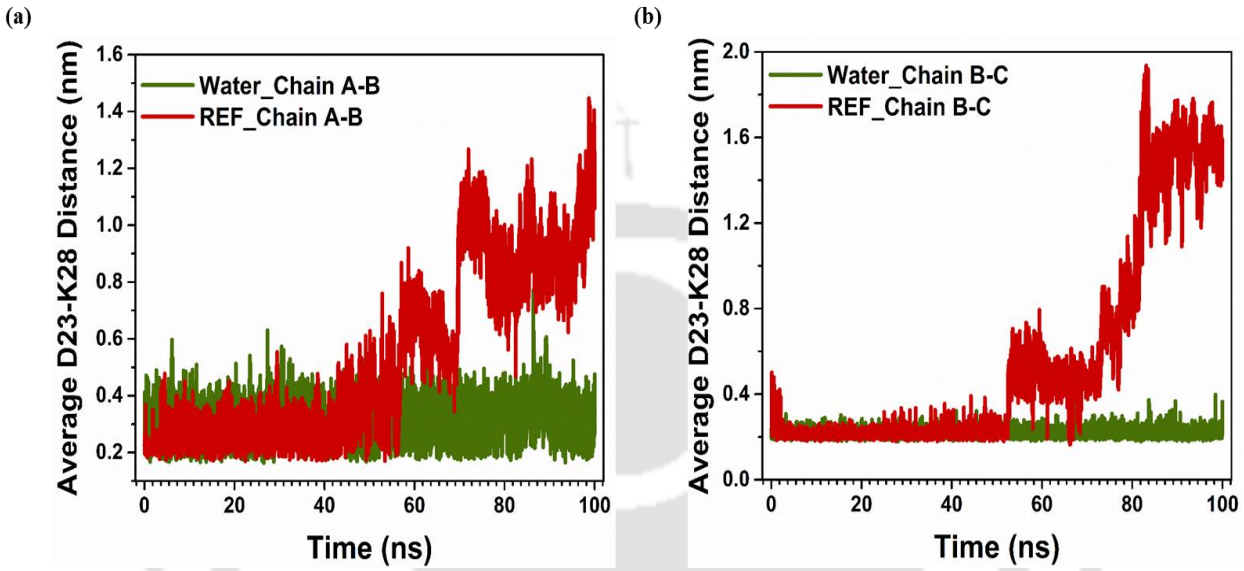

Fig. 5.13. Average D23-K28 distance for Aβ-water and Aβ-REF system (a) between Chain A-B and (b) between Chain B-C.

The profound increment in D23-K28 distance between chain C and D for Aβ-REF (0.54 nm) from Aβ-Water (0.216 nm) system infers breaking of D23-K28 bond in the presence of REF (Fig. 5.14a). The considerable increase of 0.65 nm in D23-K28 average distance (Fig. 5.14b) from Aβ-Water (0.22 nm) to the Aβ-REF system (0.87 nm) points towards the deformation of D23-K28 salt bridge between chain D and E in the presence of REF. The results thus obtained are found to concur with the breaking of salt bridges of Aβ fibril in the presence of copper ions[87], C-60 fullerene[88], and surfactin[89] molecules, leading to destabilization of Aβ oligomer. The relevance of salt bridge disruption in destabilizing the entire Aβ oligomer in the presence of brazilin[22] and a

flavonoid derivative[46] also supports the current observations. Conclusively, the salt bridges, including inter and intra-peptide, are highly compromised due to an increased distance between them. Such an increment in the distance is explained by bulky phenolic rings of the REF, which tries to enter the protofibrillar cavity and thus, destabilizes the entire pentameric structure.

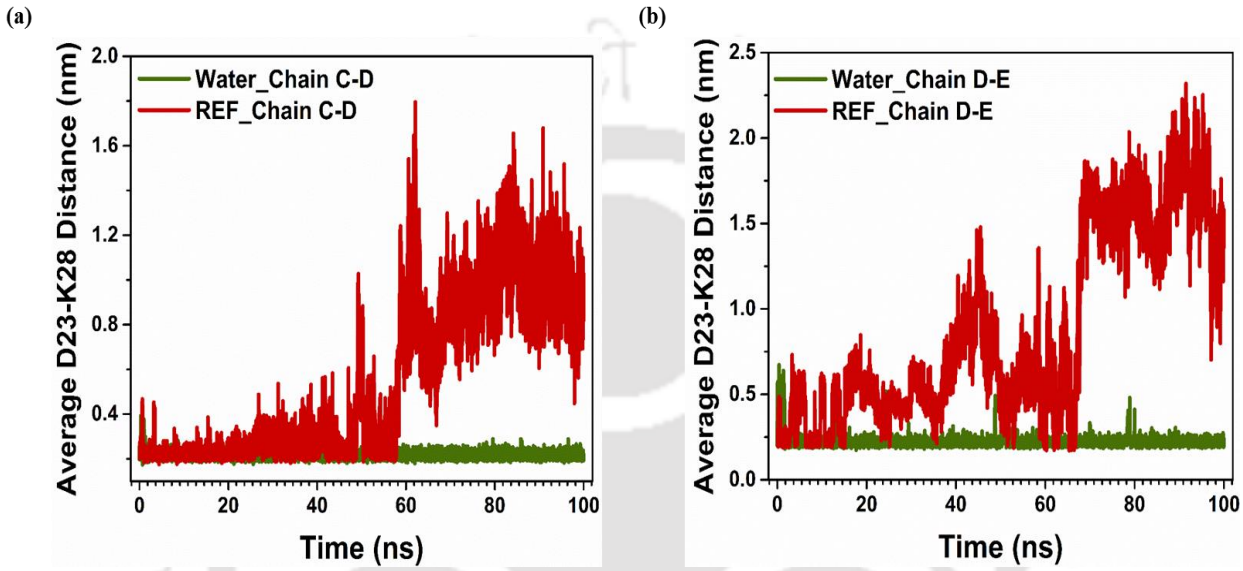

Fig. 5.14. Average D23-K28 distance for Aβ-water and Aβ-REF system (a) between Chain C-D, and (b) between Chain D-E.

5.3.6.3 Hydrophobic contacts

In addition to the electrostatic interactions, hydrophobic interactions also govern the folding and stability of proteins.[90,91] The burying of hydrophobic residues inside the solvent inaccessible cavity provides such high strength to amyloid fibrils.[92–94] According to the principle of PASA (Principle of Amyloid Self-Assembly), the fibrillar structure, which possesses the maximum number of inter and intra-peptide hydrophobic interactions, is the most stable and favorable oligomer structure

during fibrillation process.[95] We have determined the inter-residual distance between F19-G38 for chain A and B, and A21 and V36 for chain D and E in both the systems (viz., Aβ-Water and Aβ-REF).

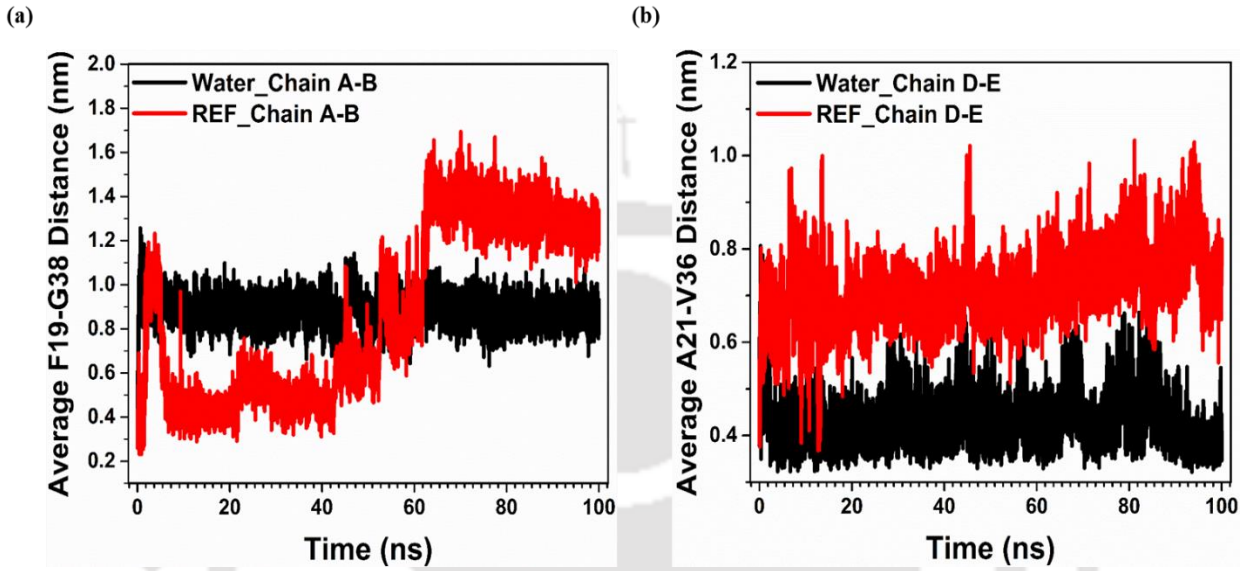

Fig. 5.15. Average F19-G38 distance for Aβ-water and Aβ-REF system (a) between Chain A-B, and (b) Average A21-V36 distance between chain D-E.

The average distance for F19-G38 for chain A and B for Aβ-REF appears to be higher compared to Aβ-Water (Fig. 5.15a). The inter-residual distance for A21-V36 pair for chain D and E are measured as 0.71 nm in Aβ-REF, which is remarkably higher from 0.43 nm in Aβ-Water system (Fig. 5.15b). Similar findings were also recorded in case of chemically synthesized drugs having anti-cholinesterase activity tested *in-vitro* and *in-silico*, causing disruption of preformed Aβ fibrils.[96] This increased distance between hydrophobic residues for both the terminal chains signals breaking of these bonds in the presence of REF, leading to the destabilization of the entire oligomeric structure.

5.3.7 Binding Free Energy analysis between Aβ oligomer and REF

The integration of the MM-PBSA method (see Method Section 2.4 for details) with MD simulation studies has been done with an objective to gain more insights on the binding affinity of phenolic compounds towards Aβ protofibril. The other objective is to verify the docking results with the MM-PBSA. The estimation of binding free energy (BFE) and various other associated energy terms allows more precision on binding by virtue of specific amino acid residues involved in binding.[97] The detailed BFE analysis for all the phenolics has been tabulated in Table 5.3, which gives an insight on the lowest value of $\Delta G_{binding}$ of REF (-82.53 kcal/mol) followed by a relatively higher value for EGT (-59.66 kcal/mol).

The van der Waals contribution seems to be slightly dominating over electrostatic interactions for both the binders (viz., REF and EGT). This observation is attributed to the involvement of hydrophobic residues in binding of REF and EGT with Aβ fibril. The $\Delta G_{binding}$ for both DHC (107.08 kcal/mol) and GDE (31.18 kcal/mol) have been obtained as a positive value, classifying them as non-binders. The trend of binding energy observed by MM-PBSA calculation testifies the docking results and establishes REF as the best binder amongst all the phenolic compounds under investigation. The detailed description of binding energy terms for REF as depicted in Table 5.3 highlights the van der Waals interactions (ΔE_{vdw}= - 89.04 ± 2.56 kcal/mol) and electrostatic interactions (ΔE_{elec}= - 75.49 ± 2.84 kcal/mol) as favorable for binding. The polar contribution to the solvation energy (ΔG_{ps}= 92.33 ± 3.75 kcal/mol) does not favor binding unlike polar contribution of ΔG_{nps} = - 10.34 ± 0.26 kcal/mol. The estimation of all these terms collectively contribute towards the binding free energy, $\Delta G_{binding}$ = - 82.53 ± 9.40 kcal/mol.

Table 5.3. Binding free energy (kcal/mol) between Aβ42 protofibril and all the Phenolics

Energy Terms	Aβ-DHC (Kcal/mol)	Aβ-EGT (Kcal/mol)	Aβ-GDE (Kcal/mol)	Aβ-REF (Kcal/mol)
ΔE_{vdW}	-0.01 ± 0.00	-105.04 ± 4.26	0.00 ± 0.00	-89.04 ± 2.56
ΔE_{elec}	123.14 ± 3.58	-73.10 ± 0.17	-0.10 ± 0.14	-75.49 ± 2.84
$\Delta E_{MM}{}^{a}$	123.13 ± 3.58	-178.14 ± 4.43	-0.10 ± 0.14	-164.52 ± 5.40
ΔG_{ps}	-15.35 ± 2.84	73.70 ± 2.36	-5.30 ± 1.40	92.33 ± 3.75
ΔG_{nps}	-0.70 ± 0.51	44.78 ± 0.46	36.58 ± 0.48	-10.34 ± 0.26
$\Delta G_{solv}{}^{b}$	-16.05 ± 3.35	118.48 ± 2.82	31.28 ± 1.88	81.99 ± 4.01
$\Delta G_{binding}{}^{c}$	107.08 ± 6.93	-59.66 ± 7.25	31.18 ± 2.02	-82.53 ± 9.40

$^{a}\Delta E_{MM} = \Delta E_{vdW} + \Delta E_{elec}$, $^{b}\Delta G_{solv} = \Delta G_{ps} + \Delta G_{nps}$, $^{c}\Delta G_{binding} = \Delta E_{MM} + \Delta G_{solv}$

A similar finding of dominating van der Waals interactions over electrostatic ones have also been reported for binding of AZD2184, a potential PET tracer with Aβ protofibril (2BEG), wherein van der Waals interaction is attributed to the hydrophobic interaction.[47]Further, the individual contribution for the entire oligomer length has been determined and illustrated in Fig. 5.16 to elucidate key residues involved in the binding of REF to Aβ oligomer. Fig. 5.16a clearly unveils the major involvement of chain A in Aβ-REF complexation.

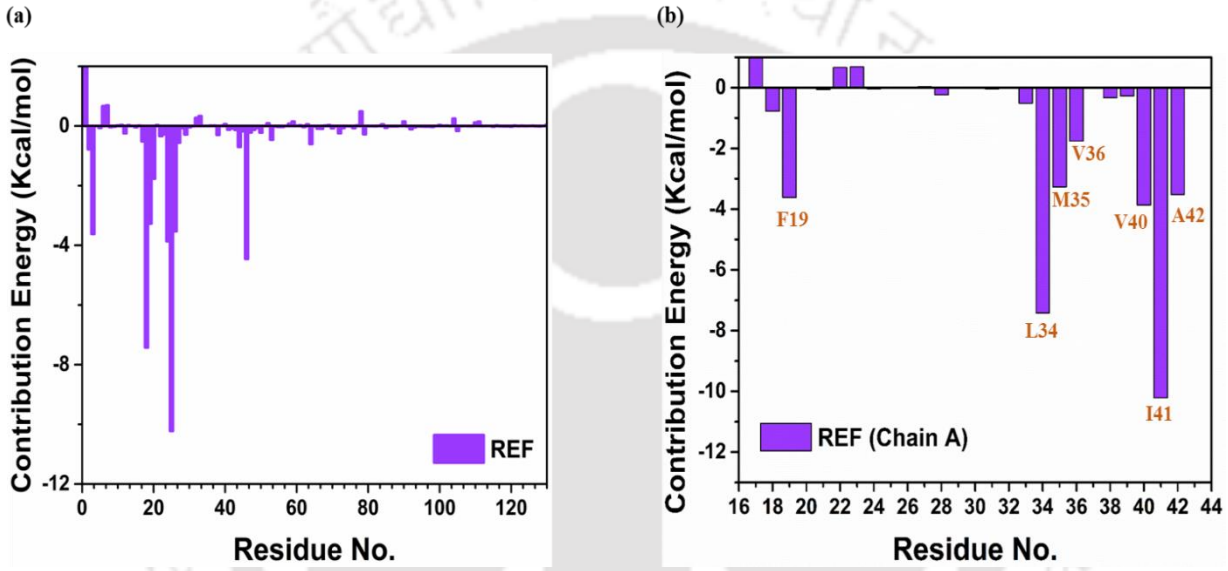

Fig. 5.16. Individual residue contribution to the total binding energy expressed in kcal/mol (a) for the entire Aβ Fibril, and (b) key residues, which contribute the most towards binding of REF with chain A, are indicated with a label in Orange.

A detailed representation of only chain A (Fig. 5.16b) residues demonstrates the involvement of F19, L34, M35, V36, V40, I41, and A42 as key residues for binding to REF. These key residues explain the dual contribution of nonpolar and electrostatic interactions towards Aβ-REF complex formation.[98] These results are also in corroboration with the binding of different

aromatic ligands like curcumin derivatives[99] and biophenols[68] to β2 site of $A\beta_{40}$ fibril involving M35 in the destabilization of these fibrils as studied by MD simulation.

Table 5.4. Inter-chain binding free energy (Kcal/mol) for chain D and E for system Aβ-Water and Aβ-REF complex evaluated by MM-PBSA method

Energy Terms	Interchain (chain D and E) binding energy for Aβ-Water (Kcal/mol)	Interchain (chain D and E) binding energy for Aβ-REF (Kcal/mol)
ΔE_{vdW}	-333.264	-195.630
ΔE_{elec}	-272.517	-81.053
ΔE_{MM^a}	-605.781	-276.683
ΔG_{ps}	443.994	198.096
ΔG_{nps}	-40.843	-23.922
ΔG_{solv^b}	403.151	174.174
$\Delta G_{binding^c}$	-202.63	-102.509

The findings from MM-PBSA analysis harmonizes well with the docking results, and substantiates the entry of REF from terminal chain A. The destabilization effect of REF on terminal chains can be viewed from Table 5.4, where the binding free energy has considerably been reduced for chain D and E in the presence of REF (-102.50 ±5.15 kcal/mol) as compared to the control system Aβ-Water (-202.62±5.73 kcal/mol). The related reports on favorable binding energy calculation of oligoproline leading to destabilization of Aβ protofibril is well synchronized with our findings.[99] The supportive results on destabilization of Aβ pentamer by a di-traizole derivate also resonates with our observation of binding of the ligand to the terminal chain.[100] Determinately, the MM-PBSA results portray the binding of ellagic acid on the terminal chain and thereby causing the destabilization of Aβ oligomer, entrenching it as a promising therapeutic agent for the treatment of AD.

5.4 CONCLUSIONS

In this chapter, the anti-amyloidogenic properties of four phenolic compounds, which include caffeic acid (DHC), epigallocatechin (EGT), gallic acid (GDE) and ellagic acid (REF) have been investigated by means of Docking and MD simulation. Molecular Docking studies discloses REF as the best binder to Aβ oligomer owing to its minimum binding energy. All these docked complexes then subjected to MD simulation subsequently, to gain acumen about the destabilization potential of these phenolics. The VMD representation of the MD trajectory showed perturbations form the oligomer structure by REF. Various parameters like RMSD, Rg, RMSF, and SASA values showed a higher magnitude in the presence of REF, indicating an unstable structure of Aβ oligomer. The destabilization effect of REF was further verified by loss in the number of H-bonds and β-sheet content. The increased distance between D23-K28, F19-G38, and A21-V36 impedes

the formation of inter and intra-chain salt bridges and hydrophobic contacts, thus evoking destabilization of Aβ oligomer due to REF. The binding free energy analysis by the MM-PBSA method corroborates nicely with the docking and simulation results. It revealed that the maximum binding affinity of REF towards chain A of Aβ oligomer is mediated predominantly by Van der Waals interactions. The key residues involved in Aβ-REF complex formation are F19, L34, M35, V36, V40, I41, and A42 from chain A. Moreover, the binding affinity between terminal chains D and E were found to be quite less in the presence of REF, thereby deviating chain E from the Aβ oligomer. The deformation of Aβ oligomer by ellagic acid not only curbs the neurotoxicity but also inhibits the formation of higher order toxic aggregates. The present work provides mechanistic details on the significant role of the ellagic acid in destabilizing Aβ oligomer. These findings pave the pathway for the investigation of other natural compounds for their neurotoxicity, alleviating potential, thereby providing suitable treatment for Alzheimer's disease.

REFERENCES

1 R. Mayeux and Y. Stern, Epidemiology of Alzheimer Disease, *Cold Spring Harbor Perspectives in Medicine*, 2012, **2**, a006239–a006239.

2 G. Evin and A. Weidemann, Biogenesis and metabolism of Alzheimer's disease Aβ amyloid peptides, *Peptides*, 2002, **23**, 1285–1297.

3 R. Kayed, Common Structure of Soluble Amyloid Oligomers Implies Common Mechanism of Pathogenesis, *Science*, 2003, **300**, 486–489.

4 M. A. Findeis, The role of amyloid β peptide 42 in Alzheimer's disease, *Pharmacology & Therapeutics*, 2007, **116**, 266–286.

5 J. Hardy, The Amyloid Hypothesis of Alzheimer's Disease: Progress and Problems on the Road to Therapeutics, *Science*, 2002, **297**, 353–356.

6 D. Mehta, R. Jackson, G. Paul, J. Shi and M. Sabbagh, Why do trials for Alzheimer's disease drugs keep failing? A discontinued drug perspective for 2010-2015, *Expert Opinion on Investigational Drugs*, 2017, **26**, 735–739.

7 P. Deshpande, N. Gogia and A. Singh, Exploring the efficacy of natural products in alleviating Alzheimer's disease, *Neural Regeneration Research*, 2019, **14**, 1321.

8 J. Xiao and R. Shao, EDITORIAL (Natural Products for Treatment of Alzheimer's Disease and Related Diseases: Understanding their Mechanism of Action), *Current Neuropharmacology*, 2013, **11**, 337–337.

9 T. T. Bui and T. H. Nguyen, Natural product for the treatment of Alzheimer's disease, *Journal of Basic and Clinical Physiology and Pharmacology*, 2017, **28**, 413–423.

10 D. J. Newman and G. M. Cragg, Natural products as sources of new drugs over the 30 years from 1981 to 2010, *Journal of Natural Products*, 2012, **75**, 311–335.

11 A. Dey, R. Bhattacharya, A. Mukherjee and D. K. Pandey, Natural products against Alzheimer's disease: Pharmaco-therapeutics and biotechnological interventions, *Biotechnology Advances*, 2017, **35**, 178–216.

12 P. Williams, A. Sorribas and M.-J. R. Howes, Natural products as a source of Alzheimer's drug leads, *Nat. Prod. Rep.*, 2011, **28**, 48–77.

13 G. D'Onofrio, D. Sancarlo, Q. Ruan, Z. Yu, F. Panza, A. Daniele, A. Greco and D. Seripa, Phytochemicals in the Treatment of Alzheimer's Disease: A Systematic Review, *Current Drug Targets*, 2017, **18**, 1487–1498.

14 Habtemariam, Natural Products in Alzheimer's Disease Therapy: Would Old Therapeutic Approaches Fix the Broken Promise of Modern Medicines?, *Molecules*, 2019, **24**, 1519.

15 K. Ono, K. Hasegawa, H. Naiki and M. Yamada, Curcumin has potent anti-amyloidogenic effects for Alzheimer's β-amyloid fibrils in vitro, *Journal of Neuroscience Research*, 2004, **75**, 742–750.

16 K. Jiménez-Aliaga, P. Bermejo-Bescós, J. Benedí and S. Martín-Aragón, Quercetin and rutin exhibit antiamyloidogenic and fibril-disaggregating effects in vitro and potent antioxidant activity in APPswe cells, *Life Sciences*, 2011, **89**, 939–945.

17 A. Pugazhendhi, R. Beema Shafreen, K. Pandima Devi and N. Suganthy, Assessment of antioxidant, anticholinesterase and antiamyloidogenic effect of Terminalia chebula, Terminalia arjuna and its bioactive constituent 7-Methyl gallic acid – An in vitro and in silico studies, *Journal of Molecular Liquids*, 2018, **257**, 69–81.

18 R. Hornedo-Ortega, G. Da Costa, A. B. Cerezo, A. M. Troncoso, T. Richard and M. C. Garcia-Parrilla, In Vitro Effects of Serotonin, Melatonin, and Other Related Indole Compounds on Amyloid-β Kinetics and Neuroprotection, *Molecular Nutrition and Food Research*, 2018, **62**, 1–12.

19 K. Ono, M. Hirohata and M. Yamada, Ferulic acid destabilizes preformed β-amyloid fibrils in vitro, *Biochemical and Biophysical Research Communications*, 2005, **336**, 444–449.

20 M. Awasthi, S. Singh, V. P. Pandey and U. N. Dwivedi, Alzheimer's disease: An overview of amyloid beta dependent pathogenesis and its therapeutic implications along with in silico approaches emphasizing the role of natural products, *Journal of the Neurological Sciences*, 2016, **361**, 256–271.

21 J. Nasica-Labouze, P. H. Nguyen, F. Sterpone, O. Berthoumieu, N.-V. Buchete, S. Coté, A.

De Simone, A. J. Doig, P. Faller, A. Garcia, A. Laio, M. S. Li, S. Melchionna, N. Mousseau, Y. Mu, A. Paravastu, S. Pasquali, D. J. Rosenman, B. Strodel, B. Tarus, J. H. Viles, T. Zhang, C. Wang and P. Derreumaux, Amyloid β Protein and Alzheimer's Disease: When Computer Simulations Complement Experimental Studies, *Chemical Reviews*, 2015, **115**, 3518–3563.

22 W. J. Du, J. J. Guo, M. T. Gao, S. Q. Hu, X. Y. Dong, Y. F. Han, F. F. Liu, S. Jiang and Y. Sun, Brazilin inhibits amyloid β-protein fibrillogenesis, remodels amyloid fibrils and reduces amyloid cytotoxicity, *Scientific Reports*, 2015, **5**, 1–10.

23 Y. Tu, S. Ma, F. Liu, Y. Sun and X. Dong, Hematoxylin inhibits amyloid β-protein fibrillation and alleviates amyloid-induced cytotoxicity, *Journal of Physical Chemistry B*, 2016, **120**, 11360–11368.

24 R. K. Saini, S. Shuaib, D. Goyal and B. Goyal, Insights into the inhibitory mechanism of a resveratrol and clioquinol hybrid against Aβ 42 aggregation and protofibril destabilization: A molecular dynamics simulation study, *Journal of Biomolecular Structure and Dynamics*, 2019, **37**, 3183–3197.

25 J. A. Lemkul and D. R. Bevan, Destabilizing Alzheimer's Aβ 42 Protofibrils with Morin: Mechanistic Insights from Molecular Dynamics Simulations, *Biochemistry*, 2010, **49**, 3935–3946.

26 Y. Jin, Y. Sun, J. Lei and G. Wei, Dihydrochalcone molecules destabilize Alzheimer's amyloid-β protofibrils through binding to the protofibril cavity, *Physical Chemistry Chemical Physics*, 2018, **20**, 17208–17217.

27 Y. Wang, D. C. Latshaw and C. K. Hall, Aggregation of Aβ(17–36) in the Presence of Naturally Occurring Phenolic Inhibitors Using Coarse-Grained Simulations, *Journal of Molecular Biology*, 2017, **429**, 3893–3908.

28 C. Martin, Y. Zhang, C. Tonelli and K. Petroni, Plants, Diet, and Health, *Annual Review of Plant Biology*, 2013, **64**, 19–46.

29 S. H. Omar, Biophenols pharmacology against the amyloidogenic activity in Alzheimer's disease, *Biomedicine & Pharmacotherapy*, 2017, **89**, 396–413.

30 K. Augustin, A. Khabbush, S. Williams, S. Eaton, M. Orford, J. H. Cross, S. J. R. Heales, M. C. Walker and R. S. B. Williams, Mechanisms of action for the medium-chain triglyceride ketogenic diet in neurological and metabolic disorders, *The Lancet Neurology*, 2018, **17**, 84–93.

31 F. Panza, M. Lozupone, V. Solfrizzi, C. Custodero, V. Valiani, A. D'Introno, E. Stella, R. Stallone, M. Piccininni, A. Bellomo, D. Seripa, A. Daniele, A. Greco and G. Logroscino, in *Role of the Mediterranean Diet in the Brain and Neurodegenerative Diseases*, eds. T. Farooqui and A. A. B. T.-R. of the M. D. in the B. and N. D. Farooqui, Academic Press, 2018, pp. 139–155.

32 D. Vauzour, M. Camprubi-Robles, S. Miquel-Kergoat, C. Andres-Lacueva, D. Bánáti, P. Barberger-Gateau, G. L. Bowman, L. Caberlotto, R. Clarke, E. Hogervorst, A. J. Kiliaan, U. Lucca, C. Manach, A. M. Minihane, E. S. Mitchell, R. Perneczky, H. Perry, A. M. Roussel, J. Schuermans, J. Sijben, J. P. E. Spencer, S. Thuret, O. van de Rest, M. Vandewoude, K. Wesnes, R. J. Williams, R. S. B. Williams and M. Ramirez, Nutrition for the ageing brain: Towards evidence for an optimal diet, *Ageing Research Reviews*, 2017, **35**, 222–240.

33 M. C. Morris, The role of nutrition in Alzheimer's disease: epidemiological evidence, *European journal of neurology*, 2009, **16 Suppl 1**, 1–7.

34 N. Gorji, R. Moeini and Z. Memariani, Almond, hazelnut and walnut, three nuts for neuroprotection in Alzheimer's disease: A neuropharmacological review of their bioactive constituents, *Pharmacological Research*, 2018, **129**, 115–127.

35 D. Sul, H.-S. Kim, D. Lee, S. S. Joo, K. W. Hwang and S.-Y. Park, Protective effect of caffeic acid against beta-amyloid-induced neurotoxicity by the inhibition of calcium influx and tau phosphorylation, *Life Sciences*, 2009, **84**, 257–262.

36 J. H. Kim, Q. Wang, J. M. Choi, S. Lee and E. J. Cho, Protective role of caffeic acid in an Aβ 25-35 -induced Alzheimer's disease model, *Nutrition Research and Practice*, 2015, **9**, 480.

37 Y. Liu, T. L. Pukala, I. F. Musgrave, D. M. Williams, F. C. Dehle and J. A. Carver, Gallic

acid is the major component of grape seed extract that inhibits amyloid fibril formation, *Bioorganic and Medicinal Chemistry Letters*, 2013, **23**, 6336–6340.

38 H. Fujiwara, M. Tabuchi, T. Yamaguchi, K. Iwasaki, K. Furukawa, K. Sekiguchi, Y. Ikarashi, Y. Kudo, M. Higuchi, T. C. Saido, S. Maeda, A. Takashima, M. Hara, N. Yaegashi, Y. Kase and H. Arai, A traditional medicinal herb Paeonia suffruticosa and its active constituent 1,2,3,4,6-penta- O -galloyl-β-d-glucopyranose have potent anti-aggregation effects on Alzheimer's amyloid β proteins in vitro and in vivo, *Journal of Neurochemistry*, 2009, **109**, 1648–1657.

39 T. Yuan, H. Ma, W. Liu, D. B. Niesen, N. Shah, R. Crews, K. N. Rose, D. A. Vattem and N. P. Seeram, Pomegranate's Neuroprotective Effects against Alzheimer's Disease Are Mediated by Urolithins, Its Ellagitannin-Gut Microbial Derived Metabolites, *ACS Chemical Neuroscience*, 2016, **7**, 26–33.

40 A. B. Jha, S. S. Panchal and A. Shah, Ellagic acid: Insights into its neuroprotective and cognitive enhancement effects in sporadic Alzheimer's disease, *Pharmacology Biochemistry and Behavior*, 2018, **175**, 33–46.

41 W. Xia and H. Mo, Potential of tocotrienols in the prevention and therapy of Alzheimer's disease, *The Journal of Nutritional Biochemistry*, 2016, **31**, 1–9.

42 H. J. Lim, S. B. Shim, S. W. Jee, S. H. Lee, C. J. Lim, J. T. Hong, Y. Y. Sheen and D. Y. Hwang, Green tea catechin leads to global improvement among Alzheimer's disease-related phenotypes in NSE/hAPP-C105 Tg mice, *Journal of Nutritional Biochemistry*, 2013, **24**, 1302–1313.

43 R. Huey, G. M. Morris, A. J. Olson and D. S. Goodsell, A semiempirical free energy force field with charge-based desolvation, *Journal of Computational Chemistry*, 2007, **28**, 1145–1152.

44 T. Lührs, C. Ritter, M. Adrian, D. Riek-Loher, B. Bohrmann, H. Döbeli, D. Schubert and R. Riek, 3D structure of Alzheimer's amyloid-β(1–42) fibrils, *Proceedings of the National Academy of Sciences*, 2005, **102**, 17342–17347.

45 S. Gupta and A. K. Dasmahapatra, Caffeine destabilizes preformed Aβ protofilaments:

insights from all atom molecular dynamics simulations, *Physical Chemistry Chemical Physics*, 2019, **21**, 22067–22080.

46 A. Kumar, S. Srivastava, S. Tripathi, S. K. Singh, S. Srikrishna and A. Sharma, Molecular insight into amyloid oligomer destabilizing mechanism of flavonoid derivative 2-(4′ benzyloxyphenyl)-3-hydroxy-chromen-4-one through docking and molecular dynamics simulations, *Journal of Biomolecular Structure and Dynamics*, 2016, **34**, 1252–1263.

47 G. Kuang, N. A. Murugan, Y. Tu, A. Nordberg and H. Ågren, Investigation of the Binding Profiles of AZD2184 and Thioflavin T with Amyloid-β(1–42) Fibril by Molecular Docking and Molecular Dynamics Methods, *The Journal of Physical Chemistry B*, 2015, **119**, 11560–11567.

48 K. R. Cousins, Computer Review of ChemDraw Ultra 12.0, *Journal of the American Chemical Society*, 2011, **133**, 8388–8388.

49 G. M. Morris, R. Huey, W. Lindstrom, M. F. Sanner, R. K. Belew, D. S. Goodsell and A. J. Olson, AutoDock4 and AutoDockTools4: Automated docking with selective receptor flexibility, *Journal of Computational Chemistry*, 2009, **30**, 2785–2791.

50 W. A. K. Humphrey Dalke Schulten, *Journal of Molecular Graphics*, 1996, 14, 33–38.

51 D. Van Der Spoel, E. Lindahl, B. Hess, G. Groenhof, A. E. Mark and H. J. C. Berendsen, *Journal of Computational Chemistry*, 2005, 26, 1701–1718.

52 C. Oostenbrink, A. Villa, A. E. Mark and W. F. Van Gunsteren, A biomolecular force field based on the free enthalpy of hydration and solvation: The GROMOS force-field parameter sets 53A5 and 53A6, *Journal of Computational Chemistry*, 2004, **25**, 1656–1676.

53 W. Huang, Z. Lin and W. F. Van Gunsteren, Validation of the GROMOS 54A7 force field with respect to β-peptide folding, *Journal of Chemical Theory and Computation*, 2011, **7**, 1237–1243.

54 A. K. Somavarapu and K. P. Kepp, The Dependence of Amyloid-β Dynamics on Protein Force Fields and Water Models, *ChemPhysChem*, 2015, **16**, 3278–3289.

55 A. W. Schüttelkopf and D. M. F. van Aalten, PRODRG : a tool for high-throughput

crystallography of protein–ligand complexes, *Acta Crystallographica Section D Biological Crystallography*, 2004, **60**, 1355–1363.

56 H. J. C. Berendsen, J. R. Grigera and T. P. Straatsma, The missing term in effective pair potentials, *Journal of Physical Chemistry*, 1987, **91**, 6269–6271.

57 H. Gohlke, C. Kiel and D. A. Case, Insights into protein-protein binding by binding free energy calculation and free energy decomposition for the Ras-Raf and Ras-RalGDS complexes., *Journal of molecular biology*, 2003, **330**, 891–913.

58 N. Homeyer and H. Gohlke, Free energy calculations by the Molecular Mechanics Poisson-Boltzmann Surface Area method, *Molecular Informatics*, 2012, **31**, 114–122.

59 S. Genheden and U. Ryde, The MM/PBSA and MM/GBSA methods to estimate ligand-binding affinities, *Expert Opinion on Drug Discovery*, 2015, **10**, 449–461.

60 R. Kumari, R. Kumar and A. Lynn, g_mmpbsa —A GROMACS Tool for High-Throughput MM-PBSA Calculations, *Journal of Chemical Information and Modeling*, 2014, **54**, 1951–1962.

61 P. K. Kanchi and A. K. Dasmahapatra, Polyproline chains destabilize the Alzheimer's amyloid-β protofibrils: A molecular dynamics simulation study, *Journal of Molecular Graphics and Modelling*, 2019, **93**, 107456.

62 R. H. Khan, M. K. Siddiqi, V. N. Uversky and P. Salahuddin, Molecular docking of Aβ 1–40 peptide and its Iowa D 23 N mutant using small molecule inhibitors: Possible mechanisms of Aβ-peptide inhibition, *International Journal of Biological Macromolecules*, 2019, **127**, 250–270.

63 Anthony J. Busti, The Inhibitory Constant (Ki) and its Use in Understanding Drug Interactions.

64 F. Peccati, S. Pantaleone, V. Riffet, X. Solans-Monfort, J. Contreras-García, V. Guallar and M. Sodupe, Binding of Thioflavin T and Related Probes to Polymorphic Models of Amyloid-β Fibrils, *Journal of Physical Chemistry B*, 2017, **121**, 8926–8934.

65 N. A. Murugan, C. Halldin, A. Nordberg, B. Långström and H. Ågren, The Culprit Is in the

Cave: The Core Sites Explain the Binding Profiles of Amyloid-Specific Tracers, *The Journal of Physical Chemistry Letters*, 2016, **7**, 3313–3321.

66 C. Yang, X. Zhu, J. Li and R. Shi, Exploration of the mechanism for LPFFD inhibiting the formation of β-sheet conformation of Aβ(1-42) in water, *Journal of Molecular Modeling*, 2010, **16**, 813–821.

67 F. Azam, N. H. Alabdullah, H. M. Ehmedat, A. R. Abulifa, I. Taban and S. Upadhyayula, NSAIDs as potential treatment option for preventing amyloid β toxicity in Alzheimer's disease: an investigation by docking, molecular dynamics, and DFT studies, *Journal of Biomolecular Structure and Dynamics*, 2018, **36**, 2099–2117.

68 F. Tavanti, A. Pedone and M. Menziani, Computational Insight into the Effect of Natural Compounds on the Destabilization of Preformed Amyloid-β(1–40) Fibrils, *Molecules*, 2018, **23**, 1320.

69 B. Han, Y. Liu, S. W. Ginzinger and D. S. Wishart, SHIFTX2: Significantly improved protein chemical shift prediction, *Journal of Biomolecular NMR*, 2011, **50**, 43–57.

70 J. Lincoff, S. Sasmal and T. Head-Gordon, The combined force field-sampling problem in simulations of disordered amyloid-β peptides, *The Journal of Chemical Physics*, 2019, **150**, 104108.

71 H.-M. Fan, R.-X. Gu, Y.-J. Wang, Y.-L. Pi, Y.-H. Zhang, Q. Xu and D.-Q. Wei, Destabilization of Alzheimer's Aβ42 Protofibrils with a Novel Drug Candidate wgx-50 by Molecular Dynamics Simulations, *The Journal of Physical Chemistry B*, 2015, **119**, 11196–11202.

72 W. M. Berhanu and U. H. E. Hansmann, Side-chain hydrophobicity and the stability of Aβ 16-22 aggregates, *Protein Science*, 2012, **21**, 1837–1848.

73 S. S. Barale, R. S. Parulekar, P. M. Fandilolu, M. J. Dhanavade and K. D. Sonawane, Molecular Insights into Destabilization of Alzheimer's Aβ Protofibril by Arginine Containing Short Peptides: A Molecular Modeling Approach, *ACS Omega*, 2019, **4**, 892–903.

74 W. Kabsch and C. Sander, Dictionary of protein secondary structure: Pattern recognition of

hydrogen-bonded and geometrical features, *Biopolymers*, 1983, **22**, 2577–2637.

75 R. K. Saini, S. Shuaib and B. Goyal, Molecular insights into Aβ 42 protofibril destabilization with a fluorinated compound D744: A molecular dynamics simulation study, *Journal of Molecular Recognition*, 2017, **30**, e2656.

76 Y. Zou, Z. Qian, Y. Chen, H. Qian, G. Wei and Q. Zhang, Norepinephrine Inhibits Alzheimer's Amyloid-β Peptide Aggregation and Destabilizes Amyloid-β Protofibrils: A Molecular Dynamics Simulation Study, *ACS Chemical Neuroscience*, 2019, **10**, 1585–1594.

77 J. Zheng, H. Jang, B. Ma, C.-J. Tsai and R. Nussinov, Modeling the Alzheimer Aβ17-42 Fibril Architecture: Tight Intermolecular Sheet-Sheet Association and Intramolecular Hydrated Cavities, *Biophysical Journal*, 2007, **93**, 3046–3057.

78 M. Sunde, L. C. Serpell, M. Bartlam, P. E. Fraser, M. B. Pepys and C. C. Blake, Common core structure of amyloid fibrils by synchrotron X-ray diffraction., *Journal of molecular biology*, 1997, **273**, 729–39.

79 K. J. Siebert, N. V. Troukhanova and P. Y. Lynn, Nature of Polyphenol−Protein Interactions, *Journal of Agricultural and Food Chemistry*, 1996, **44**, 80–85.

80 J. E. Donald, D. W. Kulp and W. F. DeGrado, Salt bridges: Geometrically specific, designable interactions, *Proteins: Structure, Function and Bioinformatics*, 2011, **79**, 898–915.

81 B. Musafia, V. Buchner and D. Arad, Complex salt bridges in proteins: Statistical analysis of structure and function, *Journal of Molecular Biology*, 1995, **254**, 761–770.

82 S. Kumar and R. Nussinov, Close-Range Electrostatic Interactions in Proteins, *ChemBioChem*, 2002, **3**, 604.

83 H. R. Bosshard, D. N. Marti and I. Jelesarov, Protein stabilization by salt bridges: concepts, experimental approaches and clarification of some misunderstandings, *Journal of Molecular Recognition*, 2004, **17**, 1–16.

84 I. Jelesarov and A. Karshikoff, in *Methods in molecular biology (Clifton, N.J.)*, 2009, vol.

490, pp. 227–260.

85 X. Ban, P. Lahiri, A. S. Dhoble, D. Li, Z. Gu, C. Li, L. Cheng, Y. Hong, Z. Li and B. Kaustubh, Evolutionary Stability of Salt Bridges Hints Its Contribution to Stability of Proteins, *Computational and Structural Biotechnology Journal*, 2019, **17**, 895–903.

86 G. Reddy, J. E. Straub and D. Thirumalai, Influence of Preformed Asp23−Lys28 Salt Bridge on the Conformational Fluctuations of Monomers and Dimers of Aβ Peptides with Implications for Rates of Fibril Formation, *The Journal of Physical Chemistry B*, 2009, **113**, 1162–1172.

87 D. Q. H. Pham, M. S. Li and G. La Penna, Copper Binding Induces Polymorphism in Amyloid-β Peptide: Results of Computational Models, *Journal of Physical Chemistry B*, 2018, **122**, 7243–7252.

88 S. A. Andujar, F. Lugli, S. Höfinger, R. D. Enriz and F. Zerbetto, Amyloid-β fibril disruption by C 60 - Molecular guidance for rational drug design, *Physical Chemistry Chemical Physics*, 2012, **14**, 8599–8607.

89 A. Verma, A. Kumar and M. Debnath, Molecular docking and simulation studies to give insight of surfactin amyloid interaction for destabilizing Alzheimer's Aβ42 protofibrils, *Medicinal Chemistry Research*, 2016, **25**, 1616–1622.

90 M. S. Dutta and S. Basu, Identifying the key residues instrumental in imparting stability to amyloid beta protofibrils – a comparative study using MD simulations of 17–42 residues, *Journal of Biomolecular Structure and Dynamics*, 2021, **39**, 431–456.

91 K. E. Marshall, K. L. Morris, D. Charlton, N. O'Reilly, L. Lewis, H. Walden and L. C. Serpell, Hydrophobic, Aromatic, and Electrostatic Interactions Play a Central Role in Amyloid Fibril Formation and Stability, *Biochemistry*, 2011, **50**, 2061–2071.

92 H. J. Dyson, P. E. Wright and H. A. Scheraga, The role of hydrophobic interactions in initiation and propagation of protein folding, *Proceedings of the National Academy of Sciences*, 2006, **103**, 13057–13061.

93 J. T. Kellis, K. Nyberg, D. S˘ail and A. R. Fersht, Contribution of hydrophobic interactions to protein stability, *Nature*, 1988, **333**, 784–786.

94 C. N. Pace, H. Fu, K. L. Fryar, J. Landua, S. R. Trevino, B. A. Shirley, M. M. Hendricks, S. Iimura, K. Gajiwala, J. M. Scholtz and G. R. Grimsley, Contribution of Hydrophobic Interactions to Protein Stability, *Journal of Molecular Biology*, 2011, **408**, 514–528.

95 B. Tarus, J. E. Straub and D. Thirumalai, Dynamics of Asp23−Lys28 Salt-Bridge Formation in Aβ 10-35 Monomers, *Journal of the American Chemical Society*, 2006, **128**, 16159–16168.

96 S. Brogi, S. Butini, S. Maramai, R. Colombo, L. Verga, C. Lanni, E. De Lorenzi, S. Lamponi, M. Andreassi, M. Bartolini, V. Andrisano, E. Novellino, G. Campiani, M. Brindisi and S. Gemma, Disease-modifying anti-Alzheimer's drugs: Inhibitors of human cholinesterases interfering with β-amyloid aggregation, *CNS Neuroscience and Therapeutics*, 2014, **20**, 624–632.

97 M. Karami, C. Jalali and S. Mirzaie, Combined virtual screening, MMPBSA, molecular docking and dynamics studies against deadly anthrax: An in silico effort to inhibit Bacillus anthracis nucleoside hydrolase, *Journal of Theoretical Biology*, 2017, **420**, 180–189.

98 F.-F. Liu, Z. Liu, S. Bai, X.-Y. Dong and Y. Sun, Exploring the inter-molecular interactions in amyloid-β protofibril with molecular dynamics simulations and molecular mechanics Poisson-Boltzmann surface area free energy calculations, *The Journal of Chemical Physics*, 2012, **136**, 145101.

99 G. Orteca, F. Tavanti, Z. Bednarikova, Z. Gazova, G. Rigillo, C. Imbriano, V. Basile, M. Asti, L. Rigamonti, M. Saladini, E. Ferrari and M. C. Menziani, Curcumin derivatives and Aβ-fibrillar aggregates: An interactions' study for diagnostic/therapeutic purposes in neurodegenerative diseases, *Bioorganic & Medicinal Chemistry*, 2018, **26**, 4288–4300.

100 A. Kaur, S. Shuaib, D. Goyal and B. Goyal, Interactions of a multifunctional di-triazole derivative with Alzheimer's Aβ 42 monomer and Aβ 42 protofibril: a systematic molecular dynamics study, *Physical Chemistry Chemical Physics*, 2020, **22**, 1543–1556.

Chapter 6

Destabilization of Aβ fibrils by Omega-3 Polyunsaturated Fatty Acids: A Molecular Dynamics study

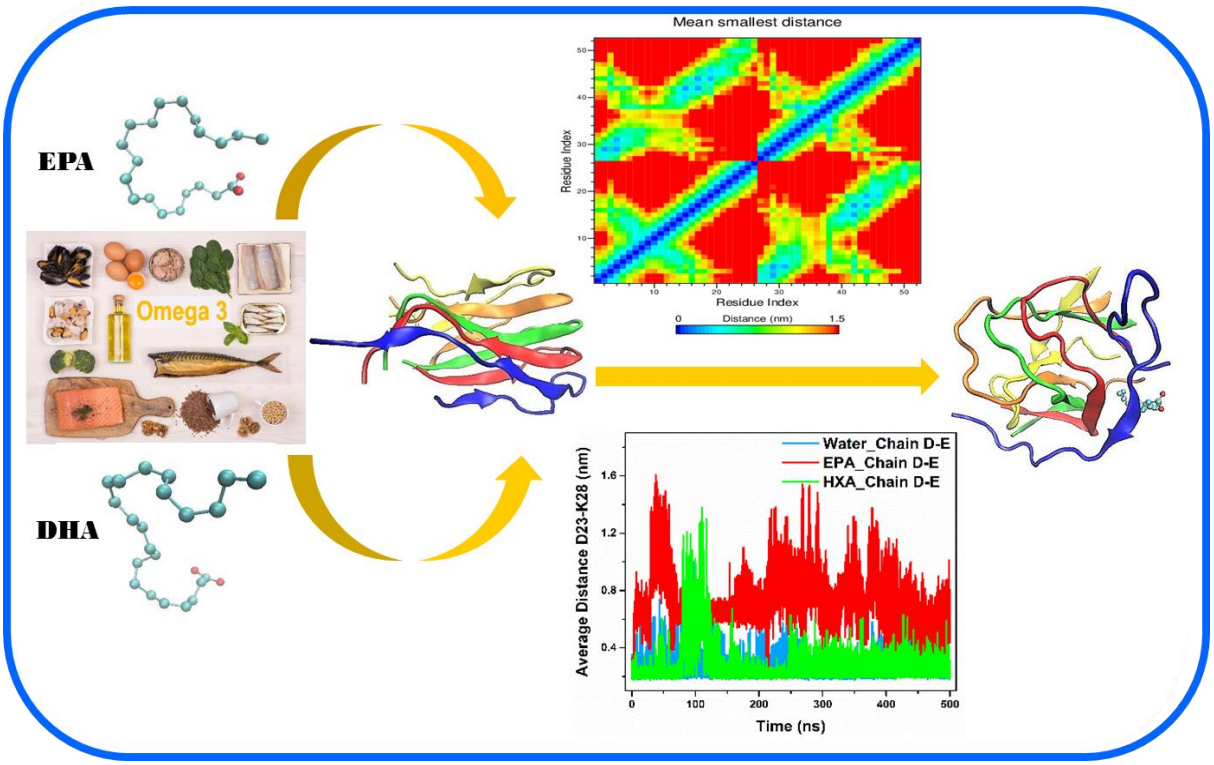

In the current study, we have investigated three ω-3 PUFAs viz., Eicosapentaenoic acid (EPA), Docosahexaenoic acid (HXA) and α-linolenic acid (LNL) by molecular dynamics simulation. The increased value of RMSD, radius of gyration, and SASA, and reduced number of H-bonds and β-

sheet content, disruption of salt bridges and hydrophobic contacts and formation of new bonds between the tail of PUFA and hydrophobic residues of Aβ fibril, leading to the destabilization of fibril. The MM-PBSA results explains the binding of EPA and HXA to Aβ fibril by interacting with different residues. The destabilization potential of EPA and HXA establishes them as promising drug leads to cure AD, and encourages prospecting of other fatty acids for therapeutic intervention in AD.

6.1 INTRODUCTION

The dementia and cognitive imbalance associated with the Alzheimer's Disease is the major concern to the global healthcare system. The dietary interventions of healthy foods are reported to delay, arrest and reverse the progression of cognitive impairment in humans.[1] Numerous epidemiological studies have also fostered the positive correlation between high adherence to Mediterranenan diet (MeDi) with lower risk of cognitive decline, lower incidences of AD, enhanced learning and memory function and lower mortality rate in AD.[2] MeDi is rich in polyphenols, flavonoids and good amount of protein, due to inclusion of various fruits, vegetables, nuts and fish. MeDi also provides a great source of healthy essential fatty acids (FAs) as well due to the presence of fish. Essential FAs are the ones that can't be synthesized by humans and hence demands dietary consumption[3] from plants or other natural sources. The omega-3 (ω-3) FAs are one such essential FAs which are long chain polyunsaturated FAs (PUFAs), having double bonds from 3rd carbon from the methyl end. The prime precursor for ω-3 FAs in humans are LNL (α-linolenic acid, C18:3).[4] The LNL is plant based PUFA, found majorly in chia seeds, flaxseeds, soybean seeds, walnuts and almonds[5] which gets metabolized inside the human body to EPA

(Eicosapentaenoic acid, C20:5) and HXA (Docosahexaenoic acid, C22:6) but with limited percentage of conversion.[6] This limited conversion and less bioavailability can be compensated by dietary supplementation of EPA and HXA. The rich sources of EPA and HXA are mainly marine fish or fish oil,[7] macroalgae and microalgae.[8]

The critical role of ω-3 PUFAs particularly EPA and HXA, in memory and learning,[9] anti-inflammation in CNS disorders,[10,11] neurotrophicity,[12] prevention of psychosis in adults[13] and lower incidence of AD[14] is exemplary. Being the major constituent of the neuronal cells, PUFAs are involved in membrane fluidity, optimal synaptic communication between cells and neuroprotection.[15] The low levels of these PUFAs are reported to have implications in overall neuropsychiatric health including AD,[16–18] thereby causing cognitive decline and commencing dementia. The fish consumption has been recommended as a part of MeDi owing to its higher contents of EPA and HXA, for maintaining cognitive resilience and memory associated functions.[19] There is a crucial evidence on permeation of EPA and HXA through BBB (Blood brain barrier) that helps in maintaining membrane integrity.[20] Passage through BBB, EPA and HXA also reinforces Aβ clearance from brain to blood thereby obviating Aβ accumulation in brain.[21] These findings emphasizes on consumption of fish, walnuts and almonds, rich in EPA and HXA for overall good health of BBB and brain.[22] In addition to that, diet supplementation with EPA and HXA was also found supportive in reducing the amyloid burden in older rats[23] and conversely their deficiency invokes depression and loss of memory.[16] These PUFAs were also reported to induce microglial phagocytosis of Aβ peptides.[24] In-vitro and cytotoxic studies on SH-SY5Y cell lines revealed the inhibitory potential of HXA by preventing $A\beta_{1\text{-}42}$ polymerization.[25] A recent report on direct interaction of EPA and HXA with Aβ peptides led to 16-84% inhibition in fibrillogenesis of the peptides.[26] These PUFAs also have stimulatory effect on IDE (Insulin

degrading enzyme) leading to degradation of Aβ peptide.[27] The reduction of amyloidogenic processing of APP by stimulating β and γ secretase by HXA[28] consonances well with the beneficial role of these ω-3 fatty acid as possible drug leads for the treatment of AD.

The computational studies not only traverse atomic-scale mechanisms by means of MD simulations but also validates results obtained by *in-vitro* studies as well.[29] A simulation study that reported adsorption of Aβ peptides over the cell membrane in the presence of PUFAs cause weaker interactions between the peptides itself. This leads to the inhibition of aggregation of Aβ peptides, thereby restricting the progression of AD.[30] A recent study on inhibition of aggregation prone fragment (KLVFFA) of Aβ peptide by HXA helps in understanding its inhibitory potential.[31] The beneficial effects of PUFAs in improving AD by various routes has been provided; however, the direct interaction and destabilization of Aβ fibrils by EPA and HXA is still not properly understood. The unavailability of enough reports instigates the need for more computational based studies to gain insight into the plausible destabilization mechanism of Aβ fibrils by PUFAs.

In the present work, the focus has been led upon investigating the atomistic details of the destabilization mechanism of Aβ fibrils by ω-3 PUFAs. The present study was conducted by MD simulation, which facilitates drug designing in lieu to formulate a clinically approved drug to treat AD. The substantial increase in RMSD and radius of gyration (R_g) demarcates disorganization of Aβ fibril structure in the presence of EPA and HXA as compared to LNL when each of the complex systems were simulated for 300 ns. To acquire more in-depth details, the Aβ-EPA and Aβ-HXA complexes have been subjected to longer simulation time of 500 ns. The disruption of H-bonds (hydrogen bonds), salt bridges and breaking of hydrophobic contacts confirms destabilization of the Aβ fibril in the presence of EPA and HXA. These PUFAs were observed to insert themselves in the hydrophobic cavity of the fibril owing to their amphipathic property. The insertion in the

cavity is due to flexibility of PUFAs and the chemical interaction involving different residues in Aβ fibril highlights amphiphilic nature of EPA and HXA. The hydrophilic carboxylic head is found to interact with positively charged lysine (K) residue; whereas, the hydrophobic carbon tail manages to form bonds with other hydrophobic residues in the fibril well testified by MM-PBSA (Molecular Mechanics Poisson-Boltzmann Surface Area) analysis. These interactions of PUFAs with different residues in Aβ fibril competes with native interactions of Aβ fibril leading to its destabilization. The results thus obtained after MD simulation establishes both EPA and HXA as potent disruptors of Aβ fibril and thus a promising drug lead for the treatment of AD.

6.2 METHODS

6.2.1 Selection of PUFAs and Aβ17-42 Fibril for Molecular Dynamics Simulation

Three-dimensional structure of $A\beta_{17-42}$ fibril (PDB ID: 2BEG)[32] was taken from the protein data bank (PDB) and was used as the receptor protein in the current study. The Aβ fibril is a pentamer structure spanning from residues 17-42, which forms the characteristic β-sheet, the prerequisite for fibrillation and stable organization of amyloid structures. The characteristic β-sheet structure is further divided into three regions - β1 region (18-26 residues), turn region (27-30 residues), and β2 region (31-42 residues) as depicted in Fig. 6.1a as derived from VMD (visual molecular dynamics) package.[33]There are five chains in 2BEG, designated as A, B, C, D, and E, having the same primary sequence, with A and E being the terminal chains. 2BEG as the representative model for Aβ fibril, employed in numerous studies owing to its well established and stable structure.[34–37] The ligands that are investigated in the study are ω-3 PUFAs viz. Eicosapentaenoic acid (EPA),

Docosahexaenoic acid (HXA) and α-linolenic acid (LNL). The PDB structures for all of these PUFAs have been taken from the ligand summary page as EPA.pdb, HXA.pdb, and LNL.pdb, respectively, and drawn by using ChemDraw[38] as shown in Fig. 6.1b-d. The definition for all the systems, for MD simulation, has been depicted in Table 6.1 as S0, S1, S2, and S3 where S0 represents the control system i.e. without ligand.

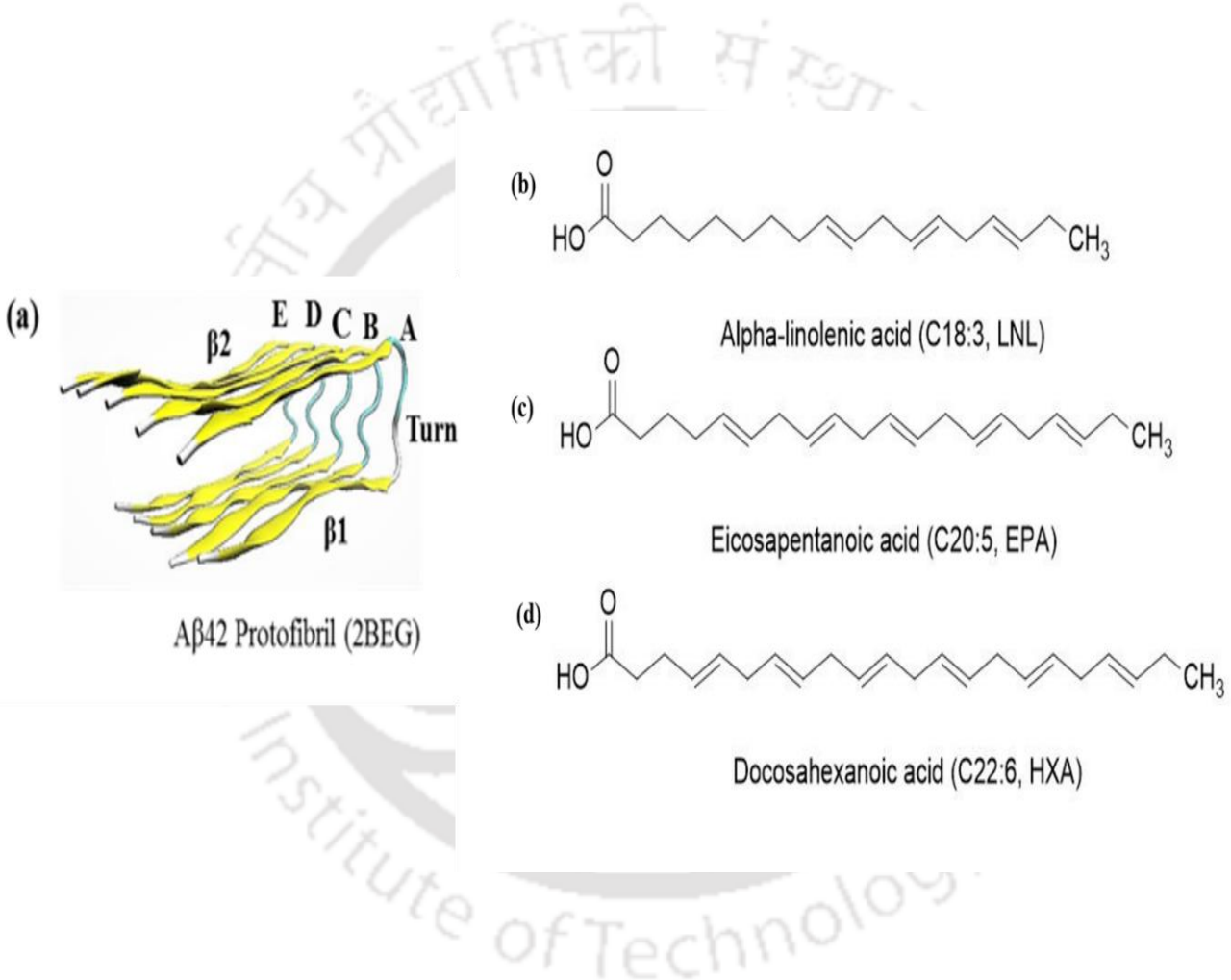

Fig. 6.2. Initial configuration of (a) Aβ fibril, (b) α-linolenic acid (LNL), (c) Eicosapentaenoic acid (EPA), and (d) Docosahexaenoic acid (HXA) taken from RSCB protein data bank.

Table 6.1. System definition for Molecular Dynamics Simulation

System Index	Receptor	Ligand	Complex Index (.gro) for MD simulation
S0	2BEG.pdb (Aβ fibril)	No ligand	Control = C0 (Aβ+Water)
S1	2BEG.pdb (Aβ fibril)	EPA.pdb (Eicosapentaenoic acid)	Test 1 = C1 (Aβ+EPA)
S2	2BEG.pdb (Aβ fibril)	HXA.pdb (Docosahexaenoic acid)	Test 2= C2 (Aβ+HXA)
S3	2BEG.pdb (Aβ fibril)	LNL.pdb (Alpha-linolenic acid)	Test 3 = C3 (Aβ+LNL)

6.2.2 Molecular Dynamics Simulation of PUFAs with Aβ fibril

The interaction between PUFAs and Aβ fibril (ω-3-Aβ) has been studied by MD simulation using GROMACS v5.1.1,[39] with GROMOS 96 54a7[40–42] force field. The same force field has been employed in various other studies as well for system definition.[35,40,43–48] The ligand topologies

obtained from rscb pdb database have been submitted to PRODRG server[49] to generate gromos defined coordinates, which are GROMACS readable. The topologies thus obtained for PUFAs in .gro format were then combined with Aβ fibril by means of random insertion to form protein-ligand complexes: C1 (Aβ-EPA), C2 (Aβ-HXA), C3 (Aβ-LNL), and C0 as (Aβ-Water) (Table 6.1). Further, the simulation procedure is the same as has been explained in section 4.2.2 of chapter 4 for 300 ns for initial screening of all the PUFAs. Further, the simulation time has been increased to 500 ns for the selected PUFAs amongst investigated molecules to gain insights into the mechanism of the interaction between protein and ligand. To check the statistical significance and reproducibility of the results, three sets of each system have been simulated and the data is represented as an average over three sets.

6.2.3 Analysis of MD generated Trajectories

We have calculated various parameters using different tools defined within the GROMACS v5.1.1 package. The parameters that were analyzed to measure structural changes in Aβ fibril structure were same as has been explained in section 4.2.3 of chapter 4. Additionally, the interchain distance for neighboring terminal chains have been calculated by g_mdmat to gain knowledge about the possible interactions via a distance matrix called contact map.

6.2.4 Binding Mode analysis by MM-PBSA

The binding free energy (BFE) of the Aβ fibril with the selected PUFA was calculated by MM-PBSA.[50–52] The package was used within the gromacs environment by g_mmpbsa tool, which

calculated the overall binding energy and individual residue contribution.[53] MM-PBSA calculates the BFE from the MD trajectory based on the following equation:

$$\Delta G^{bind} = \Delta E_{MM} + \Delta G^{psolv} + \Delta G^{npsolv} - T\Delta S$$

where,$\Delta E_{MM}$is the molecular mechanics contribution in vacuum, $\Delta G^{psolv}$is the polar contribution of solvation energy, calculated by the Poisson-Boltzmann equation and $\Delta G^{npsolv}$is the nonpolar contribution towards binding, determined by solvent accessible surface area (SASA) model. The high computational demand limits the calculation of entropy contribution. Moreover, the relative change in entropy contribution (ΔS) towards free energy calculation is negligible and thus can be ignored.[54–57] The calculation of BFE in the present study was done on the last 20 ns trajectory with Δt = 100 ps to reduce the computational time. The energetic contribution of individual residues was also quantified to identify key residues actively involved in binding with PUFAs. The solute and solvent dielectric constants were taken as 4 and 80, respectively.

6.3 RESULTS AND DISCUSSIONS

6.3.1 Molecular dynamics Simulation of PUFAs with Aβ fibril

The simulation studies were conducted for 300 ns for all the three PUFA compounds to test their destabilization potency. The system definition has been tabulated in Table 6.1 in methods section. The global stability parameters like Cα-RMSD, Rg and SASA, have been calculated for all the complex systems, which demarcated a trend of EPA and HXA being destabilizers of equal strength as compared to LNL. The Cα-RMSD value for Aβ fibril has been calculated for the entire protein, and for the terminal chain E, separately. The higher value is observed from the time trajectory of

Cα-RMSD for the entire protein (Fig. 6.2a) and for the chain E (Fig. 6.2b) for Aβ-EPA and Aβ-HXA systems as compared to the Aβ-Water. This increase in RMSD clearly establishes the destabilization of the Aβ fibril in the presence of EPA and HXA. However, LNL is found to be not much effective as a potential disruptor. The corresponding average Cα-RMSD values for the entire protein and for the chain E has been plotted for all the systems under investigation as probability density functions (PDFs) in Fig. 6.2 c and d.

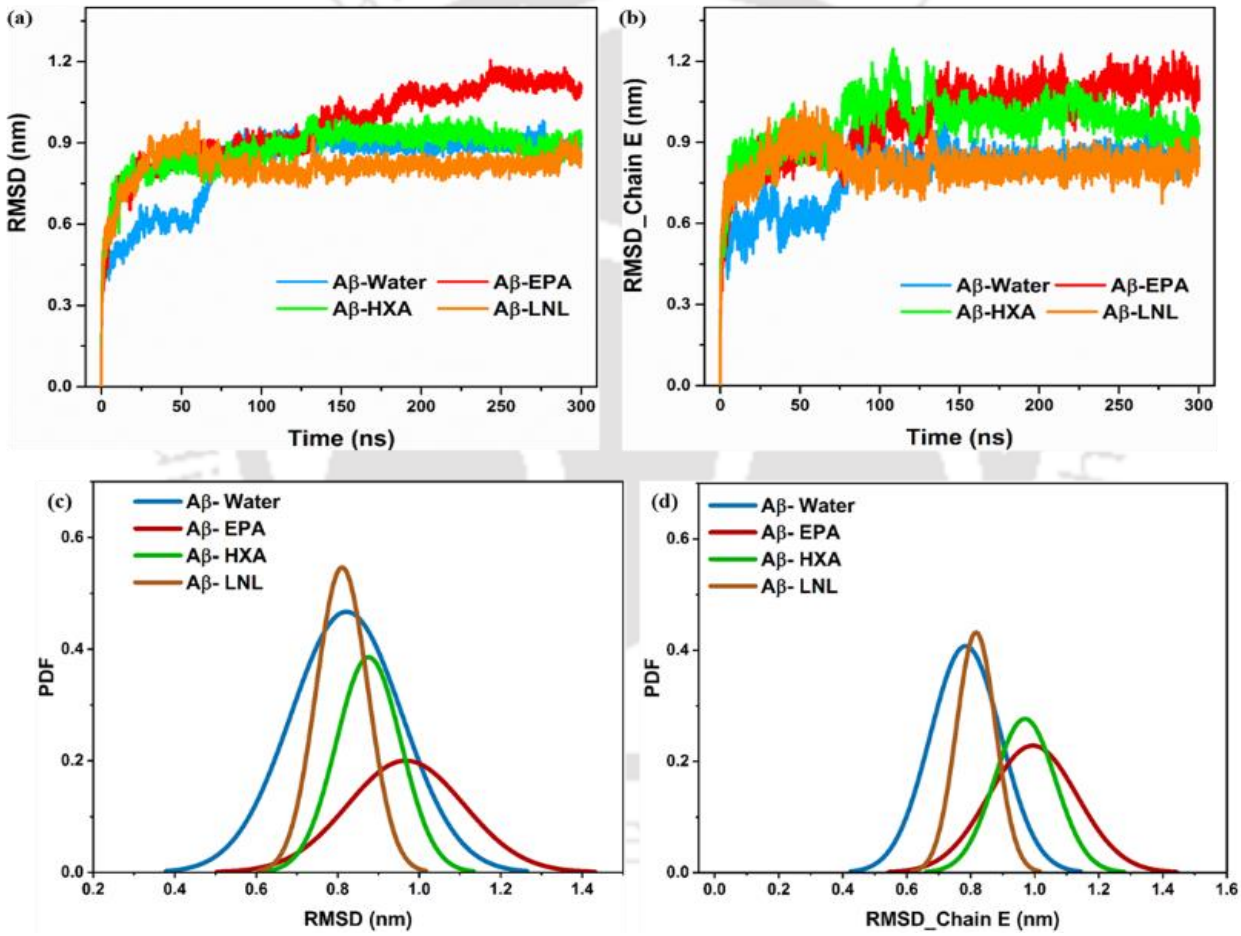

Fig. 6.3. Time trajectory and PDFs for Cα-RMSD of Aβ in water and all 3 PUFAs (a and c) for whole protein and (b and d) for chain E.

The increase in average RMSD value of 0.967 nm for Aβ-EPA system cause shift in the curve as compared to Aβ-water system. From Fig. 6.2c, it is clearly observed that Aβ-LNL system records sharpest peak with average value of 0.810 nm close to 0.821 nm of Aβ-Water system. The marginal increased RMSD value of 0.875 nm in Aβ-HXA system directs towards further investigation. Similarly, from Fig. 6.2d, increased RMSD value for chain E highlights on the potential of EPA and HXA as better destabilizer as compared to LNL. The demonstrated structural instability of Aβ fibril is also reported by other natural compounds which supports our findings.[36]

The higher Rg value for Aβ-EPA and Aβ-HXA as compared to the Aβ-water system as (Fig. 6.3a and c) indicates the decreased compactness of the fibrillar structure in the presence of these PUFAs. The trend of SASA (Fig. 6.3b and d) may not be enough to claim destabilization potential of HXA. However, a marginal increase of SASA by EPA and decrease in the presence of LNL motivates further testing of EPA and HXA, discarding LNL at this stage itself. A similar increase in Rg and SASA values of Aβ protofibril by a flavonoid derivative[58] and arginine containing short peptides[43] respectively leading to destabilization of Aβ protofibril corroborates well with our findings. These observations helped in eliminating LNL for extended run and thereby restricting further investigations to EPA and HXA only to look for the better destabilizer amongst the two.

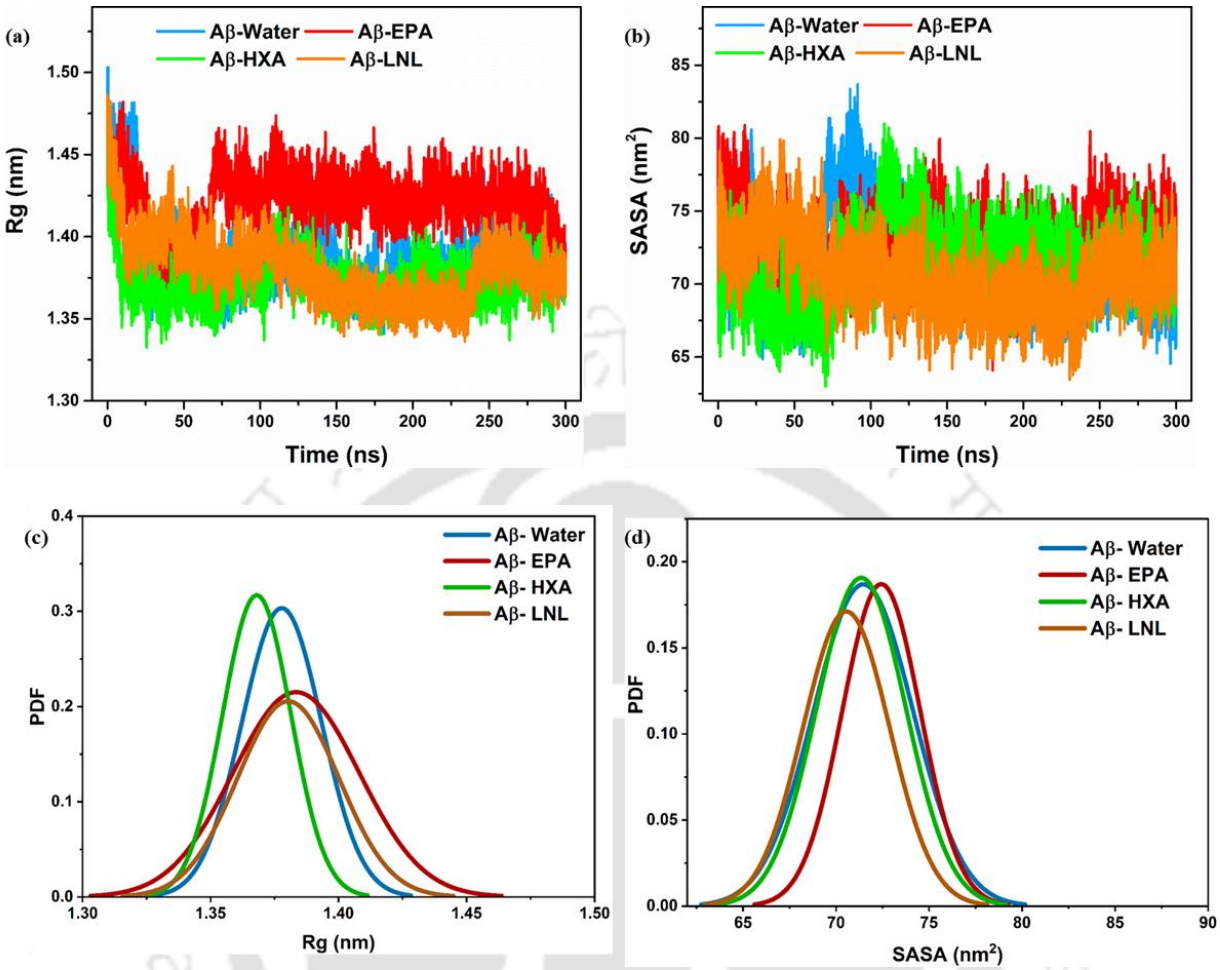

Fig. 6.4. Time trajectory and PDFs for (a and c) Rg and (b and d) SASA of 2BEG in water and all 3 PUFAs.

The extension of production run up to 500 ns for three systems, Aβ-water (C0), Aβ-EPA (C1) and Aβ-HXA (C2) has been visualized and computed with several other parameters to gain atomistic details on the destabilization mechanism of these PUFAs. The VMD visualization of the final configuration of C0, C1 and C2 system has been presented in Fig. 6.4a-c, respectively. The snapshots (Fig. 6.4a-c) of the trajectory for Aβ fibril showed binding of the PUFA molecules with

Aβ fibril leading to high degree of perturbations in the fibril indicating destabilization potential of EPA and HXA.

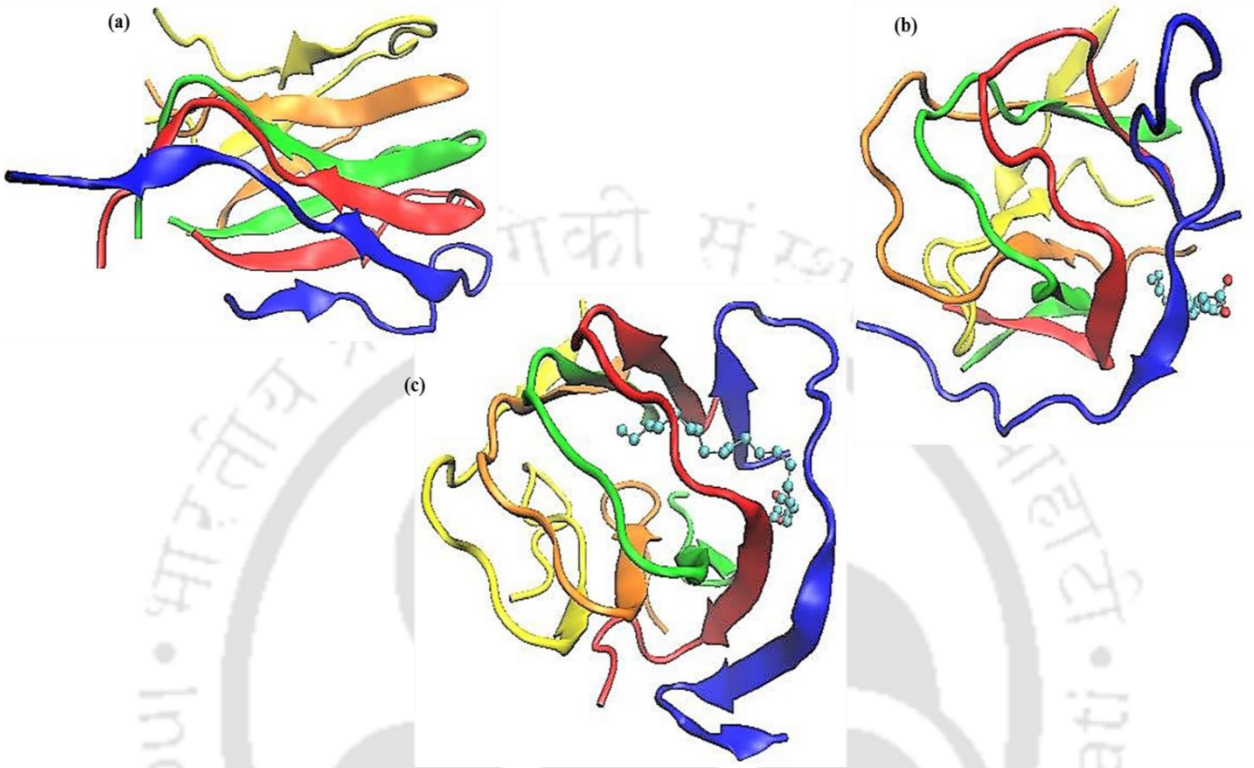

Fig. 6.5. Final Configuration of Aβ in (a) water, (b) 1 EPA molecule and (c) 1 HXA molecule.

The binding possibility can be explained from the inherent conformational flexibility of the n-3 PUFA molecules, which introduce fluidity in the biomembrane upon incorporation. Such modification in the microenvironment of the biomembrane leads to execution of wide range of biological functions.[59] The presence of different side chain groups in Aβ fibril and amphiphilic PUFA molecule makes the conformational rearrangement is such a way that facilitates effective interactions between these two.[60] Both the ligands are observed in linear conformation with disoriented Aβ fibril, establishing the destabilization of the fibril. A similar disorganized conformation of Aβ fibril was observed in the presence of caffeine,[37] which supports the current

observation. Both the EPA and HXA molecules were observed to access hydrophobic cavity of the Aβ fibril via entry from the terminal chain, which is in parity with the interaction behavior of other phenolic compounds.[48] The ability to insert themselves in the fibrillar cavity is associated with intrinsic flexibility of these molecules.[61,62] In addition to the final trajectory, the snapshots at 300 ns and 400 ns have been illustrated in Fig. 6.5 wherein, Fig. 6.5a and b for C0, Fig. 6.5c and d for C1 and Fig. 6.5e and f for C2 system, respectively. The Aβ fibril in the presence of water showed a little twisting at the ends of the organized structure with intact representation of coil (grey), turn (cyan) and β-sheet (yellow) content. The disoriented structure of Aβ fibril in the presence of EPA and HXA at various time points of the run ensures the steady progression of the destabilization phenomena instead of an arbitrary loosening of the fibril.

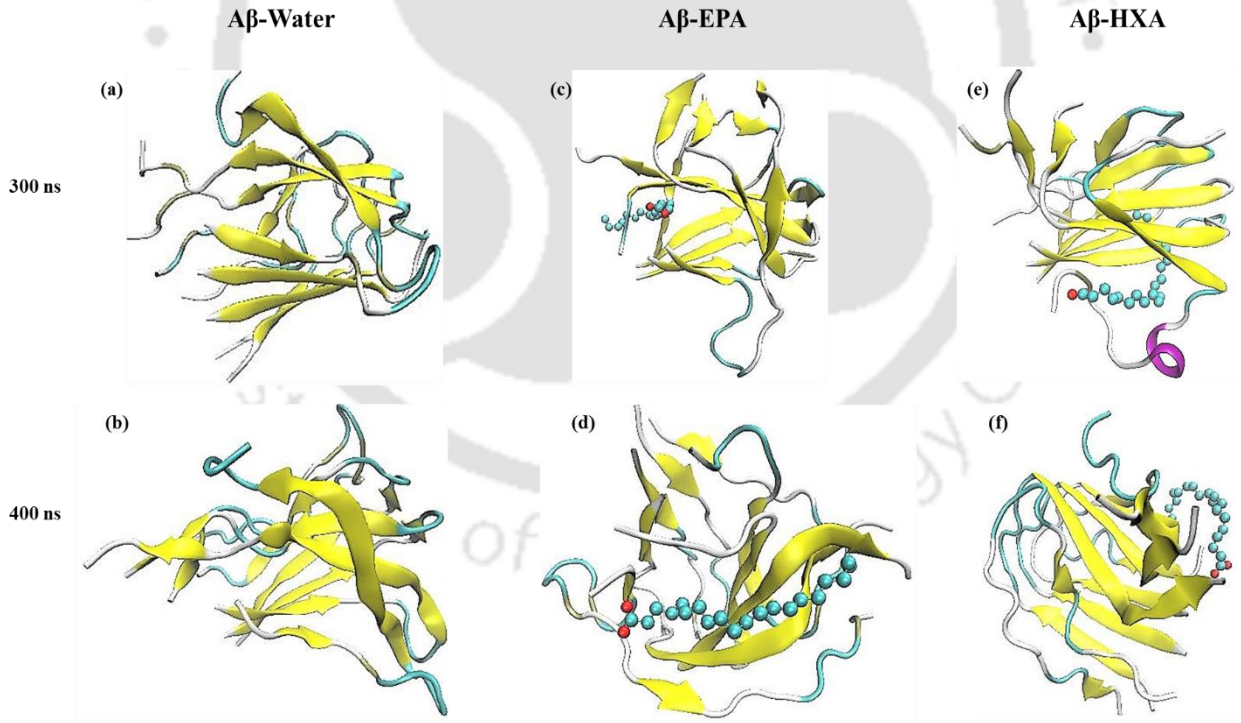

Fig. 6.6. Different snapshots of Aβ in (a,b) water, (c,d) 1 EPA molecule and (e,f) 1 HXA molecule.

The C_α-RMSD, R_g and SASA have been analyzed to check the integrity of the Aβ fibril in the presence of EPA and HXA for an extended production run of 500 ns. The time trajectory and corresponding average for Cα-RMSD value for the entire protein, Chain E and turn region has been plotted for all the three systems in Fig. 6.6a-c and d-f respectively. The average value for Cα-RMSD for the entire protein as depicted in Fig. 6.6d was recorded as 0.760, 1.016 and 0.918 nm for C0, C1 and C2 systems, respectively. A similar increase in Cα-RMSD value has been observed for the terminal chain E (Fig. 6.6e), and the turn region (Fig. 6.6f) of the Aβ fibril in the presence of EPA and HXA as compared to the Aβ-Water system.

The current observations resonate well with high Cα-RMSD value on account of destabilization of Aβ fibril by a natural novel drug, wgx-50.[63] The color scheme considered for three systems is blue for Aβ-Water, red for Aβ-EPA and green for Aβ-HXA system, which is maintained in other parametric analyses as well, if not mentioned otherwise. The observations from Fig. 6.2 and Fig. 6.6 emphasize on representation of chain E as the most affected chain of the pentamer. Henceforth, various parameters have been depicted for chain E separately to gauge the extent of destabilization.

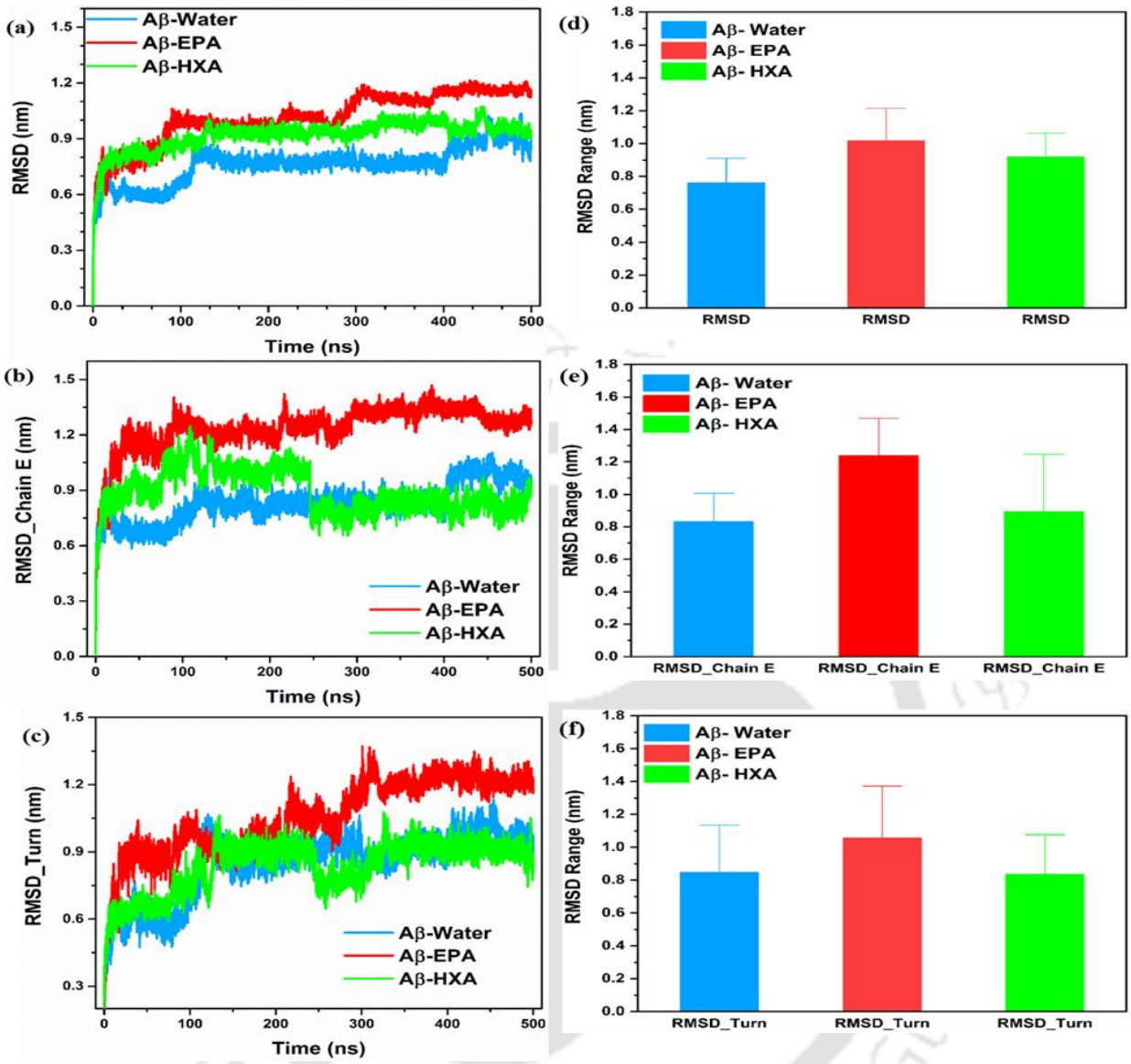

Fig. 6.7. Time trajectory and bar charts for Cα-RMSD of Aβ in water, EPA and HXA (a and d) whole protein, (b and e) chain E and (c and f) Turn region.

The Rg value, indicative of the flexibility, and SASA value, giving an account of hydrophobic and hydrophilic composition of a protein structure[64] have been determined. These two parameters have been plotted as time trajectory and interval plots with 95% confidence interval (CI) around mean value in Fig. 6.7 Herein, Fig. 6.7a and c represents Rg and Fig. 6.7b and d

denotes SASA value for all the three systems. The mean Rg value of 1.377 nm, 1.388 nm and 1.368 nm for C0, C1 and C2 system have been plotted in Fig. 6a and c indicates consideration of EPA as a potential destabilizer. The increased SASA value observed for Aβ-EPA system from Aβ-water system (see Fig. 6.7b and d) compliments the selection of EPA as a fibrillar disruptor. However, a clear and detailed picture about role of HXA has been discussed in the next sections.

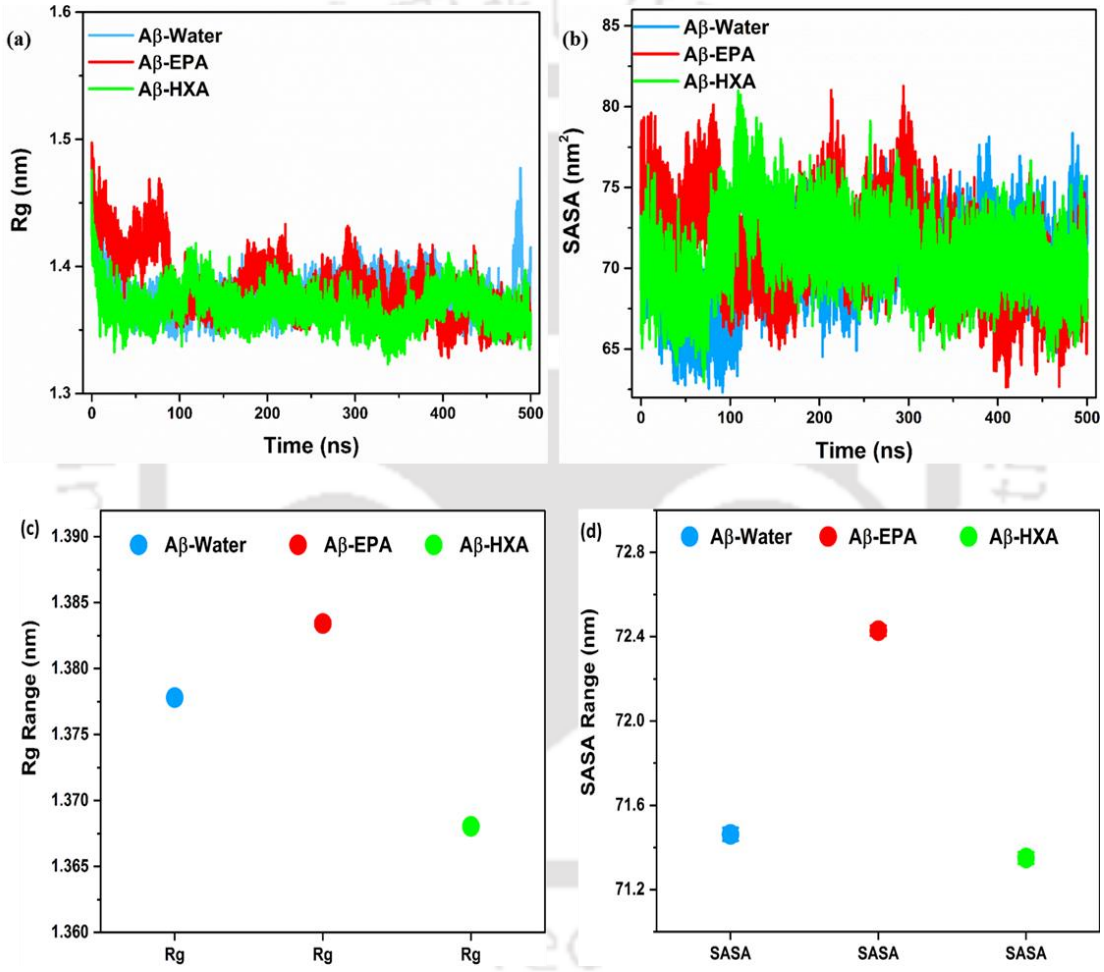

Fig. 6.8. Time trajectory and interval plots for (a and c) Rg and (b and d) SASA of Aβ in water, EPA and HXA. (the interval plots shows the mean value as the preferred interval for that data)

The increased RMSD, R_g and SASA values demonstrating structural instability of Aβ fibril is also reported by other natural compounds which supports our findings.[36] Conclusively, higher values observed for Cα-RMSD, Rg, and SASA translates the potency of both PUFA molecules (EPA and HXA) as a promising destabilizing agent of Aβ fibrils, thereby curing AD. All these global stability parameters demand further in-depth analysis to gain insight on the molecular details of the interaction between PUFAs and Aβ fibril.

6.3.2 Secondary structure determination

The secondary structure plays a decisive role in the overall stability, longevity and functionality of the protein. The stability of Aβ fibrils has been attributed to their higher β-sheet content, which directs the formation of an organized β-fibrillar structure. The DSSP[65] tool delivers the time evolution profile of possible secondary structure configurations achievable by Aβ fibril. The percentage content of the different possible secondary structures for all the three systems C0, C1 and C2 has been tabulated in Table 6.2. The coil content for C1 and C2 was recorded as 45% and 42%, which is considerably higher than C0 (37%). Contrarily, a marked decrease in β-sheet and β-bridge content for C1 and C2 systems as compared to C0 (Table 6.2) implicates the loss of the structural stability and integrity of the Aβ fibril.

The secondary structure profiling for Aβ-Water, Aβ-EPA and Aβ-HXA has been shown in Fig. 6.8a, b and c, wherein a prominent decrease in β-sheet along with rise in coil and turn content are recorded for the C1 and C2 systems as compared to the C0. The significant decrease in the β-sheet content ensures an obstruction to the formation of higher order aggregates barring neurotoxicity of Aβ fibrils.

Table 6.2. Secondary structure for (a) - Aβ-Water, (b) - Aβ-EPA and (c) - Aβ-HXA

Secondary Structure (%)	Aβ-Water	Aβ-EPA	Aβ-HXA
Coil	37 ± 0.57	45 ± 0.57	42 ± 0.57
β-Sheet	38 ± 0.57	37 ± 0.57	33 ± 0.57
β-Bridge	5 ± 0.57	4 ± 0.57	3 ± 0.57
Bend	14 ± 0.57	12± 0.57	16 ± 1
Turn	3 ± 0.57	2 ± 0.00	3 ± 0.00
α-helix	0 ± 0.00	0 ± 0.00	0 ± 0.00
3-helix	0 ± 0.00	1 ± 0.57	0 ± 0.00
Chain_Separator	3 ± 0.00	3 ± 0.00	3 ± 0.00

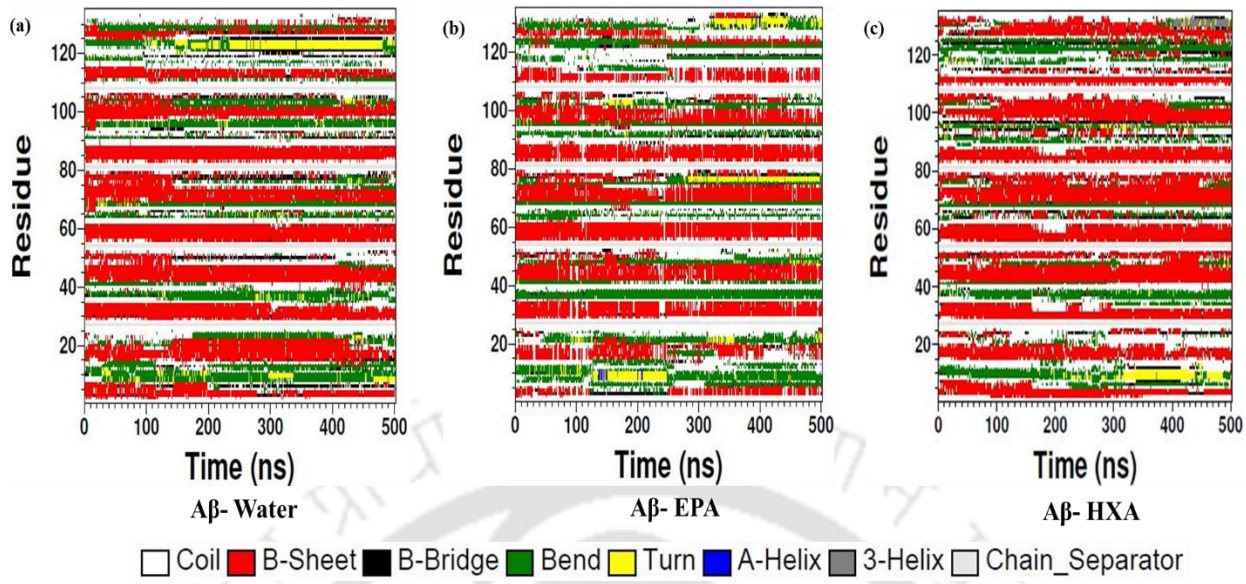

Fig. 6.9. DSSP Secondary Structure evolution with time for (a) Aβ-Water (b) Aβ-EPA and (c) Aβ-HXA molecule.

6.3.3. Backbone Stability

The integrity of the fibrillar backbone, gauged by the probability of bond formation owing to the distance between Cα of K28 residues of neighboring chains were determined. The same has been plotted as time trajectory (Fig. 6.9a and b) and as corresponding bar charts Fig. 6.9c and d based on the mean value.

The average K28-K28 distance for neighboring terminal chains (viz., A-B and D-E) were found to be increased beyond the cut off limit of bond formation in the presence of EPA and HXA. Fig. 6.9a and c depicts striking increase in K28-K28 distance from 0.49 nm (Aβ-Water) to 0.65 and 0.64 nm for Aβ-EPA and Aβ-HXA for chain A-B respectively. A similar noticeable increase for chain D-E has been observed from time trajectory and bar charts from Fig. 6.9b and d,

respectively as 0.85 nm for Aβ-EPA from 0.39 nm from Aβ-Water, Fig. 6.9b and d). Such an enhancement in the distance between these residues conciliates bond formation and hence compromising on the stability of the Aβ fibril.

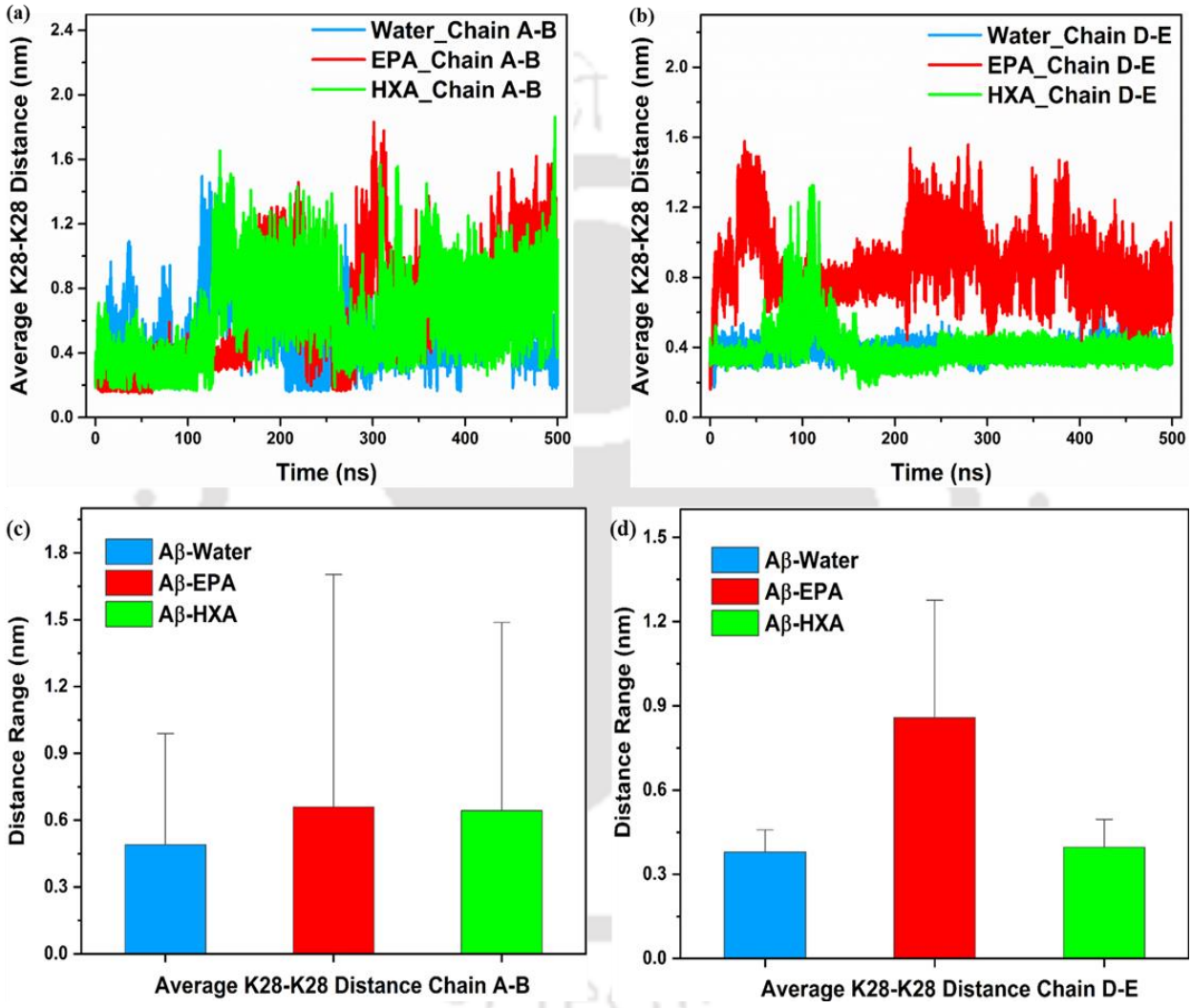

Fig. 6.10. Time trajectory and bar charts for K28-K28 Cα Distance for Aβ in water, EPA and HXA for (a and c) Chain A-B and (b and d) Chain D-E.

6.3.4 Effect of PUFAs on various bonds in Aβ fibril

There are various types of intra- and inter-molecular bonds that imparts stability to any protein structure at different levels (viz., primary to quaternary). These bonds broadly encompass H-bonds, covalent bonds, salt bridges, and hydrophobic contacts. Herein, we present a detailed analysis of the change in these molecular interactions in the presence of EPA and HXA.

6.3.4.1 Hydrogen-Bonds

The theoretical[66] and experimental[67] studies outline the importance of an extensive H-bond network contributing towards the stability of Aβ fibrils. We have calculated the average number of H-bonds for the entire protein, β1, and turn region, which showed a decreasing tendency in the presence of EPA and HXA molecule (refer Table 6.3). The average number of H-Bonds for inter-peptide chain D-E was observed to be 10.1 and 10.4 for C1 and C2 system, which is less as compared to 11.3 for C0. A similar decrease of 31.74% and 29.06% in C1 and C2 systems, respectively from C0 (Table 6.3) for intra-chain E peptide, testifies the degradation of H-bonds in Aβ fibril upon interaction with PUFAs. These observations are in close agreement with the destabilization of Aβ fibril by wgx-50, a novel compound from Sichuan pepper, which also showed a drastic decrease in both intra- and inter- chain H-bonds.[63] The H-bond disruption of Aβ fibril in the presence of PUFAs would prohibit further fibrillar growth and elongation.

Table 6.3. Average number of H-bonds for Aβ-Water, Aβ-EPA, and Aβ-HXA systems

No. of H-Bonds	Aβ-Water	Aβ-EPA	Aβ-HXA
Overall Protein	75.1 ± 1.0	74.3 ± 0.8	75.2 ± 0.4
Chain C-D	16.7 ± 0.5	14.3 ± 0.8	15.8 ± 0.8
Chain D-E	11.3 ± 0.6	10.1 ± 0.5	10.4 ± 0.5
β1 Region	25.7 ± 0.9	22.3 ± 0.5	25.1 ± 0.4
Turn Region	4.2 ± 0.7	3.6 ± 0.3	4.9 ± 0.1
Chain E-E	6.7 ± 0.8	4.6 ± 0.4	4.8 ± 0.1

6.3.4.2 Salt-Bridge formation

Electrostatic interactions between oppositely charged residues in any protein structure are called salt bridges.[68,69] Salt bridges impart the stability to the protein and influence its structural conformation, pattern recognition, function, degradation pattern, and catalytic activity.[70] In the present study, we have calculated the average distance between intra and inter D23 and K28 residues for the terminal chain E for all the three systems (viz., C0, C1 and C2). The same plots

have been drawn here also, with time trajectory and interval plots with 95% CI around mean value in Fig. 6.10a and b and Fig. 6.10c and d, respectively.

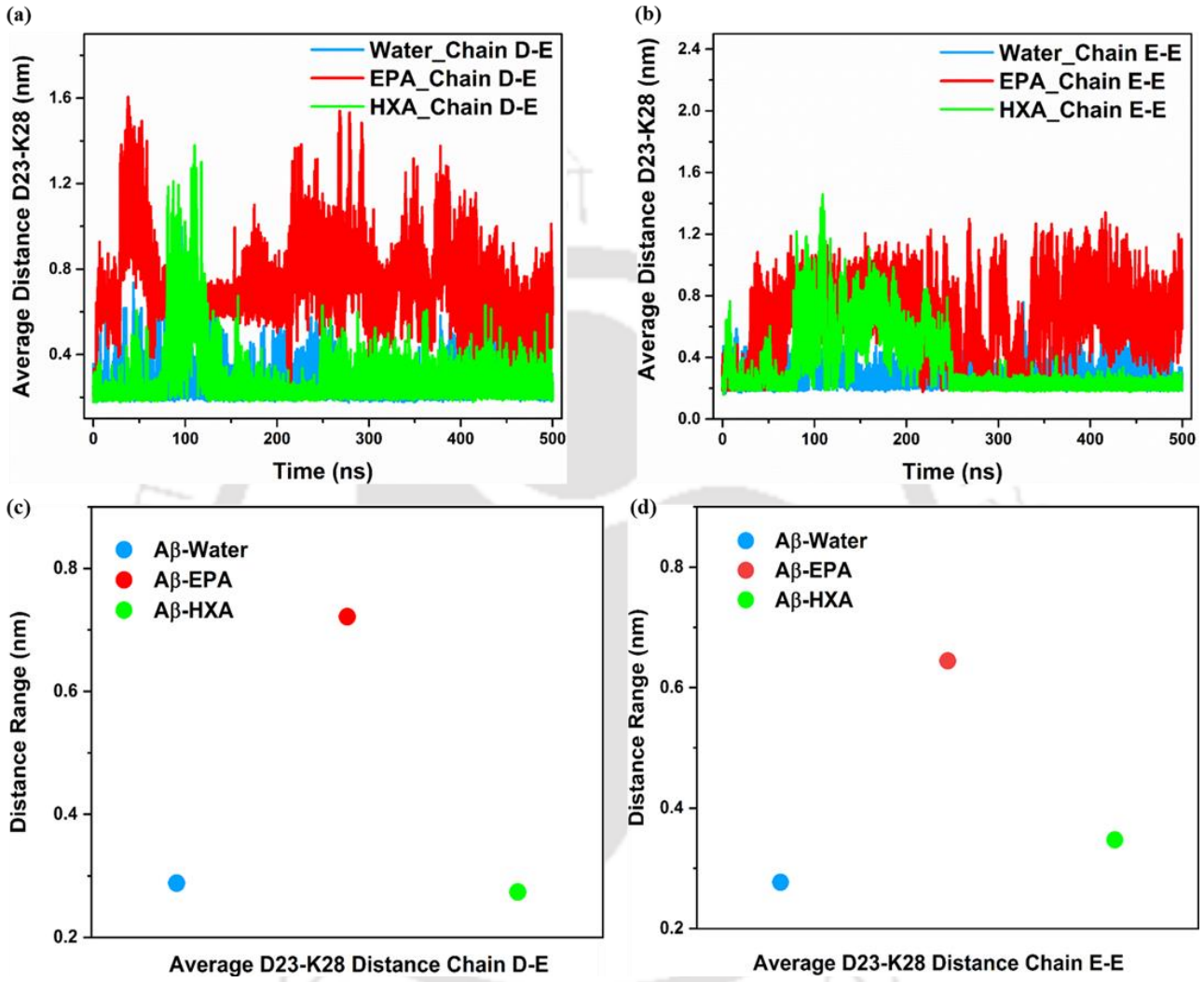

Fig. 6.11. Time trajectory and interval plots for D23-K28 Distance for Aβ in water, EPA and HXA PUFAs for (a and c) Chain D-E and (b and d) Chain E-E.

The average distance for these residues was found to be increased in the presence of Aβ-EPA (Fig. 6.10a and c); however, not much changes were observed in Aβ-HXA (Fig. 6.10b and d), indicating the ineffectiveness of HXA towards breaking of salt bridges between D23 and K28 residues in the Aβ fibril. The inter-residual distance between D23 of chain D and K28 of neighboring chain E was measured as 0.72 nm for Aβ-EPA, which is considerably pronounced as compared to 0.28 nm in Aβ-Water system (Fig. 6.10a and c). A similar increase to 0.37 nm for intra-peptide chain E (D23-K28) for Aβ-EPA system from 0.27 nm in Aβ-Water system (Fig. 6.10b and d) was measured.

Such increased distances indicate bond breaking, and hence misalignment of Aβ fibril around the terminal chain. The results thus obtained are found to be concurrent with the breaking of salt bridges of Aβ fibril in the presence of copper ions,[71] C-60 fullerene,[72] and surfactin[73] molecules, leading to the destabilization of Aβ fibril. The salt bridge disruption in destabilizing the entire Aβ fibril in the presence of brazillin[44] corroborates with the current findings.

6.3.4.3 Inter-Chain Distance Matrix

We have determined the residue-residue contact between terminal chain D and E by contact map analysis. As depicted in Fig. 6.11a, there is a portrayal of contacts throughout chain D and E for Aβ-water system. These residual contacts were fairly compromised for Aβ-EPA and Aβ-HXA systems (Fig. 6.11b and c), which can be viewed from presence of blank spaces in the matrix.

The illustration of contact map analysis for the Aβ-HXA systems provides a well-founded idea on the reduced contacts between chain D and E, thereby moving E chain apart from the parent fibrillar structure. Evidently, the contacts between terminal chains are disrupted, which confirms

the destabilization of the Aβ fibril. These observations are found in parity with the interchain matrix observed in the presence of flavonoid derivative.[58]

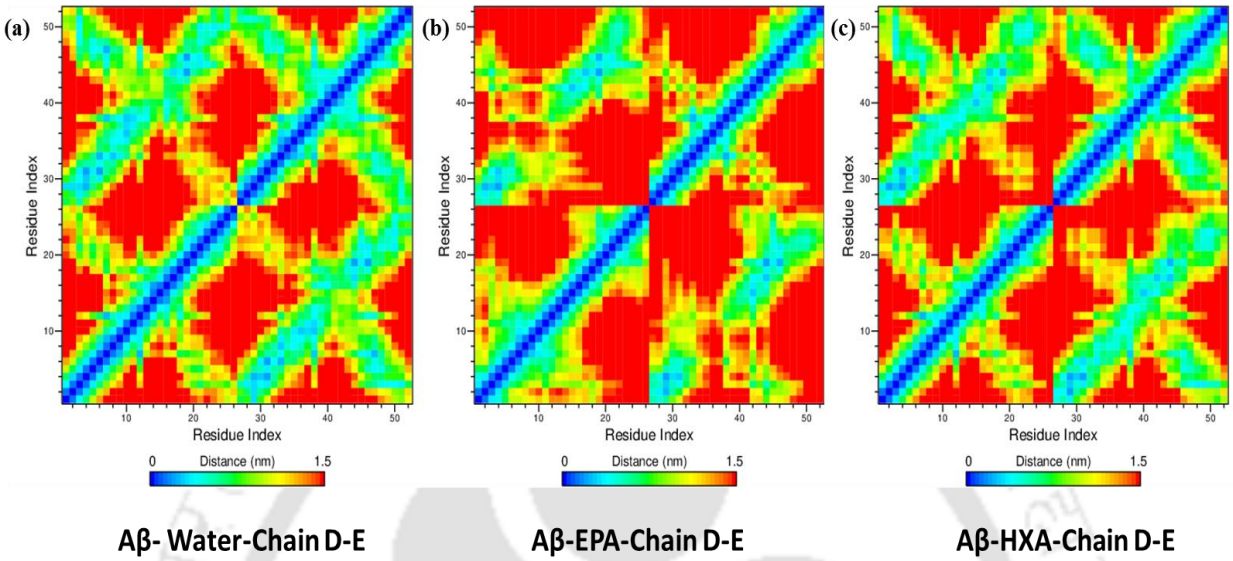

Fig. 6.12. Interchain Distance matrix for chain D-E (a) Aβ-Water (b) Aβ-EPA and (c) Aβ-HXA.

6.3.4.4 Hydrophobic contacts

The major contributors towards the folding pattern and stability of the protein are electrostatic and hydrophobic interactions. The burying of hydrophobic residues inside the solvent inaccessible cavity provides remarkable high strength to amyloid fibrils.[74] According to the principle of PASA (Principle of Amyloid Self-Assembly), the fibrillar structure, which possesses the maximum number of inter- and intra-peptide hydrophobic interactions, is the most stable and favorable fibril structure during fibrillation process.[75] There have been various hydrophobic residual contacts that play a crucial role in the structural organization and strengthening of the Aβ fibril. The hydrophobic contact pairs reported for the current pentamer Aβ structure are A21-V36, L34-V36

and F19-G38,[76] interacting in both intra- and inter-peptide manner. We have calculated mean distance between these residues as a function of time to estimate the probability of bond formation between them. The inter-residual distance between A21 of chain C and V36 of chain D (Fig. 6.12a and c) was estimated as 0.52 nm for Aβ-water system, which was increased to 0.72 nm in the presence of EPA, and to 0.75 nm when HXA was inserted, impeding A21-V36 bond formation. A considerable increase in the distance between L34 and V36 residue was also recorded for chain D and E (Fig. 6.12b and d).

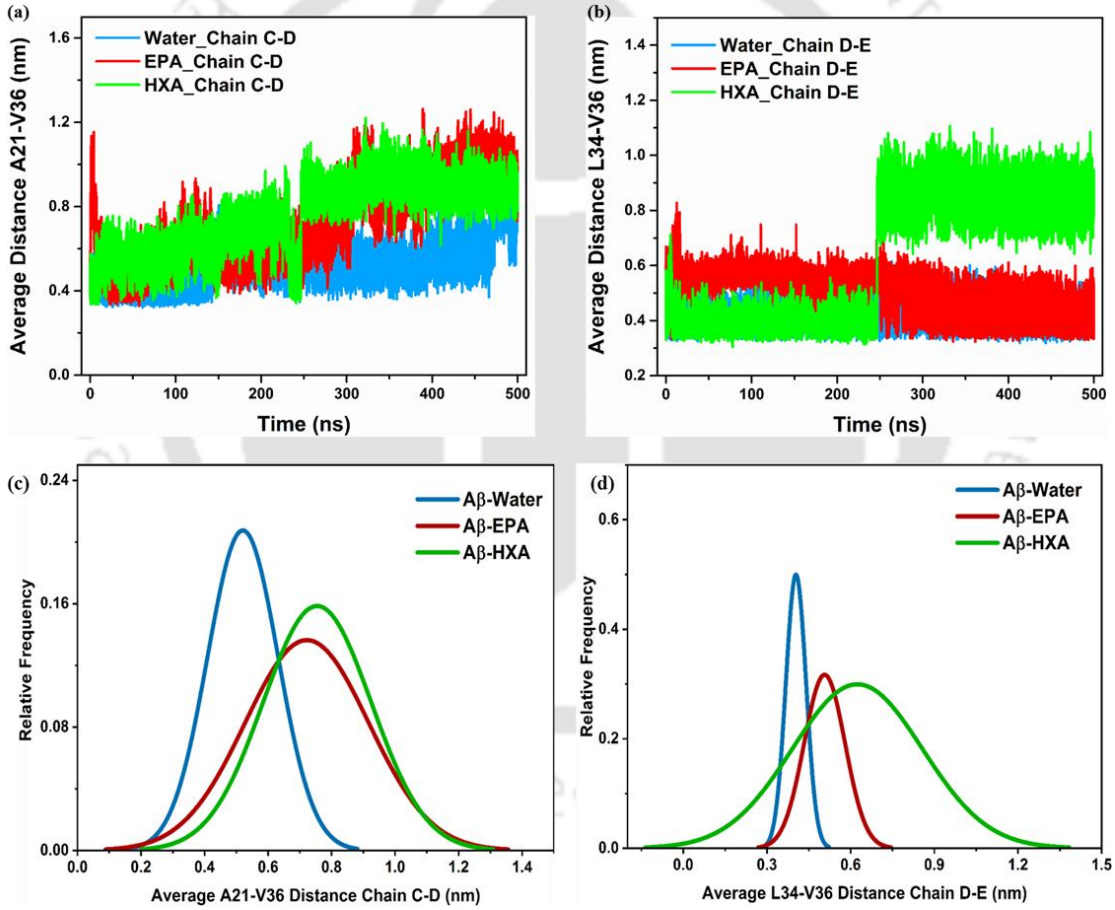

Fig. 6.13. Time trajectory and PDFs for A21-V36 Distance for Aβ in water, EPA and HXA PUFAs for (a and c) Chain C-D and (b and d) Chain D-E.

The L34-V36 distance for Aβ-Water system was recorded as 0.40 nm, which was increased to 0.50 and 0.62 in Aβ-EPA and Aβ-HXA systems, respectively, hindering the bond formation. The shift in the PDFs curves towards higher values of A21-V36 and L34-V36 distance observed for Aβ-EPA and Aβ-HXA systems in Fig. 6.12c and d, clearly highlights on the destabilization potential of both the PUFAs.

A distinct differentiation from time trajectory and interval plots, can also be viewed in chain A-B and B-C for A21-V36 residual contact for C1 and C2 system (see Fig. 6.13a-d), which supports the destabilization of Aβ fibril.

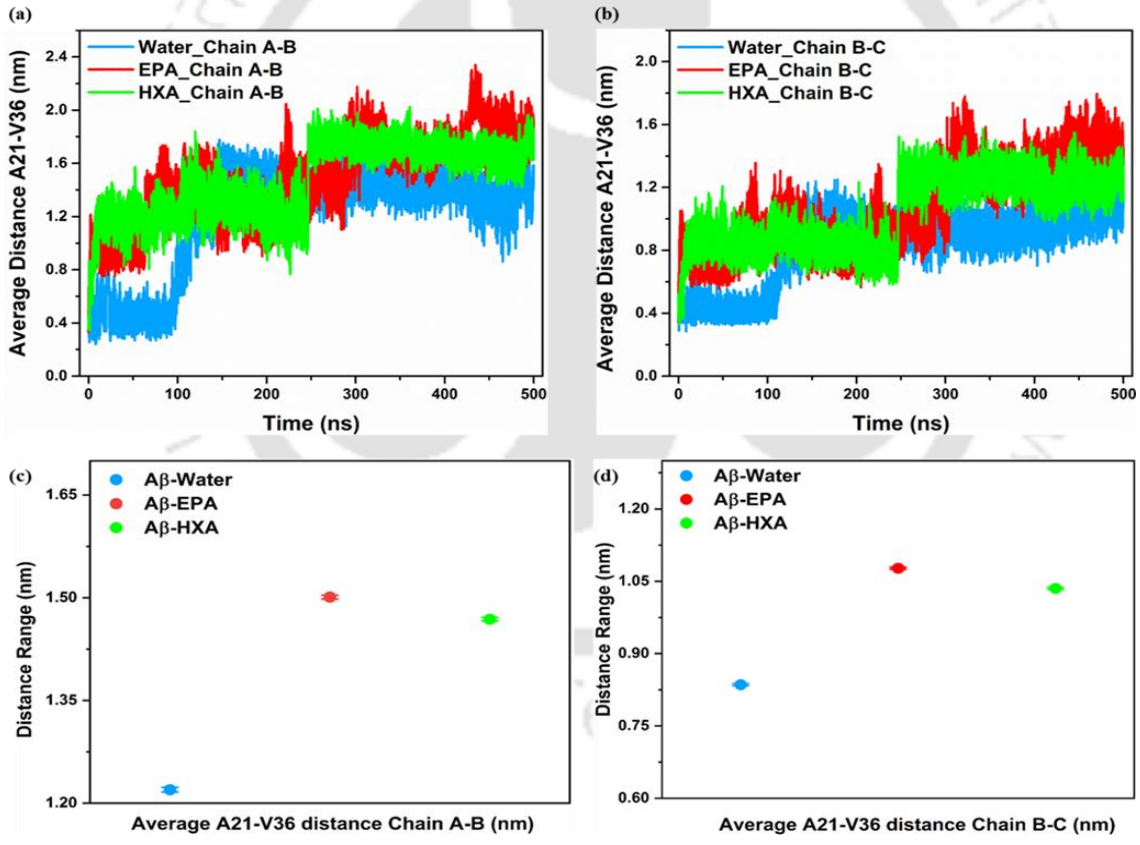

Fig. 6.14. Time trajectory and interval plots for A21-V36 Distance for Aβ in water, EPA and HXA ligands for (a and c) Chain A-B and (b and d) Chain B-C.

Furthermore, the average distance of F19-G38 for chain D and E (both intra and inter pairs) have been analyzed and plotted in Fig 6.14a-d. The mean distance for neighboring chains C-D (Fig. 6.14a) and D-E (Fig. 6.14b) pairs was observed to be 0.86 and 0.61 nm for C1 and 0.66 and 0.62 nm for C2 system which is considerably higher as compared to 0.55 nm and 0.43 nm in C0 system. A simultaneous increase in the intra-residual distance for chain D-D and E-E can also be viewed in Fig. 6.14c and 6.14d, respectively. The corresponding time trajectory to the average F19-G38 distance for all these four selections have been plotted in Fig. 6.15a-d, which well compliments with the above findings.

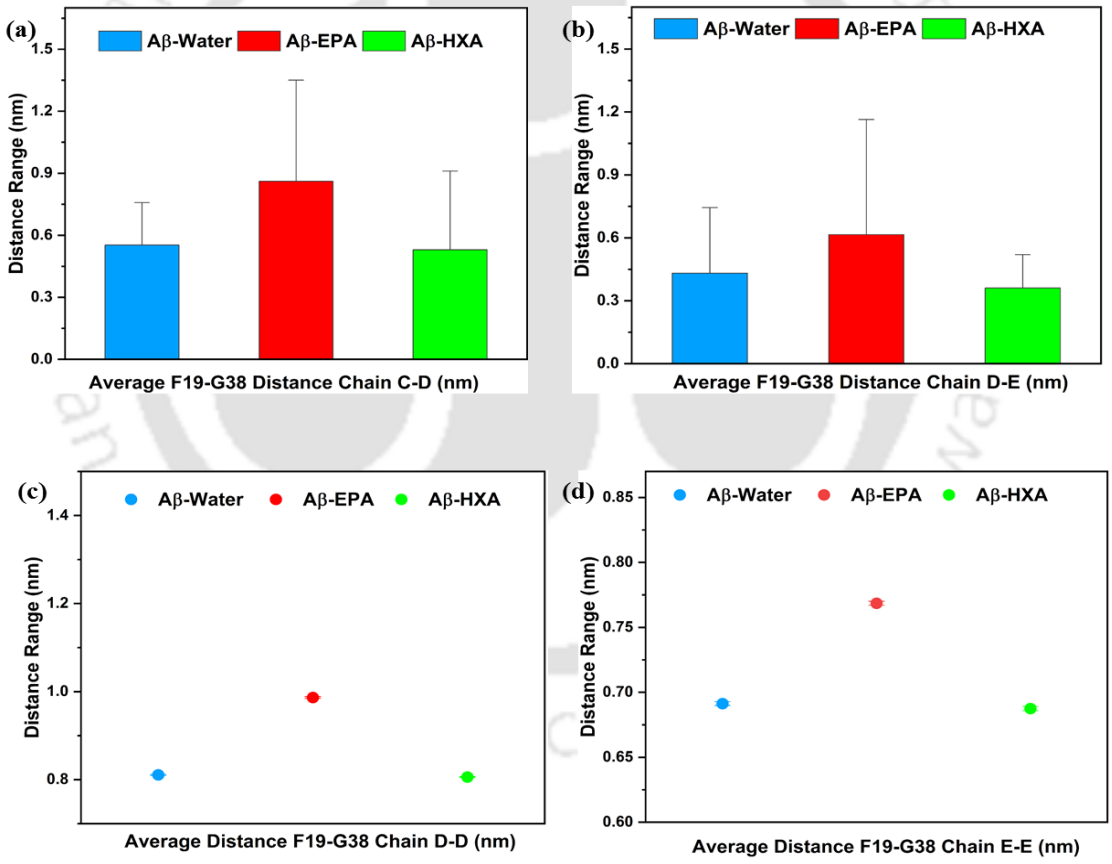

Fig. 6.15. Average F19-G38 Distance for Aβ in water, EPA and HXA for (a) Chain C-D, (b) Chain D-E (c) Chain D-D and (d) Chain E-E.

The average mean distance for the other end of Aβ fibril (viz., A-B, B-C, A-A and C-C) for F19-G38 pair has been plotted in Fig. 6.16a-d with corresponding time trajectory in Fig. 6.17a-d. Both Fig. 6.16a-d and 6.17a-d shows that there is no bond formation between these residues, which is attributed to an increased distance between F19-G38, thereby disarraying the pentamer structure. All these observations clearly manifest the obstruction in bond formation, which disarrange the organized Aβ structure.

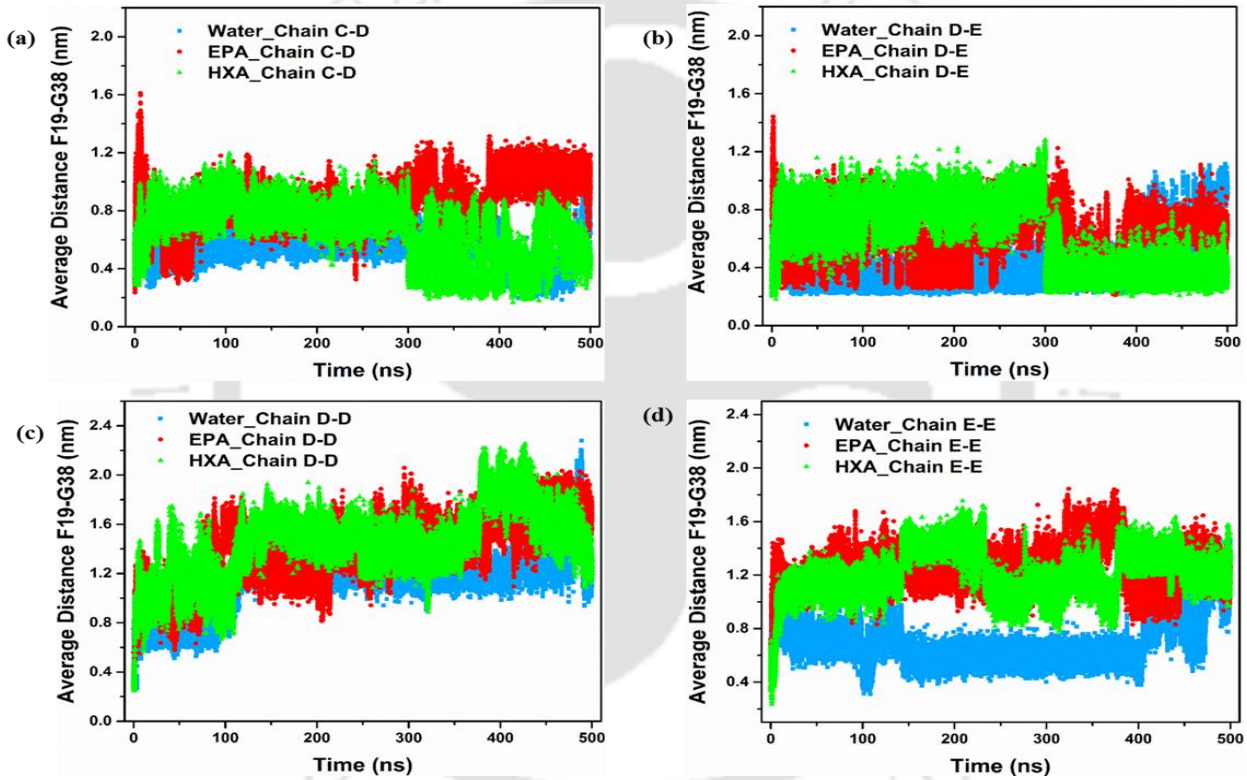

Fig. 6.16. Time trajectory for F19-G38 Distance for Aβ in water, EPA and HXA ligands for (a) Chain C-D, (b) Chain D-E (c) Chain D-D and (d) Chain E-E.

Similar findings were also recorded in case of chemically synthesized drugs having anti-cholinesterase activity tested *in-vitro* and *in-silico*, causing disruption of preformed Aβ fibrils.[77]

This increased distance between hydrophobic residues for the terminal chains implies breaking of these bonds in the presence of PUFAs, leading to the disruption of the entire fibrillar structure of Aβ fibrils.

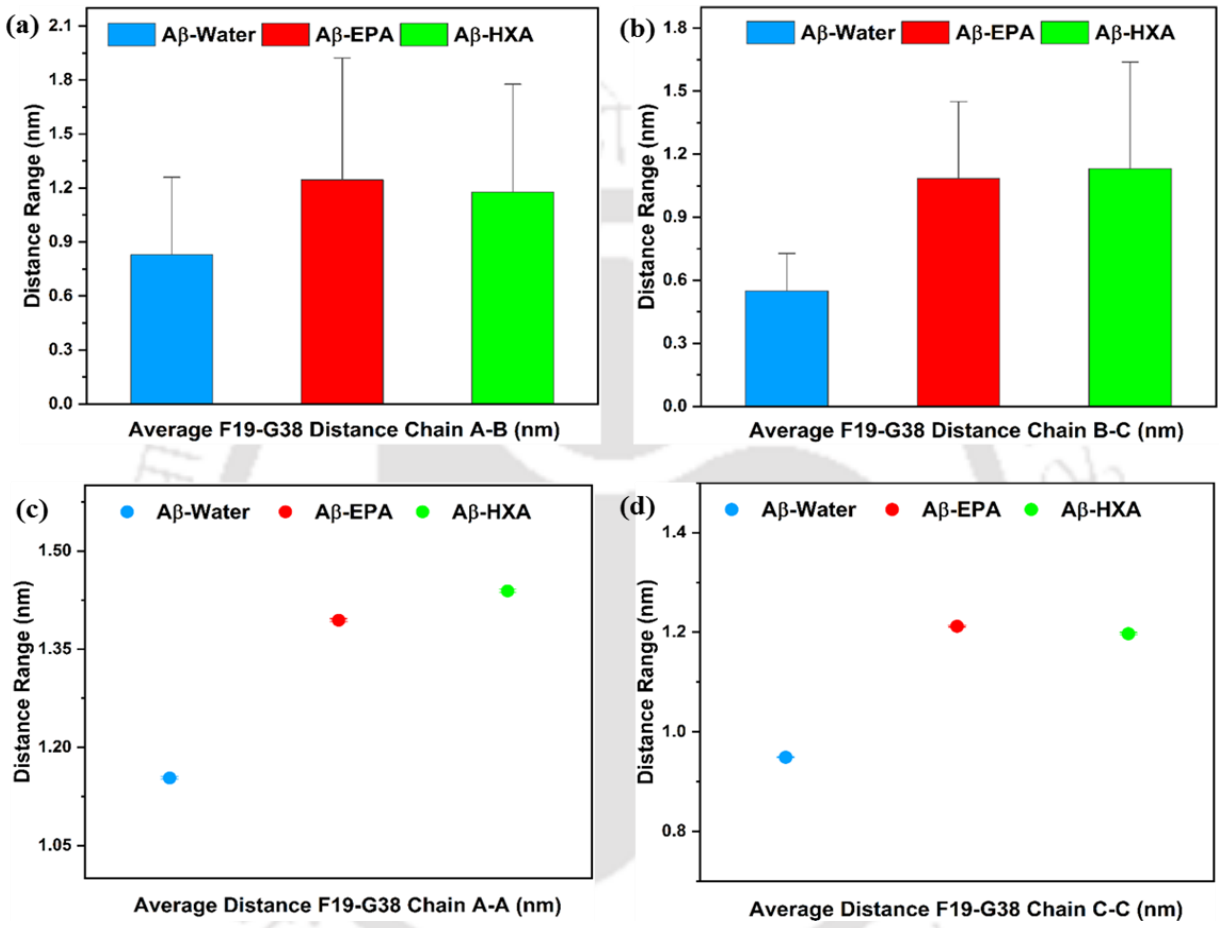

Fig. 6.17. Average values of F19-G38 Distance for Aβ in water, EPA and HXA ligands for (a) Chain A-B, (b) Chain B-C (c) Chain A-A and (d) Chain C-C.

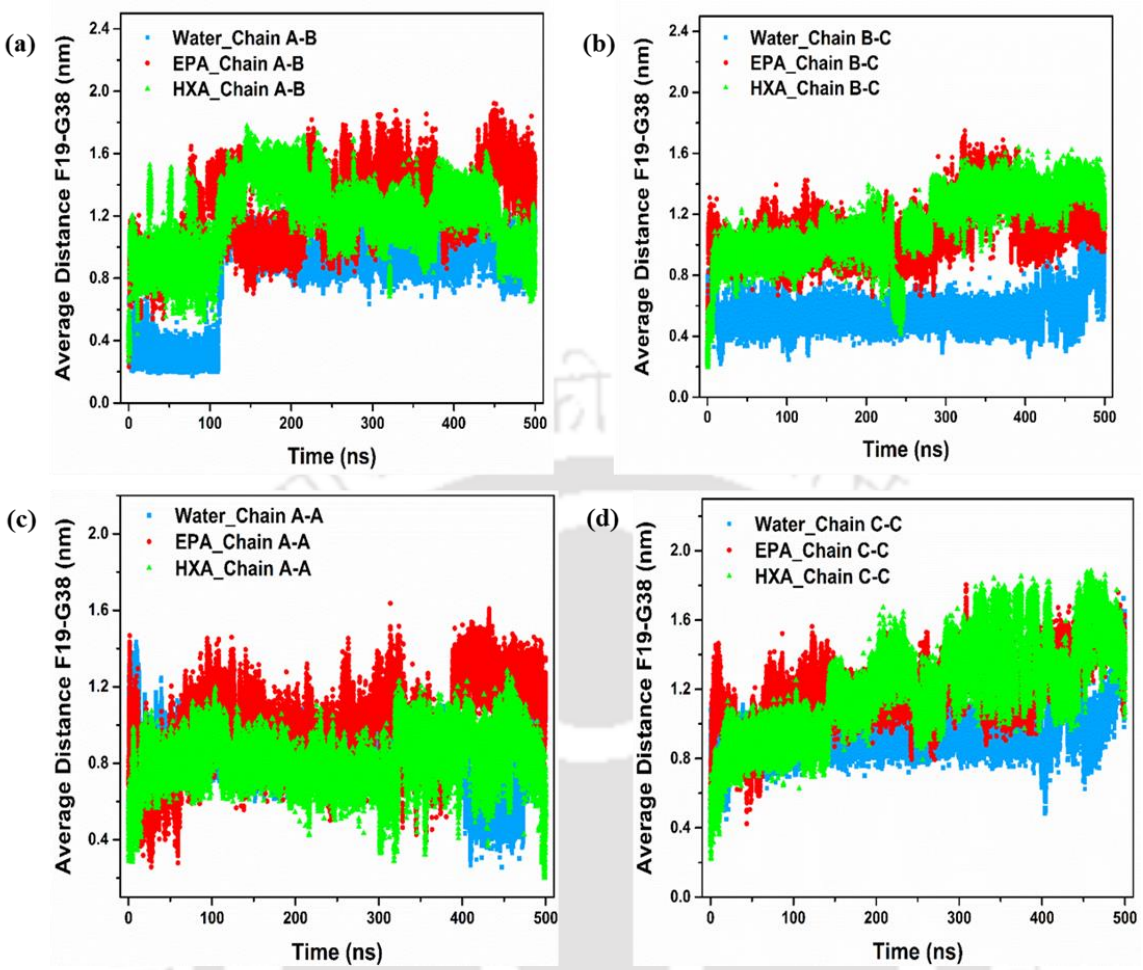

Fig. 6.18. Time trajectory of F19-G38 Distance for Aβ in water, EPA and HXA ligands for (a) Chain A-B, (b) Chain B-C (c) Chain A-A and (d) Chain C-C.

6.3.5 Binding Free Energy analysis between Aβ fibril and PUFAs

The integration of the MM-PBSA method with MD simulation studies has been done with an objective to gain more insights on the binding affinity of the neighboring terminal chains in the presence of PUFAs. The detailed inter-chain binding free energy (BFE) analysis for chain A-B and D-E for C0, C1 and C2 has been tabulated in Table 6.4. The lowest $G_{binding}$ observed for

chain A-B (-454.5 ± 8.4 kcal/mol) for Aβ-Water system mentioned in Table 6.4 clearly indicates the highest affinity of these two chains. On the contrary, the higher $G_{binding}$ of -87.5 ± 7.9 kcal/mol and -20.9 ± 8.9 kcal/mol for Aβ-EPA and Aβ-HXA respectively, specifies the lesser binding affinity between chains A-B in presence of these PUFAs. A similar level of separation of terminal chain E from the fibril is attributed to the higher $G_{binding}$ value for Aβ-EPA (-151.7 ±10.3 kcal/mol) and Aβ-HXA (-63.7 ± 11.6 kcal/mol) system as compared to -189 ±10.8 kcal/mol for Aβ-Water (Table 6.4). The estimation of various other associated energy terms, such as, ΔE_{MM}, ΔG^{psolv}, and ΔG^{npsolv} provide more precision on binding by specific amino acid residues involved in binding.[78] The ΔE_{vdW} or chain A-B for Aβ-EPA and Aβ-HXA systems has been recorded as -243.7 ± 1.6 kcal/mol and -228.2 ± 1.8 kcal/mol, respectively. The ΔE_{elec} for chain A-B has been calculated as -66.7 ± 2.3 kcal/mol and -3.3 ± 2.3 kcal/mol for Aβ-EPA and Aβ-HXA, respectively. The notable lower value for ΔE_{vdW} as compared to ΔE_{elec} explain the dominance of van der Waals contribution over electrostatic interactions for chain A-B in the presence of both the binders (viz., EPA and HXA). The similar observation has been made for chain D-E as well in presence of both the ligands. The dominance of van der Waals interactions is attributed to the involvement of hydrophobic residues in binding of PUFAs with Aβ fibril, which corroborates well with the disruption of hydrophobic interactions, as explained in above section. The van der Waals interactions dominating over electrostatic ones have also been reported for binding of AZD2184, a potential PET tracer with Aβ fibril (2BEG), attributed to the hydrophobic interaction.[34]

Table 6.4. Binding Free Energy (kcal/mol) between Chains A-B and D-E of the Aβ42 Fibril in Water, EPA and HXA.

Energy Terms	Inter-chain (A-B) BFE Aβ-Water (Kcal/mol)	Inter-chain (A-B) BFE Aβ-EPA (Kcal/mol)	Inter-chain (A-B) BFE Aβ-HXA (Kcal/mol)	Inter-chain (D-E) BFE Aβ-Water (Kcal/mol)	Inter-chain (D-E) BFE Aβ-EPA (Kcal/mol)	Inter-chain (D-E) BFE Aβ-HXA (Kcal/mol)
ΔE_{vdW}	-361.1 ± 2.5	-243.7 ± 1.6	-228.2 ± 1.8	-333.9 ± 3.4	-301.9 ± 2.4	-313.8 ± 3.2
ΔE_{elec}	-679.5 ± 1.3	-66.7 ± 2.3	-3.3 ± 2.3	-267.6 ± 2.8	-72.8 ± 4.2	-83 ± 3.7
$\Delta E_{MM}{}^{a}$	-1040.6 ±3.8	-310.4 ± 3.9	-231.6 ± 4.2	-601.6 ± 6.3	-374.7 ±6.7	-396.9 ±6.9
ΔG_{ps}	631 ± 1.2	252.9 ± 2.5	240.9 ± 2.9	455.8 ± 1.8	261.4 ± 1.2	372.8 ± 2.6
ΔG_{nps}	-44.9 ± 3.3	-30 ± 1.3	-30.2 ± 1.7	-43.2 ± 2.6	-38.4 ± 2.3	-39.7 ± 1.9
$\Delta G_{solv}{}^{b}$	586 ± 4.5	222.8 ±3.9	210.6 ± 4.7	412.6 ±4.5	223.0 ±3.6	333.1 ±4.6
ΔG_{bindin}	-454.5 ± 8.4	-87.5 ± 7.9	-20.9 ± 8.9	-189.0 ±10.8	-151.7±10.3	-63.7 ± 11.6

[a] $\Delta E_{MM} = \Delta E_{vdW} + \Delta E_{elec}$, [b] $\Delta G_{solv} = \Delta G_{ps} + \Delta G_{nps}$, [c] $\Delta G_{binding} = \Delta E_{MM} + \Delta G_{solv}$

Further, the individual contribution for the entire Aβ fibril has been determined and illustrated in Fig. 6.18a and b for EPA and HXA respectively. This has been done to elucidate the key residues involved in the binding of PUFAs to the Aβ fibril. Fig. 6.18a unveils the major involvement of L17 and K28 form all the five chains of the pentamer highlighted with different symbols and color. The contribution from V18 and I32 from chain A, L34 from chain B, and V36 from chain C indicates the hydrophobic interactions pertaining to the hydrophobic residues involved. Similarly, for HXA binding Fig. 6.18b demarcates L17 and K28 from all five chains. Additionally, the contribution form V18, F19 and I31 from Chain A, V18, I32 and L34 from chain B, and L34 from chain C highlights the Van der Walls interaction. These key residues explain the dual contribution of nonpolar and electrostatic interactions towards Aβ-EPA and Aβ-HXA complex formation.[79]

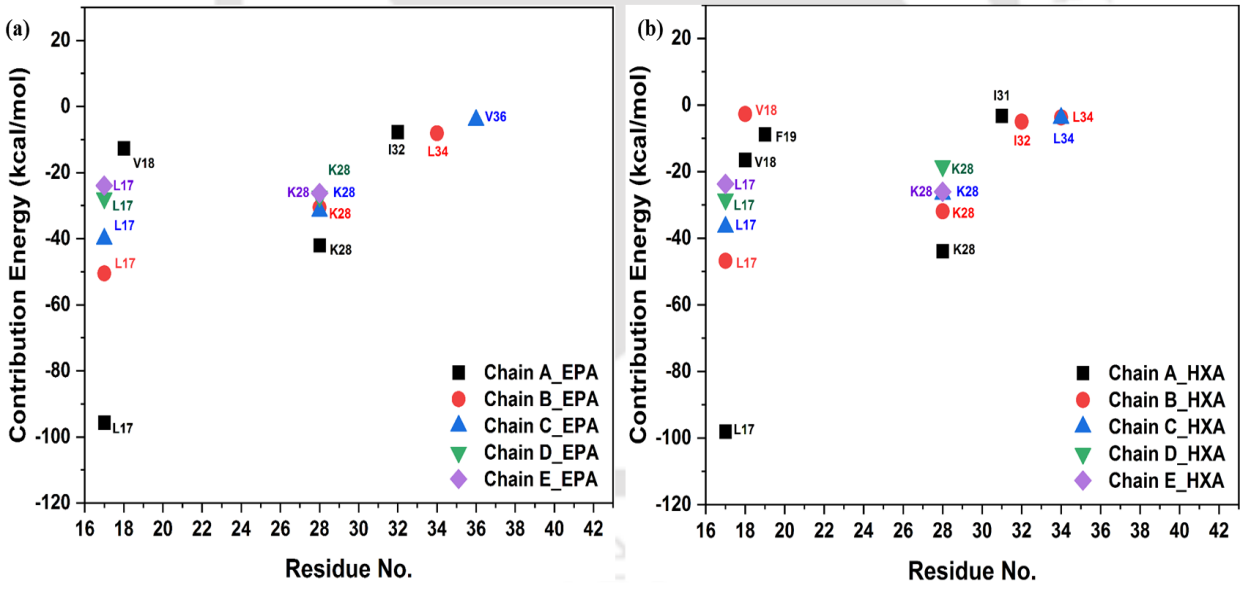

Fig. 6.19. Individual residue contribution to the total binding energy expressed in kcal/mol for all chains of Aβ fibril for (a) EPA and (b) HXA. The key residues highlighted for both the PUFA molecule.

The individual residues involved in binding of EPA to Aβ-fibril are L17 and V18 from β1 region, K28 from turn region and I32, L34 and V36 from β2 region, from all the five chains. Similarly, the contribution from L17, V18 and F19 (β1 region), K28 (turn region) and I31 and L34 (β2 region) from Aβ fibril in binding to HXA has been observed. The residues involved in binding synchronizes with the breaking of native salt bridges and various hydrophobic contacts present in the Aβ fibril. The involvement of L17, V18 and F19 residues in Aβ-HXA complex formation are in close agreement for Aβ peptide and HXA binding, leading to inhibition of fibrillation.[31] The presence of same residues were also reported in binding of PUFAs with Aβ fibril[26] studied by docking, clearly testifies our results. The binding pattern of different aromatic PUFAs, such as, curcumin derivatives[46] and biophenols[48] to Aβ fibril supports the current observation. Our results well corroborate with the binding pattern of oligoproline[55] with Aβ fibril and di-triazole derivate[57] with the terminal chain leading to the destabilization of the fibrillary structure. The MM-PBSA results reveal the mechanistic details on the binding of PUFAs to the Aβ fibril by interacting with different residues over the entire chain length. The access to fibrillar cavity by EPA and HXA led to destabilization of Aβ fibril, establishing it as a promising therapeutic agent for the treatment of AD.

6.4 CONCLUSIONS

The destabilization of amyloid fibrils is considered to be one of the most promising therapeutic strategies for AD. The natural compounds are believed to be suitable drug candidates owing to their biocompatibility and dietary consumption. The present work focuses on the screening of three major ω-3 fatty acids (PUFAs) for their destabilization potential on Aβ fibrils. The anti-

amyloidogenic properties of three PUFAs viz., Eicosapentaenoic acid (EPA), Docosahexaenoic acid (HXA), and α-linolenic acid (LNL) have been studied by MD simulation. After initial screening of PUFAs for 300 ns, EPA and HXA were considered for further extended run up to 500 ns. The VMD representation of the MD trajectory thus obtained for both Aβ-EPA and Aβ-HXA systems showed maximum perturbations and deflections of the terminal chains of Aβ fibril due to the insertion of these PUFAs in the fibrillar cavity. The increased values of RMSD, Rg, and SASA in the presence of EPA and HXA as compared to Aβ-water system, indicate a disoriented structure of Aβ fibril. The increased distance between D23-K28 inhibits the formation of inter and intra-chain salt bridges by EPA, without significant effect of HXA. However, the destabilization effect of both PUFAs was verified by loss in the number of H-bonds and β-sheet content. The increase in average distance for hydrophobic pairs (viz., K28-K28, A21-V36 and F19-G38) prevents sustenance of these interactions, thus promoting destabilization of Aβ fibril in the presence of PUFAs. This explains the destabilization potential of both EPA and HXA on Aβ fibril. The BFE analysis by MM-PBSA tool demarcates less binding affinity of the terminal chains A-B and D-E in the presence of EPA and HXA compared to the control system, pertinent to high binding energy. The involvement of positively charged residue (K28) and hydrophobic residues (viz., L17, V18, F19, I31, I32, L34 and V36) collectively elucidates electrostatic and van der Waals interactions between PUFAs and Aβ fibril, owing to amphiphilic nature of the PUFAs. The electrostatic interaction is observed between polar carboxylic head and K28 residue, whereas the long non-polar carbon tail interacts with hydrophobic residues (L17, I31, I32, L34 and V36). The minor dominance of van der Waals interactions over electrostatic interaction can be assessed from the higher contribution of hydrophobic residues involved in binding. This led to the insertion of these two PUFA molecules in the fibrillar cavity thereby assisting the destabilization of the pentamer.

The deflection of terminal chains, A and E from the parent pentamer structure is observed on account of the decreased binding affinity, attributed to the increase in the BFE as measured by MM-PBSA method.

The deformation of Aβ fibril by ω-3 PUFAs not only curbs the neurotoxicity concerns but also inhibits the formation of higher order toxic aggregates upon interacting with upcoming monomers. The present work provides the mechanistic details on the significant role of the PUFAs in destabilizing preformed Aβ fibril, thereby providing a promising cure to AD. The better interaction and destabilization of Aβ fibril due to amphiphilic fatty acid makes them promising drugs to cure AD, as they can access fibrillar cavity much better than other small molecules. These findings pave the pathway for the investigation of other natural amphiphilic compounds to measure their destabilization potency. Such compounds can be utilized for better targeting of Aβ fibrils thereby providing suitable treatment for Alzheimer's disease.

REFERENCES

1 G. K. Bhatti, A. P. Reddy, P. H. Reddy and J. S. Bhatti, Lifestyle Modifications and Nutritional Interventions in Aging-Associated Cognitive Decline and Alzheimer's Disease, *Frontiers in Aging Neuroscience*, 2020, **11**, 1–15.

2 A. J. Karstens, L. Tussing-Humphreys, L. Zhan, N. Rajendran, J. Cohen, C. Dion, X. J. Zhou and M. Lamar, Associations of the Mediterranean diet with cognitive and neuroimaging phenotypes of dementia in healthy older adults, *The American Journal of Clinical Nutrition*, 2019, **109**, 361–368.

3 N. Kaur, V. Chugh and A. K. Gupta, Essential fatty acids as functional components of foods- a review, *Journal of Food Science and Technology*, 2014, **51**, 2289–2303.

4 D. R. Tocher, M. B. Betancor, M. Sprague, R. E. Olsen and J. A. Napier, Omega-3 long-chain polyunsaturated fatty acids, EPA and DHA: Bridging the gap between supply and demand, *Nutrients*, 2019, **11**, 1–20.

5 P. Abete, G. Testa, G. Galizia, D. Della-Morte, F. Cacciatore and F. Rengo, PUFA for Human Health: Diet or Supplementation?, *Current Pharmaceutical Design*, 2009, **15**, 4186–4190.

6 J. T. Brenna, Efficiency of conversion of α-linolenic acid to long chain n-3 fatty acids in man, *Current Opinion in Clinical Nutrition and Metabolic Care*, 2002, **5**, 127–132.

7 E. Derbyshire, Oily Fish and Omega-3s Across the Life Stages: A Focus on Intakes and Future Directions, *Frontiers in Nutrition*, 2019, **6**, 1–10.

8 E. Santigosa, D. Constant, D. Prudence, T. Wahli and V. Verlhac-Trichet, A novel marine algal oil containing both EPA and DHA is an effective source of omega-3 fatty acids for rainbow trout (Oncorhynchus mykiss), *Journal of the World Aquaculture Society*, 2020, **51**, 649–665.

9 A. N. Fonteh, M. Cipolla, A. J. Chiang, S. P. Edminster, X. Arakaki and M. G. Harrington, Polyunsaturated Fatty Acid Composition of Cerebrospinal Fluid Fractions Shows Their Contribution to Cognitive Resilience of a Pre-symptomatic Alzheimer's Disease Cohort,

Frontiers in Physiology, 2020, **11**, 1–14.

10 S. Layé, A. Nadjar, C. Joffre and R. P. Bazinet, Anti-Inflammatory Effects of Omega-3 Fatty Acids in the Brain: Physiological Mechanisms and Relevance to Pharmacology, *Pharmacological Reviews*, 2018, **70**, 12–38.

11 J. F. J. Bogie, M. Haidar, G. Kooij and J. J. A. Hendriks, Fatty acid metabolism in the progression and resolution of CNS disorders, *Advanced Drug Delivery Reviews*, 2020, **159**, 198–213.

12 P. Benatti, G. Peluso, R. Nicolai and M. Calvani, Polyunsaturated Fatty Acids: Biochemical, Nutritional and Epigenetic Properties, *Journal of the American College of Nutrition*, 2004, **23**, 281–302.

13 D. Mongan, C. Healy, H. J. Jones, S. Zammit, M. Cannon and D. R. Cotter, Plasma polyunsaturated fatty acids and mental disorders in adolescence and early adulthood: cross-sectional and longitudinal associations in a general population cohort, *Translational Psychiatry*, 2021, **11**, 321.

14 D. M. van Lent, S. Egert, S. Wolfsgruber, L. Kleineidam, L. Weinhold, H. Wagner-Thelen, W. Maier, F. Jessen, A. Ramirez, M. Schmid, M. Scherer, S. G. Riedel-Heller and M. Wagner, Eicosapentaenoic acid is associated with decreased incidence of alzheimer's dementia in the oldest old, *Nutrients*, 2021, **13**, 1–16.

15 C. Luo, H. Ren, X. Yao, Z. Shi, F. Liang, J. X. Kang, J. Wan, Z. Pei, K.-P. Su and H. Su, Enriched Brain Omega-3 Polyunsaturated Fatty Acids Confer Neuroprotection against Microinfarction, *EBioMedicine*, 2018, **32**, 50–61.

16 M. Bove, E. Mhillaj, P. Tucci, I. Giardino, S. Schiavone, M. G. Morgese and L. Trabace, Effects of n-3 PUFA enriched and n-3 PUFA deficient diets in naïve and Aβ-treated female rats, *Biochemical Pharmacology*, 2018, **155**, 326–335.

17 S. Aarti and B. Priyanka, REVIEW ON THERAPEUTIC EFFECTS MEDIATED BY OMEGA-3 FATTY ACIDS IN ALZHEIMER'S DISEASE, *Asian Journal of Pharmaceutical and Clinical Research*, 2018, **11**, 54.

18 C. Song, C.-H. Shieh, Y.-S. Wu, A. Kalueff, S. Gaikwad and K.-P. Su, The role of omega-

3 polyunsaturated fatty acids eicosapentaenoic and docosahexaenoic acids in the treatment of major depression and Alzheimer's disease: Acting separately or synergistically?, *Progress in Lipid Research*, 2016, **62**, 41–54.

19 Y. Xie, L. Yan, H. Zeng, W. Chen, J.-H. Lu, J.-B. Wan, H. Su and X. Yao, Fish oil protects the blood–brain barrier integrity in a mouse model of Alzheimer's disease, *Chinese Medicine*, 2020, **15**, 29.

20 M. Ouellet, V. Emond, C. T. Chen, C. Julien, F. Bourasset, S. Oddo, F. LaFerla, R. P. Bazinet and F. Calon, Diffusion of docosahexaenoic and eicosapentaenoic acids through the blood–brain barrier: An in situ cerebral perfusion study, *Neurochemistry International*, 2009, **55**, 476–482.

21 L. Yan, Y. Xie, S. K. Satyanarayanan, H. Zeng, Q. Liu, M. Huang, Y. Ma, J. B. Wan, X. Yao, K. P. Su and H. Su, Omega-3 polyunsaturated fatty acids promote brain-to-blood clearance of β-Amyloid in a mouse model with Alzheimer's disease, *Brain, Behavior, and Immunity*, 2020, **85**, 35–45.

22 H. Ren, C. Luo, Y. Feng, X. Yao, Z. Shi, F. Liang, J. X. Kang, J. Wan, Z. Pei and H. Su, Omega-3 polyunsaturated fatty acids promote amyloid-β clearance from the brain through mediating the function of the glymphatic system, *The FASEB Journal*, 2017, **31**, 282–293.

23 G. P. Lim, A Diet Enriched with the Omega-3 Fatty Acid Docosahexaenoic Acid Reduces Amyloid Burden in an Aged Alzheimer Mouse Model, *Journal of Neuroscience*, 2005, **25**, 3032–3040.

24 E. Hjorth, M. Zhu, V. C. Toro, I. Vedin, J. Palmblad, T. Cederholm, Y. Freund-Levi, G. Faxen-Irving, L. O. Wahlund, H. Basun, M. Eriksdotter and M. Schultzberg, Omega-3 fatty acids enhance phagocytosis of alzheimer's disease-related amyloid-β42 by human microglia and decrease inflammatory markers, *Journal of Alzheimer's Disease*, 2013, **35**, 697–713.

25 K. Miwa, M. Hashimoto, S. Hossain, M. Katakura and O. Shido, Evaluation of the inhibitory effect of docosahexaenoic acid and arachidonic acid on the initial stage of amyloid β1-42 polymerization by fluorescence correlation spectroscopy, *Advances in*

Alzheimer's Disease, 2013, **02**, 66–72.

26 A. El Shatshat, A. T. Pham and P. P. N. Rao, Interactions of polyunsaturated fatty acids with amyloid peptides Aβ40 and Aβ42, *Archives of Biochemistry and Biophysics*, 2019, **663**, 34–43.

27 M. O. W. Grimm, J. Mett, C. P. Stahlmann, V. J. Haupenthal, T. Blümel, H. Stötzel, H. S. Grimm and T. Hartmann, Eicosapentaenoic acid and docosahexaenoic acid increase the degradation of amyloid-β by affecting insulin-degrading enzyme, *Biochemistry and Cell Biology*, 2016, **94**, 534–542.

28 M. O. W. Grimm, J. Kuchenbecker, S. Grosgen, V. K. Burg, B. Hundsdorfer, T. L. Rothhaar, P. Friess, M. C. De Wilde, L. M. Broersen, B. Penke, M. Peter, L. Vígh, H. S. Grimm and T. Hartmann, Docosahexaenoic acid reduces amyloid β production via multiple pleiotropic mechanisms, *Journal of Biological Chemistry*, 2011, **286**, 14028–14039.

29 J. Nasica-Labouze, P. H. Nguyen, F. Sterpone, O. Berthoumieu, N.-V. Buchete, S. Coté, A. De Simone, A. J. Doig, P. Faller, A. Garcia, A. Laio, M. S. Li, S. Melchionna, N. Mousseau, Y. Mu, A. Paravastu, S. Pasquali, D. J. Rosenman, B. Strodel, B. Tarus, J. H. Viles, T. Zhang, C. Wang and P. Derreumaux, Amyloid β Protein and Alzheimer's Disease: When Computer Simulations Complement Experimental Studies, *Chemical Reviews*, 2015, **115**, 3518–3563.

30 N. Ntarakas, I. Ermilova and A. P. Lyubartsev, Effect of lipid saturation on amyloid-beta peptide partitioning and aggregation in neuronal membranes: molecular dynamics simulations, *European Biophysics Journal*, 2019, **48**, 813–824.

31 H. Zhou, S. Liu, Q. Shao, D. Ma, Z. Yang and R. Zhou, Mechanism by which DHA inhibits the aggregation of KLVFFA peptides: A molecular dynamics study, *The Journal of Chemical Physics*, 2018, **148**, 115102.

32 T. Lührs, C. Ritter, M. Adrian, D. Riek-Loher, B. Bohrmann, H. Döbeli, D. Schubert and R. Riek, 3D structure of Alzheimer's amyloid-β(1–42) fibrils, *Proceedings of the National Academy of Sciences*, 2005, **102**, 17342–17347.

33 W. Humphrey, A. Dalke and K. Schulten, VMD: visual molecular dynamics., *Journal of*

molecular graphics, 1996, **14**, 33–8, 27–8.

34 G. Kuang, N. A. Murugan, Y. Tu, A. Nordberg and H. Ågren, Investigation of the Binding Profiles of AZD2184 and Thioflavin T with Amyloid-β(1–42) Fibril by Molecular Docking and Molecular Dynamics Methods, *The Journal of Physical Chemistry B*, 2015, **119**, 11560–11567.

35 J. A. Lemkul and D. R. Bevan, Destabilizing Alzheimer's Aβ 42 Protofibrils with Morin: Mechanistic Insights from Molecular Dynamics Simulations, *Biochemistry*, 2010, **49**, 3935–3946.

36 R. K. Saini, S. Shuaib, D. Goyal and B. Goyal, Insights into the inhibitory mechanism of a resveratrol and clioquinol hybrid against Aβ 42 aggregation and protofibril destabilization: A molecular dynamics simulation study, *Journal of Biomolecular Structure and Dynamics*, 2019, **37**, 3183–3197.

37 S. Gupta and A. K. Dasmahapatra, Caffeine destabilizes preformed Aβ protofilaments: insights from all atom molecular dynamics simulations, *Physical Chemistry Chemical Physics*, 2019, **21**, 22067–22080.

38 K. R. Cousins, Computer Review of ChemDraw Ultra 12.0, *Journal of the American Chemical Society*, 2011, **133**, 8388–8388.

39 D. Van Der Spoel, E. Lindahl, B. Hess, G. Groenhof, A. E. Mark and H. J. C. Berendsen, *Journal of Computational Chemistry*, 2005, 26, 1701–1718.

40 C. Oostenbrink, A. Villa, A. E. Mark and W. F. Van Gunsteren, A biomolecular force field based on the free enthalpy of hydration and solvation: The GROMOS force-field parameter sets 53A5 and 53A6, *Journal of Computational Chemistry*, 2004, **25**, 1656–1676.

41 W. Huang, Z. Lin and W. F. Van Gunsteren, Validation of the GROMOS 54A7 force field with respect to β-peptide folding, *Journal of Chemical Theory and Computation*, 2011, **7**, 1237–1243.

42 A. K. Somavarapu and K. P. Kepp, The Dependence of Amyloid-β Dynamics on Protein Force Fields and Water Models, *ChemPhysChem*, 2015, **16**, 3278–3289.

43 S. S. Barale, R. S. Parulekar, P. M. Fandilolu, M. J. Dhanavade and K. D. Sonawane, Molecular Insights into Destabilization of Alzheimer's Aβ Protofibril by Arginine Containing Short Peptides: A Molecular Modeling Approach, *ACS Omega*, 2019, **4**, 892–903.

44 W. Du, J. Guo, M. Gao, S. Hu, X. Dong, Y. Han, F. Liu, S. Jiang and Y. Sun, Brazilin inhibits amyloid β-protein fibrillogenesis, remodels amyloid fibrils and reduces amyloid cytotoxicity, *Scientific Reports*, 2015, **5**, 7992.

45 F.-F. Liu, X.-Y. Dong, L. He, A. P. J. Middelberg and Y. Sun, Molecular Insight into Conformational Transition of Amyloid β-Peptide 42 Inhibited by (−)-Epigallocatechin-3-gallate Probed by Molecular Simulations, *The Journal of Physical Chemistry B*, 2011, **115**, 11879–11887.

46 G. Orteca, F. Tavanti, Z. Bednarikova, Z. Gazova, G. Rigillo, C. Imbriano, V. Basile, M. Asti, L. Rigamonti, M. Saladini, E. Ferrari and M. C. Menziani, Curcumin derivatives and Aβ-fibrillar aggregates: An interactions' study for diagnostic/therapeutic purposes in neurodegenerative diseases, *Bioorganic & Medicinal Chemistry*, 2018, **26**, 4288–4300.

47 R. K. Saini, S. Shuaib and B. Goyal, Molecular insights into Aβ 42 protofibril destabilization with a fluorinated compound D744: A molecular dynamics simulation study, *Journal of Molecular Recognition*, 2017, **30**, e2656.

48 F. Tavanti, A. Pedone and M. Menziani, Computational Insight into the Effect of Natural Compounds on the Destabilization of Preformed Amyloid-β(1–40) Fibrils, *Molecules*, 2018, **23**, 1320.

49 S. Przybylska, Lycopene – a bioactive carotenoid offering multiple health benefits: a review, *International Journal of Food Science & Technology*, 2020, **55**, 11–32.

50 H. Gohlke, C. Kiel and D. A. Case, Insights into protein-protein binding by binding free energy calculation and free energy decomposition for the Ras-Raf and Ras-RalGDS complexes., *Journal of molecular biology*, 2003, **330**, 891–913.

51 N. Homeyer and H. Gohlke, Free energy calculations by the Molecular Mechanics Poisson-Boltzmann Surface Area method, *Molecular Informatics*, 2012, **31**, 114–122.

52 S. Genheden and U. Ryde, The MM/PBSA and MM/GBSA methods to estimate ligand-binding affinities, *Expert Opinion on Drug Discovery*, 2015, **10**, 449–461.

53 R. Kumari, R. Kumar and A. Lynn, g_mmpbsa —A GROMACS Tool for High-Throughput MM-PBSA Calculations, *Journal of Chemical Information and Modeling*, 2014, **54**, 1951–1962.

54 Y. Zou, Z. Qian, Y. Chen, H. Qian, G. Wei and Q. Zhang, Norepinephrine Inhibits Alzheimer's Amyloid-β Peptide Aggregation and Destabilizes Amyloid-β Protofibrils: A Molecular Dynamics Simulation Study, *ACS Chemical Neuroscience*, 2019, **10**, 1585–1594.

55 P. K. Kanchi and A. K. Dasmahapatra, Polyproline chains destabilize the Alzheimer's amyloid-β protofibrils: A molecular dynamics simulation study, *Journal of Molecular Graphics and Modelling*, 2019, **93**, 107456.

56 S. Gupta and A. K. Dasmahapatra, Destabilization potential of phenolics on Aβ fibrils: mechanistic insights from molecular dynamics simulation, *Physical Chemistry Chemical Physics*, 2020, **22**, 19643–19658.

57 A. Kaur, S. Shuaib, D. Goyal and B. Goyal, Interactions of a multifunctional di-triazole derivative with Alzheimer's Aβ 42 monomer and Aβ 42 protofibril: a systematic molecular dynamics study, *Physical Chemistry Chemical Physics*, 2020, **22**, 1543–1556.

58 A. Kumar, S. Srivastava, S. Tripathi, S. K. Singh, S. Srikrishna and A. Sharma, Molecular insight into amyloid oligomer destabilizing mechanism of flavonoid derivative 2-(4′ benzyloxyphenyl)-3-hydroxy-chromen-4-one through docking and molecular dynamics simulations, *Journal of Biomolecular Structure and Dynamics*, 2016, **34**, 1252–1263.

59 J. M. S. Law, D. H. Setiadi, G. A. Chass, I. G. Csizmadia and B. Viskolcz, Flexibility of "Polyunsaturated Fatty Acid Chains" and Peptide Backbones: A Comparative ab Initio Study, *The Journal of Physical Chemistry A*, 2005, **109**, 520–533.

60 S. R. Shaikh, J. J. Kinnun, X. Leng, J. A. Williams and S. R. Wassall, How polyunsaturated fatty acids modify molecular organization in membranes: Insight from NMR studies of model systems, *Biochimica et Biophysica Acta - Biomembranes*, 2015, **1848**, 211–219.

61 A. C. Rustan and C. A. Drevon, Fatty Acids: Structures and Properties, *Encyclopedia of Life Sciences*, 2005, 1–7.

62 W. Stillwell and S. R. Wassall, Docosahexaenoic acid: membrane properties of a unique fatty acid, *Chemistry and Physics of Lipids*, 2003, **126**, 1–27.

63 H.-M. Fan, R.-X. Gu, Y.-J. Wang, Y.-L. Pi, Y.-H. Zhang, Q. Xu and D.-Q. Wei, Destabilization of Alzheimer's Aβ42 Protofibrils with a Novel Drug Candidate wgx-50 by Molecular Dynamics Simulations, *The Journal of Physical Chemistry B*, 2015, **119**, 11196–11202.

64 W. M. Berhanu and U. H. E. Hansmann, Side-chain hydrophobicity and the stability of Aβ 16-22 aggregates, *Protein Science*, 2012, **21**, 1837–1848.

65 W. Kabsch and C. Sander, Dictionary of protein secondary structure: Pattern recognition of hydrogen-bonded and geometrical features, *Biopolymers*, 1983, **22**, 2577–2637.

66 J. Zheng, H. Jang, B. Ma, C.-J. Tsai and R. Nussinov, Modeling the Alzheimer Aβ17-42 Fibril Architecture: Tight Intermolecular Sheet-Sheet Association and Intramolecular Hydrated Cavities, *Biophysical Journal*, 2007, **93**, 3046–3057.

67 M. Sunde, L. C. Serpell, M. Bartlam, P. E. Fraser, M. B. Pepys and C. C. Blake, Common core structure of amyloid fibrils by synchrotron X-ray diffraction., *Journal of molecular biology*, 1997, **273**, 729–39.

68 J. E. Donald, D. W. Kulp and W. F. DeGrado, Salt bridges: Geometrically specific, designable interactions, *Proteins: Structure, Function and Bioinformatics*, 2011, **79**, 898–915.

69 B. Musafia, V. Buchner and D. Arad, Complex salt bridges in proteins: Statistical analysis of structure and function, *Journal of Molecular Biology*, 1995, **254**, 761–770.

70 X. Ban, P. Lahiri, A. S. Dhoble, D. Li, Z. Gu, C. Li, L. Cheng, Y. Hong, Z. Li and B. Kaustubh, Evolutionary Stability of Salt Bridges Hints Its Contribution to Stability of Proteins, *Computational and Structural Biotechnology Journal*, 2019, **17**, 895–903.

71 D. Q. H. Pham, M. S. Li and G. La Penna, Copper Binding Induces Polymorphism in

Amyloid-β Peptide: Results of Computational Models, *Journal of Physical Chemistry B*, 2018, **122**, 7243–7252.

72 S. A. Andujar, F. Lugli, S. Höfinger, R. D. Enriz and F. Zerbetto, Amyloid-β fibril disruption by C 60 - Molecular guidance for rational drug design, *Physical Chemistry Chemical Physics*, 2012, **14**, 8599–8607.

73 A. Verma, A. Kumar and M. Debnath, Molecular docking and simulation studies to give insight of surfactin amyloid interaction for destabilizing Alzheimer's Aβ42 protofibrils, *Medicinal Chemistry Research*, 2016, **25**, 1616–1622.

74 C. N. Pace, H. Fu, K. L. Fryar, J. Landua, S. R. Trevino, B. A. Shirley, M. M. Hendricks, S. Iimura, K. Gajiwala, J. M. Scholtz and G. R. Grimsley, Contribution of Hydrophobic Interactions to Protein Stability, *Journal of Molecular Biology*, 2011, **408**, 514–528.

75 B. Tarus, J. E. Straub and D. Thirumalai, Dynamics of Asp23−Lys28 Salt-Bridge Formation in Aβ 10-35 Monomers, *Journal of the American Chemical Society*, 2006, **128**, 16159–16168.

76 C. Ritter, M. Adrian, D. Riek-loher, B. Bohrmann, H. Do, D. Schubert and R. Riek, 3D structure of Alzheimer ' s amyloid- ␣ (1 – 42) fibrils, *Proceedings of the National Academy of Sciences of the United States of America*, 2005, **102**, 17342–17347.

77 S. Brogi, S. Butini, S. Maramai, R. Colombo, L. Verga, C. Lanni, E. De Lorenzi, S. Lamponi, M. Andreassi, M. Bartolini, V. Andrisano, E. Novellino, G. Campiani, M. Brindisi and S. Gemma, Disease-Modifying Anti-Alzheimer's Drugs: Inhibitors of Human Cholinesterases Interfering with β -Amyloid Aggregation, *CNS Neuroscience & Therapeutics*, 2014, **20**, 624–632.

78 M. Karami, C. Jalali and S. Mirzaie, Combined virtual screening, MMPBSA, molecular docking and dynamics studies against deadly anthrax: An in silico effort to inhibit Bacillus anthracis nucleoside hydrolase, *Journal of Theoretical Biology*, 2017, **420**, 180–189.

79 F.-F. Liu, Z. Liu, S. Bai, X.-Y. Dong and Y. Sun, Exploring the inter-molecular interactions in amyloid-β protofibril with molecular dynamics simulations and molecular mechanics Poisson-Boltzmann surface area free energy calculations, *The Journal of Chemical Physics*, 2012, **136**, 145101.

Chapter 7

Lycopene Destabilizes Preformed Aβ Fibrils: Mechanistic Insights from All-Atom Molecular Dynamics Simulation

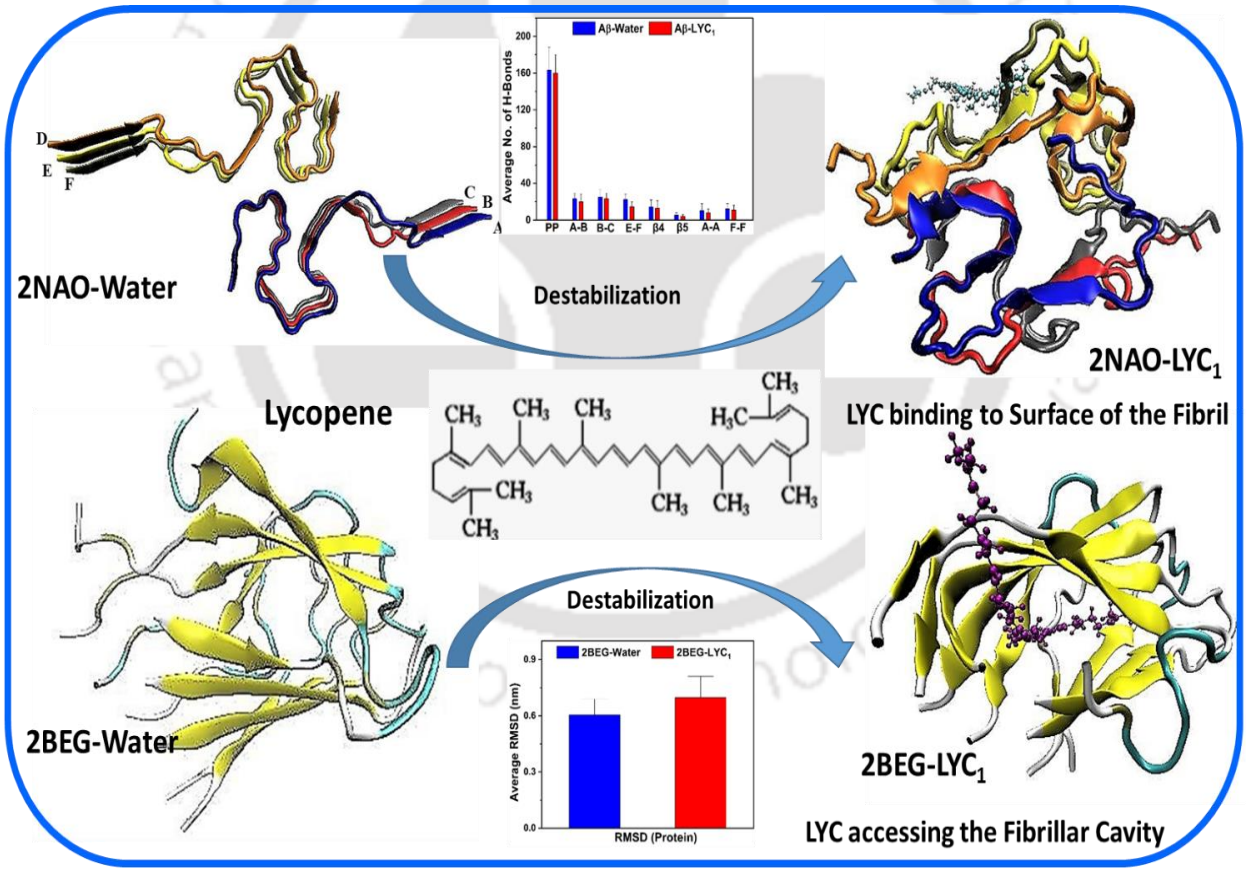

In this chapter, lycopene, a major antioxidant natural compound from terpenes (largest family of secondary metabolites from plants) have been tested for its destabilization potential on Aβ fibril.

This involves investigating the underpinning mechanism of destabilization of lycopene on different polymorphic forms of Aβ fibril viz. PDB ID: 2NAO and 2BEG via molecular dynamics (MD) simulation. The destabilization of the fibrils is evident by breakage of inherent H-bonds and hydrophobic interactions and lesser β-sheet content in the presence of one lycopene molecule. The larger size and inherent rigidity of the lycopene molecule allows binding to the upper surface of the 2NAO. However, the availability of the larger fibrillar cavity in 2BEG allows lycopene to access the cavity unlike 2NAO. The destabilization observed by lycopene on two major polymorphs of Aβ fibril explains its potency towards developing an effective therapeutic approach in treating AD.

7.1 INTRODUCTION

The significant role of the natural compounds in managing symptoms or treating Alzheimer's Disease has been established well in recent times. There have been reports about crucial role of alkaloids, polyphenolic compounds and omega-3 fatty acids, however the role of terpenoids remained elusive and uninvestigated.

The terpenoids family is the largest class of volatile secondary metabolites from plants having diverse structures that imparts fragrance, pigments and taste in the plants.[1] The terpenoids play a crucial role in plant growth, development and overall physiological processes.[2] These bioactives are reported largely for their pharmacological value as antioxidants, anti-tumor agents, anti-inflammatory and neuroprotection. The neuroprotective and anti-aging properties of lycopene (a terpenoid) has been established by *in-vivo* studies in rat model.[3] This finding triggers the investigation towards destabilization potential of lycopene on Aβ fibril to look for a prospective treatment for AD.

Lycopene ($C_{40}H_{56}$) is a dominant carotenoid, which is responsible for pink to red pigmentation in tomatoes, papaya, watermelons, apricots, guava and pink grapefruit.[4,5] The coloration depends on the concentration of the lycopene present in different sources. Lycopene is a linear, polyunsaturated hydrocarbon with thirteen double bonds, in which eleven are conjugated bonds (C=C), existing in all-trans form.[6] This naturally occurring lipophilic[7] compound needs dietary consumption, as humans can't synthesize it on their own.[8] The free radicals and lipid peroxyl radicals scavenging capacity of lycopene is reported as highest amongst the different carotenoids.[9,10] The therapeutic role of lycopene in cardiovascular disease, non-alcoholic fatty liver, malignant tumor has already been established owing to its antioxidant,[11] anti-inflammatory and anti-proliferative properties[12]. The higher lycopene blood levels are inversely related to age, plasma lipid levels, total cholesterol and triglycerides points towards the possible connection between dementia and its concentration.[13,14]

The role of lycopene in treatment and prevention of various neurodegenerative diseases like Alzheimer's (AD) and Parkinson's disease (PD) have also been reported, attributed to its antioxidative properties.[15,16] The positive correlation between lycopene levels and anti-ageing effects has been exemplary wherein the younger people has higher blood concentration levels of lycopene.[9,17] Lycopene has been found to mitigate the neuroinflammatory markers thereby diminishing the Aβ deposition in the hippocampus tissues.[18] The significant suppression of neuroinflammation and thereby curbing neuronal apoptosis by lycopene explains its neuroprotective ability. The down-regulation of neuroinflammatory cytokines by lycopene helps in ameliorating the spatial learning and memory impairment, making it a suitable cognitive promoter.[19] The administration of lycopene reported to manage dopamine levels in the rat study demonstrates its potential role in treating PD .[16,20] The epidemiological studies confirm that higher

the lycopene level, higher is the cognitive enhancement, and hence lower is risk of death from AD.[21–24].

The Aβ, main culprit behind AD, that induced cognitive impairment, has been found to be diminished by lycopene loaded microemulsion.[25] Lycopene treatment reported for reduction in the secretion of $A\beta_{42}$ peptides in SH-SY5Y cells establishes its potency for treatment of AD.[26] The penetrance of lycopene in the blood brain barrier, its natural storage in the brain and pool of promising *in-vitro* studies adds to the preferential and potent choice of lycopene as a drug for treating disorders of central nervous system, especially, AD.[27]

The profound capabilities of neuroprotection, cognitive enhancement and anti–ageing of lycopene collectively encourage the determination of its destabilization potential on Aβ fibrils. In the present study, lycopene has been considered as the representative molecule from terpenes family to determine its destabilization potential on Aβ fibril by molecular dynamics (MD) simulation. For this, one molecule of lycopene has been introduced in hexameric Aβ fibril (PDB ID: 2NAO) and simulated for 500 ns. Two systems viz. Aβ-Water and Aβ-LYC_1 after simulation, have been analyzed by determining various parameters like RMSD, R_g, SASA, RMSF and Secondary structure content. The crucial role of H-bonds, salt bridges and hydrophobic contacts have been assessed by minimum distance analysis between interacting residues. The increase in RMSD, R_g, SASA and RMSF in Aβ-LYC_1, are indicative of destabilized fibril obtained in the presence of the lycopene. The binding profile of lycopene has been observed to be on the outer surface of chain F of the fibril. The binding was mediated by G9, K16 and V18 (van der Waals) and Y10 and F20 (π-π interactions) residues of the fibril with the methyl groups and C=C bonds of the ligand, respectively. The interaction between the fibril and lycopene translates into breaking of inherent H-bonds and hydrophobic interactions, leading to the destabilization of the fibril. The

low β-sheet content exhibits the disorientation of the fibrillar structure inhibiting further higher order aggregation. The higher concentration of the lycopene (sixty molecules i.e. Aβ-LYC_{60}) has also been assessed for higher destabilization but a linear correlation is not observed. The destabilization of other virulent polymorphic form of Aβ fibril (PDB ID: 2BEG) has also been investigated for destabilization by lycopene. The ability of the lycopene to access fibrillar cavity of pentameric form explains the destabilization of the fibril. The disorganization of 2BEG is evaluated by increased RMSD and lower β-sheet content with simultaneous increase in the coil conformation. These findings collectively establish the potency and prophecy of lycopene towards destabilization of the different polymorphic forms of Aβ fibrils, and paves the pathway for formulation of lycopene (and different terpenes) as a suitable drug to treat AD.

7.2 METHODS

7.2.1 MD simulation of Aβ fibril and Lycopene

Protein- The Aβ fibril considered for the current study is the disease relevant, dimeric, LS shaped fibril that appears as a double horseshoe structure.[28] Each monomeric unit consists of three chains making it a hexameric fibril wherein chains are arranged in two subunits as A, B, C, and D, E and F as depicted in Fig. 7.1a. All the six chains are full length residues from 1 to 42 wherein residues 1-14 are reported to be partially ordered and in β-strand conformation. Residues 15-42 are relatively densely packed and form the double horseshoe-shaped structure consisting of maximally buried residues with hydrophobic side chains. The fibrillar sequence is further divided into five β-sheet regions observed for all chains: β1 (residues 2-6), β2 (residues 15-18), β3 (residues 26-28),

β4 (residues 30-32), and β5 (residues 39-42). Each chain has characteristic cross β-sheet, the prerequisite for fibrillation and stable organization of amyloids.

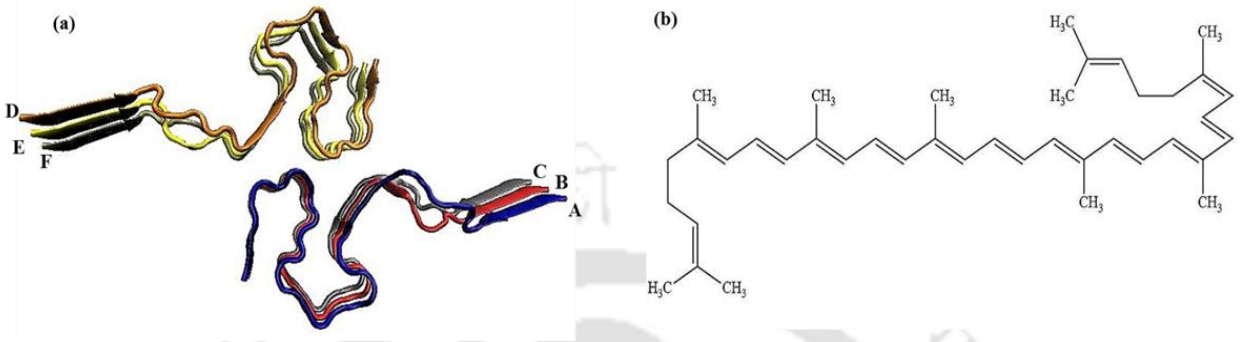

Fig. 7.1. (a)-VMD representation of 2NAO.pdb (Aβ fibril) and (b)-ChemDraw structure of Lycopene.

Ligand- Lycopene is the acyclic tetraterpene with eight isoprene units as represented by ChemDraw representation in Fig. 7.1b.[29] It has been designated as LYC in the entire manuscript. The structure for LYC has been obtained by automated topology builder (ATB). The obtained pdb coordinates further, are defined according to the GROMOS 96 54a7 force field to obtain the LYC.itp (topology file) that is gromacs readable.[30] This is further used for setting up the simulation system, as explained in the subsequent sections.

Simulation Systems- In order to study the destabilization effect of lycopene on Aβ fibril, the topology for protein and ligand has been combined, applying the same force field. The MD simulation of the systems has been performed using GROMACS v5.1.1[31] with GROMOS 96 54a7[32–34] force field. This force field has extensively been employed in various other reported studies.[32,35–41] There are two systems reported in the present study – S1 and S2 (Table 7.1). S2

consists of Aβ fibril, water with one molecule of lycopene, while S1 consists of Aβ fibril and water, and serves as a reference system.

Table 7.1. Systems definition for Molecular Dynamics Simulation

System Index	Receptor	Ligand (Lycopene, LYC.pdb)	Complex Index (.gro) for MD simulation
S0	2NAO.pdb	No ligand	Control= S0.gro (Aβ-Water)
S1	2NAO.pdb	One Molecule of LYC.pdb	Test 1 = S1.gro (Aβ-LYC_1)

The systems under investigation were solvated in a 10 × 10 × 10 nm^3 cubic box with water, represented by the SPC/E water model wherein protein is kept in the center of the box, and placed at least 1.0 nm from the box edge.[42] Further, the simulation procedure is the same as has been explained in section 4.2.2 of chapter 4 with production run for 500 ns. Three sets of each system have been simulated here also and the data is represented as an average over three sets. The repeatability gives the statistical significance and reproducibility of the results. The visualizations of MD trajectories were done using VMD (visual molecular dynamics).[43]

7.2.2 **Analysis of MD generated trajectories**

We have calculated various parameters using different tools defined within the GROMACS v5.1.1 package. The parameters that were analyzed to measure structural changes in Aβ fibril structure were same as has been explained in section 4.2.3 of chapter 4. Additionally, the contacts between different residues have been determined by calculating the possible number of contacts and

average minimum distance between them by g_mindist tool. The contact maps have been drawn for neighboring chains by using g_mdmat tool.

7.3 RESULTS AND DISCUSSIONS

7.3.1 Validation of simulation data with experimental results

Before proceeding towards measuring different parameters to assess destabilization of the fibril due to lycopene, MD ensembles obtained after 500 ns simulation were monitored for convergence. In the present study the NMR chemical shifts for backbone Cα and Cβ atoms of 2NAO.pdb given in original pdb structure and ensembles obtained after 500 ns simulation of Aβ-LYC_1 system has been compared by the help of SHIFTX2 package.[44] The higher correlation represented by R^2 value of 0.99 and 0.98 for Cα and Cβ, respectively (Fig. 7.2a and b) signifies validation of PDB structure (experimental) and simulated ensemble.

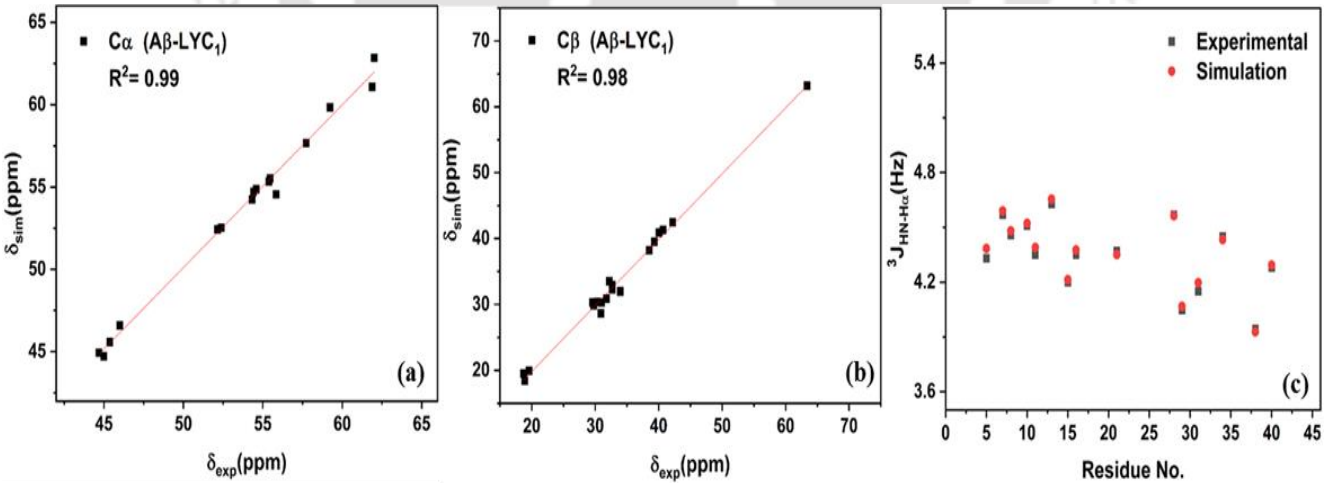

Fig. 7.2. Correlation between the theoretical and experimental NMR chemical shifts. (a)-Cα and (b)-Cβ atoms of $A\beta_{42}$ fibril structure and (c)-Comparison of simulated $^3J_{HN\text{-}H\alpha}$ coupling constants of the $A\beta_{42}$ residues (red) with experimental measurements (black).

The similar validation for PDB ID: 2BEG has also been reported [45,46] which well supports the validation of PDB ID: 2NAO as well by the same method. Three-bond J-coupling constants illustrated in Fig. 7.2c, calculated by Karplus equation using Vuister and bax parameters[47,48] have been found as 4.34 Hz for experimental and 4.36 Hz for simulated one. The close agreement found for Three-bond J-coupling constants reported by Chong et al. for Aβ monomer (PDB ID: 1IYT) are well in accordance with current findings.[49]

7.3.2 Visual inspection of the trajectories of the systems

The visual inspection of both the systems (viz., S1 and S2) considered for MD simulation has been presented in Fig. 7.3 and 7.4, respectively. Fig. 7.3a and 7.3b represent the initial configuration (i.e. at zero ns) and after the completion of production run of 500 ns respectively for S1 system. At the end of the simulation, a twisted structure of the fibril is observed (Fig. 7.3b). The twisting without unwinding indicates that the secondary structure remains intact with a stable fibrillar structure. Similar reports for the Aβ fibril (PDB ID: 2BEG) with enhanced stability and packing of the side chains of the fibril without structural modification substantiates the current observations.[50,51]

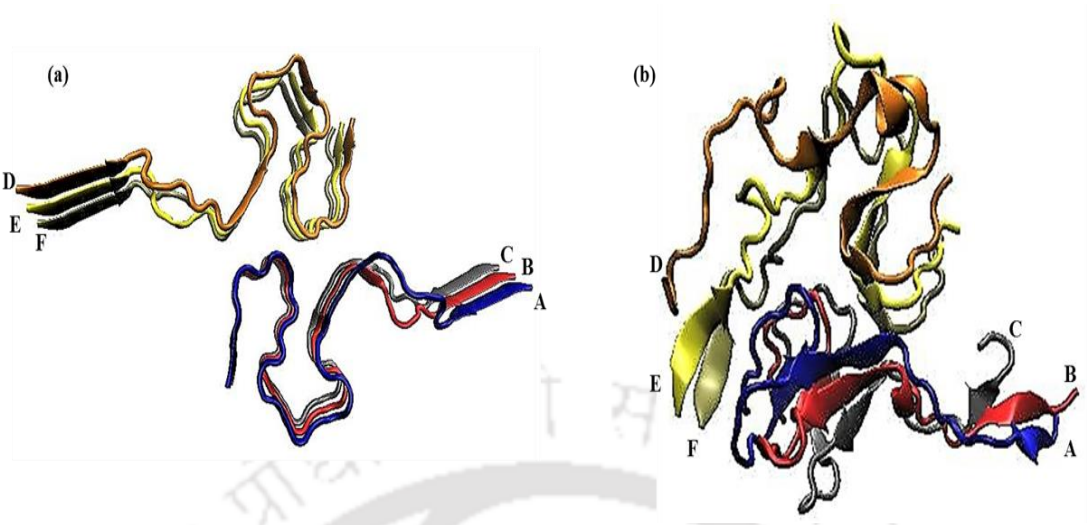

Fig. 7.3. VMD representation of snapshots of Aβ-Water at (a)-Initial and (b)-Final configuration.

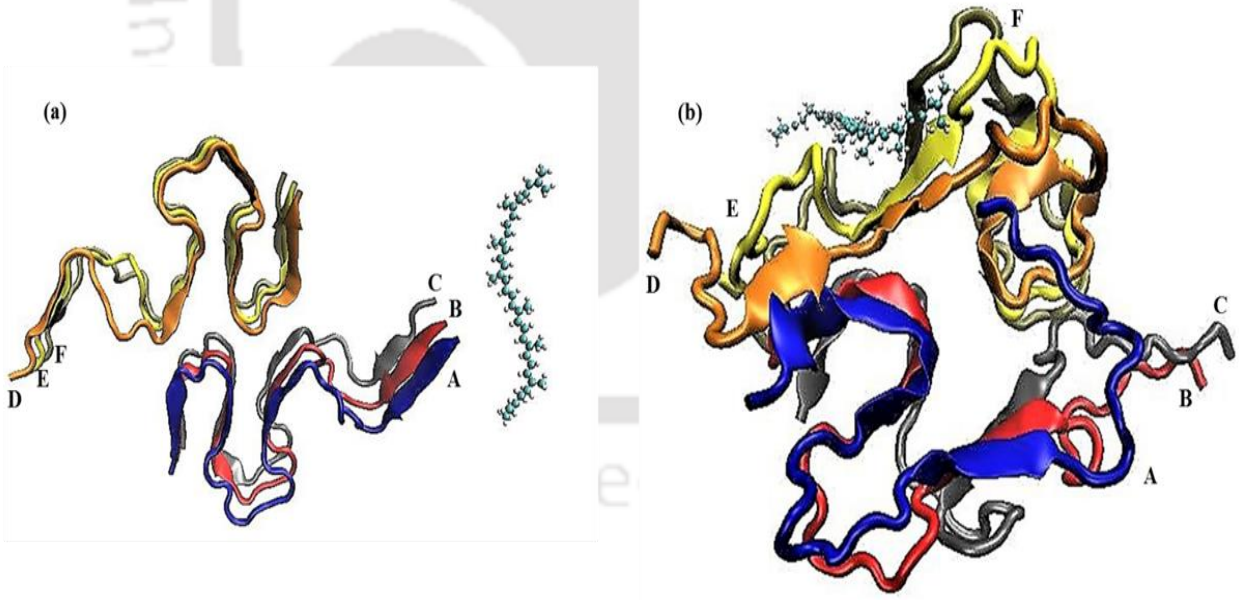

Fig. 7.4. VMD representation of snapshots of Aβ-LYC$_1$ at (a)-Initial and (b)-Final configuration.

Fig. 7.4a shows the combined system of Aβ fibril and lycopene molecule. After running the system for 500 ns, the fibril was observed to be highly perturbed and destabilized in the presence of lycopene molecule (Fig. 7.4b). The ligand is found to be interacting with the upper surface of the fibril suggesting the hindrance of the lycopene in accessing fibrillar cavity due to its rigidity and large size. The rigidity of the lycopene structure mainly arises from the presence of large numbers consecutive C=C bonds. The switching of β-sheet configuration to coil or helical (Fig. 7.4b) indicates the decrease in the β-sheet content, pointing towards the destabilization of the fibril in the presence of lycopene.

Such high level of perturbations and twisting of the Aβ fibril as compared to the native hexameric structure, highlights destabilization of the fibril and thus establishes lycopene as the promising therapeutic bioactive against AD. The current observations are in parity with the destabilized structure of Aβ fibril obtained upon interaction with ferulic acid,[52] fatty acids,[53] and THC[54]. Below, we discuss the mechanistic details of the destabilization of Aβ fibril by lycopene.

7.3.3 Structural analysis of Aβ fibril upon Lycopene interaction

The structural stability of any protein or fibril depends on the global stability parameters such as, RMSD, R_g, RMSF and SASA values. The Cα-RMSD value was calculated and depicted in Fig. 7.5a for different selections like the entire protein, chain A, chain F, and four β regions (viz., β1, β3, β4 and β5). The data for chain B, C, D and E and β2 region has not been presented and selected for further studies, as not much changes have been observed for them. The mean value of Cα-RMSD for the entire protein has increased from 0.95 ± 0.29 (Aβ-Water) to 1.05 ± 0.49 (Aβ-LYC_1) nm in the presence of lycopene (Fig. 7.5a).

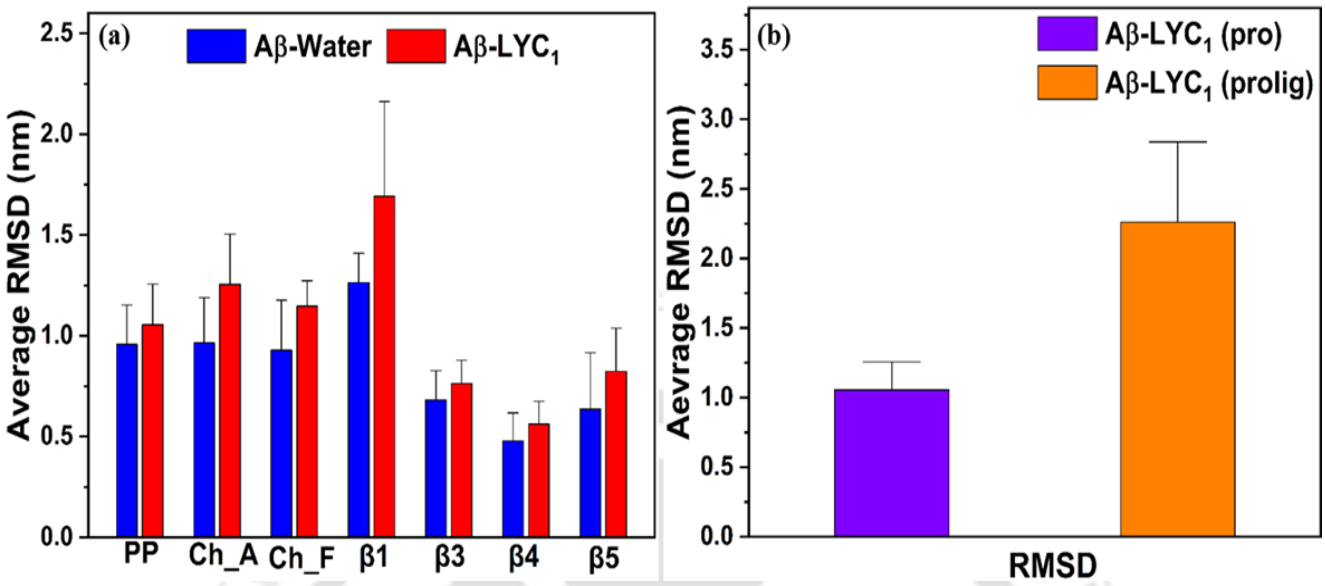

Fig. 7.5. Average Cα-RMSD value for (a)-Different selections (Aβ-Water (blue) and Aβ-LYC$_1$ (red) and (b)-pro (Violet) and prolig (orange) in Aβ-LYC$_1$.

In view of the deeper investigation, the Cα-RMSD for individual chains A and F has also been calculated and drawn in Fig. 7.5a. The selection of only these two chains is attributed to the absence of significant deviation observed for Cα-RMSD for any other chains. We have observed that Cα-RMSD of A and F chain of Aβ-LYC$_1$ system has been increased from 0.96 to 1.25 nm and 0.90 to 1.25 nm, respectively.

The corresponding time evolution of Cα-RMSD for all these selections has been depicted in Fig. 7.6a-c, wherein the Aβ-LYC$_1$ shows higher value compared to the Aβ-Water system, indicating significant destabilization of the fibril in the presence of lycopene. Typically, the stability of an Aβ-fibril is largely governed by β regions, responsible for cross-β arrangement important for amyloid formation.[55] In this view, the Cα-RMSD for β1, β3, β4 and β5 regions have been calculated and depicted in Fig. 7.5a, wherein the average value for Aβ-LYC$_1$ system has been

found higher to the Aβ-Water. The higher Cα-RMSD value for these four β regions for Aβ-LYC$_1$ system point towards the destabilization of the entire fibril in the presence of lycopene. The time evolution of Cα-RMSD for β1, β3, β4 and β5 regions is illustrated in Fig. 7.6d-g where it was found to be increased in the presence of lycopene.

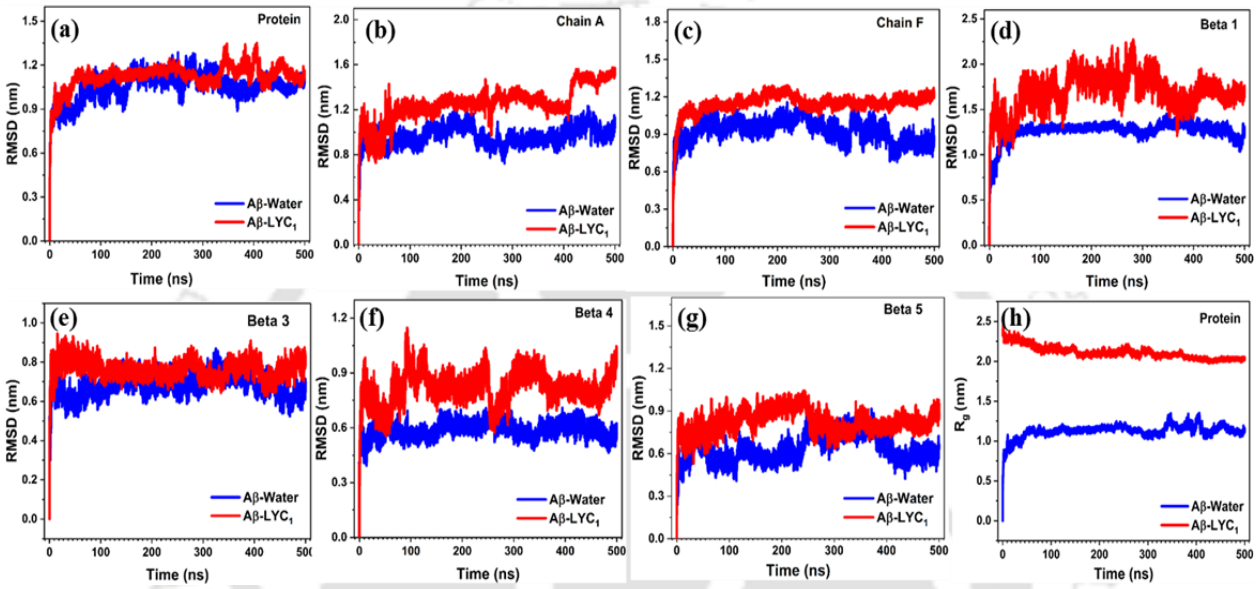

Fig. 7.6. Time evolution of Cα-RMSD value of Aβ-Water (blue) and Aβ-LYC$_1$ (red) for (a)-Protein, (b)-Chain A and (c)-Chain F (d)-Beta1, (e)-Beta3, (f)-Beta4, (g)-Beta5 and (h)-R_g for protein.

The increment of Cα-RMSD from 1.05 nm in protein (pro) only to 2.26 nm in protein-ligand (prolig) for Aβ-LYC$_1$ system (Fig. 7.5b), indicates contribution of lycopene towards destabilization of the fibril. A similar observation on higher Cα-RMSD value for prolig system as compared to the protein only construing destabilization has been reported with caffeine as the ligand, is in close agreement with the present findings.[56]

Radius of gyration (R_g) measure the overall compactness of the fibril. Any loss of compactness is an indication of disorganization of the fibril, leading to destabilization. We have measured R_g for both S1 and S2 systems and found that R_g of S2 is 2.11 nm compared to 1.12 nm in S1 (Fig. 7.7a). This large enhancement in R_g is a strong evidence of destabilization of the fibril in the presence of lycopene. Our result matches qualitatively with the destabilization of Aβ fibril by D744 (a fluorinated compound)[46] and Caffeine[56] where a similar increase in R_g have been observed. Time evolution of R_g has been presented in Fig. 7.6h wherein the stark difference has been observed for Aβ-LYC_1 as compared to Aβ-Water.

The extent of destabilization has also been evaluated by average RMSF (Fig. 7.7b) and SASA (Fig. 7.7c) values for the entire protein. Both the RMSF and SASA values have been found to be marginally increased for S2 as compared to S1, indicating destabilization of the fibril in the presence of lycopene. The increased RMSF value (Fig. 7.7b), which accounts for increased flexibility of the fibrillar chains, is consistent with observations, where morin,[57] wgx-50,[58] ellagic acid[59] have been used as ligands. The increased average SASA value (Fig. 7.7c) reflects the increased hydrophilicity of the fibril in the presence of lycopene, resulting in higher mobility and thus larger disorientation similar to reported for dihydrochalcone[60] and ellagic acid[59] molecule.

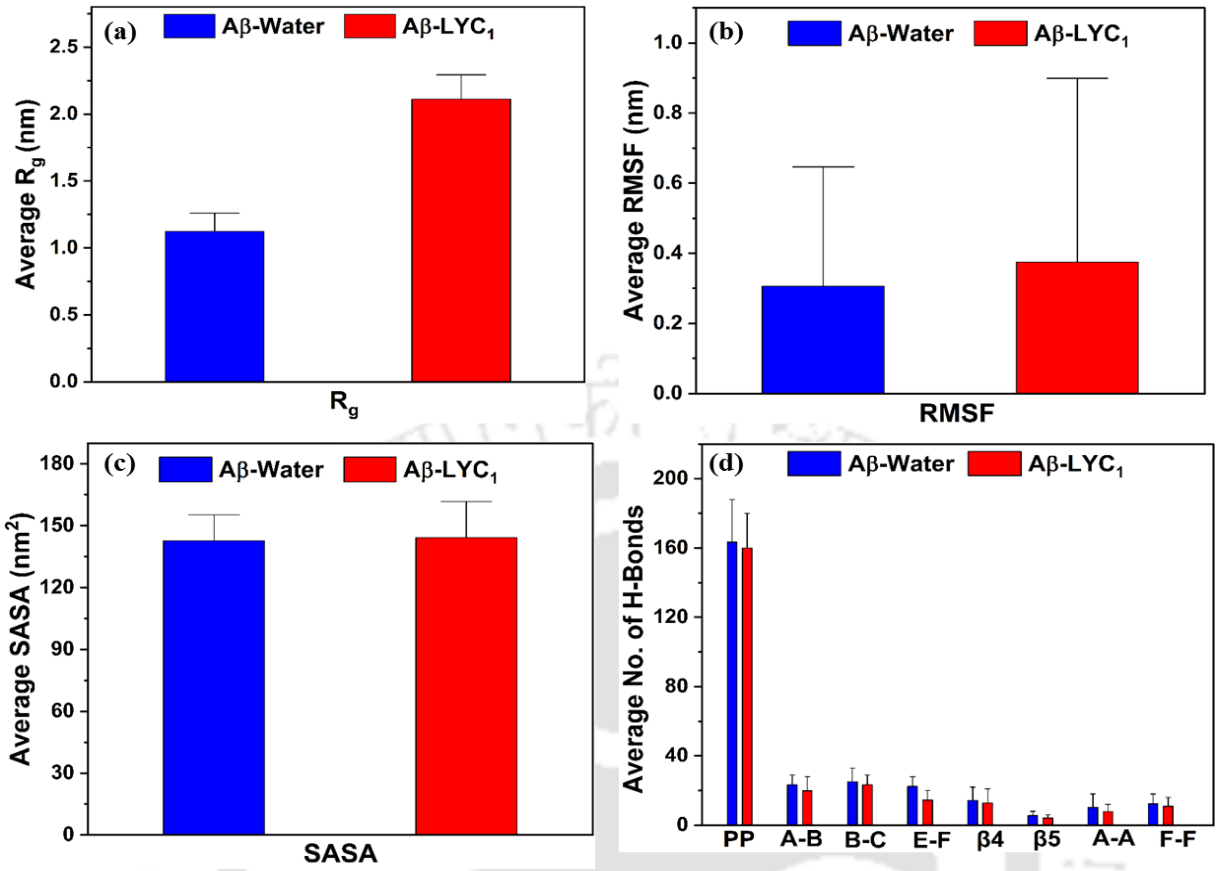

Fig. 7.7. Average value of (a)-R_g and (b)-RMSF, (c)-SASA and (d)-Average no. of H-bonds across various selection (Aβ-Water (blue) and Aβ-LYC_1 (red)).

7.3.4 Effect of Lycopene on H-bonds

Hydrogen bonds (intra- and inter-chain) plays a crucial role in formation, stability and integrity of different structural motifs of proteins. Stability of α-helix and β-sheet structures are largely governed by hydrogen bonds (H-bonds) both in a single protein and in an aggregate (viz. fibril). The average number of H-bonds for the entire protein, inter-chain (A-B, B-C, E-F) and intra-chain (A-A and F-F), two beta regions (β4 and β5 region) have been determined for both the systems and presented in Fig. 7.7d. Other selections (viz. inter-chain C-D and D-E and intra-chain B-B, C-

C, D-D and E-E and β1, β2 and β3 regions) have been ignored due to lack of observational changes in the number of H-bonds between two systems under investigation. The notable decrease in the average number of H-bonds recorded for various selections in Aβ-LYC_1 system as observed from Fig. 7.7d and Table 7.2, indicates breakage of inherent H-bond network in the presence of lycopene, suggesting a disorganized structure.

Table 7.2. Average No. of H-bonds with % reduction for each selection

S. No.	Average No. of H-Bonds	Aβ-Water	Aβ-LYC_1	% Reduction
1	**PP**	163.40 ± 0.34	159.90 ± 0.34	2.06 ± 0.39
2	**Chain A-B**	23.33 ± 0.15	19.87 ± 0.35	14.83 ± 0.43
3	**Chain B-C**	24.99 ± 0.46	23.33 ± 0.19	6.64 ± 0.34
4	**Chain E-F**	22.36 ± 0.15	14.48 ± 0.32	35.24 ± 0.32
5	**β4**	5.47 ± 0.37	4.11 ± 0.10	24.86 ± 0.77
6	**β5**	7.75 ± 0.39	6.63 ± 0.10	14.45 ± 0.32
7	**Chain A-A**	10.68 ± 0.32	7.85 ± 0.50	26.49 ± 0.32
8	**Chain F-F**	12.27 ± 0.16	10.89 ± 0.16	11.24 ± 0.19

The reduction of H-bonds for E-F and A-A is 35.24 % and 26.49 %, respectively, which suggests that chain A and F are the most affected chains in the entire hexamer. Similarly, β4 and β5 region reported loss of 24.86 % and 14.45 % respectively, suggesting instability in these regions leading to instability of the fibril. The loss of number of H-bonds by BSB (beta sheet breaker) peptides,[61] MOS_2 based nanomaterial,[62] and biflavonoid[63] leading to distortion of the fibril, are in close agreement with our results.

7.3.5 Effect of Lycopene on Inter-Chain Interactions

The inter-chain interactions driven by inter-residue contacts play a pivotal role in imparting the strength and structural stability to any protein. The important pairs of contacts that are responsible for the stability of the fibril are identified as: Q15-M35 and L17-M35.[28] Fig. 7.8 represents the inter-chain average distance for Q15-M35 contact for A-D, B-E and C-F and L17-M35 contact for A-D and C-F. The average distance of Q17-M35 contact for inter-chain A-D, B-E and C-F (Fig. 7.8a) has been observed at increased value for Aβ-LYC_1 as compared to Aβ-Water system, suggesting breakage of these contacts leading to the destabilization of the fibril. Similarly, the average distance of L17-M35 contact for inter-chain A-D and C-F for Aβ-LYC_1 has been increased significantly (Fig. 7.8b) compared to Aβ-Water. However, not much change has been observed for chain B-E for Aβ-LYC_1 over Aβ-Water system. Our observations well-match with the reported results based on dihydrochalcone,[60] and flavonoid derivative,[64] ellagic acid,[59] brazilin,[36] and a flavonoid compound[40] as the ligand. The higher value for average distance of inter-chain residues, observed in Aβ-LYC_1 system elucidates the mechanistic details behind destabilization of the fibril.

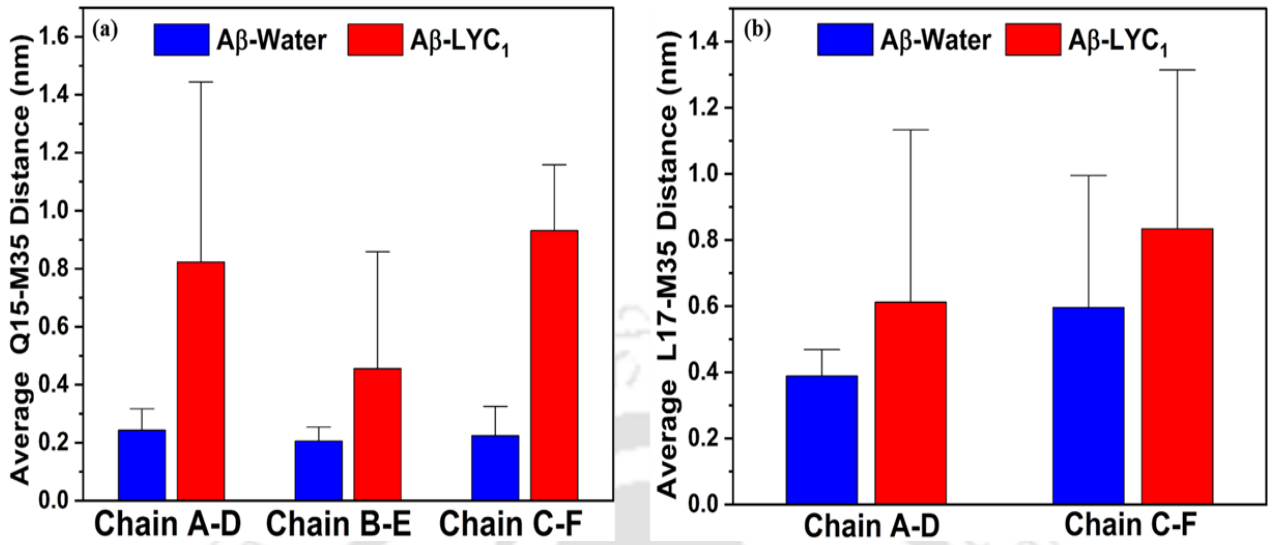

Fig. 7.8. Inter-Chain (a)-Q15-M35 distance for Chain A-D, Chain B-E and Chain C-F and (b)-L17-M35 distance for Chain A-D and Chain C-F (Aβ-Water (blue) and Aβ-LYC$_1$ (red)).

7.3.6 Effect of Lycopene on Intra-Chain Interactions

The intra-chain interactions, consisting of salt bridges and hydrophobic interactions, are believed to be a major contributor towards strength and stability of Aβ-fibril.[65,66] The average distance of K28-A42 (salt bridge), L17-L34 and I31-V36 (hydrophobic bonding) for both the chains (A and F) and both the systems (S1 and S2) has been determined and illustrated in Fig. 7.9. The average distance for Aβ-Water (viz., S1) system for all these pairs have been found within 0.5 nm (Fig. 7.9a-c), indicative of bond formation between them and thus govern the stability to chain A and F. The K28-A42 distance of chain-A in Aβ-LYC$_1$ system has been increased to ~ 0.95 nm from ~ 0.50 nm in Aβ-water (Fig. 7.9a), indicating breakage of salt-bridge, and hence instability in the fibril.

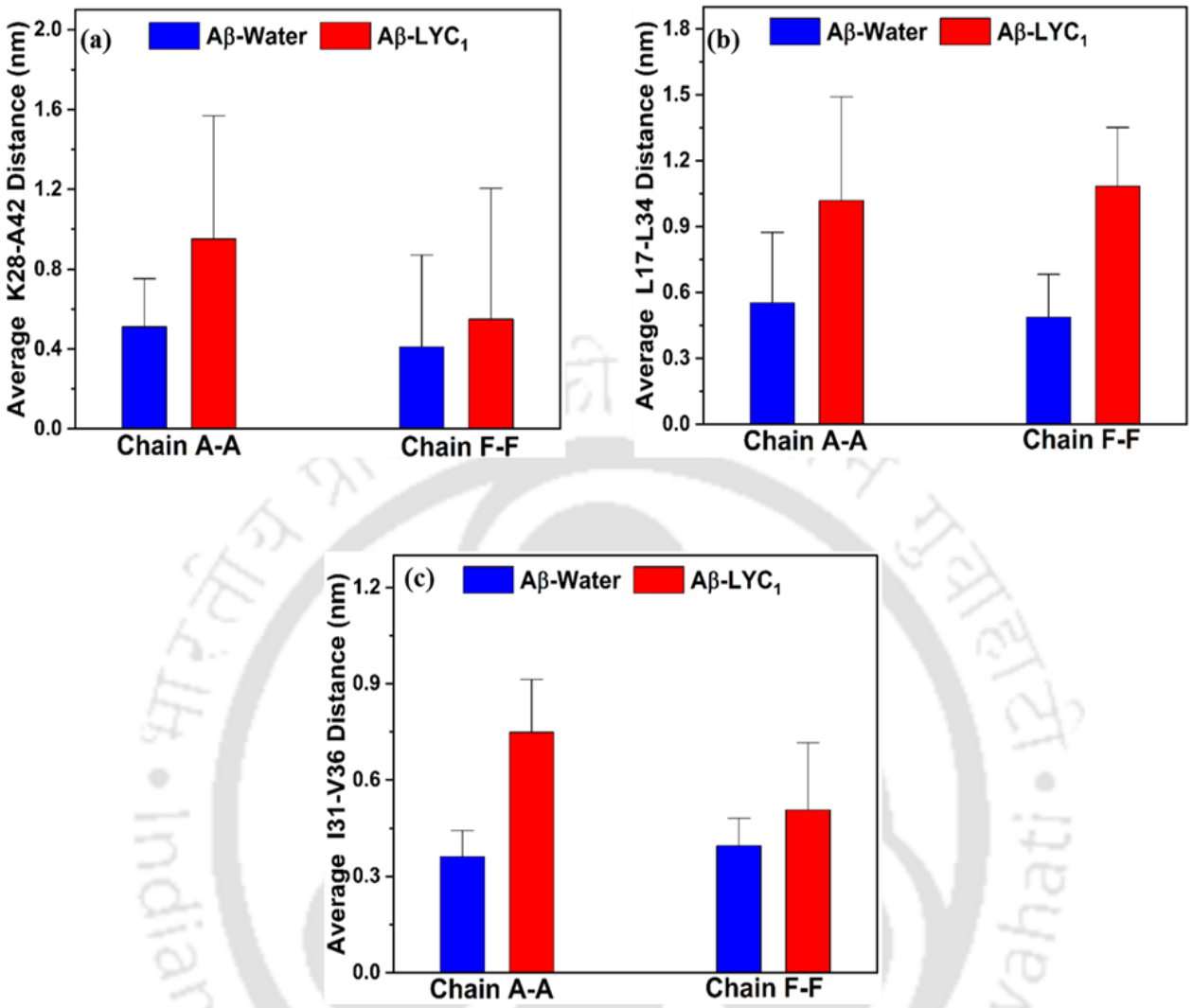

Fig. 7.9. Intra-Chain average distance for chains (A and F) for (a)-K28-A42 (b)-L17-L34, and (c)-I31-V36 for Aβ-Water (blue), Aβ-LYC$_1$ (red)).

The breaking of same salt bridge can be observed for chain F on account of increased intra-residual distance to 0.54 nm in Aβ-LYC$_1$ from 0.41 nm in Aβ-Water (Fig. 7.9a). Similar breakage of salt-bridge has also been observed of an LS shaped neurotoxic fibril (PDB ID: 5OQV).[67] The disruption of salt-bridges reported in the presence of serotonin and melatonin[68] causing destabilization of the fibril are in concordance to our findings. The role of hydrophobic interactions has been exemplary for such high stability and strength of the amyloid fibrils[50,69,70] and symbolic to the fibrillization

process.[71] The distance between L17-L34 has been found to be increased to 1.01 nm (chain A) and 1.08 nm (chain F) for Aβ-LYC_1 system from 0.55 nm and 0.48 nm in Aβ-Water system, respectively (Fig. 7.9b) indicating breakage of this bond for both chains A and F. Similarly, the average distance for I31-V36 pair in Fig. 7.9c suggest breaking of these bonds in Aβ-LYC_1 on account of increased value of 0.74 nm for chain A as compared to 0.36 nm (Aβ-Water). The destabilization of the fibril on account of breaking of intra-chain interactions in the presence of lycopene is well supported by substantial destabilization of the fibril reported by polyunsaturated fatty acids,[53] bis-tacrine compounds,[67] and arginine containing short peptides.[35]

7.3.7 Secondary Structure conformations in presence of Lycopene

The secondary structure analysis by the DSSP tool delivers the time evolution profile of possible secondary structure configurations achievable by Aβ fibril. The higher β-sheet content in Aβ fibril drives its amyloidogenesis, ensuing such stability and longevity of the fibril. A comparative graphical description for the secondary structure profile for the entire fibril illustrated in Fig. 7.10a and b for Aβ-Water and Aβ-LYC_1, respectively, depicts loss of β-sheet and β-bridge content in Aβ-LYC_1. All the secondary structure contents have been quantified and tabulated in Table 7.3 for both the systems, with % change (increase or decrease) recorded in Aβ-LYC_1 compared to Aβ-Water system. The decrease of 23.33% β-sheet and 50% β-bridge content with simultaneous increase of 20% coil and 40% turn explains the disorganization of the fibril in Aβ-LYC_1. To gain more insights on the most affected chains by lycopene, the time evolution DSSP profile for chains A and F have been plotted separately for both the systems in Fig. 7.10c-f.

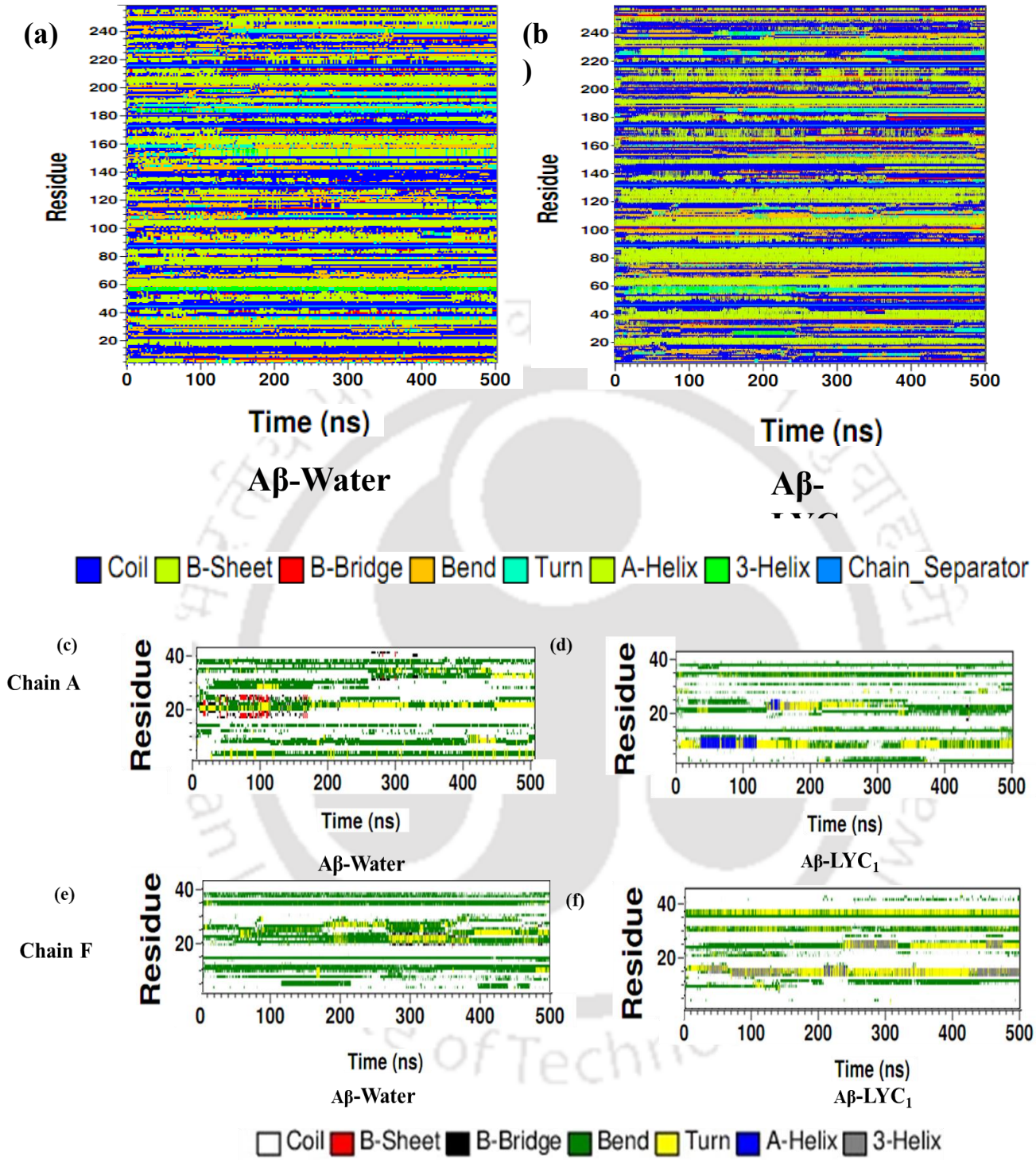

Fig. 7.10. The DSSP time evolution for 500 ns for all the six chains for (a)-Aβ-Water and (b)-Aβ-LYC$_1$. A comparative representation for chain A in upper panel (c and d) for Aβ-Water and Aβ-LYC$_1$ system and chain F in lower panel (e and f) for Aβ-Water and Aβ-LYC$_1$.

The presence of β-sheet and β-bridge in Aβ-Water in chain A and F can be viewed from Fig. 7.10c and e, respectively. In contrast to Aβ-Water, the emergence of α-helix and 3-helix in chain A and F, respectively, in Aβ-LYC_1 has been observed (Fig. 7.10d and f). The observed higher helical content in Aβ-LYC_1 corresponds well with the higher hydrophilicity, and thus higher SASA values as reported above (see section 7.3.3).[72] A similar reduction in β sheet content of Aβ fibril, leading to its destabilization in the presence of caffeine,[56] a fluorinated derivative of curcumin[40] and norepinephrine[73] is found to be coherent with the current findings. The lowered β-sheet and higher helical content collectively establishes the destabilization of the fibril, and inhibition to form higher order aggregates in the presence of lycopene.

Table 7.3. Secondary Structure content for whole protein for both the systems

Secondary Structure (%) Whole Protein	**Aβ-Water Whole Protein**	**Aβ-LYC_1 Whole Protein**	**% Change (Increase (+) or Decrease (-)**
Coil	40	48	(+) 20
β-Sheet	30	23	(-) 23.33
β-Bridge	4	2	(-) 50
Bend	15	19	(+) 26.66
Turn	5	7	(+) 40
α-helix	0	1	(+) 100

3-helix	1	2	(+) 100
Chain_Separator	2	2	0

7.3.8 Binding of Lycopene molecule with the Aβ fibril

The binding or interaction profile of any ligand with the protein is of highest significance and forms the basis of any biological activity. The minimum average distance between the ligand and all the six chains have been determined by g_mindist and plotted in Fig. 7.11a. Lycopene appears to be interacting with the chain F of the fibril due to their closest proximity. The minimum distance between lycopene and chain F of the fibril corroborates well with the increased RMSD value (Fig. 7.4a) and loss of native contacts of the fibril (Fig. 7.11b). The corroborated findings can be viewed by contact maps in Fig. 7.11b, wherein the inherent contacts are found to be less between chain A-B, B-C and E-F in Aβ-LYC$_1$ (lower panel) as compared to the Aβ-Water (upper panel).

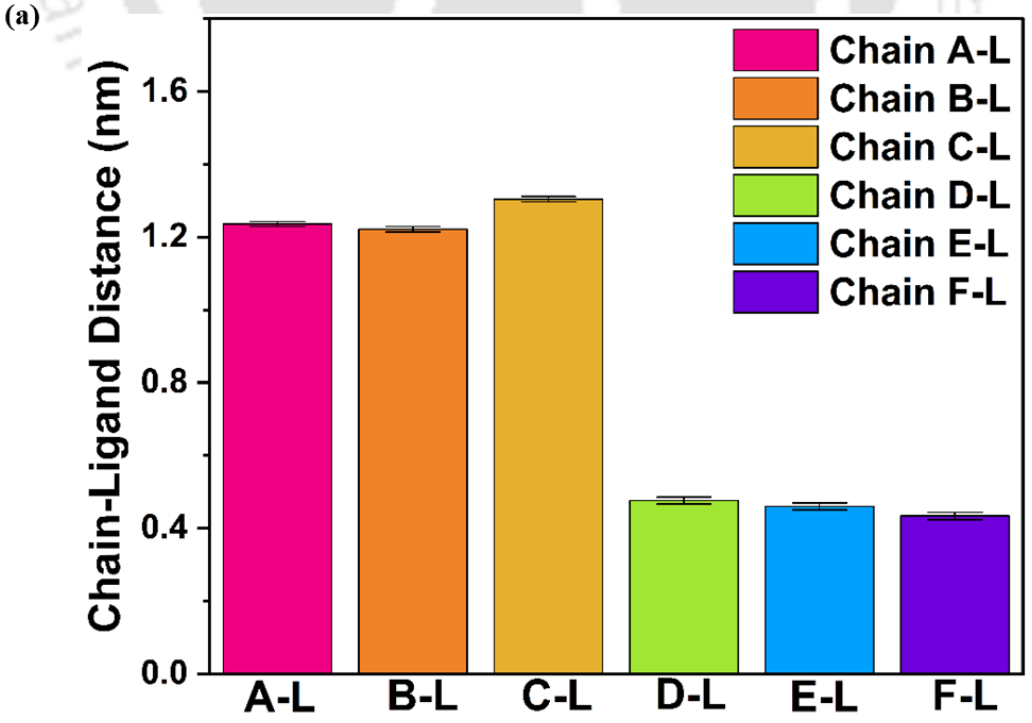

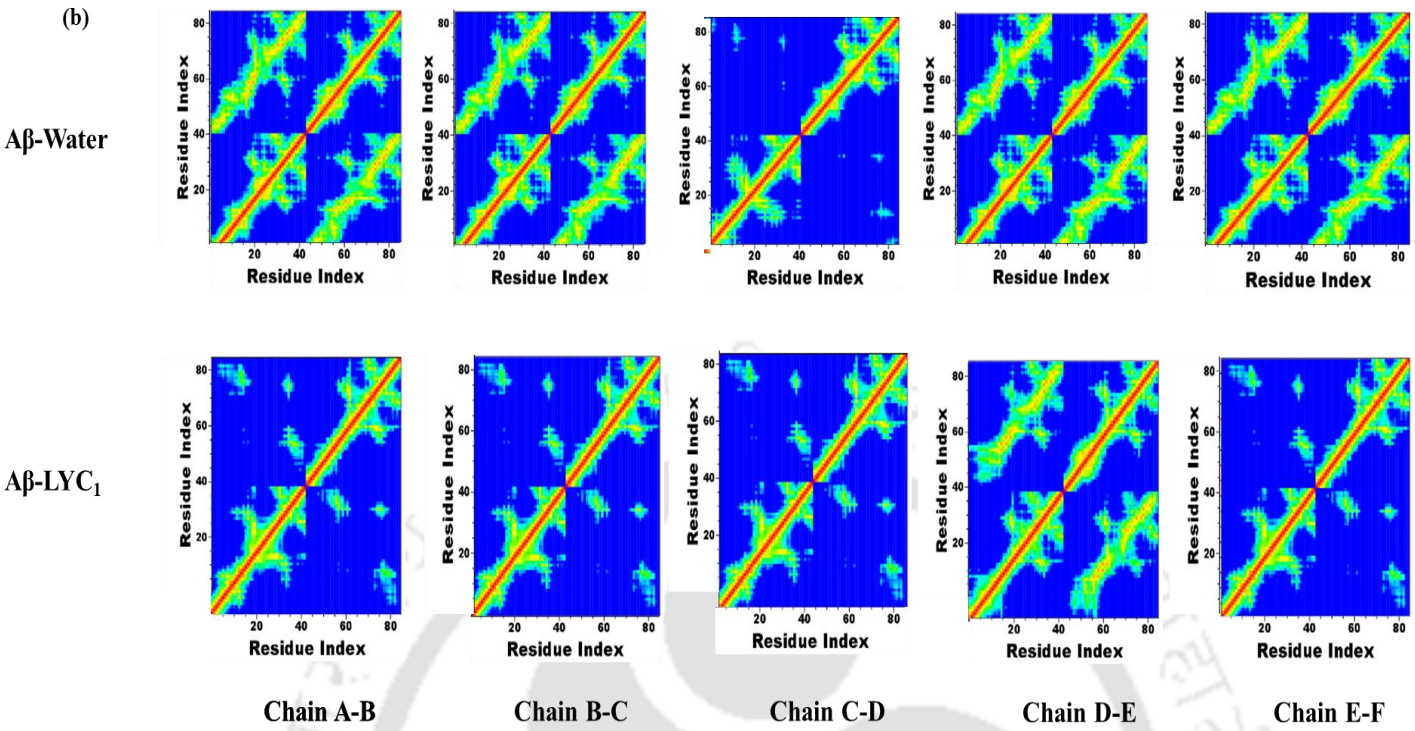

Fig. 7.11. (a)-Average distance between individual chains of Aβ fibril and ligand (LYC) and (b)-Contact maps between all neighboring chains in Aβ-Water (upper panel) and Aβ-LYC$_1$ (lower panel).

The loss of native contacts points towards the destabilization of the fibril in the presence of lycopene. Similar findings of breaking of inherent contacts in Aβ fibril in the presence of curcumin and tetracycline are found in parity with our observations.[74] From Fig. 7.12, it can be clearly observed that the lycopene binds to the upper surface of the fibril via Gly9, Tyr10, Lys16, Val18 and Phe20 residues of chain F involved in interaction. The distance between interacting entities of ligand and fibril has also been depicted with dashed line in Fig. 7.12. The number of contacts, average minimum distance and kind of interaction depending on the property of the residue is tabulated in Table 7.4.

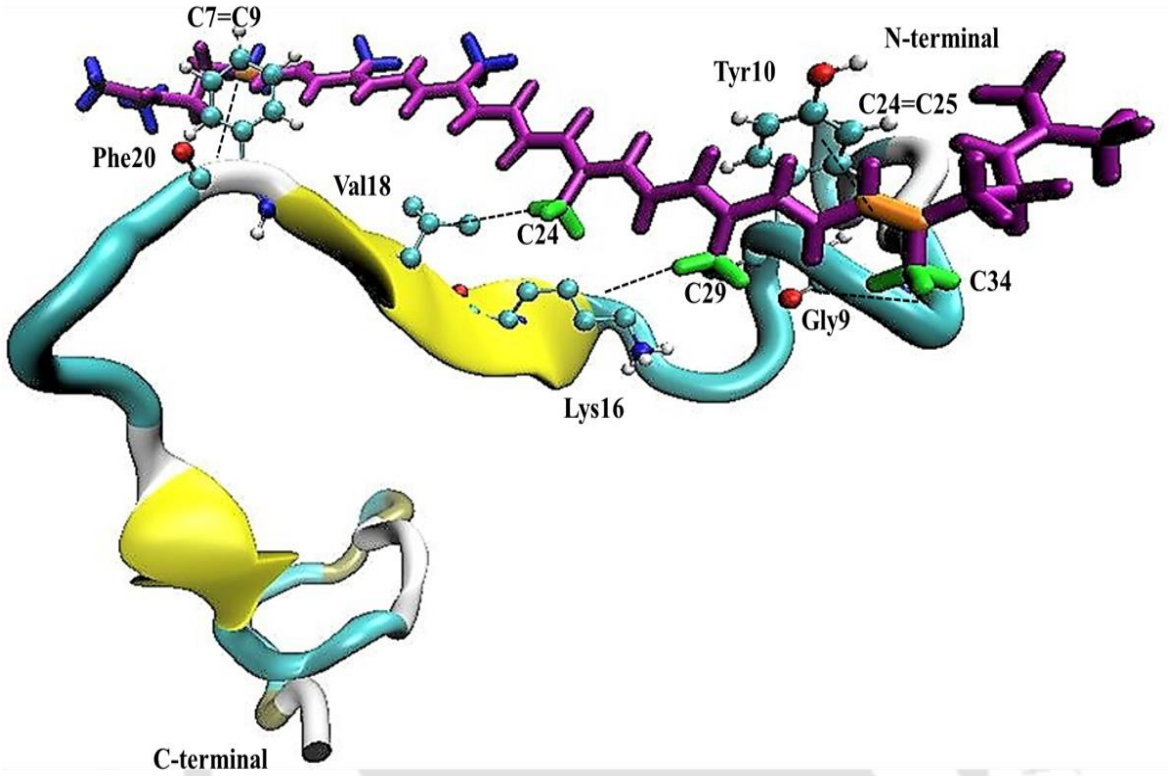

Fig. 7.12. VMD representation (new cartoon) depicting interactions between lycopene with the chain F of the fibril (Methyl Groups in Green and Blue, C=C in Orange colour, Residues in CPK representation).

Herein, the G9, K16 and V18, being the hydrophobic residues, are able to show van der Waals interactions with the methyl groups present in the ligand. The possibility of π–π interaction has been reported for Y10 and F20 of chain F of the fibril and C24=C25 and C7=C9 of the lycopene owing to the aromatic residues and sp^2 hybridized carbons of the ligand respectively. This interaction pattern explains the bonding regions of the lycopene on the surface of the fibril, thereby perturbs its native contacts causing destabilization. The existence of these bonds both van der Waals and π–π interaction, as tabulated in Tabel 7.4, have been postulated by calculating the

average mean distance between these residues, thereby giving the mean distance (that comes in the cut off range to form a bond) and number of contacts.

Table 7.4. Residues involved in binding of chain F of 2NAO.pdb and Lycopene

S. No.	Residue from chain F	Secondary Structure Conf.	Ligand Part	Number of Contacts	Average Minimum Distance (nm)	Kind of Interaction
1.	Gly9 (G9)	Turn	C34 (methyl group)	19	3.50	Van der Waals
2.	Tyr10 (Y10)	Turn	C24=C25	32	2.75	π–π interaction
3.	Lys16 (K16)	β-sheet	C29 (methyl group)	20	3.21	Van der Waals
4.	Val18 (V18)	β-sheet	C24 (methyl group)	14	2.77	Van der Waals
5.	Phe20 (F20)	Coil	C7=C9	21	3.25	π–π interaction

This kind of surface-mediated interaction indicates the inherent rigidity and bulky size of lycopene and explains the efficacy of the lycopene in destabilizing higher order fibrils like 2NAO without even need for accessing their cavity. The molecular details gained by MD simulation for

interaction and thus destabilization of the Aβ fibril by lycopene, establishes lycopene as a potential drug candidate in treating AD.

7.3.9 Relation between high Lycopene concentration and destabilization

In order to understand the relation between higher concentration of the lycopene and extent of destabilization, sixty molecules (viz., 10:1) have been added to the same Aβ fibril (viz., 2NAO) by random insertion method. The system is denoted as Aβ-LYC_{60} and simulated of 500 ns following the same strategy as explained in the method section (section 7.2.1). The VMD representation of Aβ-LYC_{60} system has been depicted in Fig. 7.13a, at zero ns which after 500 ns of simulation is found to be destabilized on account of perturbations observed in Fig. 7.13b.

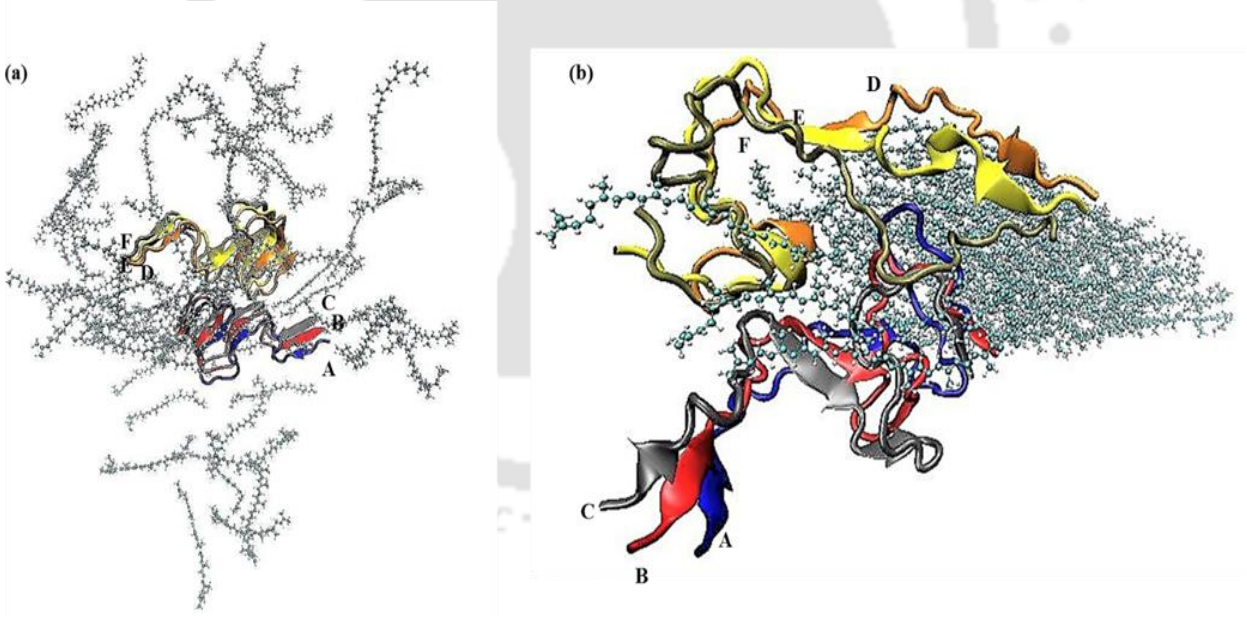

Fig. 7.13. VMD representation of snapshots of Aβ-LYC_{60} at (a)-Initial and (b)-Final configuration.

Various parameters has been measured such as, RMSD, R_g, SASA and number of H-bonds Fig. 7.14a-e compares the results of RMSD, R_g, RMSF, SASA and number of H-bonds for Aβ-water respectively for Aβ-Water, Aβ-LYC_1, and Aβ-LYC_{60} systems. It can be seen that Aβ-LYC_{60} system shows a marginal effect in destabilizing the fibril. The introduction of higher number of lycopene molecules (sixty) does not present a linear correlation with the extent of destabilization, suggesting the possibility of self-aggregation of lycopene molecules, as can be seen from Fig. 7.14b. Interaction between the like molecules exhibits the possible reason behind self-aggregation. The self-aggregation of lycopene molecules restricts the interaction with the fibril.

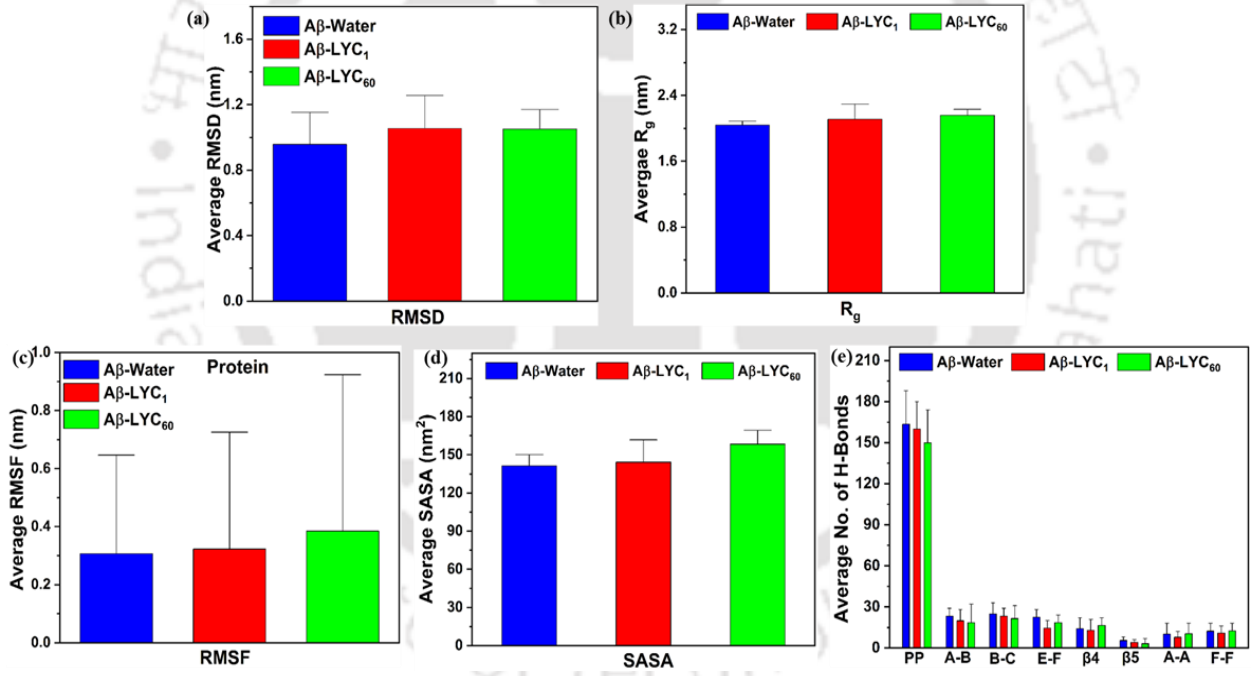

Fig. 7.14. Average value of (a)-RMSD, (b)-R_g, (c)-RMSF (d)-SASA and (e)-Average no. of H-bonds across various selection for Aβ-Water (blue), Aβ-LYC_1 (red) and Aβ-LYC_{60} (green).

The quantification of average distance for inter-chain (Q15-M35) have also been measured and plotted in Fig. 7.15a-c for chain A-D, B-E and C-F. However, no significant difference from the Aβ-LYC_1 system was observed.

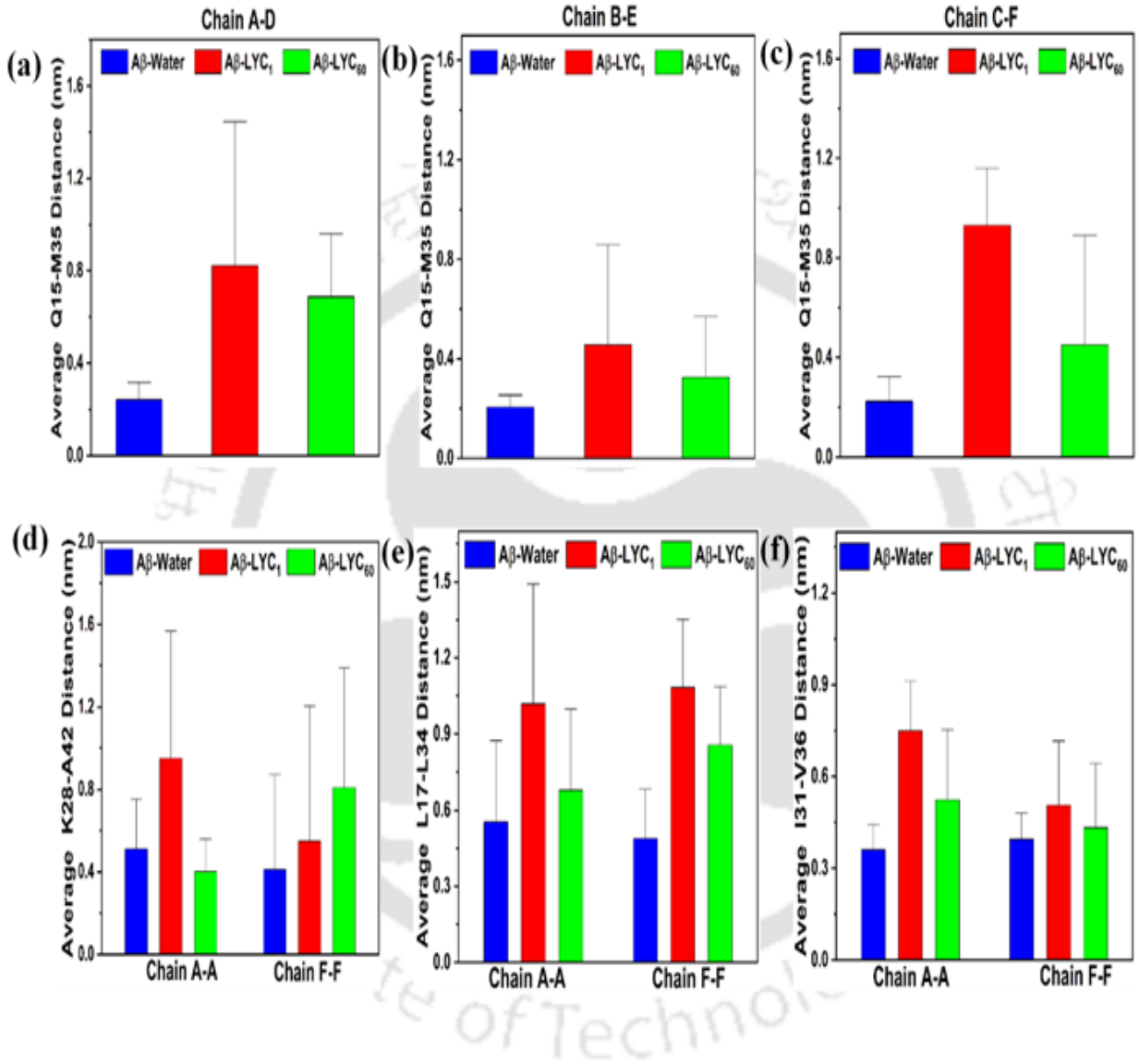

Fig. 7.15. Inter-chain average Q15-M35 distance for (a)-Chain A-D, (b)-Chain B-E and (c)-Chain C-F (upper panel) and Intra-chain average distance for chains (A and F) for (a)-K28-A42, (b)- L17-L34 and (c)-I31-V36 residues (lower panel) where Aβ-Water (blue), Aβ-LYC_1 (red) and Aβ-LYC_{60} (green).

The similar or higher or even lesser values has been observed for Aβ-LYC_{60} system for intra-chain (K28-A42, L17-L34 and I31-V36 residues) contacts, depicted in Fig. 7.15d-f respectively. All these observations collectively suggest the lack of direct correlation between destabilization and higher concentration of lycopene molecules.

7.3.10 Interaction of Lycopene with U-shaped neurotoxic Aβ fibril (2BEG.pdb)

In order to measure the destabilization effect of lycopene on the other disease relevant polymorphic form of Aβ fibril, U-shaped neurotoxic fibril (PDB ID: 2BEG) has been considered. The 2BEG is the pentameric structure with five chains having three β regions with 17-42 residue length for all chains.[75] In this direction, one lycopene molecule has been placed randomly with the 2BEG and simulated for 100 ns employing the same simulation strategy as explained in section 7.2.1 for 2NAO. The VMD representation of the final snapshot (at 100 ns) for 2BEG in water (2BEG-Water) and 2BEG with lycopene (2BEG-LYC_1) has been drawn in Fig. 7.16a and b respectively. The terminal chain in 2BEG-LYC_1 is observed to lose its β-sheet content replacing it with the random coil as compared to the 2BEG-Water (Fig. 7.16b), indicating destabilization of the fibril in the presence of lycopene.

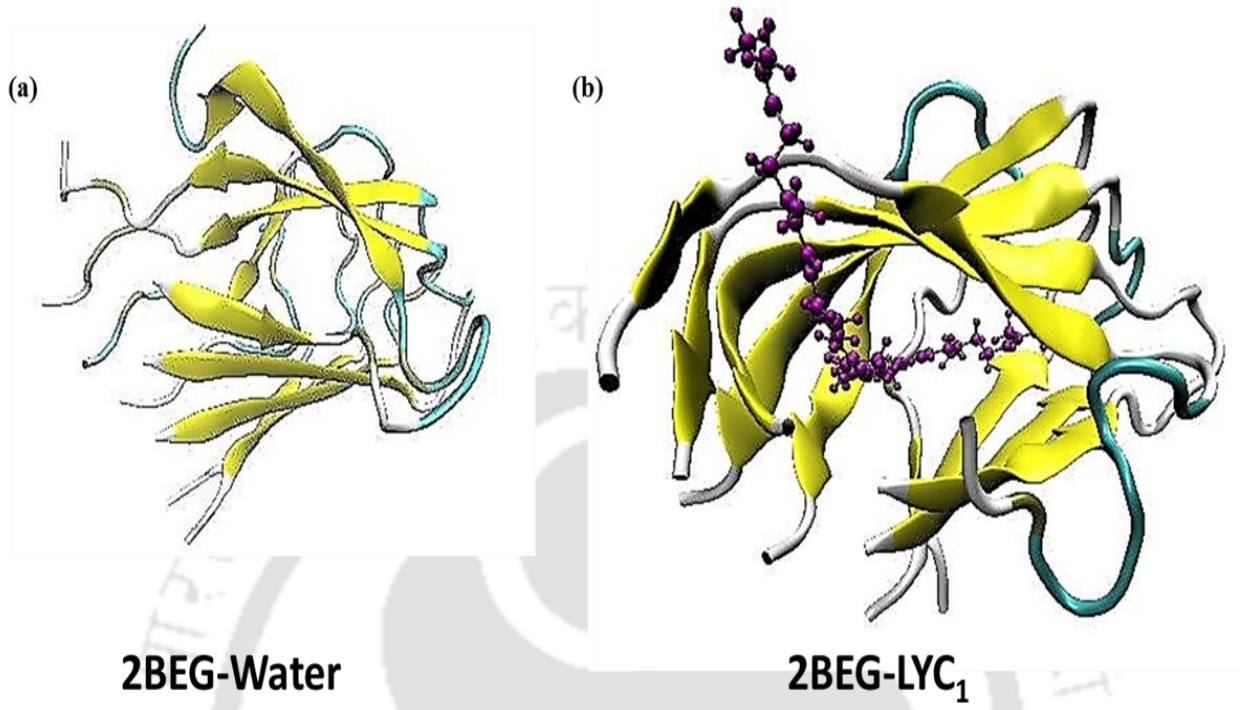

Fig. 7.16. VMD representation of final configuration of 2BEG.pdb for (a)-2BEG-Water and (b)-2BEG-LYC$_1$.

The increased RMSD value from 0.60 nm in 2BEG-Water to 0.69 nm in 2BEG-LYC$_1$ system (Fig. 7.17a) supports the observation on destabilization of the fibril. The lack of observable changes in R_g, RMSF and SASA values in Fig. 7.17b-d points towards the large size and inherent rigidity of the lycopene molecule.

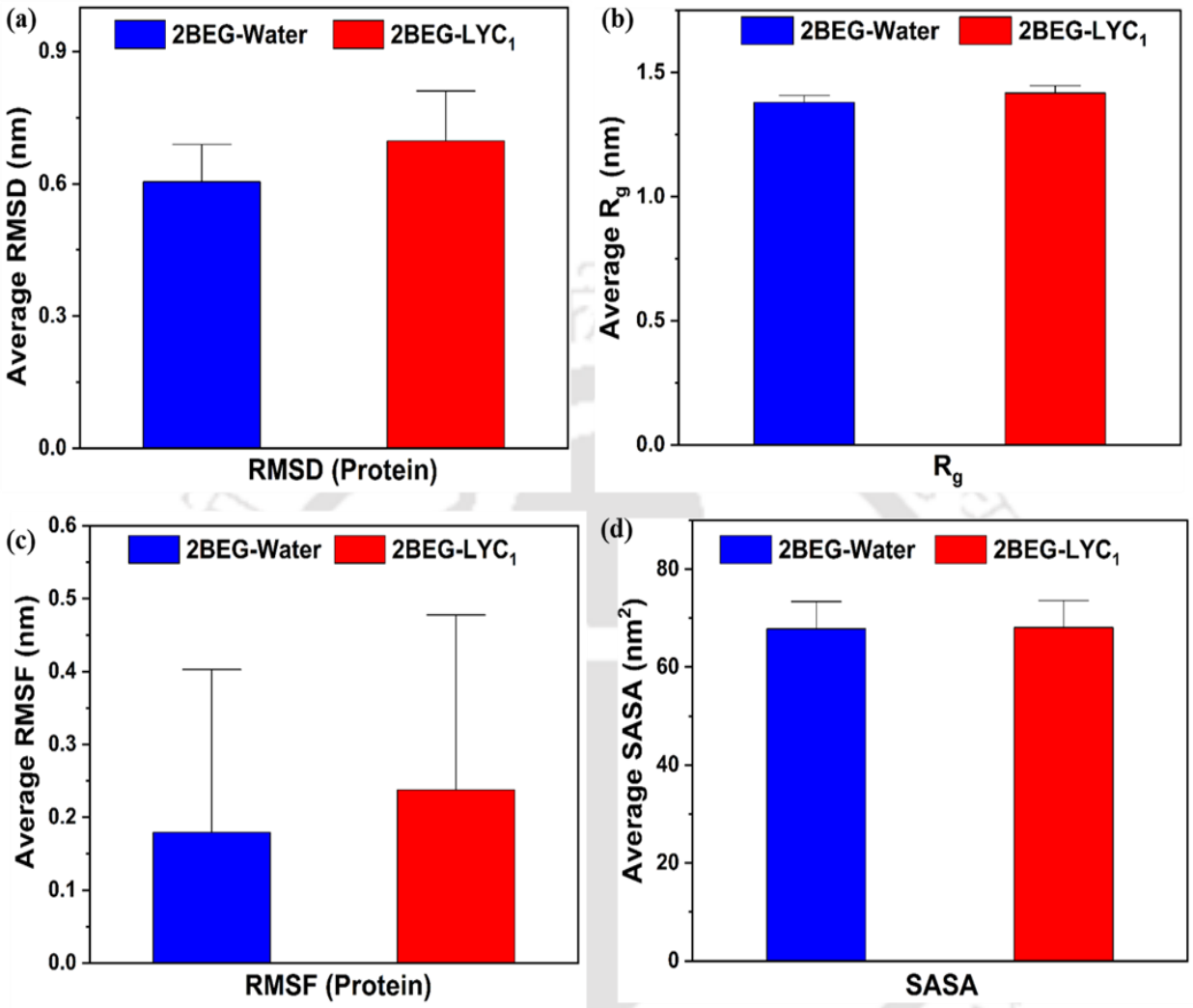

Fig. 7.17. Average value of 2BEG-Water (blue) and 2BEG-LYC$_1$ (red) (a)-RMSD, (b)-R$_g$, (c)-RMSF and (d)-SASA.

However, the overall increment in the coil content with simultaneous decrease in β-sheet content (Fig. 7.18b) supports the destabilization of 2BEG.pdb in the presence of lycopene. Similar findings about destabilization of the Aβ fibril (PDB ID: 2BEG) on account of increased RMSD value and decrease in β-sheet content by arginine containing short peptides are in parity with our observations.[35]

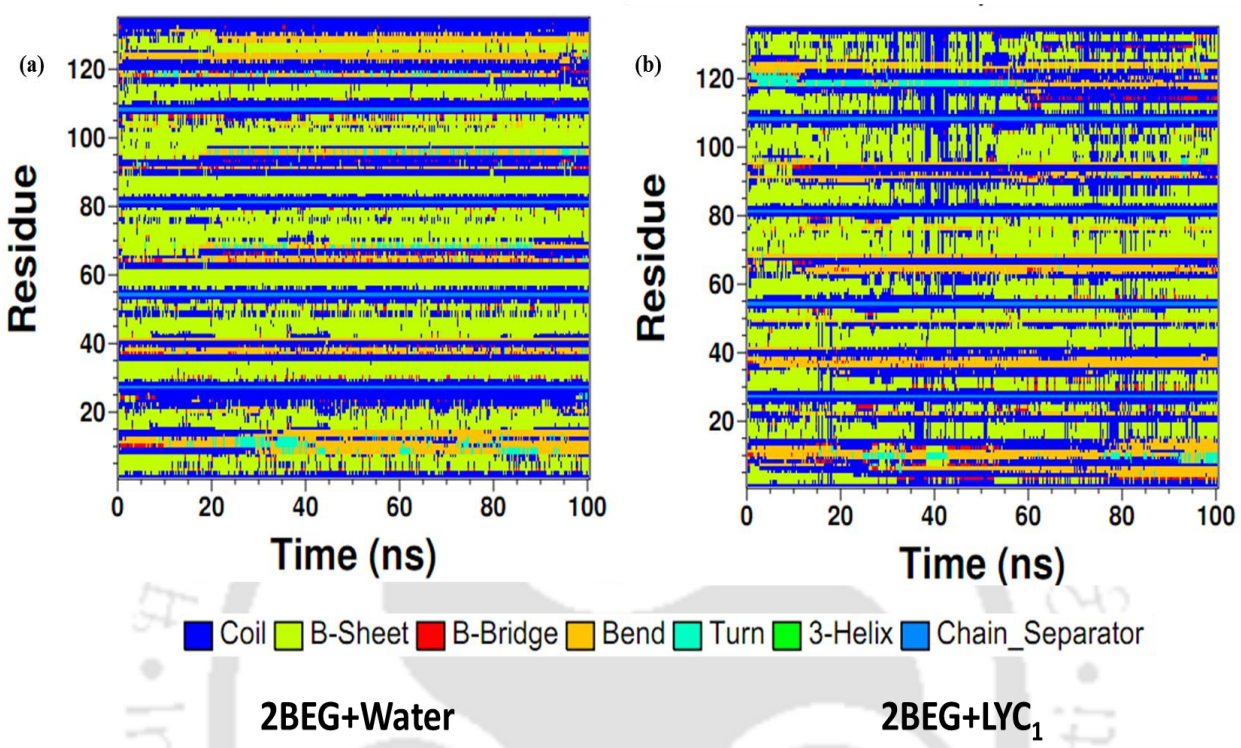

Fig. 7.18. The DSSP time evolution for 100 ns for all the five chains for (a)-2BEG-Water and (b)-2BEG-LYC$_1$.

In both the Aβ polymorphs (viz., 2NAO and 2BEG), the destabilization is observed in the presence of lycopene. However, the binding sites are different - lycopene binds to the upper surface of 2NAO and fibrillar cavity in 2BEG. The stark difference observed in the access of the fibril by the same ligand (lycopene) is insightful in preparing the ligand for effective destabilization towards a promising therapeutic treatment for AD. Conclusively, from all the data and findings, lycopene has been found to promote disorientation and destabilization of Aβ fibrils inhibiting their further

aggregation and neurotoxicity, and hence, establishes the potency of lycopene as a suitable lead compound as a therapeutic agent for AD

7.4 CONCLUSION

The tomatoes which are an imperative part of the mediterranean diet and also consumed globally in different cuisines in varied forms, are the richest source of lycopene. This carotenoid (lycopene) is tested for its destabilization potential on Aβ fibrils (PDB ID: 2NAO and 2BEG) in the current study. The mechanistic details provided by MD simulation highlight the interaction of lycopene to the upper surface of the chain F of 2NAO. The binding was mediated by G9, K16 and V18 residues by van der Waals and Y10 and F20 by π-π interactions with the methyl groups and C=C bonds of the lycopene, respectively. The binding of lycopene on the outer surface of the fibril is attributed to the large size of the fibril, as well as the ligand itself. Lycopene is a large-size molecule with high number of C-atoms forming a planar structure due to the presence of alternate C=C (viz., sp^2 hybridized) bond. Therefore, the molecule possesses an inherent rigidity, which restricts in accessing the cavity of the fibril. The interaction of lycopene with fibril is translated in breaking of several inherent H-bonds and hydrophobic interactions in the fibril. The lowering of β-sheet content and increase in coil and helical configuration governs the disorientation of the fibril in the presence of lycopene. Interestingly, the linear correlation between the higher lycopene content and the extent of destabilization has not been observed, implying the effectiveness of lycopene in lower dosages for curing AD. The destabilization of other polymorphic form (PDB ID: 2BEG) is also observed in the presence of lycopene, wherein lycopene successfully accesses the cavity of the fibril. The easiness of lycopene in accessing the cavity of 2BEG may be attributed to the relatively

smaller size of the fibril compared to 2NAO. The increased RMSD value and lowering of β-sheet content explains the disorientation of the 2BEG.pdb in the presence of lycopene.

The current study indicates the crucial role of lycopene in destabilizing the major neurotoxic polymorphs of Aβ fibrl and establishes the lycopene as the potential preventive and therapeutic choice to cure AD. Additionally, the present study also paves the pathway for screening and testing of other carotenoids and terpenoids as well to check their destabilization potential on Aβ fibrils. However, further detailed *in-vitro* and *in-vivo* studies are required to develop lycopene as effective drug lead compound for treatment of AD.

REFERENCES

1 D. Cox-Georgian, N. Ramadoss, C. Dona and C. Basu, in *Medicinal Plants*, Springer International Publishing, Cham, 2019, pp. 333–359.

2 K.-H. Wagner and I. Elmadfa, Biological Relevance of Terpenoids, *Annals of Nutrition and Metabolism*, 2003, **47**, 95–106.

3 X. LEI, L. LEI, Z. ZHANG and Y. CHENG, Neuroprotective effects of lycopene pretreatment on transient global cerebral ischemia-reperfusion in rats: The role of the Nrf2/HO-1 signaling pathway, *Molecular Medicine Reports*, 2016, **13**, 412–418.

4 E. Mourvaki, S. Gizzi, R. Rossi and S. Rufini, Passionflower Fruit—A 'New' Source of Lycopene?, *Journal of Medicinal Food*, 2005, **8**, 104–106.

5 D. Heber and Q.-Y. Lu, Overview of Mechanisms of Action of Lycopene, *Experimental Biology and Medicine*, 2002, **227**, 920–923.

6 H. Jackson, C. L. Braun and H. Ernst, The Chemistry of Novel Xanthophyll Carotenoids, *The American Journal of Cardiology*, 2008, **101**, S50–S57.

7 S. Przybylska, Lycopene – a bioactive carotenoid offering multiple health benefits: a review, *International Journal of Food Science & Technology*, 2020, **55**, 11–32.

8 J. V. Woodside, A. J. McGrath, N. Lyner and M. C. McKinley, Carotenoids and health in older people, *Maturitas*, 2015, **80**, 63–68.

9 I. M. Petyaev, Lycopene Deficiency in Ageing and Cardiovascular Disease, *Oxidative Medicine and Cellular Longevity*, 2016, **2016**, 1–6.

10 N. J. Engelmann, S. K. Clinton and J. W. Erdman, Nutritional Aspects of Phytoene and Phytofluene, Carotenoid Precursors to Lycopene, *Advances in Nutrition*, 2011, **2**, 51–61.

11 A. W. Schüttelkopf and D. M. F. van Aalten, PRODRG : a tool for high-throughput crystallography of protein–ligand complexes, *Acta Crystallographica Section D Biological Crystallography*, 2004, **60**, 1355–1363.

12 L. Abar, A. R. Vieira, D. Aune, C. Stevens, S. Vingeliene, D. A. Navarro Rosenblatt, D. Chan, D. C. Greenwood and T. Norat, Blood concentrations of carotenoids and retinol and lung cancer risk: an update of the WCRF-AICR systematic review of published prospective studies, *Cancer Medicine*, 2016, **5**, 2069–2083.

13 S. T. Mayne, B. Cartmel, F. Silva, C. S. Kim, B. G. Fallon, K. Briskin, T. Zheng, M. Baum, G. Shor-Posner and W. J. Goodwin, Plasma Lycopene Concentrations in Humans Are Determined by Lycopene Intake, Plasma Cholesterol Concentrations and Selected Demographic Factors, *The Journal of Nutrition*, 1999, **129**, 849–854.

14 R. Re, G. D. Mishra, C. W. Thane and C. J. Bates, Tomato consumption and plasma lycopene concentration in people aged 65 y and over in a British national survey, *European Journal of Clinical Nutrition*, 2003, **57**, 1545–1554.

15 B. Joshi, S. K. Kar, P. K. Yadav, S. Yadav, L. Shrestha and T. K. Bera, Therapeutic and medicinal uses of lycopene: a systematic review, *International Journal of Research in Medical Sciences*, 2020, **8**, 1195.

16 K. S. Cho, M. Shin, S. Kim and S. B. Lee, Recent Advances in Studies on the Therapeutic Potential of Dietary Carotenoids in Neurodegenerative Diseases, *Oxidative Medicine and Cellular Longevity*, 2018, **2018**, 1–13.

17 R. D. Semba, S. S. Chang, K. Sun, S. Talegawkar, L. Ferrucci and L. P. Fried, Serum carotenoids and pulmonary function in older community-dwelling women, *The journal of nutrition, health & aging*, 2012, **16**, 291–296.

18 C.-B. Liu, R. Wang, Y.-F. Yi, Z. Gao and Y.-Z. Chen, Lycopene mitigates β-amyloid induced inflammatory response and inhibits NF-κB signaling at the choroid plexus in early stages of Alzheimer's disease rats, *The Journal of Nutritional Biochemistry*, 2018, **53**, 66–71.

19 A. K. Sachdeva and K. Chopra, Lycopene abrogates Aβ(1-42)-mediated neuroinflammatory cascade in an experimental model of Alzheimer's disease, *Journal of Nutritional Biochemistry*, 2015, **26**, 736–744.

20 V. Matteo, M. Pierucci, G. Giovanni, L. K. Dragani, S. Murzilli, A. Poggi and E. Esposito, in *Birth, Life and Death of Dopaminergic Neurons in the Substantia Nigra*, eds. G. Giovanni, V. Di Matteo and E. Esposito, Springer Vienna, Vienna, 2009, pp. 333–341.

21 Q. Dai, A. R. Borenstein, Y. Wu, J. C. Jackson and E. B. Larson, Fruit and Vegetable Juices and Alzheimer's Disease: The Kame Project, *The American Journal of Medicine*, 2006, **119**, 751–759.

22 J. Min and K. Min, Serum Lycopene, Lutein and Zeaxanthin, and the Risk of Alzheimer's Disease Mortality in Older Adults, *Dementia and Geriatric Cognitive Disorders*, 2014, **37**,

246–256.

23 E. Kesse-Guyot, V. A. Andreeva, V. Ducros, C. Jeandel, C. Julia, S. Hercberg and P. Galan, Carotenoid-rich dietary patterns during midlife and subsequent cognitive function, *British Journal of Nutrition*, 2014, **111**, 915–923.

24 D. M. Williams, S. Hägg and N. L. Pedersen, Circulating antioxidants and Alzheimer disease prevention: a Mendelian randomization study, *The American Journal of Clinical Nutrition*, 2019, **109**, 90–98.

25 W. Ning, R. Lv, N. Xu, X. Hou, C. Shen, Y. Guo, Z. Fan, N. Cao and X.-P. Liu, Lycopene-Loaded Microemulsion Regulates Neurogenesis in Rats with Aβ-Induced Alzheimer's Disease Rats Based on the Wnt/β-catenin Pathway, *Neural Plasticity*, 2021, **2021**, 1–15.

26 W. Chen, L. Mao, H. Xing, L. Xu, X. Fu, L. Huang, D. Huang, Z. Pu and Q. Li, Lycopene attenuates Aβ1-42 secretion and its toxicity in human cell and Caenorhabditis elegans models of Alzheimer disease, *Neuroscience Letters*, 2015, **608**, 28–33.

27 H. Kaur, S. Chauhan and R. Sandhir, Protective Effect of Lycopene on Oxidative Stress and Cognitive Decline in Rotenone Induced Model of Parkinson's Disease, *Neurochemical Research*, 2011, **36**, 1435–1443.

28 M. A. Wälti, F. Ravotti, H. Arai, C. G. Glabe, J. S. Wall, A. Böckmann, P. Güntert, B. H. Meier and R. Riek, Atomic-resolution structure of a disease-relevant Aβ(1–42) amyloid fibril, *Proceedings of the National Academy of Sciences*, 2016, **113**, E4976–E4984.

29 K. R. Cousins, Computer Review of ChemDraw Ultra 12.0, *Journal of the American Chemical Society*, 2011, **133**, 8388–8388.

30 A. K. Malde, L. Zuo, M. Breeze, M. Stroet, D. Poger, P. C. Nair, C. Oostenbrink and A. E. Mark, An Automated Force Field Topology Builder (ATB) and Repository: Version 1.0, *Journal of Chemical Theory and Computation*, 2011, **7**, 4026–4037.

31 D. Van Der Spoel, E. Lindahl, B. Hess, G. Groenhof, A. E. Mark and H. J. C. Berendsen, *Journal of Computational Chemistry*, 2005, 26, 1701–1718.

32 C. Oostenbrink, A. Villa, A. E. Mark and W. F. Van Gunsteren, A biomolecular force field based on the free enthalpy of hydration and solvation: The GROMOS force-field parameter sets 53A5 and 53A6, *Journal of Computational Chemistry*, 2004, **25**, 1656–1676.

33 W. Huang, Z. Lin and W. F. Van Gunsteren, Validation of the GROMOS 54A7 force field with respect to β-peptide folding, *Journal of Chemical Theory and Computation*, 2011, **7**,

1237–1243.

34 A. K. Somavarapu and K. P. Kepp, The Dependence of Amyloid-β Dynamics on Protein Force Fields and Water Models, *ChemPhysChem*, 2015, **16**, 3278–3289.

35 S. S. Barale, R. S. Parulekar, P. M. Fandilolu, M. J. Dhanavade and K. D. Sonawane, Molecular Insights into Destabilization of Alzheimer's Aβ Protofibril by Arginine Containing Short Peptides: A Molecular Modeling Approach, *ACS Omega*, 2019, **4**, 892–903.

36 W.-J. Du, J.-J. Guo, M.-T. Gao, S.-Q. Hu, X.-Y. Dong, Y.-F. Han, F.-F. Liu, S. Jiang and Y. Sun, Brazilin inhibits amyloid β-protein fibrillogenesis, remodels amyloid fibrils and reduces amyloid cytotoxicity, *Scientific Reports*, 2015, **5**, 7992.

37 J. A. Lemkul and D. R. Bevan, Destabilizing Alzheimer's Aβ 42 Protofibrils with Morin: Mechanistic Insights from Molecular Dynamics Simulations, *Biochemistry*, 2010, **49**, 3935–3946.

38 F.-F. Liu, X.-Y. Dong, L. He, A. P. J. Middelberg and Y. Sun, Molecular Insight into Conformational Transition of Amyloid β-Peptide 42 Inhibited by (−)-Epigallocatechin-3-gallate Probed by Molecular Simulations, *The Journal of Physical Chemistry B*, 2011, **115**, 11879–11887.

39 G. Orteca, F. Tavanti, Z. Bednarikova, Z. Gazova, G. Rigillo, C. Imbriano, V. Basile, M. Asti, L. Rigamonti, M. Saladini, E. Ferrari and M. C. Menziani, Curcumin derivatives and Aβ-fibrillar aggregates: An interactions' study for diagnostic/therapeutic purposes in neurodegenerative diseases, *Bioorganic & Medicinal Chemistry*, 2018, **26**, 4288–4300.

40 R. K. Saini, S. Shuaib and B. Goyal, Molecular insights into Aβ 42 protofibril destabilization with a fluorinated compound D744: A molecular dynamics simulation study, *Journal of Molecular Recognition*, 2017, **30**, e2656.

41 F. Tavanti, A. Pedone and M. Menziani, Computational Insight into the Effect of Natural Compounds on the Destabilization of Preformed Amyloid-β(1–40) Fibrils, *Molecules*, 2018, **23**, 1320.

42 H. J. C. Berendsen, J. R. Grigera and T. P. Straatsma, The missing term in effective pair potentials, *Journal of Physical Chemistry*, 1987, **91**, 6269–6271.

43 W. Humphrey, A. Dalke and K. Schulten, VMD: Visual molecular dynamics, *Journal of Molecular Graphics*, 1996, **14**, 33–38.

44 B. Han, Y. Liu, S. W. Ginzinger and D. S. Wishart, SHIFTX2: significantly improved protein chemical shift prediction, *Journal of Biomolecular NMR*, 2011, **50**, 43–57.

45 R. K. Saini, S. Shuaib, D. Goyal and B. Goyal, Insights into the inhibitory mechanism of a resveratrol and clioquinol hybrid against Aβ 42 aggregation and protofibril destabilization: A molecular dynamics simulation study, *Journal of Biomolecular Structure and Dynamics*, 2019, **37**, 3183–3197.

46 R. K. Saini, S. Shuaib and B. Goyal, Molecular insights into Aβ 42 protofibril destabilization with a fluorinated compound D744: A molecular dynamics simulation study, *Journal of Molecular Recognition*, 2017, **30**, e2656.

47 G. W. Vuister and A. Bax, Quantitative J correlation: a new approach for measuring homonuclear three-bond J(HNH.alpha.) coupling constants in 15N-enriched proteins, *Journal of the American Chemical Society*, 1993, **115**, 7772–7777.

48 M. Karplus, Contact electron-spin coupling of nuclear magnetic moments, *The Journal of Chemical Physics*, 1959, **30**, 11–15.

49 S.-H. Chong, J. Yim and S. Ham, Structural heterogeneity in familial Alzheimer's disease mutants of amyloid-beta peptides, *Molecular BioSystems*, 2013, **9**, 997.

50 J. Zheng, H. Jang, B. Ma, C.-J. Tsai and R. Nussinov, Modeling the Alzheimer Aβ17-42 Fibril Architecture: Tight Intermolecular Sheet-Sheet Association and Intramolecular Hydrated Cavities, *Biophysical Journal*, 2007, **93**, 3046–3057.

51 N. L. Fawzi, K. L. Kohlstedt, Y. Okabe and T. Head-Gordon, Protofibril assemblies of the arctic, dutch, and flemish mutants of the alzheimer's Aβ1-40 peptide, *Biophysical Journal*, 2008, **94**, 2007–2016.

52 A. Sgarbossa, S. Monti, F. Lenci, E. Bramanti, R. Bizzarri and V. Barone, The effects of ferulic acid on β-amyloid fibrillar structures investigated through experimental and computational techniques, *Biochimica et Biophysica Acta - General Subjects*, 2013, **1830**, 2924–2937.

53 S. Gupta and A. K. Dasmahapatra, Destabilization of Aβ fibrils by omega-3 polyunsaturated fatty acids: a molecular dynamics study, *Journal of Biomolecular Structure and Dynamics*, 2021, **0**, 1–18.

54 P. K. Kanchi and A. K. Dasmahapatra, Destabilization of the Alzheimer's amyloid-β protofibrils by THC: A molecular dynamics simulation study, *Journal of Molecular*

Graphics and Modelling, 2021, **105**, 107889.

55 O. S. Makin, E. Atkins, P. Sikorski, J. Johansson and L. C. Serpell, Molecular basis for amyloid fibril formation and stability, *Proceedings of the National Academy of Sciences of the United States of America*, 2005, **102**, 315–320.

56 S. Gupta and A. K. Dasmahapatra, Caffeine destabilizes preformed Aβ protofilaments: insights from all atom molecular dynamics simulations, *Physical Chemistry Chemical Physics*, 2019, **21**, 22067–22080.

57 J. A. Lemkul and D. R. Bevan, Destabilizing Alzheimer's Aβ 42 Protofibrils with Morin: Mechanistic Insights from Molecular Dynamics Simulations, *Biochemistry*, 2010, **49**, 3935–3946.

58 H.-M. Fan, R.-X. Gu, Y.-J. Wang, Y.-L. Pi, Y.-H. Zhang, Q. Xu and D.-Q. Wei, Destabilization of Alzheimer's Aβ42 Protofibrils with a Novel Drug Candidate wgx-50 by Molecular Dynamics Simulations, *The Journal of Physical Chemistry B*, 2015, **119**, 11196–11202.

59 S. Gupta and A. K. Dasmahapatra, Destabilization potential of phenolics on Aβ fibrils: mechanistic insights from molecular dynamics simulation, *Physical Chemistry Chemical Physics*, 2020, **22**, 19643–19658.

60 Y. Jin, Y. Sun, J. Lei and G. Wei, Dihydrochalcone molecules destabilize Alzheimer's amyloid-β protofibrils through binding to the protofibril cavity, *Physical Chemistry Chemical Physics*, 2018, **20**, 17208–17217.

61 V. Jani, U. Sonavane and R. Joshi, Destabilization potential of beta sheet breaker peptides on Abeta fibril structure: an insight from molecular dynamics simulation study, *RSC Advances*, 2021, **11**, 23557–23573.

62 S. K. Mudedla, N. A. Murugan, V. Subramanian and H. Agren, Destabilization of amyloid fibrils on interaction with MoS 2 -based nanomaterials, *RSC Advances*, 2019, **9**, 1613–1624.

63 P. K. Windsor, S. P. Plassmeyer, D. S. Mattock, J. C. Bradfield, E. Y. Choi, B. R. Miller and B. H. Han, Biflavonoid-Induced Disruption of Hydrogen Bonds Leads to Amyloid-β Disaggregation, *International Journal of Molecular Sciences*, 2021, **22**, 2888.

64 A. Kumar, S. Srivastava, S. Tripathi, S. K. Singh, S. Srikrishna and A. Sharma, Molecular insight into amyloid oligomer destabilizing mechanism of flavonoid derivative 2-(4′ benzyloxyphenyl)-3-hydroxy-chromen-4-one through docking and molecular dynamics

simulations, *Journal of Biomolecular Structure and Dynamics*, 2016, **34**, 1252–1263.

65 K. E. Marshall, K. L. Morris, D. Charlton, N. O'Reilly, L. Lewis, H. Walden and L. C. Serpell, Hydrophobic, Aromatic, and Electrostatic Interactions Play a Central Role in Amyloid Fibril Formation and Stability, *Biochemistry*, 2011, **50**, 2061–2071.

66 H. R. Bosshard, D. N. Marti and I. Jelesarov, Protein stabilization by salt bridges: concepts, experimental approaches and clarification of some misunderstandings, *Journal of Molecular Recognition*, 2004, **17**, 1–16.

67 S. Brogi, S. Butini, S. Maramai, R. Colombo, L. Verga, C. Lanni, E. De Lorenzi, S. Lamponi, M. Andreassi, M. Bartolini, V. Andrisano, E. Novellino, G. Campiani, M. Brindisi and S. Gemma, Disease-Modifying Anti-Alzheimer's Drugs: Inhibitors of Human Cholinesterases Interfering with β -Amyloid Aggregation, *CNS Neuroscience & Therapeutics*, 2014, **20**, 624–632.

68 Y. Gong, C. Zhan, Y. Zou, Z. Qian, G. Wei and Q. Zhang, Serotonin and Melatonin Show Different Modes of Action on Aβ42Protofibril Destabilization, *ACS Chemical Neuroscience*, 2021, **12**, 799–809.

69 M. S. Dutta and S. Basu, Identifying the key residues instrumental in imparting stability to amyloid beta protofibrils – a comparative study using MD simulations of 17–42 residues, *Journal of Biomolecular Structure and Dynamics*, 2021, **39**, 431–456.

70 H. J. Dyson, P. E. Wright and H. A. Scheraga, The role of hydrophobic interactions in initiation and propagation of protein folding, *Proceedings of the National Academy of Sciences*, 2006, **103**, 13057–13061.

71 B. Tarus, J. E. Straub and D. Thirumalai, Dynamics of Asp23−Lys28 Salt-Bridge Formation in Aβ 10-35 Monomers, *Journal of the American Chemical Society*, 2006, **128**, 16159–16168.

72 B. Sharma, S. Kalita, A. Paul, B. Mandal and S. Paul, The role of caffeine as an inhibitor in the aggregation of amyloid forming peptides: a unified molecular dynamics simulation and experimental study, *RSC Advances*, 2016, **6**, 78548–78558.

73 Y. Zou, Z. Qian, Y. Chen, H. Qian, G. Wei and Q. Zhang, Norepinephrine Inhibits Alzheimer's Amyloid-β Peptide Aggregation and Destabilizes Amyloid-β Protofibrils: A Molecular Dynamics Simulation Study, *ACS Chemical Neuroscience*, 2019, **10**, 1585–1594.

74 I. Jahan and S. M. Nayeem, Destabilization of Alzheimer's Aβ 42 protofibrils with acyclovir, carmustine, curcumin, and tetracycline: insights from molecular dynamics simulations, *New Journal of Chemistry*, 2021, **45**, 21031–21048.

75 T. Lührs, C. Ritter, M. Adrian, D. Riek-Loher, B. Bohrmann, H. Döbeli, D. Schubert and R. Riek, 3D structure of Alzheimer's amyloid-β(1–42) fibrils, *Proceedings of the National Academy of Sciences*, 2005, **102**, 17342–17347.

Chapter 8

Enhanced Stability of a Disaggregated Aβ Fibril on Removal of Ligand Inhibits Refibrillation: An All Atom Molecular Dynamics Simulation Study

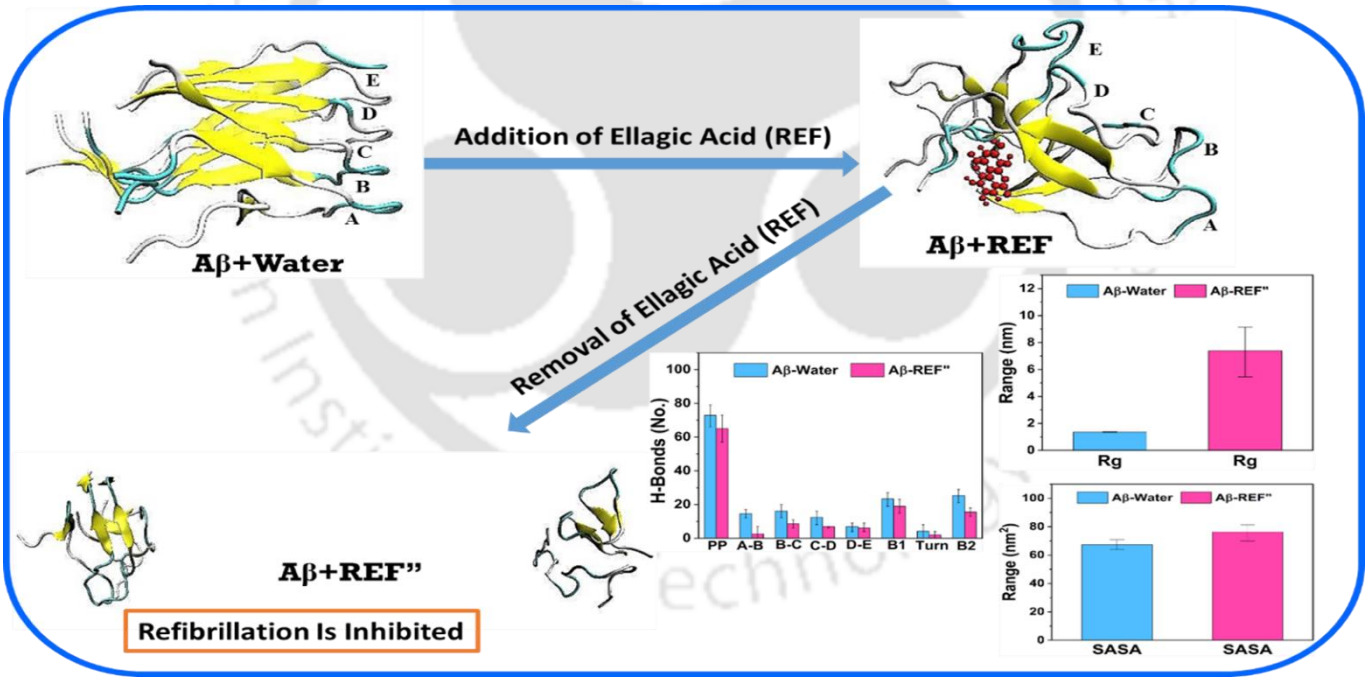

In the current study, the effect of removal of ligand has been measured for its probability for refibrillation or enhanced stability of the destabilized complex. For this, the ellagic acid and caffeine has been removed from their destabilized complex and simulated for 1 μs. The resultant

increased RMSD, R_g, and SASA values in Aβ-REF" system indicates enhanced stability of the destabilized structure. The lesser number of H-bonds and β-sheet explains enhanced destabilization in Aβ-REF" system. The higher Gibbs free energy of the misaligned structure of Aβ-REF" ensures irreversibility to the organized structure due to its inability to cross such high energy barrier. The observed stability of the disaggregated structure, despite ligand elimination, establishes the effectiveness of the destabilization technique as a promising therapeutic approaches towards treating AD.

8.1 INTRODUCTION

In general, any drug demands the ADME (Absorption, Distribution, Metabolism and Excretion) studies to satisfy the drugability concerns and enhance its drug likeliness.[1] The elimination of hydrophobic drugs needs some biotransformation processes to make it more polar to be excreted in urine, as kidney being the chief organ for elimination.[2] However, the hydrophilic drugs can be cleared via renal function owing to their water solubility. The excretion of potential polyphenolic destabilizers like caffeic acid[3] and ellagic acid[4] gets removed by kidney as reported. However, irreversibility of the nutraceutical effect of any drug, after the drug is eliminated from the human body, is a major concern and needs thorough investigation. The sustainability of the therapeutic effect needs to be tested even after removal of the administered drug to enhance the therapeutic value of the drug.

The deformed Aβ fibril can acquire two pathways upon ligand removal viz. refibrillation and enhanced stability of the disorganized fibril. Therefore, investigation of the stability of the destabilized fibril holds importance due to its biological relevance. There is a pool of scientific

literature that highlights the significance of specific residues that have crucial role in β-sheet organization, salt bridge formation and several hydrophobic interactions for the formation of Aβ fibril.[5,6] The MD simulation tool[7] comes handy in determining the sustainability of the deformation caused by the ligand. The unavailability of enough reports in this direction instigates the need for more computational based studies to gain insights into the stability of destabilized Aβ fibril after ligand removal. The extent of deformation in Aβ fibril, if observed, will facilitate the consideration of destabilization approach as the promising therapeutics.

In the present work, the focus has been devoted in assessing the state of a deformed Aβ fibril as a consequence of the removal of the ligand. The Aβ fibril has been studied by all–atom MD simulation for 1 μs both with water (control/ Aβ-Water) and after ligand removal (test/ Aβ-REF") system. The rationale behind this experiment is to check for the sustained deformation in Aβ fibril by calculating various parameters. The substantial increase in RMSD and radius of gyration (R_g) in Aβ-REF" demarcates enhanced disorganization of Aβ fibril even after removal of the ligand. The disruption of H-bonds (hydrogen bonds), salt bridges and other hydrophobic contacts, decrease in β-sheet content indicates enhanced destabilization of the already deformed Aβ fibril. The increased inter-chain distance led to the drifting of the terminal chains from the pentamer. The correlation between increased SASA value and higher ΔG_{ps} (polar solvation energy) explains less interaction amongst residues and more with the solvent, supporting unfolding of the fibril. The higher Gibbs free energy impedes crossing of the energy barrier by such misaligned and destabilized structure in Aβ-REF". This in turn ensures irreversibility of the disoriented structure and impedes formation of higher order aggregates as well. The current findings proposed low β-sheet content, higher SASA value and higher polar solvation energy as main drivers behind the irreversibility of the disorganized fibrils to native conformation. These

observations, reported for the first time, summarizes the effectiveness of the destabilization technique, attributed to the irrevocability of the destabilized fibril to its original structure explaining therapeutic efficacy towards AD.

8.2 METHODS

8.2.1 Defining the simulation system: Eliminating Ellagic acid (REF) from Aβ-REF complex

This is well known fact that any drug that is being administered in the body, is eliminated from the human system. This further demands the re-administration in the human system to bind to the desired receptor or protein again. The current work identifies the stability of Aβ fibril after the removal of bound ligand, REF (ellagic acid). Removal of ligand can have two possibilities- refibrillation of the destabilized Aβ fibril to its native well organized structure or enhanced destabilization. The simulated Aβ-REF complex (destabilized structure) as explained in previous study[8] has been considered and ligand coordinates have been removed, thereby obtaining the starting configuration for further simulation. The coordinate file after ligand removal, contains protein structure and named as destab.gro and this test system has been designated as Aβ-REF" with REF removed which is tested against the control system of Aβ-Water

8.2.2 Molecular Dynamics Simulation of Aβ-Water and Aβ-REF" Systems

The all-atom MD simulation of Aβ-Water (control) and Aβ-REF" (test) systems has been performed using GROMACS v5.1.1[9] with GROMOS 96 54a7[10–12] force field with SPC/E water

model for solvation.[13] The total numbers of atoms were 206201 and 31403 in Aβ-REF" and Aβ-Water system, respectively. Further the simulation procedure has been carried out the same way as described in section 4.2.2 of chapter 4. The only point of difference is the length of the production run which is 1000 ns or 1μs in the current study. The statistical significance and reproducibility have been ensured by conducting three sets of simulation and plotting average data for all the parameters discussed in following section. The visualizations of MD trajectories were analyzed using VMD (Visual Molecular Dynamics) package,[14] similar to previous chapters.

8.2.3 Analysis of MD generated trajectories

The Aβ fibril is a pentamer structure (PDB ID: 2BEG) with five chains as A, B, C, D, and E, having the same primary sequence, with A and E being the terminal chains. The fibrillar length is from 17-42, with 1-16 residues being disordered and hence avoided for simulation and analysis. Each chain has characteristic cross β-sheet, the prerequisite for fibrillation and stable organization of amyloids. The fibrillar sequence is further divided into three regions - β1 region (18-26 residues), turn region (27-30 residues), and β2 region (31-42 residues) as depicted in Fig. 8.1a as derived from VMD package.[15]

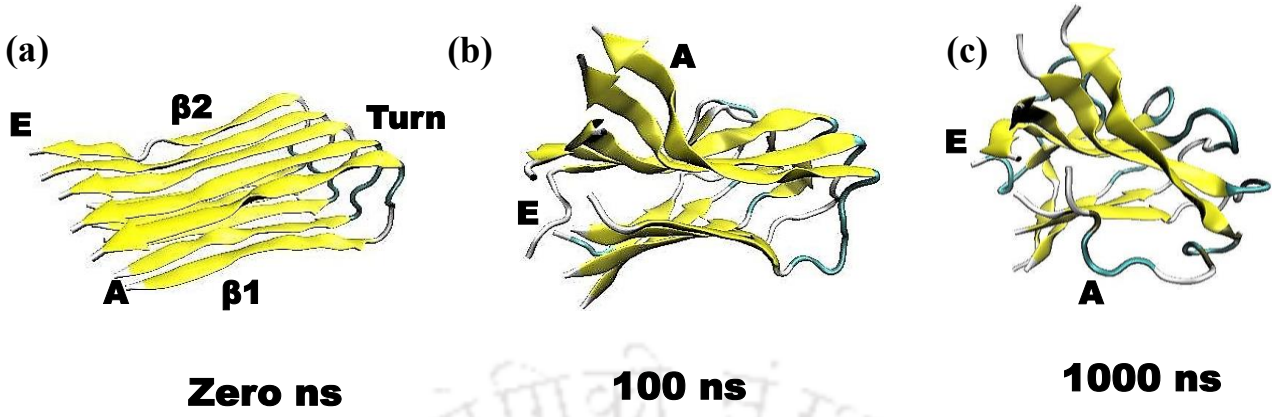

Fig. 8.1. Snapshots of Aβ-Water at different time. Twisting of the fibril without major changes in the system indicates stability of the structure after simulation.

We have calculated various parameters using different tools defined within the GROMACS v5.1.1 package to assess the structural information of simulated structure. The various parameters like Cα-RMSD, Rg, SASA, RMSF, H-bonds, secondary structure configurations, average minimum distance between key residues and contact maps have been determined the same way as previous chapters. Additionally, free energy landscape has been obtained by using g_sham, an inbuilt tool in gromacs by considering Cα-RMSD and H-bonds as important components across entire protein. The free energy landscape provides details on the possible configuration of the protein. The detailed description for all the tools with commands has been given in Appendix A.

8.2.4 Binding Mode analysis by MM-PBSA

The binding free energy (BFE) for chain A-B and D-E for Aβ-Water and Aβ-REF" system was calculated by MM-PBSA tool (Molecular Mechanics Poisson-Boltzmann Surface Area).[16–18] MM-PBSA calculates the BFE from the MD trajectory based on the following equation [1]:

$$\Delta G^{bind} = \Delta E_{MM} + \Delta G^{psolv} + \Delta G^{npsolv} - T\Delta S \qquad \textbf{[8.1]}$$

where,, $\Delta E_{MM}$is the molecular mechanics contribution in vacuum consisting of ΔE_{vdW} and ΔE_{elec}, $\Delta G^{psolv}$is the polar contribution of solvation energy, calculated by the Poisson-Boltzmann equation and ΔG^{npsolv} is the nonpolar contribution towards binding, determined by solvent accessible surface area (SASA) model. The high computational demand limits the calculation of entropy contribution. Moreover, the relative change in entropy contribution (ΔS) towards free energy calculation is negligible and thus has been ignored.[8,19–21] The calculation of BFE in the present study was done on the last 20 ns trajectory with Δt = 100 ps to reduce the computational time. The BFE was calculated for both the terminal pairs so as to determine their ability to remain intact to the parent pentamer. The solute and solvent dielectric constants were taken as 4 and 80, respectively.

8.3 RESULTS AND DISCUSSIONS

8.3.1 Visualization of Molecular dynamics trajectory of Aβ-Water and Aβ-REF”

The simulation studies were conducted for 1 μs for both the systems to assess the effect of ligand removal on destabilized Aβ fibril. The visualization of the configuration of Aβ-Water by VMD has been represented as snapshots captured at zero ns, 100 ns and 1000 ns in Fig. 8.1 a-c, respectively. The depiction for Aβ-REF” system for the same time points has been given as well, in Fig. 8.2a-c wherein Fig. 8.2a represents the starting point of the simulation followed by simulated structure at 100 ns (Fig. 8.2b) and 1000 ns (Fig. 8.2c). A marginal twisting that has been observed at the ends of the organized structure for Aβ-Water system (Fig. 8.1c) imparts more stability to the fibril, which is well-matched with observations reported by others.[22] The VMD snapshots are illustrated in new cartoon form, highlighting their secondary structure configuration with coil (grey), turn (cyan) and β-sheet (yellow) for both the systems in Fig. 8.1 and 8.2a-c. As viewed from Fig. 8.2b, higher level of perturbations and disorganization has been observed in Aβ fibril in Aβ-REF” system at 100 ns itself, which increased to further extent at 1000 ns (Fig. 8.2c).

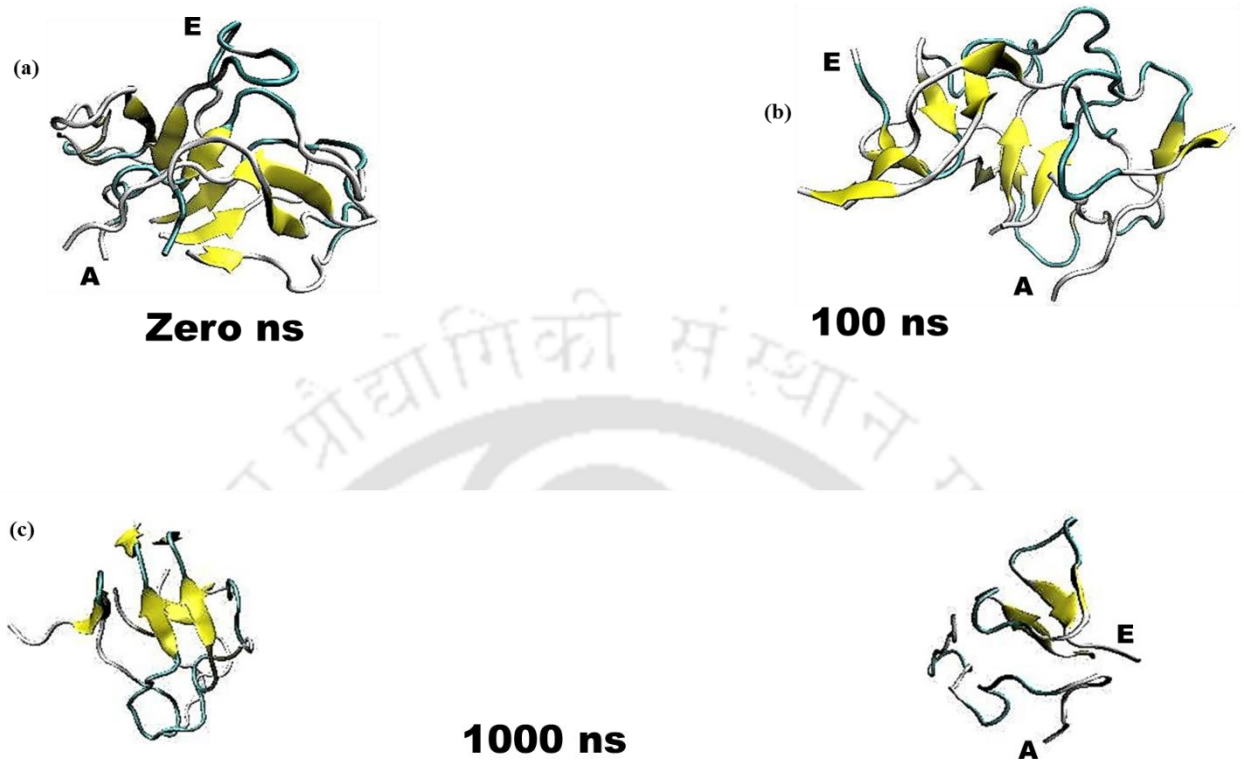

Fig. 8.2. Snapshots of Aβ-REF" at different time intervals. The destabilization of the Aβ fibril is observed at 100 ns which extends to higher disorganization at 1000 ns with drifting of the terminal chains A and E from the parent pentamer.

The breaking of the Aβ pentamer in trimer and dimer wherein, the terminal chains A and E breaks apart from the parent pentamer structure (refer Fig. 8.2c) was observed indicating highly perturbed structure. The current observation strongly suggests that there is extremely low possibility of refibrillation of the highly misaligned and unstructured fibril.[23] The misaligned structure of Aβ fibril thus obtained, shares structural similarity with the stable states that are explained as stable intermediates during aggregation process inhibiting reversibility to form organized fibril and further aggregation as well.[24] The extent of destabilization thus observed in

Aβ-REF" system envisages the importance of destabilization approach as the better therapeutic intervention for AD.

8.3.2 Global stability parameters of Aβ-Water and Aβ-REF"

The global stability parameters like Cα-RMSD, R_g and SASA, have been calculated for both the systems, which demarcated a trend of enhanced destabilization in the Aβ-REF" system as compared to the control one. In Fig. 8.3, Cα-RMSD have been plotted for various selections such as, the entire protein (Fig. 8.3a), individual chains (Fig. 8.3b-f respectively) and different regions (viz., β1, turn and β2 in Fig. 8.3g-i, respectively). The trend for different selection groups are depicted in black for Aβ-Water and red for Aβ-REF" system in all the graphs. In all these Figures, the average Cα-RMSD value has been found to be significantly higher for Aβ-REF" as compared to the Aβ-Water for all the selections. The average Cα-RMSD value for the entire protein has been recorded as 4.50 nm for Aβ fibril in Aβ-REF", which is noticeably higher than 0.58 nm in case of Aβ-Water system. Similarly, the average Cα-RMSD value has been recorded as 7.18 nm for chain A in Aβ-REF" system which is significantly higher as compared to 1.15 nm in case of Aβ-Water. Such remarkably high Cα-RMSD values clearly indicates towards the enhanced destabilization of the already destabilized fibril, thereby minimizing propensity for refibrillation. The considerable increase of 2.32 nm in Cα-RMSD for chain E in Aβ-REF" (3.48 nm) from 1.16 nm in Aβ-Water indicates higher degree of deformation. The drifting of both the terminal chains from the parent

pentamer as viewed from Fig. 8.3b and 8.3f is well augmented by spiked Cα-RMSD values reported for Aβ-REF" system as compared to the control system.

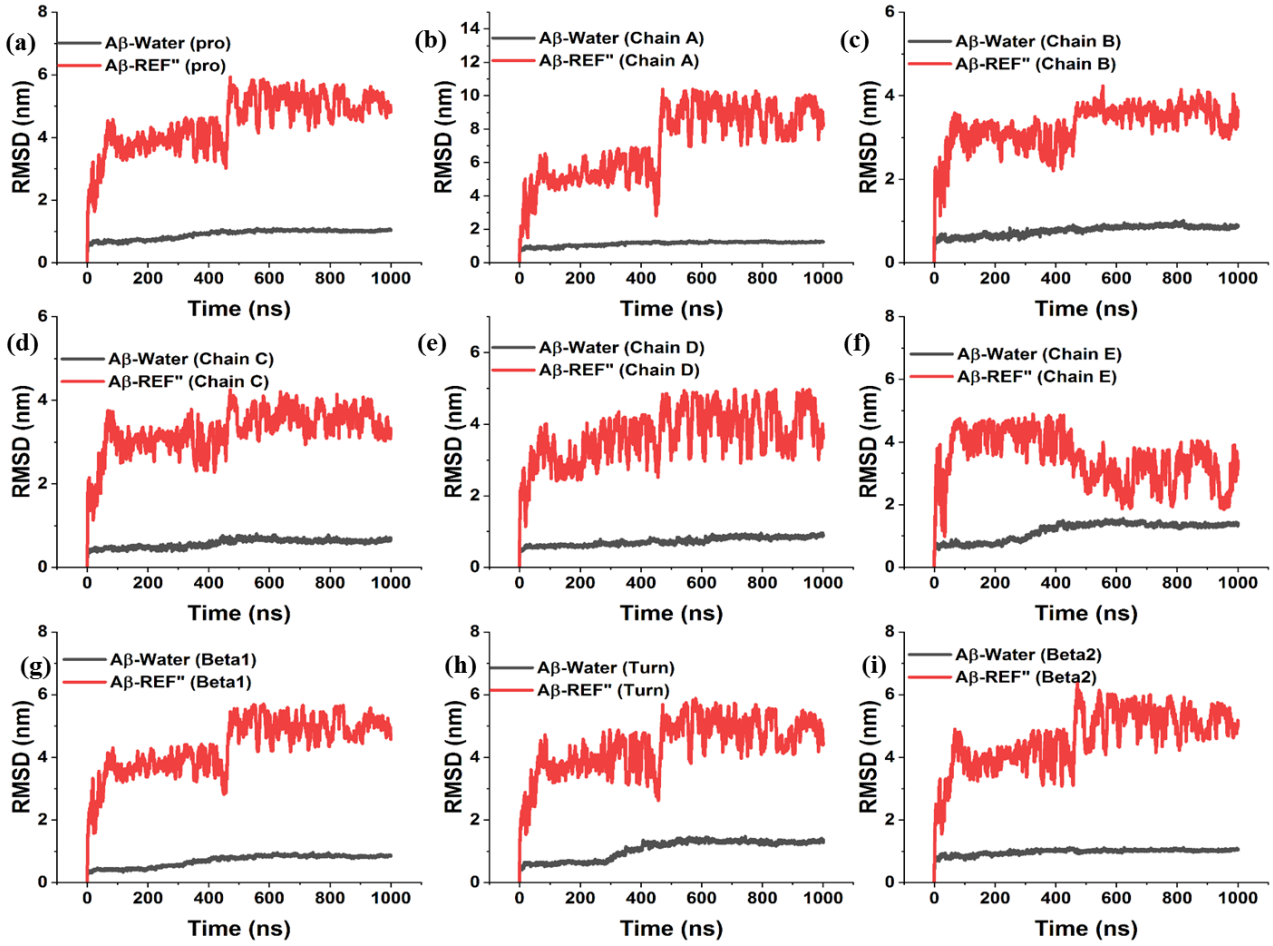

Fig. 8.3. Time evolution of Cα-RMSD of Aβ-Water (black) and Aβ-REF" (red) for different selections. The increased Cα-RMSD value for protein, chain A, B, C, D and E and β1, turn and β2 region in Aβ-REF" system indicates disorganization as compared to the Aβ-Water.

The current findings are found in parity with increased Cα-RMSD value for Aβ fibril as reported for Omega-3 PUFAs, leading to destabilization.[25] Such observations direct towards the

irreversible destabilization in the Aβ fibril on account of introduction and then removal of ligand, reinstating the destabilization as a promising approach to treat AD.

The R_g value, which is an indicative of the flexibility, and SASA value accounting for hydrophobic and hydrophilic composition of a protein structure[26] have been determined. The bar charts based on the mean values have been plotted for R_g and SASA values in Fig. 8.4a and 8.4b, respectively. The higher R_g value of 7.38 ± 0.45 nm measured for Aβ fibril in Aβ-REF" system is found considerably higher than the 1.35 ± 0.34 nm as recorded in Aβ-water (Fig. 8.4a). The higher SASA value of 76.40 ± 0.45 nm^2 in Aβ-REF" in comparison with 67.10 ± 0.25 nm^2 in Aβ-Water system (Fig. 8.4b) highlight greater unfolding of the Aβ fibril upon ligand elimination.

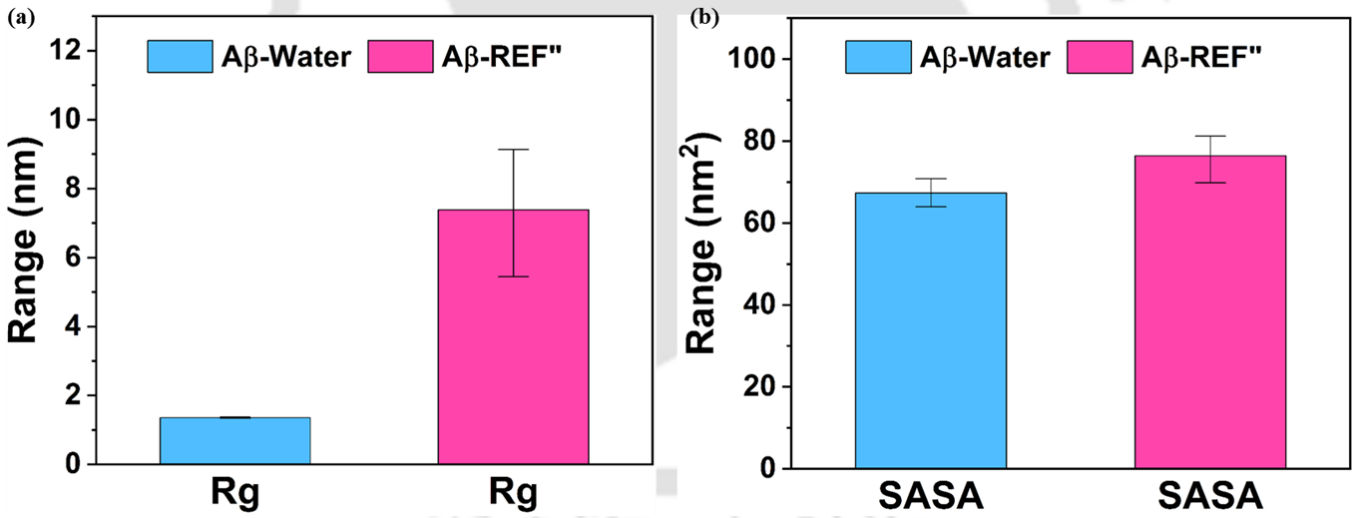

Fig. 8.4. Average value of (a) R_g and (b) SASA for Aβ-Water (blue) and Aβ-REF" (pink). The increased R_g and SASA for Aβ-REF" indicates higher flexibility, lesser compactness and more interaction with the solvent molecules as compared to the Aβ-Water, which is compact and organized.

The higher R_g value for Aβ fibril when interacted with flavonoids wherein non-toxic amorphous aggregates are formed, well supports the current findings.[27] The current results are well synchronized with the destabilization effect observed by ellagic acid due to increased SASA of the protein.[8] The increased R_g and SASA values for Aβ fibril in Aβ-REF" system demarcates the decreased compactness and higher accessibility of the fibril to the solvent molecules. As a result, the obtained misaligned structure becomes more stable compared to the initial one, and therefore inhibits the refibrillation to the original state.

8.3.3 Secondary structure determination: The decisive role of secondary conformations in the structural determination, stability, longevity and functionality of the protein is well known. The stability of Aβ fibrils is largely governed by higher β-sheet content, which manifests the formation of a well-organized cross β motif. The DSSP[28] tool delivers the time evolution profile of possible secondary structure configurations achievable by Aβ fibril as depicted in Fig. 8.5. The higher number of β-sheet content denoted by green color in Fig. 8.5a reflects stability and organized structure of Aβ fibril in Aβ-Water. However, the β-sheet content is highly compromised and replaced by coil (dark blue) and bend (orange) content in Aβ-REF" (Fig. 8.5b), marking further destabilization.

The percentage content of the different possible secondary structures for both the systems (viz., Aβ-Water and Aβ-REF") has been tabulated in Table 8.1. The β-sheet content shows a large reduction from 40% in Aβ-Water to 18% in Aβ-REF", whereas, the bend content shows an enhancement from 12% in Aβ-Water to 21% in Aβ-REF" (Table 8.1). The secondary structure profiling for Aβ-Water and Aβ-REF" clearly demonstrates the enhanced destabilization of the

already disarranged Aβ fibril upon ligand removal. The significant decrease in the β-sheet content ensures an obstruction to reorganization of the fibril and formation of higher order aggregates as well, barring neurotoxicity of otherwise toxic Aβ fibrils.

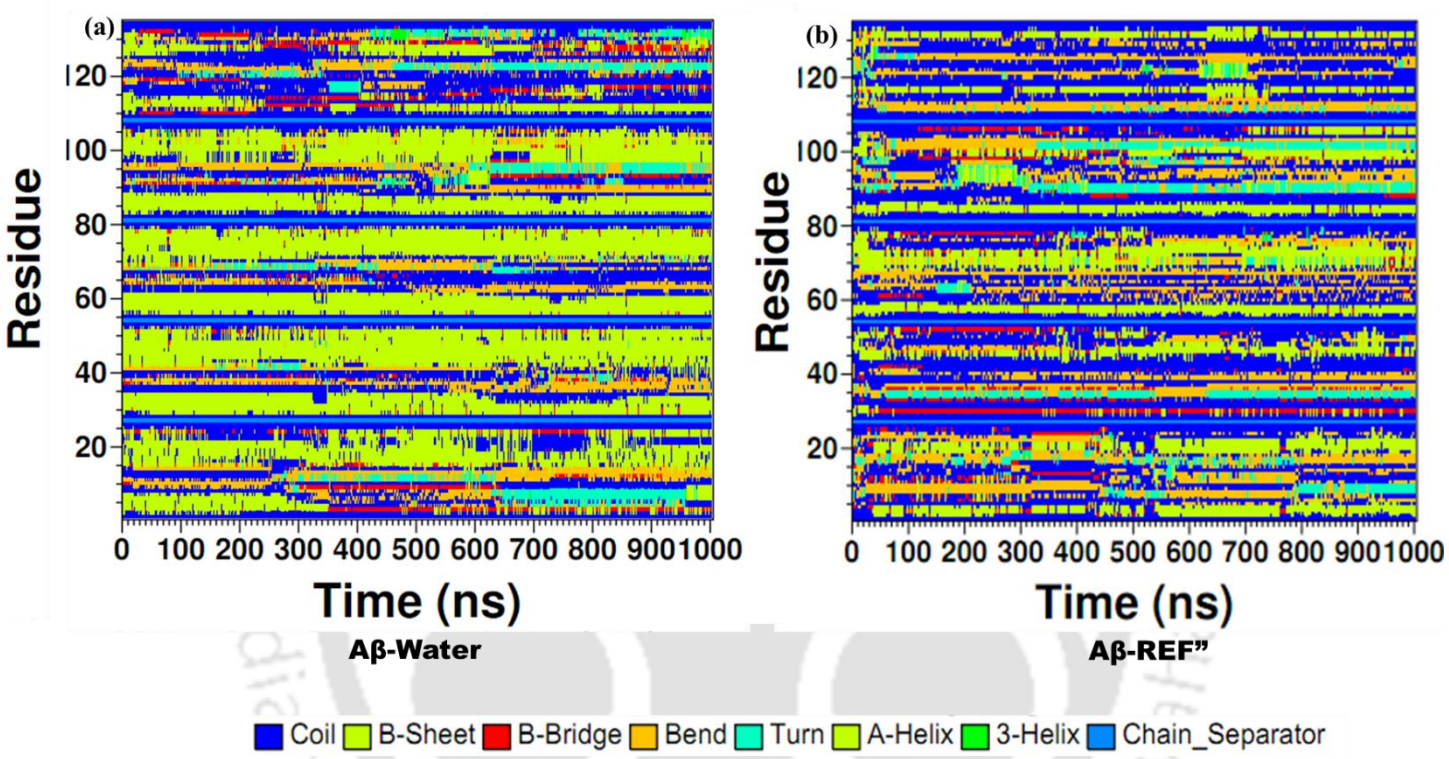

Fig. 8.5. DSSP representation of secondary structures for (a) Aβ-Water and (b) Aβ-REF". The lower β-sheet content and higher coil content in Aβ-REF" indicates destabilization of the fibril in off-pathway aggregates rather than the organized neurotoxic Aβ fibrils in Aβ-Water.

A similar reduction in β-sheet content of Aβ fibril leading to its destabilization in the presence of caffeine,[27] D744 (a fluorinated derivative of curcumin)[29], and norepinephrine[30] is found to be coherent with the current findings. The loss in β-sheet content and remarkable increase

in the coil and bend content assures destabilization to a greater extent and formation of off-pathway aggregates which further locks the conformation for further fibrillization.

Table 8.1. Secondary structures for (a) Aβ-Water and (b) Aβ-REF"

Secondary Structure (%)	Aβ-Water	Aβ-REF"
Coil	37	47
β-Sheet	40	18
β-Bridge	4	4
Bend	12	21
Turn	4	6
α-helix	0	1
3-helix	0	0
Chain_Separator	3	3

The results have been corroborated well by interaction of neobavaisoflavone on Aβ fibril wherein loss in β sheet content leads to the formation of amorphous or off–pathway aggregates.[23] Such highly disoriented structure due to high helical and low β sheet content suggests similarity with the amorphous aggregates, as reported by *in-vitro* interaction of ferulic acid with Aβ fibril.[31] The amorphous aggregates ensures the non-neurotoxicity and inability to form ordered fibrils further.

8.3.4 Effect on different bonds in Aβ fibril upon removal of ligand

8.3.4.1 Hydrogen-Bonds: The theoretical[32] and experimental[33] studies outlines the importance of an extensive H-bond network contributing towards the stability of Aβ fibrils. The average number of H-bonds for various selections such as, the entire protein, chain A-B, B-C, C-D and D-E, β1, turn and β2 region have been determined, and depicted in Fig. 8.6. The substantial decrease in H-bonds for the entire protein and neighboring inter-chain selections (Fig. 8.6) manifests such high degree of disarrangement of Aβ fibril.

The average number of H-bonds for above-mentioned selection groups have also been tabulated in Table 8.2, which shows marked decline in Aβ-REF" as compared to Aβ-water system. The average number of H-Bonds for inter-peptide chain A-B was recorded to be 14.543 ± 0.45 for Aβ-Water, which decreased to 2.571 ± 0.34 in Aβ-REF". This 82.32% reduction clearly highlight upon the breakage of H-bonds between chains A-B, pointing towards outward movement of chain A from the pentamer. Additionally, the turn region for all the chains is highly affected with 53.51% reduction in H-bonds in Aβ-REF" from Aβ-water system, suggesting greater relaxation of the entire Aβ fibril after removal of the ligand.

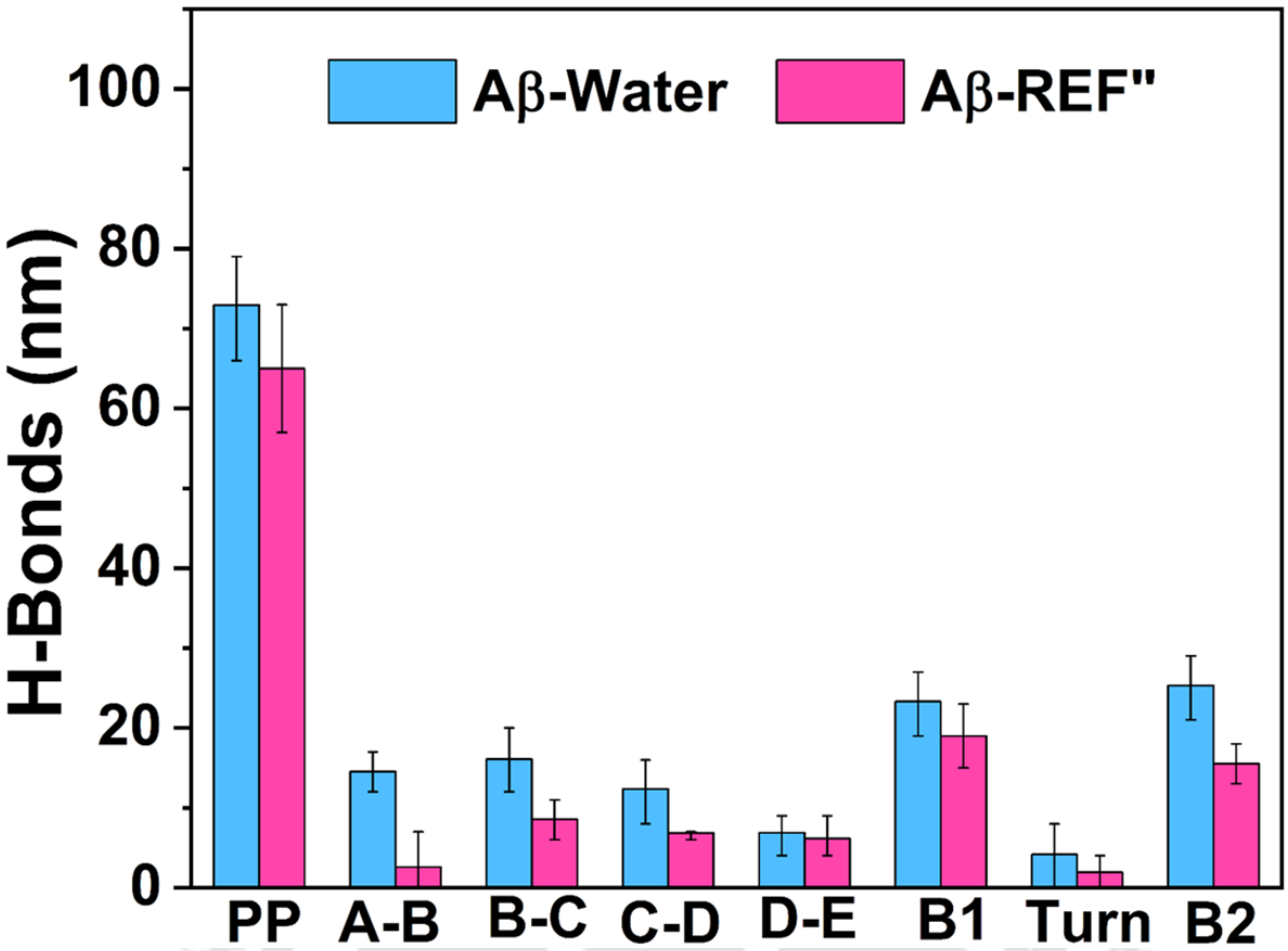

Fig. 8.6. Average number of H-bonds for Aβ-Water (blue) and Aβ-REF" (pink) for different pairs. The lesser H-bonds observed for Aβ-REF" system in entire protein, inter-chain A-B, B-C, C-D and D-E and intra-region β_1, turn and β_2 indicates the compromised stability and integrity of the fibril.

These observations are in close agreement with the destabilization of Aβ fibril by wgx-50, a novel compound from Sichuan pepper on account of drastic decrease in both intra- and inter-chain H-bonds.[34] The low number of H-bonds recorded for Aβ fibril in Aβ-REF" points out further prevention of refibrillation and elongation despite removal of the ligand.

Table 8.2. Number of H-bonds and % reduction for (a) Aβ-Water and (b) Aβ-REF"

Average number of H-Bonds	Aβ-Water	Aβ-REF"	% Reduction
Pro-Pro	74.779	64.997	13.08
Chain A-B	14.543	2.571	82.32
Chain B-C	16.081	8.548	46.84
Chain C-D	12.352	6.854	44.51
Chain D-E	6.884	6.153	10.61
β1	23.292	18.992	18.46
Turn	4.167	1.937	53.51
β2	25.292	15.536	38.57

8.3.4.2 Backbone Stability by K28-K28 residue interactions: The interaction between K28-K28 residues are key interactions that holds the integrity of the backbone of any protein structure. The average minimum distance between K28-K28 residues for all neighboring chain combination (viz., A-B, B-C, C-D and D-E) has been measured. The same has been plotted as interval plots with 95 % CI (confidence interval) around mean value in Fig. 8.7. Aβ-Water and Aβ-REF" are represented blue and pink color, respectively.

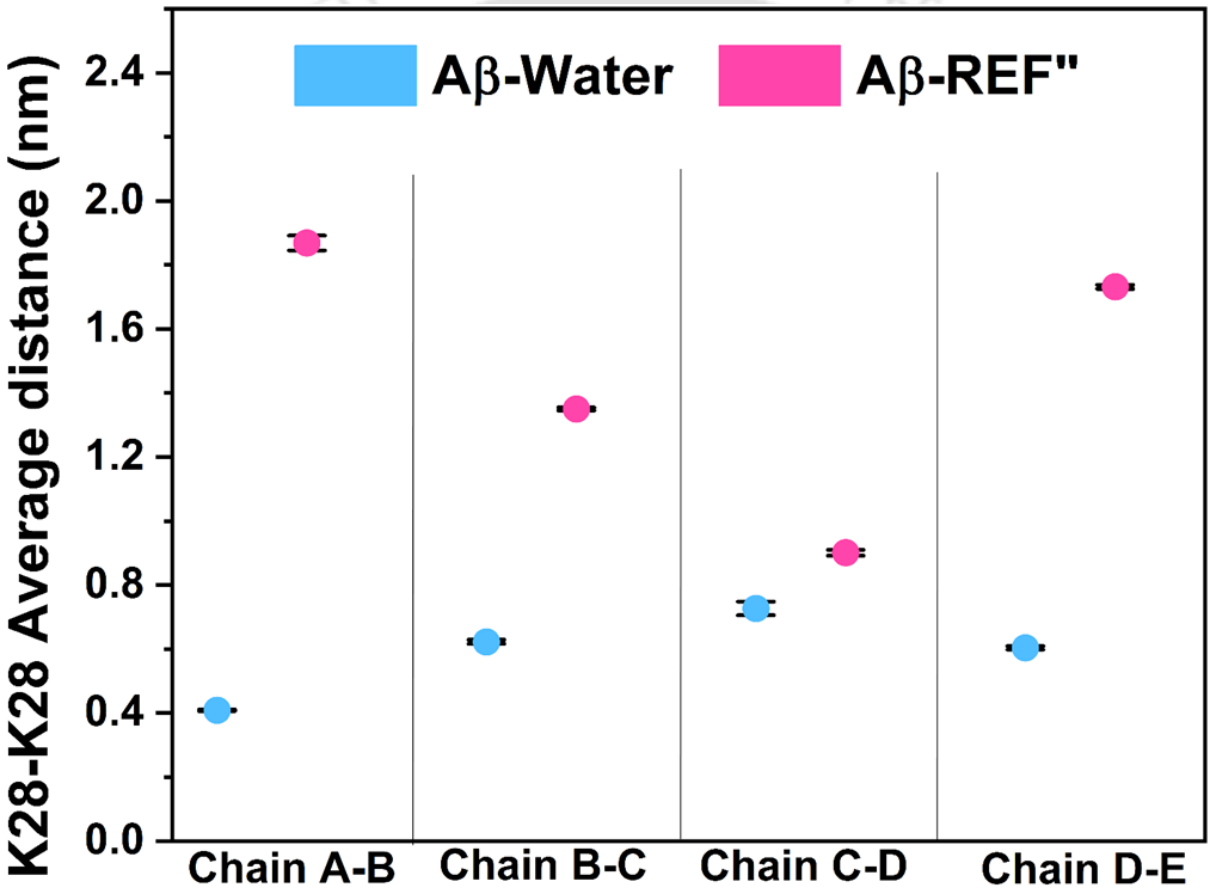

Fig. 8.7. Average K28-K28 Distance for Aβ-Water (blue) and Aβ-REF" (pink) for different pairs. The increased distance observed for inter-chain A-B, B-C and D-E in Aβ-REF" system indicates breaking of K28-K28 bonds at these places and thus the destabilization of the Aβ fibril in this system as compared to the Aβ-Water.

In Fig. 8.7, the value denoted in pink is found to be very high than values in blue for all the selection groups. The average value for chain A-B was measured to be 0.40 nm for Aβ-Water which has been increased to 1.86 nm for Aβ-REF" system, pointing on the breakage of the bond and thereby disorganization of the Aβ pentamer. The similar increment in K28-K28 residue leading to destabilization has been reported in Aβ fibril when caffeine has been introduced.[35] The instability introduced in backbone, disorganize the entire protein and conciliates prevention of reorganization of Aβ fibril. This reinstates the ligand removal approach as one of the promising therapeutics to treat AD.

8.3.4.3. Salt-Bridge formation by D23-K28 Residues: Salt bridges[36,37] are electrostatic interactions that impart stability to the protein and influence its structural conformation which in turn governs pattern recognition, function, degradation pattern, and catalytic activity.[38] In the present study, we have calculated the average distance between D23 and K28 residues for all inter- and intra-chain combinations for both Aβ-Water and Aβ-REF" systems. The average values have been plotted as bar graphs for all the selections in Fig. 8.8, with Aβ-Water and Aβ-REF" represented by blue and pink color respectively.

The inter-residual distance between D23 of chain A and K28 of neighboring chain B was measured as 1.09 nm for Aβ-Water that has been increased to 2.63 nm in Aβ-REF". Similarly, the considerable increase in the average distance from Aβ-Water to Aβ-REF" has been recorded for chain B-C (from 0.45 nm to 2.67 nm) and chain C-D (from 0.87 nm to 1.95 nm) as well. The intra-chain D23-K28 residual distance has been found to be increased for terminal chain E, which indicates it's drifting apart from the Aβ fibril. From Fig. 8.8, it can clearly be inferred that such a

pronounced increase in the distance between D23-K28 residues results in disorganized Aβ fibril structure, and marks enhanced destabilization.

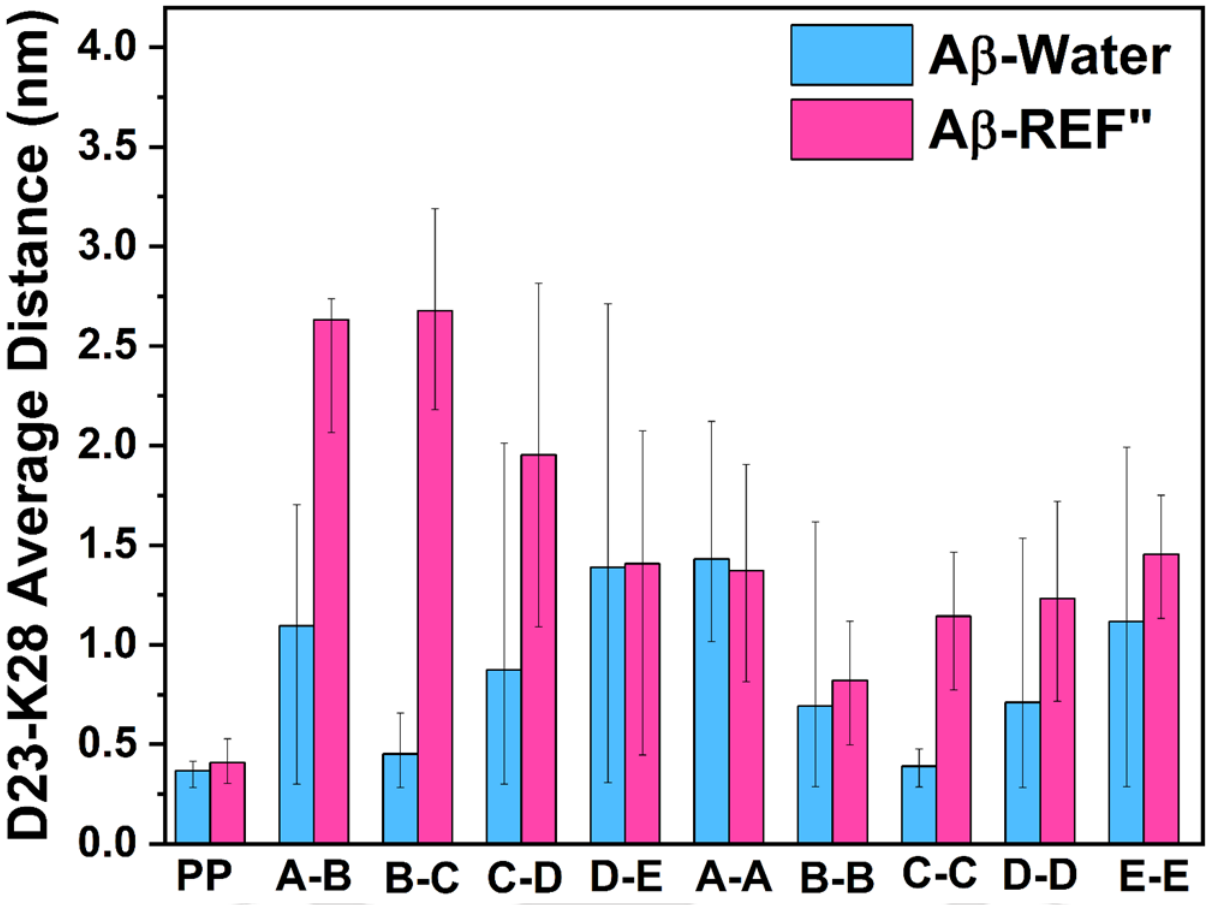

Fig. 8.8. Average D23-K28 Distance for Aβ-Water (blue) and Aβ-REF" (pink) for different pairs. The increased distance observed for inter-chain A-B, B-C and C-D and intra-chain C-C, D-D and E-E in Aβ-REF" system indicates breaking of D23-K28 bonds at these places and thus the destabilization of the Aβ fibril in this system as compared to the Aβ-Water.

The results thus obtained are found to be concurrent with the breaking of salt bridges of Aβ fibril in the presence of copper ions,[39] C-60 fullerene,[40] surfactin[41] molecules, and beta sheet

breakers[42] leading to the destabilization of Aβ fibril. This explains the importance of ligand removal approach for enhanced destabilization as promising method for treating AD.

8.3.4.4 Hydrophobic contacts: The major contributors towards the folding pattern and stability of the protein are hydrophobic interaction due to presence of hydrophobic residues. The burying of hydrophobic residues inside the solvent inaccessible cavity provides such remarkable strength to amyloid fibrils.[43] According to the principle of PASA (Principle of Amyloid Self-Assembly), the most stable fibrillar structure possesses the maximum number of inter- and intra-peptide hydrophobic interactions.[44] The crucial hydrophobic contact pairs reported for the current pentamer Aβ structure are L34-V36, A21-V36, and F19-G38.[45] All these residues interact in both intra- and inter-peptide manner to provide structural stability to the Aβ fibril.

We have calculated mean distance between these residues to estimate the probability of bond formation between them. The inter-residual distance between all neighboring pairs (viz., chain A-B, B-C, C-D and D-E) has been depicted in Fig. 8.9 as bar graphs representing average mean values with Aβ-water in blue and Aβ-REF" represented in pink. The inter-residual distance between L34 of chain A and V36 of chain B was estimated as 0.43 nm for Aβ-Water, which was increased to 2.65 nm in Aβ-REF" system (Fig. 8.9), highlighting bond breakage. The value recorded for average distance of L34-V36 between chains D-E has been found to be 0.41 nm for Aβ-Water that has been increased to 0.93 nm in Aβ-REF" system. The significant increase in the mean distance implies inhibition of bond formation between L34 and V36 for all the neighboring chains construing the organization and stability of the Aβ fibril upon ligand removal.

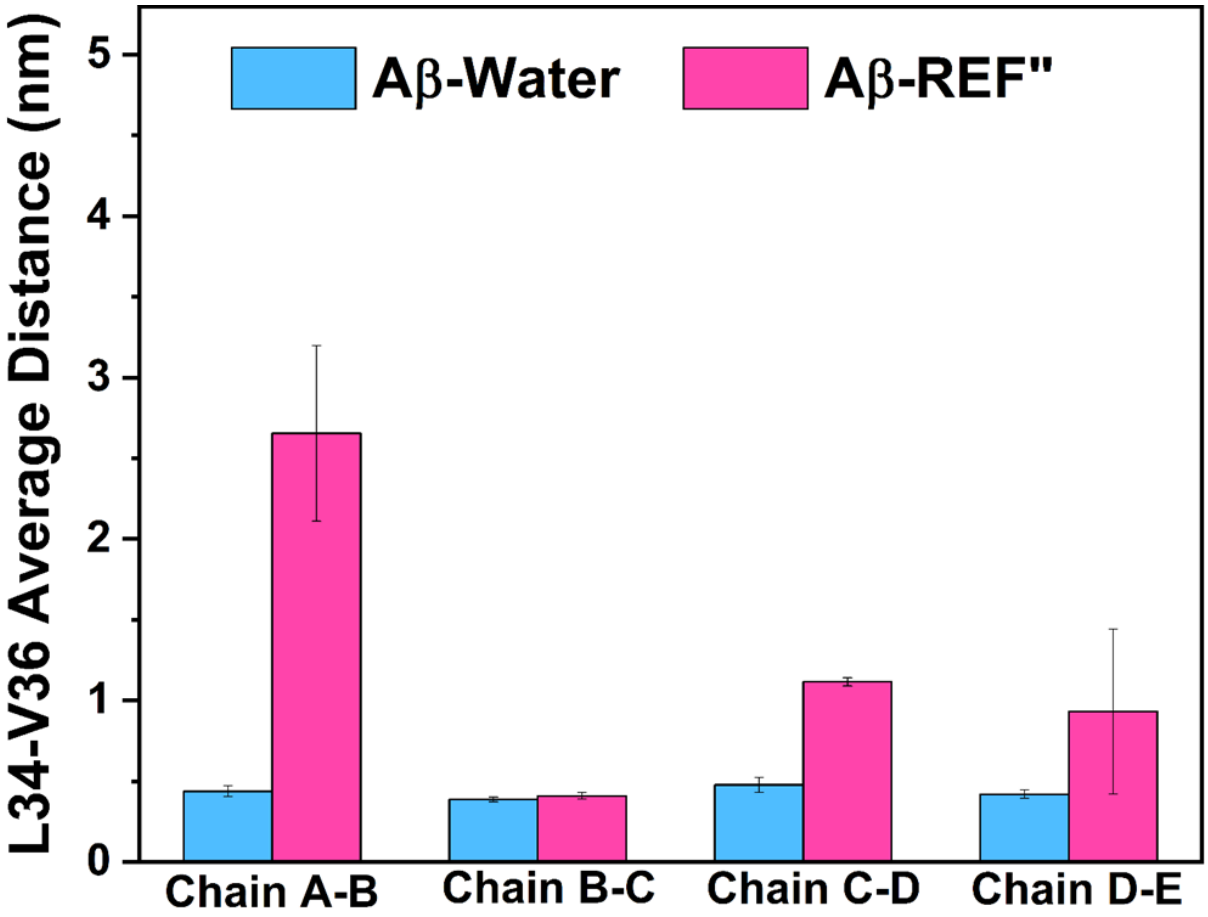

Fig. 8.9. Average L34-V36 Distance for Aβ-Water (blue) and Aβ-REF" (pink) for different pairs. The increased distance observed for inter-chain A-B, C-D and D-E in Aβ-REF" system indicates breaking of L34-V36 bonds at these places and thus the destabilization of the Aβ fibril in this system as compared to the Aβ-Water.

Likewise, the hydrophobic residue interaction between A21 and V36 for all the chains (inter and intra) has been accessed and plotted as interval plots in Fig. 8.10. The mean distance between chain A and B for residue A21 and V36 has been found to be 2.51 nm in Aβ-REF" which is remarkably higher than Aβ-Water (0.79 nm) system (Fig. 8.10). The similar sharp increment of 1.24 nm, 0.3 nm and 0.71 nm has been reported for Chain B-C, C-D and D-E respectively in Aβ-

REF" system. Such increase in intra- and inter-chain distance in Aβ-REF" system, points towards compromised bond stability thereby, affecting the entire pentamer structure. Additionally, the increased mean distance between A21 and V36 within the same chain impedes the bond formation thereby further destabilizing the already misaligned structure in Aβ-REF" system, as depicted in Fig. 8.10.

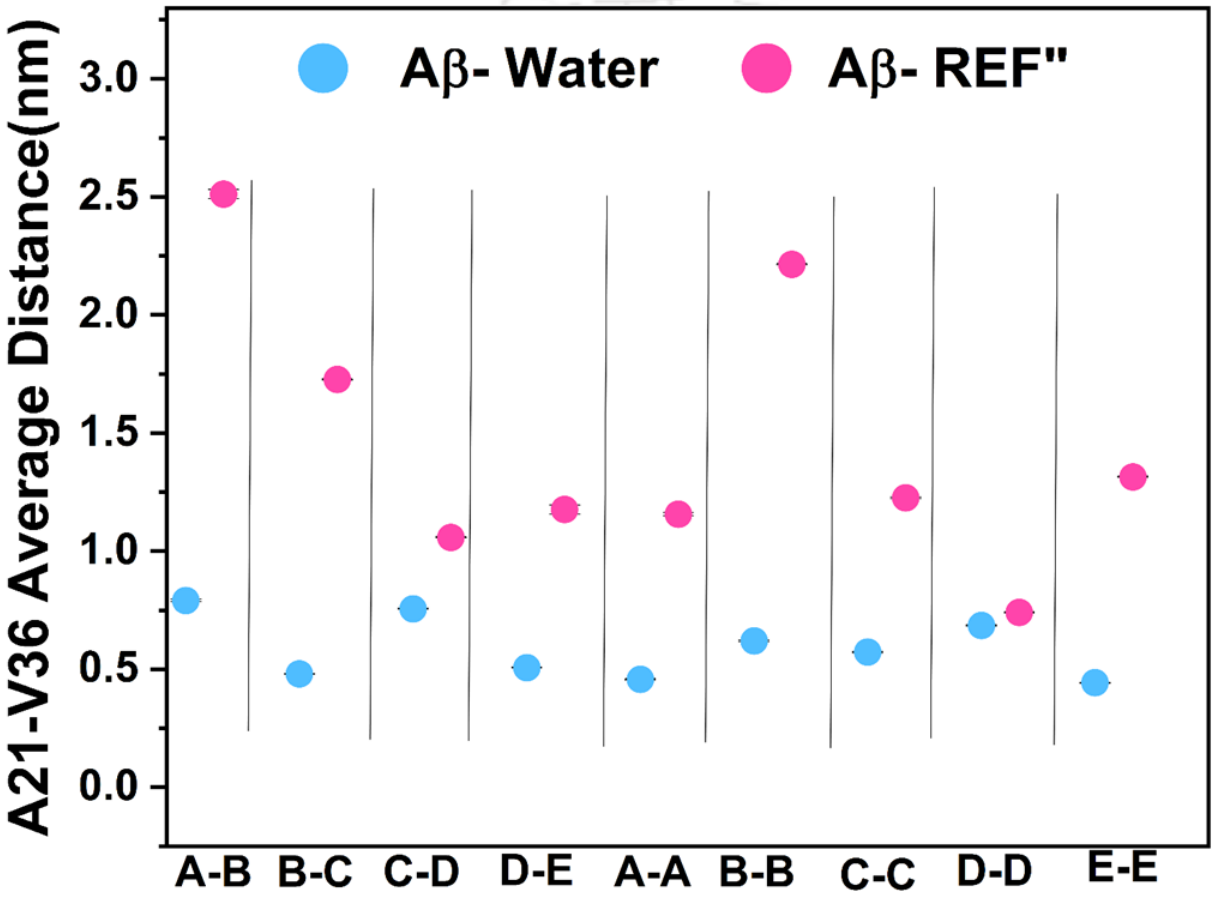

Fig. 8.10. Average A21-V36 Distance for Aβ-Water (blue) and Aβ-REF" (pink) for different pairs. The increased distance observed for inter-chain A-B, B-C and D-E and intra-chain A-A, B-B, C-C and E-E in Aβ-REF" system indicates breaking of A21-V36 bonds at these places and thus the destabilization of the Aβ fibril in this system as compared to the Aβ-Water.

One more key interaction between F19-G38 has been calculated for its ability for bond formation which is a function of the distance between these residues. The average mean distance for inter-chain in Aβ fibril (viz., A-B, B-C, C-D and D-E) and intra-chain peptide interaction (viz. A-A, B-B, C-C, D-D and E-E) for F19-G38 pair has been plotted as an interval plot in Fig. 8.11.

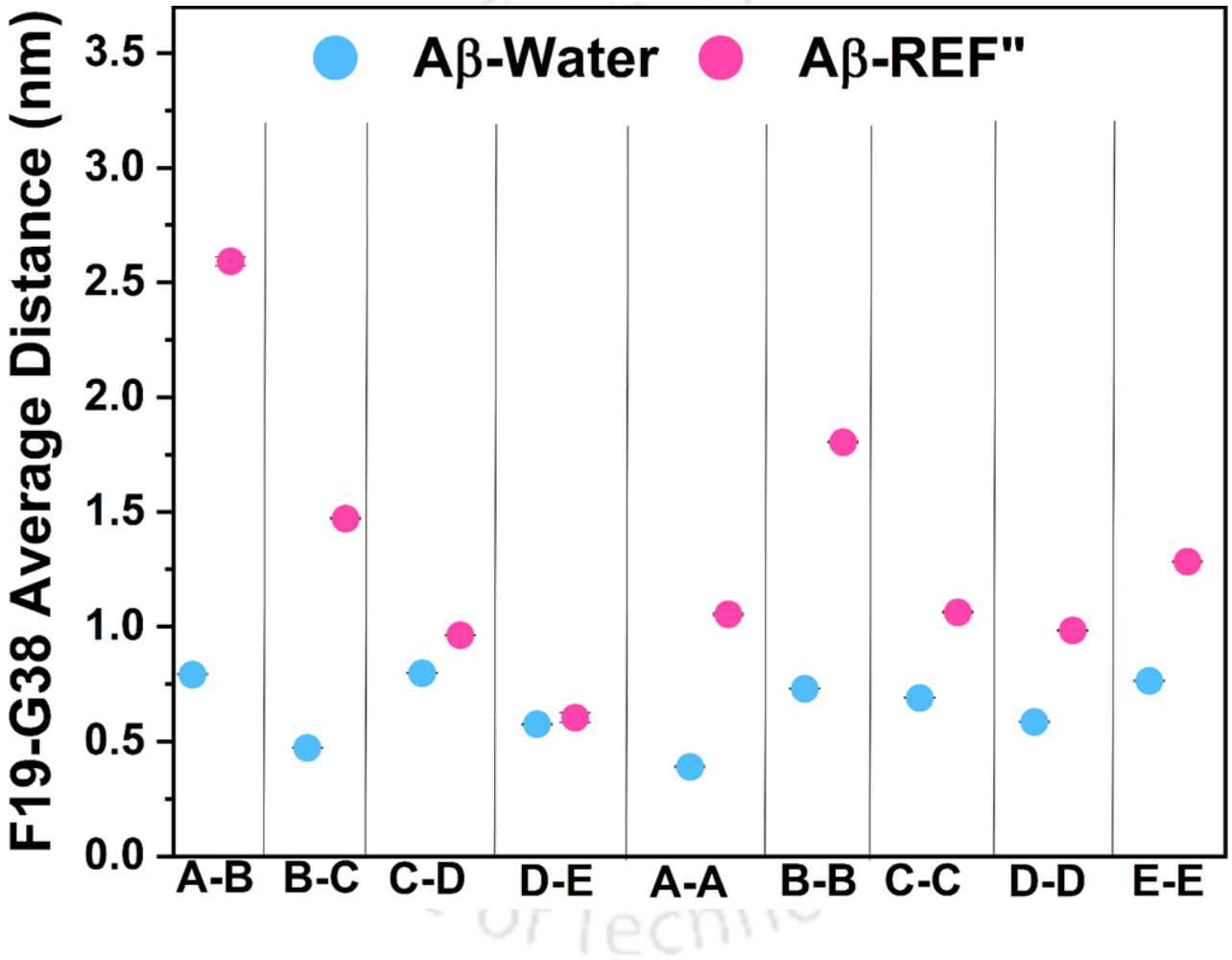

Fig. 8.11. Average F19-G38 Distance for Aβ-Water (blue) and Aβ-REF" (pink) for different pairs. The increased distance observed for inter-chain A-B and B-C and intra-chain A-A, B-B, C-C, D-D and E-E in Aβ-REF" system indicates breaking of F19-G38 bonds at these places and thus the destabilization of the Aβ fibril in this system as compared to the Aβ-Water.

Although there has been an increase in the mean distance for all the selections under study, but chain A has been found to be the most affected one. The increased distance of 1.8 nm for chain A-B and 0.67 nm for chain A-A from Aβ-Water to Aβ-REF" system clearly highlight the obstruction of bond formation between these chains leading to drifting of chain A from the pentamer. Similarly, the obstruction in bond formation in F19-G38 residues for intra and inter chains of all other peptide chains manifest the highly disorganized Aβ fibril structure as viewed in Fig. 8.2c. This increased distance between hydrophobic residues for all the chains implies breaking of these bonds in the Aβ-REF" system, leading to the misalignment and disruption of the entire fibrillar structure of Aβ fibril. The similar findings have been reported for Aβ fibril where destabilization is attributed to breaking of hydrophobic interactions when serotonin and melatonin has been introduced.[46] The current observation highlight upon the irreversible destabilization of Aβ fibril achieved by removal of ligand thereby pinning importance of destabilization approach as a better therapeutic intervention for AD.

8.3.5 Inter-Chain Distance Matrix: The residue-residue contact between neighboring chains at both the terminals of the fibril has been determined via a distance matrix. The contact map analysis has been depicted in Fig. 8.12 for chain A-B (upper panel) and D-E (lower panel) for both the systems under investigation. Herein, representation for Aβ-Water and Aβ-REF" has been depicted in left and right side respectively in both the panels. It is clearly evident that the residue – residue contacts for both the chain A-B and D-E has been highly repressed in Aβ-REF" as compared to Aβ-Water (Fig. 8.12). The portrayal of blank spaces in distance matrices demonstrates the breaking of bonds in chain A-B (Fig. 8.12b) and D-E (Fig. 8.12d) indicates drifting of these chains from the parent Aβ fibril thereby pointing enhanced destabilization on Aβ-REF".

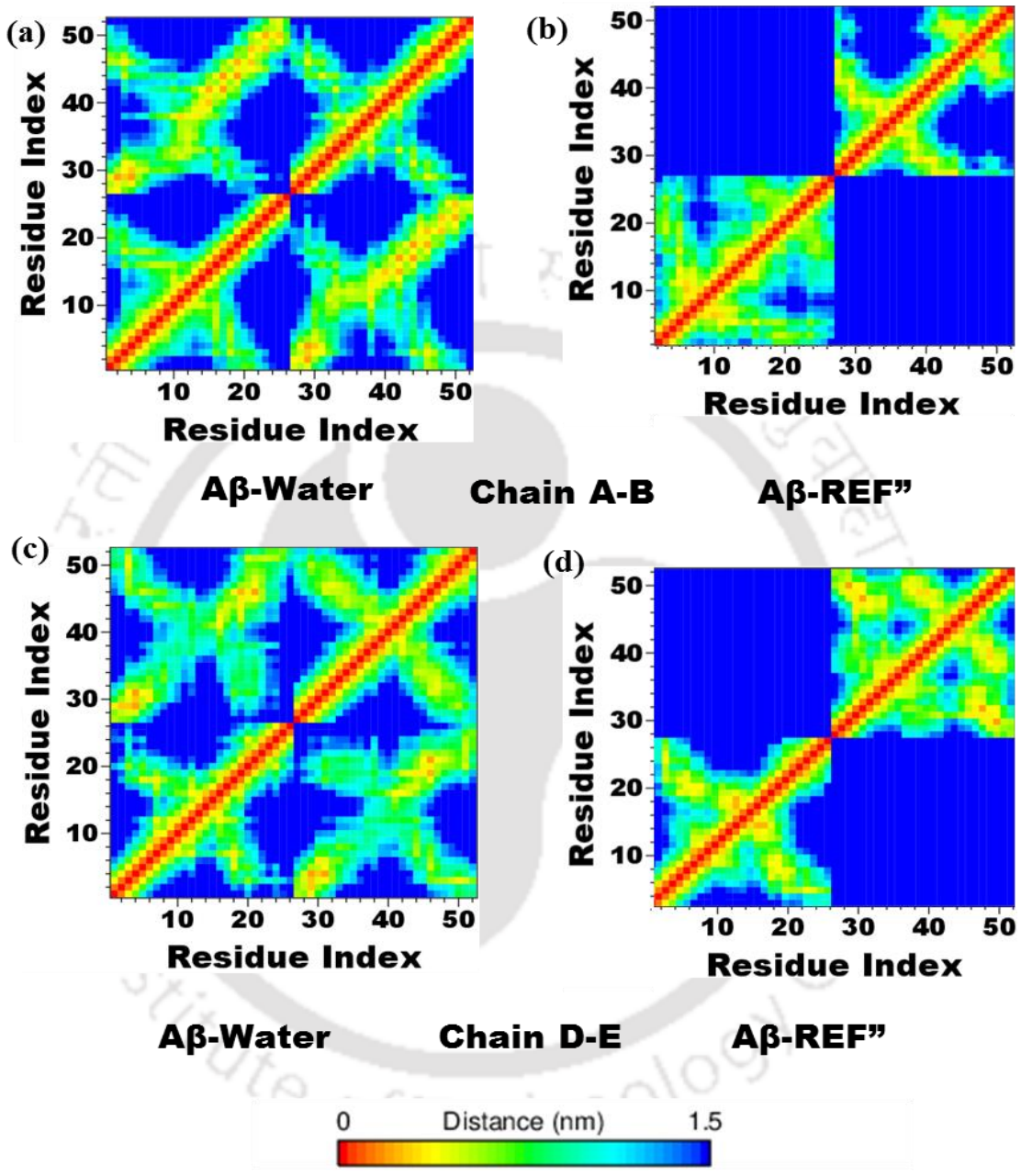

Fig. 8.12. Inter-chain distance matrix for Aβ-Water (left) and Aβ-REF" (right) for chain A-B (upper panel) and for Aβ-Water (left) and Aβ-REF" (right) for chain D-E (lower panel). No contacts have been observed for chain A-B and D-E in Aβ-REF" system explaining drifting of chains A and E from the parent pentamer.

The similar contact maps have been represented in various other reports with norepinephrine[30], omega-3 PUFAs[25] and D744 (a curcumin derivative)[29] with evidence on breakage of chains, which very well corroborates with our findings.

The breaking of residual contacts is resultant of the increased inter-chain distance between neighboring chains as depicted in Fig. 8.13 which compliments well with the contact map analysis depicted in Fig. 8.12.

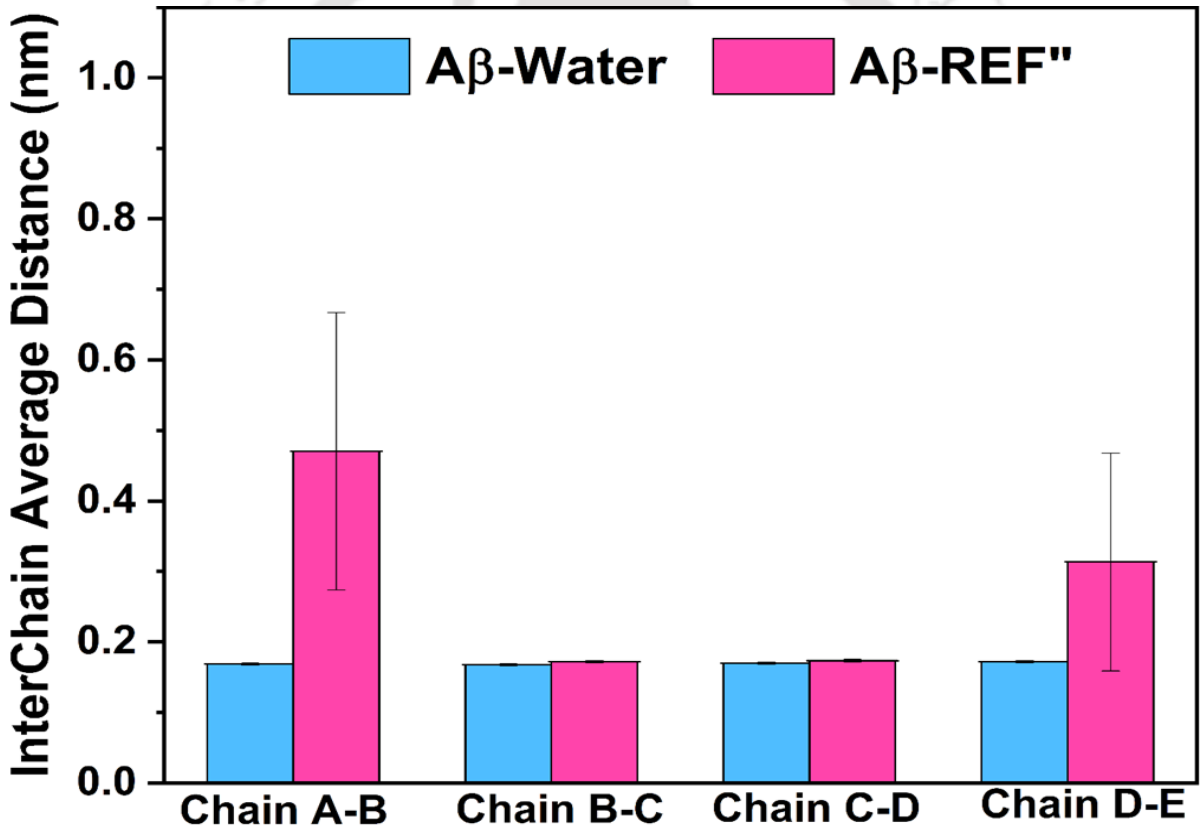

Fig. 8.13. Average Inter-chain distance for Aβ-Water (blue) and Aβ-REF" (pink) for different pairs. The increased distance observed for inter-chain A-B and D-E in Aβ-REF" system indicates drifting of chains A and E from the parent pentamer structured as compared to the Aβ-Water.

The inter-chain distance computed by g_mindist tool has been recorded as 0.16 nm in Aβ-Water that has been increased to 0.47 nm in Aβ-REF", indicating the drifting apart of chain A from the organized fibril. Similarly, a considerable increase of 0.14 nm in Aβ-REF" for distance between chain D-E has been observed, indicating moving apart of chain E from the pentamer (Fig. 8.13). The unaltered distance observed for both the chains, B-C and C-D in both Aβ-Water (control) and Aβ-REF" (test) systems, indicated sustenance of their native structure. The corroboration between breaking of residual contacts on account of increased inter-chain distance explains the misaligned structure as observed in Fig. 8.2c. The consideration of destabilization approach has got one more evidence for its therapeutic intervention.

8.3.6 Free Energy Landscape: The free energy landscape (FEL) is the representation of the Gibbs free energy (kcal/mol) that demonstrates the folding pattern and motion in the protein. The FEL helps in understanding the dominant motions and conformational changes that are induced on introduction or removal of ligand. The FEL is constructed via principal component analysis (PCA) traversing the protein trajectory. This helps in resolution of the folding dynamics of the trajectories despite they look very similar upon visual inspection.[47] In the current work, we have constructed a 2D FEL for both the systems Aβ-Water and Aβ-REF" under investigation as a function of Cα-RMSD value and number of H-bonds for the entire protein (intra- and inter-chain). As depicted in Fig. 8.14, FEL highlight minima energy basins in blue and highest energy states in red for both Aβ-Water (left panel) and Aβ-REF" (right panel). The blue spots, concentrated in a single region, signifying the stable and folded state of Aβ fibril in the absence of ligand interaction. Contrarily, more number of highly scattered regions of the blue spots observed in Aβ-REF" system

highlight upon the unfolded and collapsed state of the pentamer, pointing enhanced destabilization in this system.

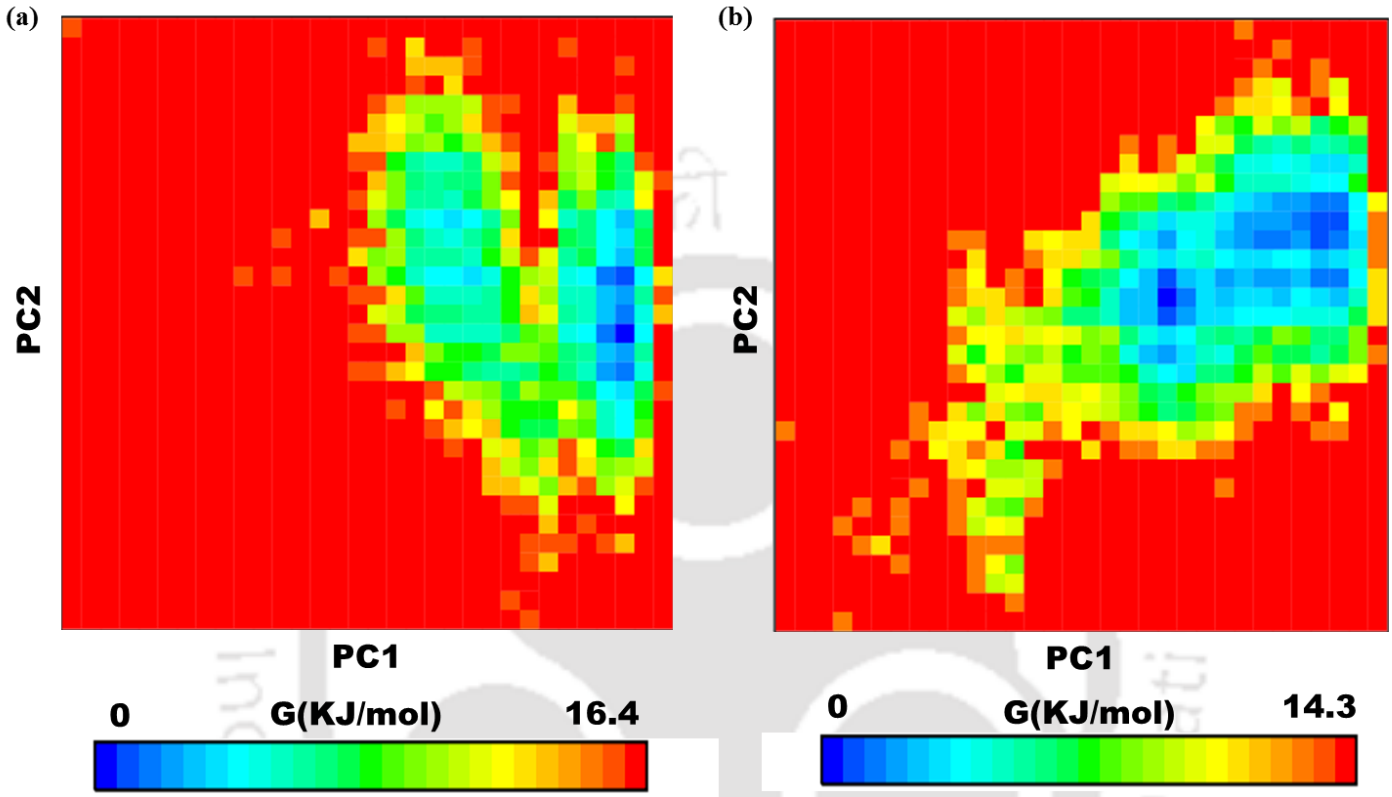

Fig. 8.14. Free Energy Landscape for (a) Aβ-Water and (b) Aβ-REF". (*PC1 = Cα-RMSD (pro), PC2 = Average number of H-bonds (pp)). Higher number of scattered blue regions observed for Aβ-REF" system indicates highly collapsed and unfolded structure of the fibril indicating destabilization of the fibril as compared to the Aβ-Water.

The higher Gibbs free energy in Aβ-REF" system indicates unfolded and disorganized state of the Aβ fibril, thereby concluding the destabilization by the natural ligand as a promising therapeutic approach. Interestingly, the FEL plot observed for Aβ-REF" can be correlated to the disappearance of the β sheet structure in terminal chain, A (Fig. 8.2c). A similar conformation has

been reported in case of hIAPP, an amyloidogenic protein, interacting with EGCG wherein the disappearance of β-sheet was observed.[48] The studies are also found in close proximity with the observations where native proteins are found to be in folded state as compared to the mutant ones on account of the lower Gibbs free energy.[49] Similar results of higher Gibbs free energy, represented by scattered blue spots, have been reported in Aβ fibril upon binding of hybrid of resveratrol and clioquinol compound.[50]

8.3.7 Binding Free Energy analysis of the terminal neighboring chains: The MM-PBSA method is integrated with MD simulation with an objective to gain deeper insights on the binding affinity of the neighboring terminal chains in the absence of ligand. The detailed inter-chain binding free energy (BFE) analysis for chain A-B and D-E for Aβ-Water and Aβ-REF" system has been tabulated in Table 8.3. The lowest $G_{binding}$ observed for chain A-B (-448.45 ± 51.39 kcal/mol) for Aβ-Water system (Table 8.3), clearly indicates the highest affinity of these two chains. On contrary, the unfavorable positive $G_{binding}$ of 3.21 ± 1.77 kcal/mol has been reported for chain A-B when ligand is removed, indicating falling apart of the interaction between these chains in Aβ-REF". Similarly, $G_{binding}$ of -103.11 ± 39.04 kcal/mol for terminal chain D-E for Aβ-Water system has been found to increase to 10.83 ± 6.47 kcal/mol for Aβ-REF", indicating the breaking of this inter-chain pair. The estimation of various other associated energy terms, such as, ΔE_{MM}, ΔG^{psolv}, and ΔG^{npsolv} provide more precision on nature of dominant interactions involved in binding.[51]

Table 8.3. MM-PBSA description for Aβ-Water and Aβ-REF" for terminal pairs

Energy Terms	Inter-chain (chain A and B) BFE for Aβ-Water (Kcal/mol)	Inter-chain (chain A and B) BFE for Aβ-REF" (Kcal/mol)	Inter-chain (chain D and E) BFE for Aβ-Water (Kcal/mol)	Inter-chain (chain D and E) BFE for Aβ-REF" (Kcal/mol)
ΔE_{vdW}	-380.614 ± 3.89	0	-316.55 ± 4.05	0
ΔE_{elec}	-678.3 ± 27.5	7.91 ± 0.13	16.14 ± 2.24	14.54 ± 0.52
$\Delta E_{MM}{}^{a}$	-1058.91 ± 31.4	7.91 ± 0.13	-300.41 ± 6.29	14.54 ± 0.52
ΔG_{ps}	660.26 ± 19.64	-5.29 ± 1.28	234.37 ± 11.86	-3.60 ± 1.99
ΔG_{nps}	-49.8 ± 0.3	0.59 ± 0.36	-37.14 ± 0.69	-0.11 ± 0.24
$\Delta G_{solv}{}^{b}$	610.46 ± 19.99	-4.7± 1.64	197.23 ± 12.55	-3.71 ± 2.18
$\Delta G_{binding}{}^{c}$	-448.45 ± 51.39	3.21 ± 1.77	-103.11 ± 39.04	10.83 ± 2.7

[a] $\Delta E_{MM} = \Delta E_{vdW} + \Delta E_{elec}$ [b] $\Delta G_{solv} = \Delta G_{ps} + \Delta G_{nps}$ [c] $\Delta G_{binding} = \Delta E_{MM} + \Delta G_{solv}$

The notable zero value for ΔE_{vdW} on account of van der Waals contributions signifies the breaking of various hydrophobic interactions between non polar residues across the fibrillar length which has been depicted in Fig. 8.9-8.11. The ΔE_{elec} that gives idea about the electrostatic interactions between charged residues in neighboring chains is found to be higher or positive in Aβ-REF" system highlighting breakage of these bonds which is in parity with the observations reported in Fig. 8.8. Interestingly, the favorable non polar contribution expressed by ΔG_{nps} in Aβ-Water and unfavorable ΔG_{nps} in Aβ-REF" is found to be contrary to the SASA values observed. The reason for the indirect relationship between SASA values in Fig. 8.4b with ΔG_{nps} calculated by MM-PBSA is the interaction of residues with water and in residues amongst themselves respectively. The increased SASA values in Aβ-REF" explains the interaction of Aβ residues to the solvent rather than the hydrophobic residues among demarcating unfolding. Correlatively, the polar solvation energy expressed by ΔG_{ps} is found to be favorable for Aβ-REF" on account of increased SASA value, which explains limited interaction amongst terminal peptides. The current findings draw a possible direct correlation between high SASA values and physical significance of polar solvation contribution in the binding or unbinding. This also corroborates well with the contribution of van der Waals interaction towards binding of the terminal chains in Aβ-Water which lacks completely in Aβ-REF". The current observation on disorganization of the entire pentamer with chain A and E drifting apart is a cumulative effect of breakage of all salt bridges and hydrophobic interactions as depicted and explained in Fig. 8.8-8.11 already.

The similar reports of the unfavorable binding energy as observed for protein-inhibitor complex, directs its non-binding towards MurA enzyme for inhibitory studies as mentioned[52] which explains no interaction between enzyme and the receptor. The positive $G_{binding}$ energy reported due to alanine mutations also indicates the destabilization and inhibition of further

elongation of the Aβ fibril.[53] Recently, positive binding energy was reported for bexarotene with Aβ dimers, indicating no binding affinity,[54] which substantiates our current findings. These observations relate towards the drifting of terminal chains from the pentamer. Simultaneously, the obtained destabilized structure on account positive energy barrier (difficult to cross) impedes irrevocability towards the organized amyloid structure. These observations helps in establishing the destabilization technique as the promiscuous therapeutic intervention for AD owing to its irreversibility.

8.3.8 Supporting studies from removal of caffeine: The efficacy of ligand removal strategy as one of the promising therapeutic approach, pertinent to the inhibition of refibrillation of the already destabilized Aβ fibril is well explained in the current work. To substantiate the same, we have also ran a 100 ns simulation following the same methodology with caffeine (CFF) removed from the destabilized structure. The destabilization effect observed in Aβ fibril upon introduction of caffeine has been explained in detail in our previous work.[35] This supporting study implies the removal of one caffeine molecule from the Aβ fibril system, denoted as Aβ-CFF", and ran for 100 ns simulation using CHARMM22* force field with all the other parameters same as the methodology section in the current work. The comparative analysis has been done in a similar way between Aβ-Water as the control system and Aβ-CFF" being the test one. The visual

inspection by VMD given in Fig. 8.15a and 8.15b, clearly indicates the detachment of one terminal chain (Fig. 8.15b) from pentamer in Aβ-CFF" system when caffeine molecule is removed.

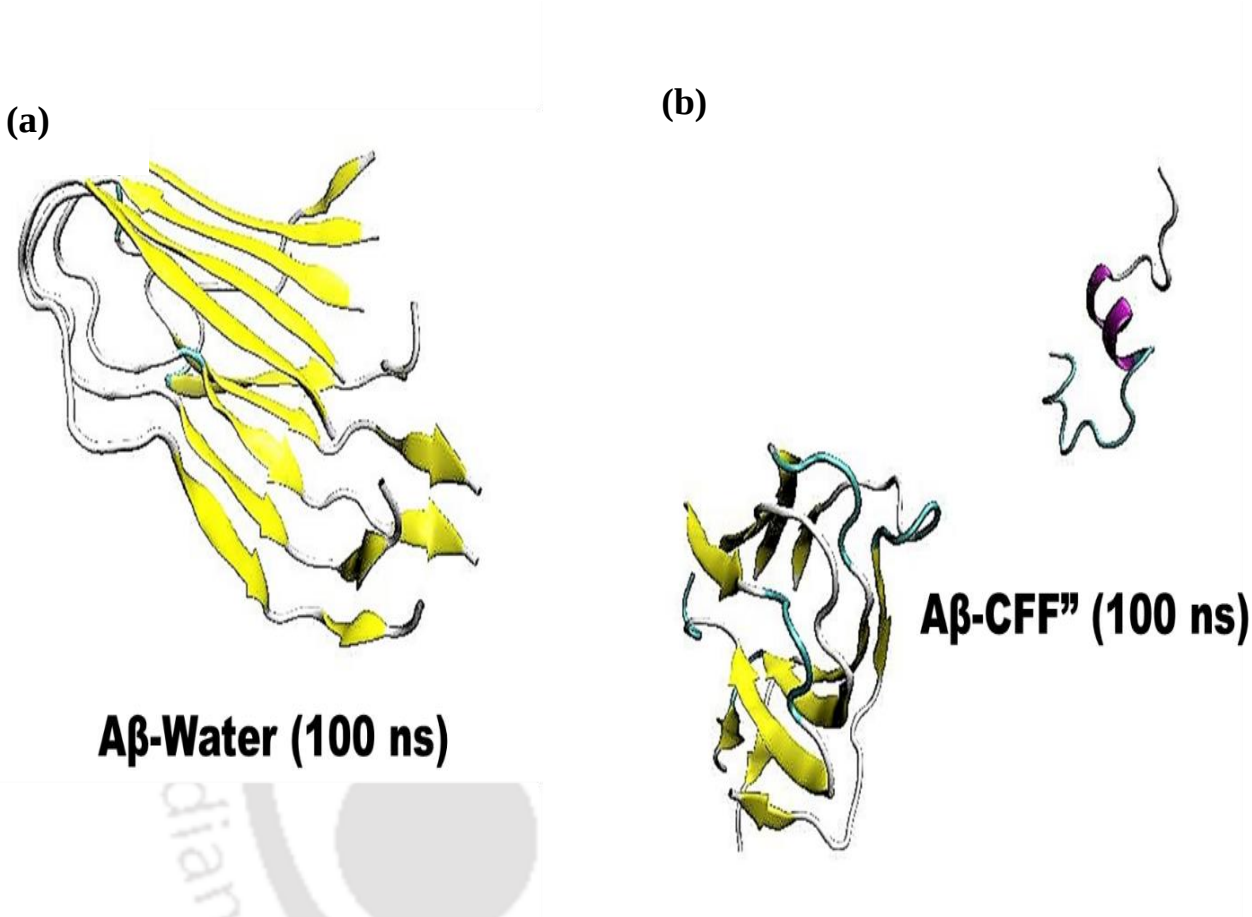

Fig. 8.15. Final snapshot of (a) Aβ-Water and (b) Aβ-CFF" system after 100 ns of simulation. The destabilization observed in Aβ-CFF" system with detachment of terminal chain explains effectiveness of the destabilization technique.

The higher fluctuations in RMSD in Aβ-CFF" in all selections, Fig. 8.16, demarcates the extent of destabilization in the entire fibril upon ligand removal.

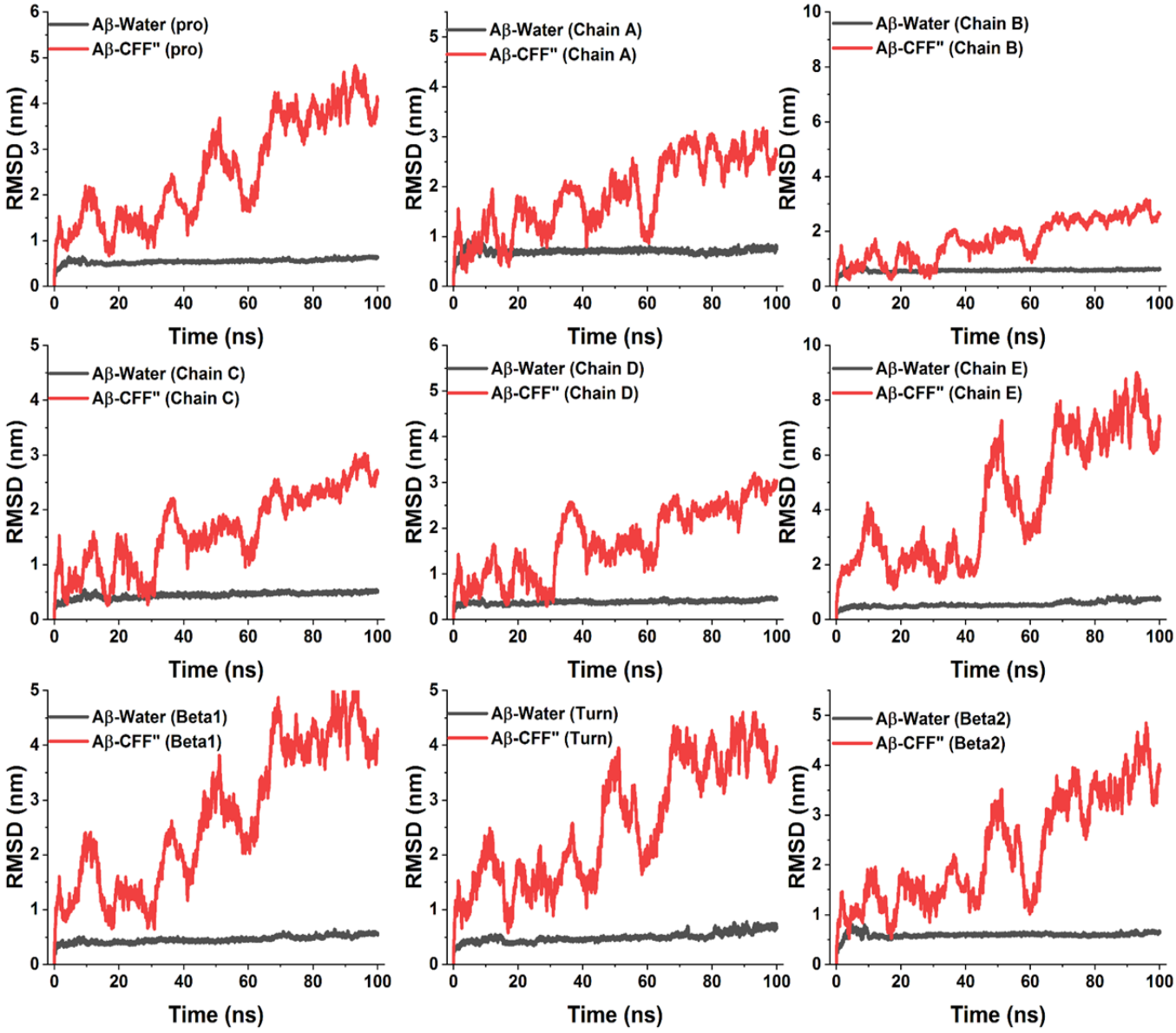

Fig. 8.16. Time evolution of Cα-RMSD of Aβ-Water (black) and Aβ-CFF" (red) for different selections. The increased Cα-RMSD value for protein, chain A, B, C, D and E and β1, turn and β2 region in Aβ-CFF" system indicates disorganization as compared to the Aβ-Water.

The increased R_g and SASA values recorded for Aβ-CFF" system as compared to Aβ-Water (Fig. 8.17a and 8.17b respectively) indicates higher unfolding of the fibril, and thus higher interaction with the solvent molecules.

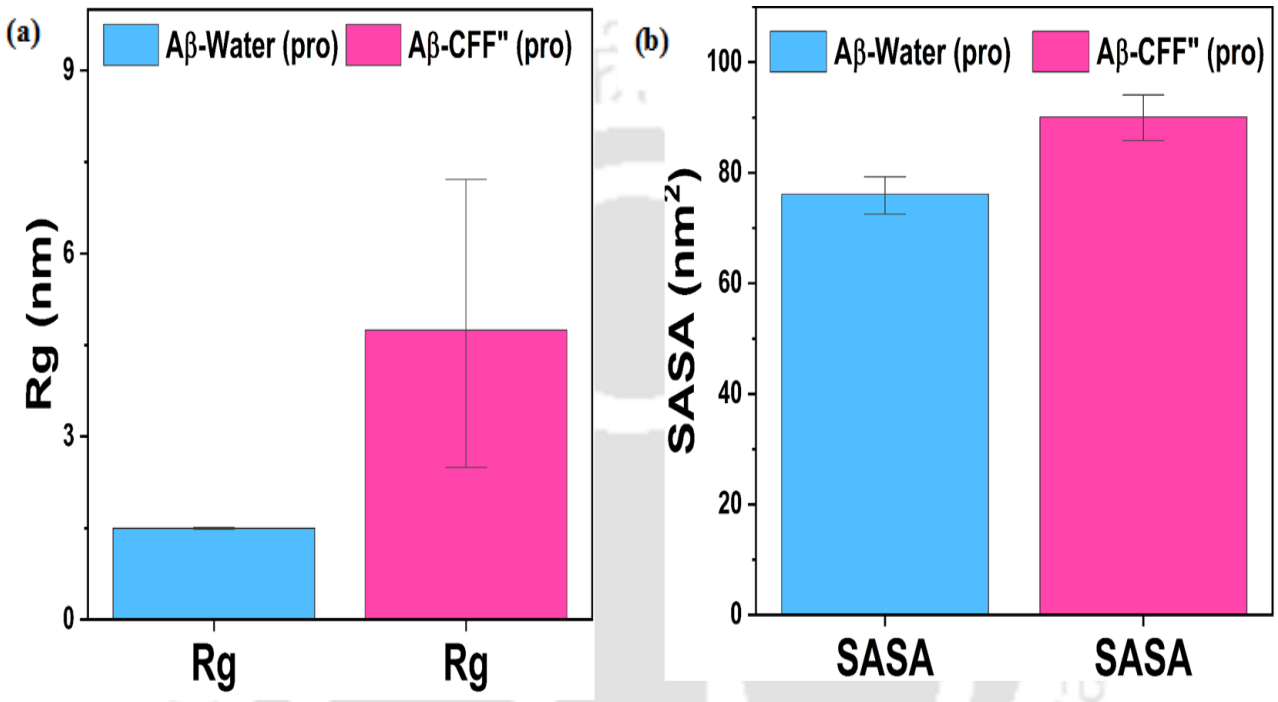

Fig. 8.17. Average value of (a) R_g and (b) SASA for Aβ-Water (blue) and Aβ-CFF" (pink). The increased R_g and SASA for Aβ-CFF" indicates higher flexibility, lesser compactness and more interaction with the solvent molecules as compared to the Aβ-Water, which is compact and organized.

The detachment of terminal chain E can be assessed from no H-bonds observed between chain D-E (Fig. 8.18a), increased inter-chain distance between chain D and E (Fig. 8.18b).

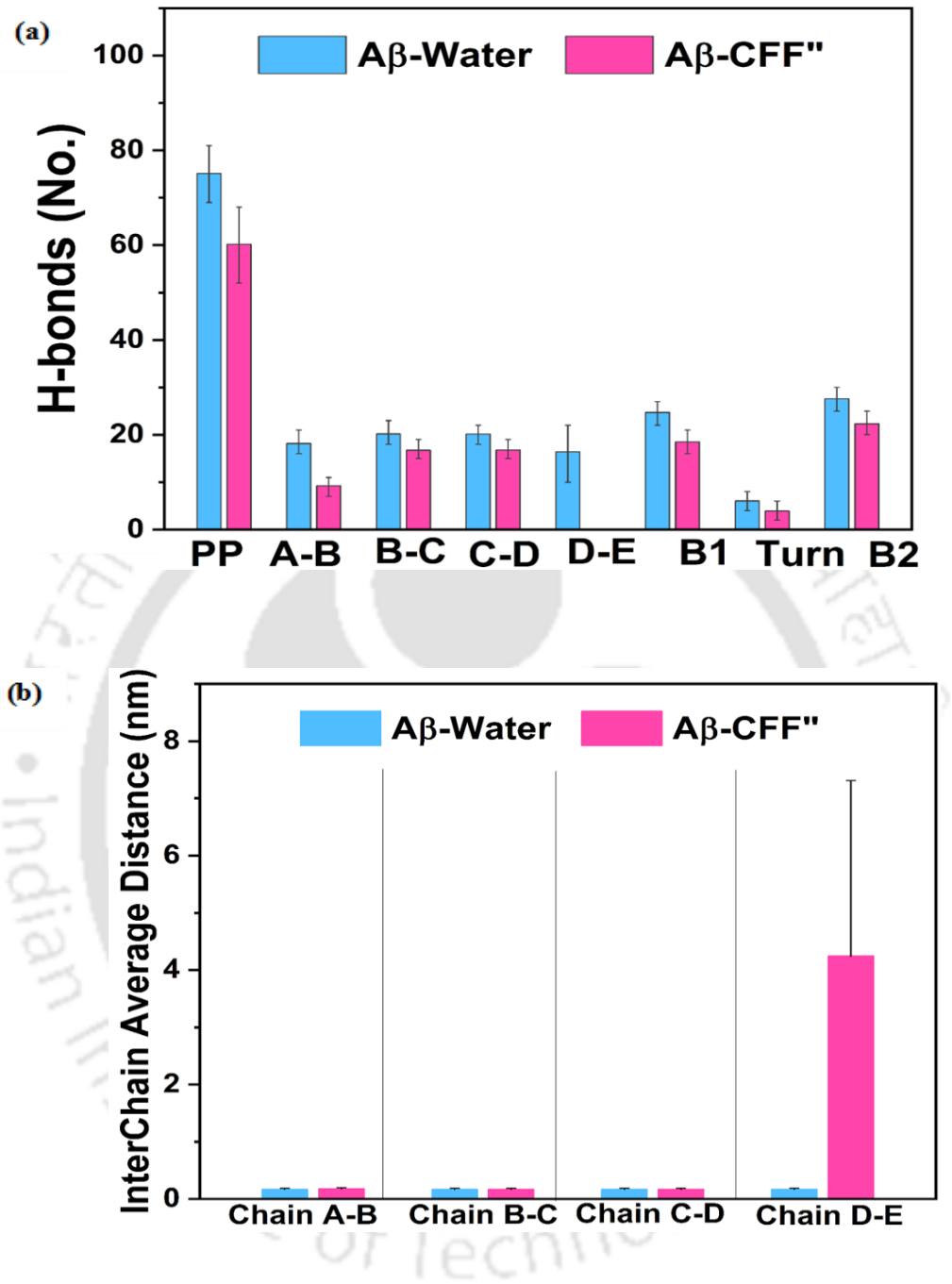

Fig. 8.18. Average numbers of (a) H-bonds and (b) Interchain Distance for Aβ-Water (blue) and Aβ-CFF" (pink) for different pairs. Less Number of H-bonds observed for all the selections indicates loss of integrity of the fibril in Aβ-CFF".

The correlation between zero H-bonds observed for chain D-E and increase in inter-chain distance for the same has led to detachment of chain E from the parent pentamer in Aβ-CFF" system. The same observation for drifting of chain E is well supported by the contact analysis map for Chain D-E in Aβ-CFF" (Fig. 8.19b), wherein no residual contacts has been observed for these terminal chains.

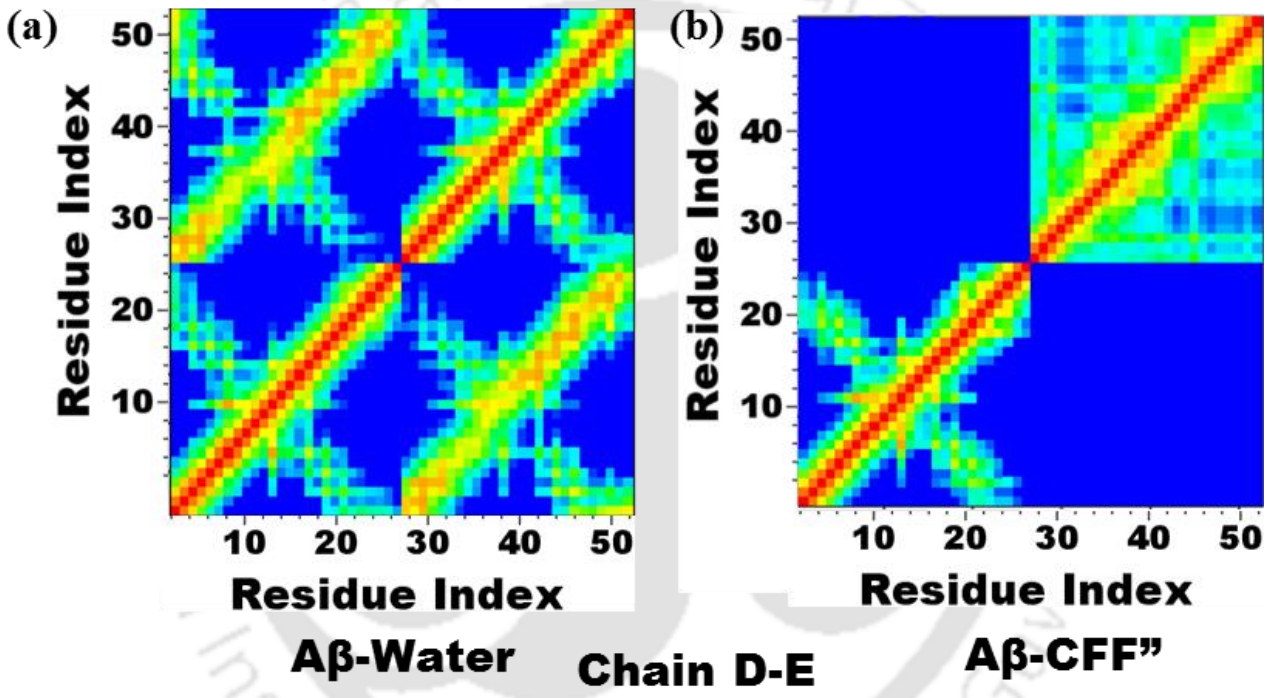

Fig. 8.19. Inter-chain distance matrix for (a) Aβ-Water (left) and (b) Aβ-CFF" (right) for chain D-E. No contacts have been observed for chain D-E in Aβ-CFF" system explains drifting of chain E from the parent pentamer.

The inhibition towards refibrillation of the Aβ fibril is inferred from the loss of β-sheet content from 49% in Aβ-Water to 38% in Aβ-CFF" system (in Fig. 8.20a and 8.20b), is well matched with the observation in Aβ-REF" system.

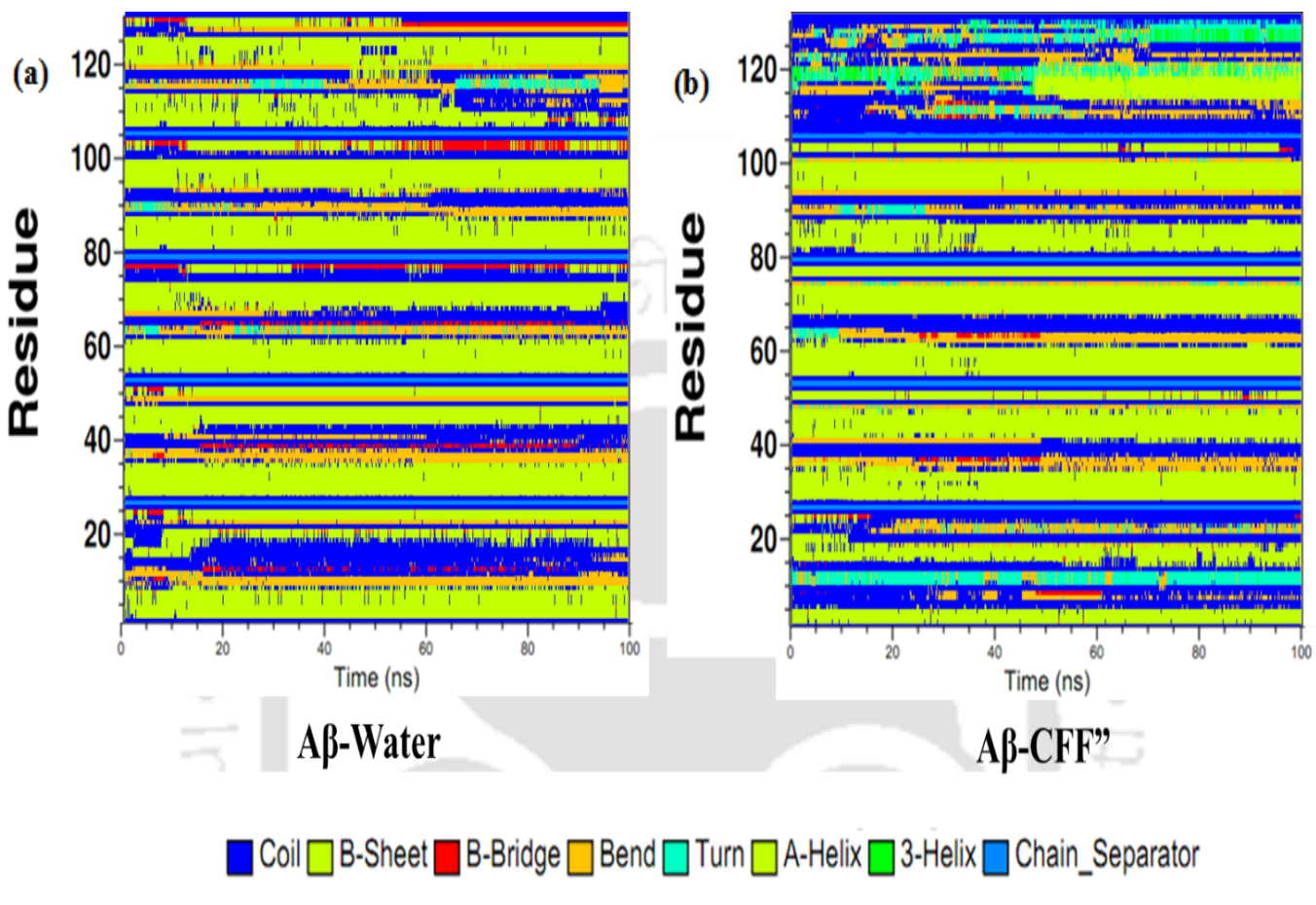

Fig. 8.20. DSSP representation of secondary structures for (a) Aβ-Water and (b) Aβ-CFF”. The lower β-sheet content and higher coil content in Aβ-CFF” indicates destabilization of the fibril in off-pathway aggregates rather than the organized neurotoxic Aβ fibrils in Aβ-Water.

The analysis from this study explains and corroborates well with the current findings of irrevocable and extended destabilization by the removal of the ligand. Interestingly, the current observations, from removal of both the ligands (viz., REF and CFF), points towards the irreversibility of the ligand removal strategy along with independency to the force fields used.

8.4 CONCLUSIONS

The present work intent to determine the stability and integrity of a destabilized Aβ fibril after the ligand or potential drug gets excreted from the system. The MD simulation has been conducted for 1 μs for both Aβ-water and Aβ-REF" systems. The VMD representation depicts drift of the terminal chains from the pentamer and loss of β-sheet conformation in chain A, in Aβ-REF" system. This explains the extent of perturbations observed in the fibril, after ligand removal, which are well explained by increased RMSD, R_g, loss of H-bonds and breaking of various key interactions involving salt bridges and hydrophobic interactions. The high helical and low β-sheet content is believed to be crucial for impedance towards the formation of the native organized state. The higher Gibbs free energy, SASA value in direct relation with the polar solvation energy are found to be the main drivers behind the irreversibility of the misaligned Aβ fibril in Aβ-REF" to its original conformation. The morphological as well as parametric similarity of the disoriented fibril thus obtained, with off-pathway aggregates, ensure inhibition of the formation of higher order fibrils further. The highly misaligned structure obtained in Aβ-REF" system points towards its irreversibility to the native conformation. A similar observation and pattern is expected in Aβ fibril upon interaction with other natural compounds too. More investigations are needed to explore in detail. The combined studies including interaction of Aβ fibril with ligand and subsequent removal of ligand can be used for a comprehensive analysis of the destabilization of the fibril. Our findings would help in understanding the prophecy of the destabilization as a promising therapeutic technique for treating AD.

REFERENCES

1 H. E. Selick, A. P. Beresford and M. H. Tarbit, The emerging importance of predictive ADME simulation in drug discovery, *Drug Discovery Today*, 2002, **7**, 109–116.

2 M. P. Doogue and T. M. Polasek, The ABCD of clinical pharmacokinetics, *Therapeutic Advances in Drug Safety*, 2013, **4**, 5–7.

3 M. H. Omar, W. Mullen, A. Stalmach, C. Auger, J. Rouanet, P. Teissedre, S. T. Caldwell, R. C. Hartley and A. Crozier, Absorption, Disposition, Metabolism, and Excretion of [3- 14 C]Caffeic Acid in Rats, *Journal of Agricultural and Food Chemistry*, 2012, **60**, 5205–5214.

4 J. C. Espín, M. Larrosa, M. T. García-Conesa and F. Tomás-Barberán, Biological Significance of Urolithins, the Gut Microbial Ellagic Acid-Derived Metabolites: The Evidence So Far, *Evidence-Based Complementary and Alternative Medicine*, 2013, **2013**, 1–15.

5 M. S. Dutta and S. Basu, Identifying the key residues instrumental in imparting stability to amyloid beta protofibrils – a comparative study using MD simulations of 17–42 residues, *Journal of Biomolecular Structure and Dynamics*, 2021, **39**, 431–456.

6 W. Kim and M. H. Hecht, Generic hydrophobic residues are sufficient to promote aggregation of the Alzheimer's Abeta42 peptide, *Proceedings of the National Academy of Sciences*, 2006, **103**, 15824–15829.

7 J. Nasica-Labouze, P. H. Nguyen, F. Sterpone, O. Berthoumieu, N.-V. Buchete, S. Coté, A. De Simone, A. J. Doig, P. Faller, A. Garcia, A. Laio, M. S. Li, S. Melchionna, N. Mousseau, Y. Mu, A. Paravastu, S. Pasquali, D. J. Rosenman, B. Strodel, B. Tarus, J. H. Viles, T. Zhang, C. Wang and P. Derreumaux, Amyloid β Protein and Alzheimer's Disease: When Computer Simulations Complement Experimental Studies, *Chemical Reviews*, 2015, **115**, 3518–3563.

8 S. Gupta and A. K. Dasmahapatra, Destabilization potential of phenolics on Aβ fibrils: mechanistic insights from molecular dynamics simulation, *Physical Chemistry Chemical Physics*, 2020, **22**, 19643–19658.

9 D. Van Der Spoel, E. Lindahl, B. Hess, G. Groenhof, A. E. Mark and H. J. C. Berendsen, *Journal of Computational Chemistry*, 2005, 26, 1701–1718.

10 C. Oostenbrink, A. Villa, A. E. Mark and W. F. Van Gunsteren, A biomolecular force field based on the free enthalpy of hydration and solvation: The GROMOS force-field parameter sets 53A5 and 53A6, *Journal of Computational Chemistry*, 2004, **25**, 1656–1676.

11 W. Huang, Z. Lin and W. F. Van Gunsteren, Validation of the GROMOS 54A7 force field with respect to β-peptide folding, *Journal of Chemical Theory and Computation*, 2011, **7**, 1237–1243.

12 A. K. Somavarapu and K. P. Kepp, The Dependence of Amyloid-β Dynamics on Protein Force Fields and Water Models, *ChemPhysChem*, 2015, **16**, 3278–3289.

13 H. J. C. Berendsen, J. R. Grigera and T. P. Straatsma, The missing term in effective pair potentials, *Journal of Physical Chemistry*, 1987, **91**, 6269–6271.

14 W. Humphrey, A. Dalke and K. Schulten, VMD: Visual molecular dynamics, *Journal of Molecular Graphics*, 1996, **14**, 33–38.

15 W. Humphrey, A. Dalke and K. Schulten, VMD: visual molecular dynamics., *Journal of molecular graphics*, 1996, **14**, 33–8, 27–8.

16 H. Gohlke, C. Kiel and D. A. Case, Insights into protein-protein binding by binding free energy calculation and free energy decomposition for the Ras-Raf and Ras-RalGDS complexes., *Journal of molecular biology*, 2003, **330**, 891–913.

17 N. Homeyer and H. Gohlke, Free energy calculations by the Molecular Mechanics Poisson-Boltzmann Surface Area method, *Molecular Informatics*, 2012, **31**, 114–122.

18 S. Genheden and U. Ryde, The MM/PBSA and MM/GBSA methods to estimate ligand-binding affinities, *Expert Opinion on Drug Discovery*, 2015, **10**, 449–461.

19 Y. Zou, Z. Qian, Y. Chen, H. Qian, G. Wei and Q. Zhang, Norepinephrine Inhibits Alzheimer's Amyloid-β Peptide Aggregation and Destabilizes Amyloid-β Protofibrils: A Molecular Dynamics Simulation Study, *ACS Chemical Neuroscience*, 2019, **10**, 1585–1594.

20 P. K. Kanchi and A. K. Dasmahapatra, Polyproline chains destabilize the Alzheimer's amyloid-β protofibrils: A molecular dynamics simulation study, *Journal of Molecular Graphics and Modelling*, 2019, **93**, 107456.

21 A. Kaur, S. Shuaib, D. Goyal and B. Goyal, Interactions of a multifunctional di-triazole derivative with Alzheimer's Aβ 42 monomer and Aβ 42 protofibril: a systematic molecular dynamics study, *Physical Chemistry Chemical Physics*, 2020, **22**, 1543–1556.

22 P. K. Kanchi and A. K. Dasmahapatra, Enhancing the binding of the β-sheet breaker peptide LPFFD to the amyloid-β fibrils by aromatic modifications: A molecular dynamics simulation study, *Computational Biology and Chemistry*, 2021, **92**, 107471.

23 D. E. Ehrnhoefer, J. Bieschke, A. Boeddrich, M. Herbst, L. Masino, R. Lurz, S. Engemann, A. Pastore and E. E. Wanker, EGCG redirects amyloidogenic polypeptides into unstructured, off-pathway oligomers, *Nature Structural & Molecular Biology*, 2008, **15**, 558–566.

24 K. Röder and D. J. Wales, Energy Landscapes for the Aggregation of Aβ 17–42, *Journal of the American Chemical Society*, 2018, **140**, 4018–4027.

25 S. Gupta and A. K. Dasmahapatra, Destabilization of Aβ fibrils by omega-3 polyunsaturated fatty acids: a molecular dynamics study, *Journal of Biomolecular Structure and Dynamics*, 2021, **0**, 1–18.

26 W. M. Berhanu and U. H. E. Hansmann, Side-chain hydrophobicity and the stability of Aβ 16-22 aggregates, *Protein Science*, 2012, **21**, 1837–1848.

27 S. A. Gargari and A. Barzegar, Simulations on the dual effects of flavonoids as suppressors of Aβ42 fibrillogenesis and destabilizers of mature fibrils, *Scientific Reports*, 2020, **10**, 16636.

28 W. Kabsch and C. Sander, Dictionary of protein secondary structure: Pattern recognition of hydrogen-bonded and geometrical features, *Biopolymers*, 1983, **22**, 2577–2637.

29 R. K. Saini, S. Shuaib and B. Goyal, Molecular insights into Aβ 42 protofibril destabilization with a fluorinated compound D744: A molecular dynamics simulation study, *Journal of Molecular Recognition*, 2017, **30**, e2656.

30 Y. Zou, Z. Qian, Y. Chen, H. Qian, G. Wei and Q. Zhang, Norepinephrine Inhibits Alzheimer's Amyloid-β Peptide Aggregation and Destabilizes Amyloid-β Protofibrils: A Molecular Dynamics Simulation Study, *ACS Chemical Neuroscience*, 2019, **10**, 1585–1594.

31 E. Bramanti, L. Fulgentini, R. Bizzarri, F. Lenci and A. Sgarbossa, B-Amyloid Amorphous Aggregates Induced By the Small Natural Molecule Ferulic Acid, *Journal of Physical Chemistry B*, 2013, **117**, 13816–13821.

32 J. Zheng, H. Jang, B. Ma, C.-J. Tsai and R. Nussinov, Modeling the Alzheimer Aβ17-42 Fibril Architecture: Tight Intermolecular Sheet-Sheet Association and Intramolecular Hydrated Cavities, *Biophysical Journal*, 2007, **93**, 3046–3057.

33 M. Sunde, L. C. Serpell, M. Bartlam, P. E. Fraser, M. B. Pepys and C. C. Blake, Common core structure of amyloid fibrils by synchrotron X-ray diffraction., *Journal of molecular biology*, 1997, **273**, 729–39.

34 H.-M. Fan, R.-X. Gu, Y.-J. Wang, Y.-L. Pi, Y.-H. Zhang, Q. Xu and D.-Q. Wei, Destabilization of Alzheimer's Aβ42 Protofibrils with a Novel Drug Candidate wgx-50 by Molecular Dynamics Simulations, *The Journal of Physical Chemistry B*, 2015, **119**, 11196–11202.

35 S. Gupta and A. K. Dasmahapatra, Caffeine destabilizes preformed Aβ protofilaments: insights from all atom molecular dynamics simulations, *Physical Chemistry Chemical Physics*, 2019, **21**, 22067–22080.

36 J. E. Donald, D. W. Kulp and W. F. DeGrado, Salt bridges: Geometrically specific, designable interactions, *Proteins: Structure, Function and Bioinformatics*, 2011, **79**, 898–915.

37 B. Musafia, V. Buchner and D. Arad, Complex salt bridges in proteins: Statistical analysis of structure and function, *Journal of Molecular Biology*, 1995, **254**, 761–770.

38 X. Ban, P. Lahiri, A. S. Dhoble, D. Li, Z. Gu, C. Li, L. Cheng, Y. Hong, Z. Li and B. Kaustubh, Evolutionary Stability of Salt Bridges Hints Its Contribution to Stability of Proteins, *Computational and Structural Biotechnology Journal*, 2019, **17**, 895–903.

39 D. Q. H. Pham, M. S. Li and G. La Penna, Copper Binding Induces Polymorphism in Amyloid-β Peptide: Results of Computational Models, *Journal of Physical Chemistry B*, 2018, **122**, 7243–7252.

40 S. A. Andujar, F. Lugli, S. Höfinger, R. D. Enriz and F. Zerbetto, Amyloid-β fibril disruption by C 60 - Molecular guidance for rational drug design, *Physical Chemistry Chemical Physics*, 2012, **14**, 8599–8607.

41 A. Verma, A. Kumar and M. Debnath, Molecular docking and simulation studies to give insight of surfactin amyloid interaction for destabilizing Alzheimer's Aβ42 protofibrils, *Medicinal Chemistry Research*, 2016, **25**, 1616–1622.

42 V. Jani, U. Sonavane and R. Joshi, Destabilization potential of beta sheet breaker peptides on Abeta fibril structure: an insight from molecular dynamics simulation study, *RSC Advances*, 2021, **11**, 23557–23573.

43 C. N. Pace, H. Fu, K. L. Fryar, J. Landua, S. R. Trevino, B. A. Shirley, M. M. Hendricks, S. Iimura, K. Gajiwala, J. M. Scholtz and G. R. Grimsley, Contribution of Hydrophobic Interactions to Protein Stability, *Journal of Molecular Biology*, 2011, **408**, 514–528.

44 B. Tarus, J. E. Straub and D. Thirumalai, Dynamics of Asp23−Lys28 Salt-Bridge Formation in Aβ 10-35 Monomers, *Journal of the American Chemical Society*, 2006, **128**, 16159–16168.

45 T. Lührs, C. Ritter, M. Adrian, D. Riek-Loher, B. Bohrmann, H. Döbeli, D. Schubert and R. Riek, 3D structure of Alzheimer's amyloid-β(1–42) fibrils, *Proceedings of the National Academy of Sciences*, 2005, **102**, 17342–17347.

46 Y. Gong, C. Zhan, Y. Zou, Z. Qian, G. Wei and Q. Zhang, Serotonin and Melatonin Show Different Modes of Action on Aβ 42 Protofibril Destabilization, *ACS Chemical Neuroscience*, 2021, **12**, 799–809.

47 G. G. Maisuradze, A. Liwo and H. A. Scheraga, Relation between Free Energy Landscapes of Proteins and Dynamics, *Journal of Chemical Theory and Computation*, 2010, **6**, 583–595.

48 Q. Wang, J. Guo, P. Jiao, H. Liu and X. Yao, Exploring the Influence of EGCG on the β-

Sheet-Rich Oligomers of Human Islet Amyloid Polypeptide (hIAPP1–37) and Identifying Its Possible Binding Sites from Molecular Dynamics Simulation, *PLoS ONE*, 2014, **9**, e94796.

49 S. P., T. K. D., G. P. D. C., S. R. and H. Zayed, Determining the role of missense mutations in the POU domain of HNF1A that reduce the DNA-binding affinity: A computational approach, *PLOS ONE*, 2017, **12**, e0174953.

50 R. K. Saini, S. Shuaib, D. Goyal and B. Goyal, Insights into the inhibitory mechanism of a resveratrol and clioquinol hybrid against Aβ 42 aggregation and protofibril destabilization: A molecular dynamics simulation study, *Journal of Biomolecular Structure and Dynamics*, 2019, **37**, 3183–3197.

51 M. Karami, C. Jalali and S. Mirzaie, Combined virtual screening, MMPBSA, molecular docking and dynamics studies against deadly anthrax: An in silico effort to inhibit Bacillus anthracis nucleoside hydrolase, *Journal of Theoretical Biology*, 2017, **420**, 180–189.

52 A. Kumar, R. Saranathan, K. Prashanth, B. K. Tiwary and R. Krishna, Inhibition of the MurA enzyme in Fusobacterium nucleatum by potential inhibitors identified through computational and in vitro approaches, *Molecular BioSystems*, 2017, **13**, 939–954.

53 A. D. Williams, S. Shivaprasad and R. Wetzel, Alanine Scanning Mutagenesis of Aβ(1-40) Amyloid Fibril Stability, *Journal of Molecular Biology*, 2006, **357**, 1283–1294.

54 P. D. Q. Huy, N. Q. Thai, Z. Bednarikova, L. H. Phuc, H. Q. Linh, Z. Gazova and M. S. Li, Bexarotene Does Not Clear Amyloid Beta Plaques but Delays Fibril Growth: Molecular Mechanisms, *ACS Chemical Neuroscience*, 2017, **8**, 1960–1969.

Chapter 9

Conclusions and Future Scopes

This chapter presents a summary of the entire thesis with a discussion on the future scope for possible treatment for AD.

9.1 Conclusions

Alzheimer's disease (AD), a progressive, geriatric and neurodegenerative disorder associated with dementia is an unsolved mystery for global healthcare system. Varied drugs and therapies have been suggested targeting this multi-faceted disease from various directions, such as, inhibition of aggregation of Aβ monomers, and destabilization of the Aβ fibrils. The skepticism about the root cause and mechanism of progression is also one of the major reasons for such delay in any cure. The inefficacy and failure of numerous drugs in the clinical trial proposed for AD till date has raised more concerns, and triggered need to explore different therapeutic approaches.

To address the above-mentioned issue, destabilization of the preformed Aβ senile plaques is proposed to be one of the new yet promising therapeutic choice. Therefore, the present work is intended to investigate the feasibility, efficacy and associated mechanism of destabilization of the preformed neurotoxic Aβ fibrils by various natural compounds. The natural compounds were selected due to their inherent biocompatibility and natural non-toxicity for the human beings. In the current study different natural compounds from various categories viz. Caffeine from alkaloids, Ellagic acid from phenolics, Eicosapentanoic acid and Hexadecanoic acid from omega-3 fatty

acids, Lycopene from terpenes has been prospected for their destabilization potential by Molecular Dynamics (MD) Simulation. All these compounds are selected based on certain advantages linked with them, such as, native capability to cross blood brain barrier (BBB), antioxidant properties, established role in neuroprotection and other health benefits. The assessment has been done by determining various parameters such as, RMSD, R_g, RMSF, SASA, number of H-bonds and secondary structure conformation. Moreover, the refibrillation possibility or stability of the destabilized structure of Aβ fibril (obtained after interaction with these ligands) have also been tested further by removing the ligand (ellagic acid and caffeine) and thereafter conducting lengthy MD simulation (1 μs). All these studies have been discussed in detailed from chapter 4 to chapter 8 in the thesis which is summarized below:

- **Chapter 4** gave mechanistic details on the interaction of caffeine (CFF) with preformed Aβ fibril wherein the destabilization of the fibril is observed. The reduction of β-sheet content and loss of H-bonds were found to be the main drivers behind destabilization of the Aβ fibril upon caffeine introduction.

- **Chapter 5** has screened four major polyphenols from plants by docking and studied by MD simulation for their destabilization potential. The outcome of the study revealed ellagic acid (REF) to be the best binder and destabilizer of Aβ fibril, wherein it binds to chain A of the fibril by accessing fibrillar cavity.

- **Chapter 6** compared the significant role of three major Omega -3 fatty acids and reported Eicosapentaenoic acid (EPA) and Docosahexaenoic acid (HXA) as potential destabilizers of the Aβ fibril. The crucial role of EPA and HXA in maintaining brain integrity and destabilization potential on Aβ fibril, makes them a suitable drug candidate for treating AD. The amphiphilic nature of fatty acids was found to be the supportive for the better

binding with the fibril, wherein polar head binds to K28 (positively charged residue) and long carbon tail to the hydrophobic residues of the fibril. This brings efficient destabilization by compromising the inherent hydrophobic interactions coupled with loss of β-sheet content.

- **Chapter 7** gave detailed analysis of lycopene (LYC), a carotenoid, belonging to terpenes (largest class of secondary plant metabolites) as a potential destabilizer of different polymorphic form of Aβ fibril. It was found to interact with the surface and cavity depending on the architecture of the fibril.

- **Chapter 8** gave insights on the fate of the destabilized fibril upon removal of the ligand. This study highlights the enhancement of the destabilized structure upon removal of the ligand (REF and CFF in this case), thereby inhibiting the refibrillation. This ensures the non-neurotoxicity and irreversibility of the deformed fibril, establishing destabilization as the promising therapeutic technique for AD. This establishes the efficacy and prophecy of destabilization of preformed Aβ fibril as a promising therapeutic approach for treating AD.

Collectively, the loss of H-bonds, breakage of salt-bridges and other key hydrophobic interactions in the fibril, upon l introduction of these natural compounds, were found to be the governing factors behind destabilization of the fibril. The collapse of highly organized structure due to the loss of β-sheet content indicates disorganization of the Aβ fibril. The access to the fibrillar cavity or interacting via the surface depend on the ligand and the architecture of the polymorph of Aβ fibril.

The important cues and findings obtained in this thesis provide a fair idea about the potency of these natural ligands towards the destabilization of the Aβ fibril as studied by MD simulation. The destabilization by natural compounds is proposed to be the best alternative therapeutic approach to treat AD which requires urgent attention from the scientific community. The exploration of various natural compounds studied by MD simulation and other advanced tools coupled with *in-vitro* and *in-vivo* studies can be useful in unveiling the mystery behind AD in near future.

9.2 Future Scope of the Research

The present work establishes the promising role of natural compounds as potential destabilizers of Aβ fibril. However, there are many future possibilities associated with the current work that are given below.

- **Formulation of a better ligand**: By combining various information on structural and molecular descriptors, a new ligand having all the qualities of these ligands can be formulated and tested. This entails the preparation of a potential ligand by structure based drug discovery approach (using a fragment) that further ensures better targeting to Aβ fibril.[1,2]

- **Newer MD simulation Tools:** The enhanced sampling of the possible configurations of the Aβ fibril and ligand can be done by metadynamics and REMD (replica exchange molecular dynamics).[3,4] The use of quantum calculations for understanding the mechanistic details about protein-ligand interactions can further be coupled.

- **Assessment of affinity and entropy for protein-ligand binding:** The binding affinity explains the role and pattern of interaction between the protein and ligand. This can be assessed well by quantum calculations and other FEP (Free Energy Perturbations) methods that can address issue of entropy calculations as well.[5] The crux of the developing any drug is based on the insights involved in protein-ligand interaction, which is a future avenue of this thesis. More insights on the best pose, the energy calculation, entropic calculations, quantitative contribution towards binding from each residue and effect of functionalization can be studied by *in-silico* methods.

- **Use of AI and ML:** AI (Artificial Intelligence) and ML (Machine Learning) tools for employing drug discovery and drug repurposing for AD can address questions for present and future in a comprehensive way.[6–10]

- ***In-vitro* and *in-vivo* investigations:** The current findings on destabilization of Aβ fibril driven by natural compounds based on MD simulation, needs further investigations by *in-vitro* and *in-vivo* methods for therapeutic treatment of AD.[11,12]

All these approaches collectively enhance the possibility of the clearance of the drug lead compound in clinical trials so as to formulate a promising treatment towards AD. The common goal is to have a responsive and efficient drug to treat AD in the near future.

REFERENCES

(1) Hajduk, P. J.; Greer, J. A Decade of Fragment-Based Drug Design: Strategic Advances and Lessons Learned. *Nature Reviews Drug Discovery* **2007**, *6* (3), 211–219.

(2) Colman, P. M. Structure-Based Drug Design. *Current Opinion in Structural Biology* **1994**, *4* (6), 868–874.

(3) Luitz, M. P.; Zacharias, M. Protein–Ligand Docking Using Hamiltonian Replica Exchange Simulations with Soft Core Potentials. *Journal of Chemical Information and Modeling* **2014**, *54* (6), 1669–1675.

(4) Wang, J.; Peng, C.; Yu, Y.; Chen, Z.; Xu, Z.; Cai, T.; Shao, Q.; Shi, J.; Zhu, W. Exploring Conformational Change of Adenylate Kinase by Replica Exchange Molecular Dynamic Simulation. *Biophysical Journal* **2020**, *118* (5), 1009–1018.

(5) Ryde, U.; Söderhjelm, P. Ligand-Binding Affinity Estimates Supported by Quantum-Mechanical Methods. *Chemical Reviews* **2016**, *116* (9), 5520–5566.

(6) Paul, D.; Sanap, G.; Shenoy, S.; Kalyane, D.; Kalia, K.; Tekade, R. K. Artificial Intelligence in Drug Discovery and Development. *Drug Discovery Today* **2021**, *26* (1), 80–93.

(7) Chan, H. C. S.; Shan, H.; Dahoun, T.; Vogel, H.; Yuan, S. Advancing Drug Discovery via Artificial Intelligence. *Trends in Pharmacological Sciences* **2019**, *40* (8), 592–604.

(8) Li, Z.; Jiang, X.; Wang, Y.; Kim, Y. Applied Machine Learning in Alzheimer's Disease Research: Omics, Imaging, and Clinical Data. *Emerging Topics in Life Sciences* **2021**, *5* (6), 765–777.

(9) Priyadharsini, M.; Sugantha Mallika, S. S.; Karuppasamy, K.; R, S. Drug Discovery for Alzheimer's Disease Using Machine Learning. In *2022 8th International Conference on Advanced Computing and Communication Systems (ICACCS)*; IEEE, 2022; pp 787–792.

(10) Lavecchia, A. Deep Learning in Drug Discovery: Opportunities, Challenges and Future Prospects. *Drug Discovery Today* **2019**, *24* (10), 2017–2032.

(11) Barai, P.; Raval, N.; Acharya, S.; Borisa, A.; Bhatt, H.; Acharya, N. Neuroprotective Effects of Bergenin in Alzheimer's Disease: Investigation through Molecular Docking, in Vitro and in Vivo Studies. *Behavioural Brain Research* **2019**, *356* (May 2018), 18–40.

(12) Li, H.; Wang, X.; Yu, H.; Zhu, J.; Jin, H.; Wang, A.; Yang, Z. Combining in Vitro and in Silico Approaches to Find New Candidate Drugs Targeting the Pathological Proteins Related to the Alzheimer's Disease. *Current Neuropharmacology* **2018**, *16* (6), 758–768.

APPENDIX A

MD Simulation Steps

The MD simulation workflow has been mentioned in methodology section as general scheme in section 3.3 of Chapter 3 (Methodology). Also, the details about the sequential process has been discussed in section 4.2.2 of Chapter 4. However, the commands that are required to execute steps in MD for protein (pro)-ligand (lig) interaction are missing, and henceforth given here. All the commands have been demarcated with a dollar sign (`$`) but the execution needs to be done without the sign. The general notation for all commands is -f means the input file, -o signifies the output file, -v stands for verbose and -s implies the supporting file or the trajectory obtained after the simulation. All the commands have been highlighted in grey colour.

Obtaining topology: The -ignh flag ignore H atoms in the PDB file; especially useful for NMR structures.

```
$ gmx_mpi pdb2gmx -f pro.pdb -ignh -o pro_processed.gro
```

Select Gromos96 53a7 from the list. After combining coordinates of the ligand, modify topol.top with the following.

Adding ligand topology:

; include Ligand topology

#include "lig.itp"

Boxing: In the command below -c centers the protein in the box and places it at least 2.0 nm from the box edge (-d 2.0). The box type is defined as a cube (-bt cubic).

```
$ gmx_mpi editconf -f conf.gro -o newbox.gro -c -bt cubic -d 2.0
```

Solvation: Herein, the -cp and -cs contains the configuration for protein and solvent respectively. The -p flag process and update the topology file called topol.top with number of solvent molecules added to the protein.

```
$ gmx_mpi solvate -cp newbox.gro -cs spc216.gro -p topol.top -o solv.gro
```

Neutralizing the system: -p is for processing and updating the topology file (topol.top), -np is the number of positive ions and -pname is for the name of the positive ion, NA stands for sodium and -s reads the input file for structure of ions.tpr.

```
$ gmx_mpi grompp -f ions.mdp -c solv.gro -p topol.top -o ions.tpr

$ gmx_mpi genion -s ions.tpr -o ions.gro -p topol.top -pname NA -np 5
```

Energy Minimization:

```
$ gmx_mpi grompp -f minim.mdp -c ions.gro -p topol.top -o em.tpr

$ gmx_mpi mdrun -v -deffnm em &

$ gmx_mpi energy -f em.edr -o potential.xvg
```

Making the index groups:

```
$ gmx_mpi make_ndx -f em.gro -o index.ndx (select protein and
ligand)
```

NVT Equilibration: Where -n reads index file and takes it as an intput.

```
$ gmx_mpi grompp -f nvt.mdp -c em.gro -p topol.top -n index.ndx -
o nvt.tpr

$ gmx_mpi mdrun -deffnm nvt -v &

$ gmx_mpi energy -f nvt.edr -o temperature.xvg
```

NPT Equilibration: The -t flag here is used to include the checkpoint file from the NVT equilibration; this file contains all the necessary state variables to continue the simulation. To conserve the velocities produced during NVT, this fie must be included.

```
$ gmx_mpi grompp -f npt.mdp -c nvt.gro -t nvt.cpt -p topol.top -n
index.ndx -o npt.tpr

$ gmx_mpi mdrun -v -deffnm npt &

$ gmx_mpi energy -f npt.edr -o pressure.xvg

$ gmx_mpi energy -f npt.edr -o density.xvg
```

The average value over the course of 100 ps is 1019 ± 3 kg m^{-3}, close to the experimental value of 1000 kg m^{-3} and the expected density of the SPC/E model of 1008 kg m^{-3}. The parameters for the SPC/E water model closely replicate experimental values for water. If the density values are very

stable over time, indicating that the system is well-equilibrated now with respect to pressure and density. This further can be submitted for final production run step.

Production run: & flag helps in running the simulation in the background, -deffnm Set the default filename for all output file options, like creates all the files with md_0_1 followed by extension and -nb selects GPU if available.

```
$ gmx_mpi grompp -f md.mdp -c npt.gro -t npt.cpt -p topol.top -o
md_0_1.tpr

$ gmx_mpi mdrun -deffnm md_0_1 -nb gpu &
```

Analysis of the Simulated Trajectory

There have been various tools that are used during MD simulation and analysis of the obtained trajectory (md_0_1.xtc). The various parameters were calculated for different selection groups to gauge destabilization potential of Aβ fibril in presence of different natural compounds.

A. Gromacs Tools

RMSD – The root mean square deviation has been calculated from the obtained trajectory. This tool helps in measuring the distance between different chains of the fibril. The -tu flag helps in selecting the time frames for evaluation i.e. fs/ ps/ ns/ us/ ms/ s.

```
$ gmx_mpi rms -s md_0_1.tpr -f md_0_1.xtc -o rmsdpro.xvg -tu ns
```

1. **RMSF** – The root mean square fluctuation has been calculated for protein from the obtained trajectory. The tool explains the fluctuations around various residues of the protein chains that explains their deviation from the parent fibril structure. The -res flag gives the output residue wise.

   ```
   $ gmx_mpi rmsf -s md_0_1.tpr -f md_0_1.xtc -res -o rmsfpro.xvg
   ```

2. **Radius of Gyration (R_g) -** This tool helps in measuring the compactness of the fibrillar structure. It is calculated by the following command.

   ```
   $ gmx_mpi gyrate -s md_0_1.tpr -f md_0_1.xtc -o gyratepro.xvg
   ```

3. **SASA –** This helps in measuring the solvent accessible surface area that helps in gauging the area that is able to interact with the water around the fibrillar structure. -or gives output residue wise.

   ```
   $ gmx_mpi sasa -s md_0_1.tpr -f md_0_1.xtc -or ressas.xvg
   ```

4. **H-Bonds –** The hydrogen bonds provides stability to the fibrillar structure. This is between different residues of the single chain and other chains too. The -num flag calculates the average number of H-bonds.

   ```
   $ gmx_mpi hbond -s md_0_1.tpr -f md_0_1.xtc -num hnumpp.xvg
   ```

5. **Minimum Distance between two residues –** This tool is used to calculate the minimum distance between different bonded residues that are important for stability of the fibrillar

structure. The tool is g_mindist that measures all kind of inter and intra interactions. The -od flag gives distance value.

```
$ gmx_mpi mindist -s md_0_1.tpr -f md_0_1.xtc -od file.xvg -tu ns
```

The different residues can be chosen by making an index file by-

```
$ gmx_mpi make_ndx -f em.gro -o index.ndx
```

selecting D23 (chain A) and K28 (chain B) and then average minimum distance between these two residues can be calculated by following command.

```
$ gmx_mpi mindist -f md_0_1_nojump.xtc -s md_0_1.tpr -n index.ndx -od D23-K28chainA-B.xvg -tu ns
```

6. **Secondary Structure by DSSP:** The secondary structure configuration has been defined by installing the dssp tool and setting its environment in the working directory of the gromacs by the following commands executed sequentially. -ver is for the version, -ssdump gives the generic data file, -sc gives scount.xvg that has information on secondary structures in %, -ta gives total area.

```
$ export DSSP=/home/path of working directory/dssp
```

```
$ chmod +x dssp
```

```
$ gmx_mpi do_dssp -f md_0_1.trr -s md_0_1.tpr -o dssp.xpm -tu ns -ver 2 -ssdump dssp.dat -sc scount.xvg -a map.xpm -ta totarea.xvg
```

The conversion of xpm (x-windows pixel maps) thus obtained, can be converted to eps (encapsulated script) by ps.m2p file containing all the information on axis and graph. The -di flag takes this as input and merge with -f (input file) and gives output (dssp.eps). With the -rainbow option, dull grayscale matrices can be turned into attractive color pictures in red or blue background as selected.

```
$ gmx_mpi xpm2ps -f dssp.xpm -o dssp.eps -by 2.5 -di ps.m2p
-rainbow red

$ ps2pdf dssp.eps dssp.pdf
```

7. **Free Energy Landscape:** The FEL represents a mapping of all possible conformations a molecule adopted during a simulation, together with their corresponding energy typically reported as the Gibbs Free Energy. FEL are represented using two variables that reflect specific properties of the system and measure conformational variability. When FEL is represented in three dimensions, the landscape shows 'valleys' of low free-energy, which represent metastable conformational states of the system, and 'hills' that account for the energetic barriers that connect these states. A perl file is given to merge two .xvg files for two different values called as principal component analysis (PCA) in this case. The following commands needs sequential execution in the working directory. The sham.pl file is freely available on GITHUB and can be downloaded from there. The -i1and -i2 stands for 1st and 2nd input files which is rmsdalpha and h-bonds value in this case. The -ls flag is applied to obtain X PixMap compatible matrix file.

```
$ perl sham.pl -i1 rmsdcalphapro.xvg -i2 hnumpp.xvg -data1 1
-data2 1 -o gsham_input.xvg

$ gmx_mpi sham -f gsham_input.xvg -ls fel.xpm

$ gmx_mpi xpm2ps -f fel.xpm -o fel.eps -rainbow red

$ ps2pdf fel.eps fel.pdf
```

Now create a python file to get a free-energy-landscape.txt file for plotting a 3D graph by the data thus obtained in origin further.

```
$ python xpm2txt.py -f fel.xpm -o fel.txt
```

B. Binding Energy Calculation by MM-PBSA

This tool has been used in Chapter 5,6 and 8 to evaluate the binding energetics of phenolic compounds with Aβ fibril we have used MM-PBSA tool which is set inside GROMACS environment. The binding free energy (BFE) of the Aβ oligomer with the selected phenolic compounds was calculated by MM-PBSA (Molecular Mechanics Poisson-Boltzmann Surface Area method).[34–36] The calculation of BFE in the present study was done on the last 20 ns trajectory with Δt = 100 ps by cutting the trajectory for selected frames. This is done by -b and -e flag which selects the time of the first and last frame to be read from the trajectory. The -skip flag skips the frames and write nth frames to the output. In case of 100 ns simulation the following command can be used:

```
$ gmx_mpi trjconv -f obatined.xtc -o new.xtc -s obtained.tpr -b 81
-e 100 -tu ns -skip 100
```

The package was used within the gromacs environment by g_mmpbsa tool, which calculated the overall binding energy and individual residue contribution.[37] MM-PBSA calculates the BFE from the MD trajectory based on the following equation:

$$\Delta G^{bind} = \Delta E_{MM} + \Delta G^{psolv} + \Delta G^{npsolv} - T\Delta S$$

where,$\Delta E_{MM}$is the molecular mechanics contribution in vacuum $\Delta G^{psolv}$is the polar contribution of solvation energy, calculated by the Poisson-Boltzmann equation; $\Delta G^{npsolv}$is the nonpolar contribution towards binding and is determined by solvent accessible surface area (SASA) model. The high computational demand limits the calculation of entropy contribution. In addition, the relative change in entropy contribution (ΔS) towards free energy calculation is negligible and thus can be ignored.[38] The tool calculates the energy from the new cut trajectory for both protein-protein (PP) and protein-ligand (PL) combination. Here -mm stands for molecular mechanic file, -mmcon gives contribution of MM energy file, -i takes the input parameter file.

```
$ g_mmpbsa -f mmpbsa.xtc -s obtained.tpr -n index.ndx -mme -mm
energy_MM.xvg -decomp -mmcon contrib_MM.dat
```

```
$ g_mmpbsa -f mmpbsa.xtc -s obtained.tpr -i mmpbsapol.mdp -n
index.ndx -nomme -pbsa -decomp -pol polar.xvg -pcon
contrib_pol.dat
```

```
$ g_mmpbsa -f mmpbsa.xtc -s md_0_1.tpr -i mmpbsa.mdp -n index.ndx
-nomme -pbsa -decomp -apol apolar.xvg -apcon contrib_apol.dat
```

All the related .mdp (parameter) files can be found in the tutorial (https://rashmikumari.github.io/g_mmpbsa/) which are user specific. The solute and solvent dielectric constants were taken as 4 and 80, respectively. The energetic contribution of individual residue was also quantified to identify key residues actively involved in binding with the phenolic compound by the following energy2bfac tool. Here -i gives the output file.

```
$ energy2bfac -s obtained.tpr -i energyMapIn.dat
```

This tool helps in comparing the binding free energy between different ligands to select the best binder. Further it helps in finding the contribution of individual residues of Aβ fibril in binding to the ligand.

List of Publications

Publications in peer-reviewed journals:

1. **S. Gupta**, A.K. Dasmahapatra, Caffeine destabilizes preformed Aβ protofilaments: insights from all-atom molecular dynamics simulations, Physical Chemistry Chemical Physics. 21 (2019) 22067–22080. https://doi.org/10.1039/C9CP04162a.
2. **S. Gupta**, A.K. Dasmahapatra, Destabilization potential of phenolics on Aβ fibrils: mechanistic insights from molecular dynamics simulation, Physical Chemistry Chemical Physics. 22 (2020) 19643–19658. https://doi.org/10.1039/D0CP02459g.
3. **S. Gupta**, A.K. Dasmahapatra, Destabilization of Aβ fibrils by omega-3 polyunsaturated fatty acids: a molecular dynamics study, Journal of Biomolecular Structure and Dynamics. 0 (2021) 1–18. https://doi.org/10.1080/07391102.2021.2009915.
4. Lycopene Destabilizes Preformed Aβ Fibrils: Mechanistic Insights from All-Atom Molecular Dynamics Simulation. **(Communicated)**
5. Enhanced Stability of a Disaggregated Aβ Fibril on Removal of Ligand Inhibits Refibrillation: An All-atom Molecular Dynamics Simulation Study. **(Communicated)**

Conferences Attended:

1. Poster presentation in Research Conclave (14th -17th March,'19) and won 2nd prize.
2. Poster presentation Oral Presentation in Reflux (28th - 29th September) and won First prize.
3. Poster presentation in CompFlu organized at IISER BHOPAL (5th - 7th Dec, 2019).